Thesis titled:

Some Unusual, Astronomically Significant Organic Molecules

submitted for the Degree of Doctor of Philosophy (Ph.D.)

by

Salvatore Peppe

B.Sc. (Hons.)

of the

Department of Chemistry

THE UNIVERSITY
OF ADELAIDE
AUSTRALIA

June 2002

Contents

Abstract

To date, astronomical surveys have confirmed the existence of over 120 molecules from a variety of extraterrestrial sources. The diversity of the molecular content of circumstellar and interstellar space can only be surmised, and there is continuing debate over the processes by which molecules are formed within these extreme environments. In this thesis we describe experimental and theoretical studies on a number of unusual organic molecules that may have tangible existences in the rarefied environments of space, or in the upper atmosphere of Earth. Stable, neutral precursors of the molecular systems investigated in this work have been generated experimentally via unequivocal pathways by the application of conventional condensed phase synthetic techniques. The molecules, once prepared, were then probed by mass spectrometry. These investigations were supported by computer-based quantum chemical calculations, by which further understanding can be gained about the structures and energetics of the systems under investigation.

Accordingly, various covalently bound, anionic and neutral oxocarbon species, C_nO_m (n = 2, m = 3, 4) were formed and studied. These systems are particularly pertinent to atmospheric chemistry. Additionally, two analogous C_3HX (X = O, S) heterocumulenic systems were investigated. Some isomers of either system, when energised, were shown to undergo gas-phase rearrangement processes.

Statement of Originality

This work contains no material which has been accepted for the award of any other degree or diploma in any university or other tertiary institution and, to the best of my knowledge and belief, contains no material previously published or written by another person, except where due reference is made in the text.

I give consent to this copy of my thesis, when deposited in the University Library, being made available for loan and photocopying.

Salvatore Peppe

13/6/2002

Date

Acknowledgments

It is a pleasure for me to acknowledge the contribution of many people to this thesis.

First and foremost, I thank my patient and long-suffering supervisor. I have indeed been privileged to have worked with such a prolific and reputable scientist as Prof. John Bowie. The remarkable depth of his knowledge and the astonishing breadth of his experience have been invaluable during the last three years, and a steady source of inspiration for me. The professionalism and high sense of duty that he has demonstrated to me, and demonstrates daily to all his students has set a high water mark in my academic experience. My gratitude also extends to him for his great generosity and trust in providing me with the all-important financial support, without which the work described in this thesis would not have been possible.

I, my contemporaries, and many others before us have been fortunate to have had the invaluable resources, skills, and guidance of Dr Suresh Dua to draw from. In all matters arising during the course of experimentation - but even more for matters far beyond the cosseted confines of academia - Suresh's timely advice, and his readiness to share it, has been instrumental in the achievement of this professional milestone. I thank Suresh for patiently and without scorn showing me the folly of my more hair-brained ideas and misconceptions, and for intervening at the crucial moment to scuttle the odd ship of fools before it set sail.

Early in my candidature, I undertook a brief foray into the heady field of instrument design, ably guided by Assoc. Prof. Mark Buntine. I am grateful for the opportunity to have experienced first-hand his enormous enthusiasm and energy. At the same time, I was also fortunate to have worked alongside Dr Gregory Metha, who was able to help me by the advice that quantum-hopped across our parallel trajectories. Of both of these "Wizards of the Wavelengths" I have more to say later.

Thanks are due to Tom Blumenthal for sharing with me some of his extensive mass spectrometry know-how, in particular with respect to the ZAB 2HF instrument. I also very much enjoyed our frequent conversations on geopolitics, and I welcome any future opportunity to revisit some of the thornier issues that we raised.

I owe an equally great debt (and absolution from responsibility from my errors) to my many friends - chemists, scientists, and laypersons alike - who patiently explained the subtleties of their specialised subjects, read my drafts, and kindly listened to my concerns for this small, local speck of cosmic dust called Planet Earth. In this regard (though not necessarily in this

order), special thanks go to Dr Pasquale Razzino, Dr Mark Jurisevic, Peter Clifford, and Andrew McAnoy. The very capable Andrew, in particular, has been a constant influence on my work, regularly providing suggestions and selflessly offering help at all times. I warmly thank him and wish him every success in the future.

I extend my gratitude also to The Chemistry Department at The University of Adelaide for providing the facilities and laboratory space. Special thanks go to John Cameron for his diligent services from the chemical store (as well as his pleasant, welcoming demeanour), and to Jeffrey Borkent for his able and reliable assistance with all things computer-related (and for taking the time and putting up with my inquisitiveness, despite everyone wanting the job done last week).

On a less formal note, the friendly social atmosphere within The Chemistry Department provided a positive environment that made working within its walls a genuine pleasure. A number of individuals have made important contributions to my enjoyment of life over the last three years. Firstly, the members of the Bowie group: a fine collection of individuals of whom I have had the privilege of associating with, both at and away from the work place. Again, I extend my sincere gratitude to Suresh for his warm hospitality, and genuine friendship. As this chapter of our lives draws to a close, I wish him success and satisfaction in his future endeavours. Additionally, I'd like to thank Andrew McAnoy, Pinmanee (Charm) Boontheung, Mark Fitzgerald, and Craig Brinkworth, who are all good friends and excellent work mates. I have also associated, in social as well as scientific capacities, with the Buntine group. Our brewing adventures [as well as the frequent appraisal (quaffing) sessions], coordinated and stimulated by Drs Buntine and Metha were sometimes hilarious, often edifying, but always extremely pleasurable. But it wasn't all about gastronomical excess. Some of the most strenuous (yet no less enjoyable) activities I have engaged in over the past few years have been the Sunday morning bicycle mini-tours through the Adelaide hills. If it is true that getting there is half the fun, then the other half surely must be actually arriving at "Shangri-la" after the long climb. I consider myself fortunate to have been able to take in the scenery, and privileged to have been allowed to share the road with Greg.

My great debt to my family and my many friends will not be obvious (to them, at least) from the (in)frequency of the occasions in which I have sought their company over the period of my candidature. I apologise unreservedly to all those who have felt somewhat abandoned by me, and wish them to know that my regard for them is in no way proportional to the paucity of time I have devoted to our relationships. Particular mention must be made of my dear

Mother and Father, without whose understanding, patience, and support I have been able to reliably count on, I may never have contemplated a trying undertaking such as a PhD. Without having even the most pedestrian comprehension of the work described in this thesis, they have nevertheless stood by me, unwaveringly, and they have assisted me throughout my whole life merely by letting me find my own way and without weighing me down with the burden of their own expectations. It is to them that I dedicate this work.

List of Figures

1.1 Molecules in The Interstellar Medium

I. Introduction

A. Space: An Imperfect Vacuum

Beyond Earth's gravity, the terrestrial atmosphere gives way not to a true vacuum, but to the rarefied environment of interplanetary space. This predominantly gaseous expanse consists primarily of electrically charged particles, but it also contains solid particles of dust, material from comets, and other gas and dust from interstellar space. In our region of space, the principal source of the matter spread throughout interplanetary space is the Sun; all the planets within the Solar System, including those as far away as Neptune and Pluto, undergo a constant bombardment by atomic particles from the Sun's corona,* in a variable *solar wind.* Nevertheless, even at the Earth's distance the particle density is exceedingly low – about 5 million particles per cubic metre. The solar wind flows into a large region of space known as the *heliosphere* which extends to a radius of about 100 AU (astronomical units),† and is bounded by the *heliopause*, beyond which interstellar gas exerts an equal pressure from outside. Accordingly, interstellar space itself is not completely devoid of matter; gas, dust, and particulate material abound, and as a result of the motion of the Sun and the Solar System around the Galaxy, the interstellar material is perceived to stream around the heliosphere in an *interstellar wind.*

The vast reaches of space extending between the stars enclose the tenuous expanse of interstellar matter in the form of gas and dust that supplies the interstellar wind, and is otherwise known as the *interstellar medium.* While exhibiting an average density of only 1 particle per cm^3‡ (there are enormous variations about this average, however), the matter

---

* An extremely hot (about 2 million K) ionised gas surrounding the sun

† 1 AU corresponds approximately to the mean distance of the Earth from the sun

‡ For comparison, the terrestrial atmosphere at sea level has a density of approximately 30×10^{18} molecules per cm^3

within the interstellar medium nevertheless represents about 10 % of the entire mass of our Galaxy. The densest regions are the cold molecular clouds, containing up to 10^{10} molecules per cm^3. These are also the coldest regions in all of interstellar space, where extant temperatures are close to absolute zero. The major constituent of the interstellar medium is the gas component, which amounts to about 99 % of its total mass. The remainder consists primarily of ellipsoidal granular particles present at an average number density of 10^{-11} grains per cm^3. The overall elemental composition of the interstellar medium is dominated by hydrogen and helium, at 93.38 % and 6.49 % respectively, but also includes the biogenic elements oxygen, carbon, nitrogen, and sulfur together contributing 0.12 %; other elements furnishing only 0.01 % to the total composition.

As a consequence of the low average density and extensive permeation by magnetic fields and cosmic ray particles, high-energy radiation which readily disrupts chemical bonds, matter is only permitted to exist within the greater part of the interstellar medium primarily in the form of single atoms. Conversely, in cool, dark astronomical environments such as the interiors of dense interstellar clouds, in expanding envelopes around dying red giant stars, in comets, and in planetary atmospheres, where both the higher densities and the presence of dust grains provides a shielding effect, a rich and ever-expanding assortment of gas phase molecules have been found. The molecular diversity in some of these environments is astonishing, and is reflected in the distribution of 123 molecules, radicals, and ions that have thus far been identified by microwave, infrared (IR), and ultraviolet (UV) spectroscopy (Table 1.1). Sensitive spectral techniques such as these have been indispensable in the detection of sparsely distributed matter where, for instance, molecules exist with fractional abundances as low as 10^{-13} relative to hydrogen (detected by rotational spectroscopy).

Although technologies involving the most sophisticated terrestrial and space-born telescopes are being applied to identify the molecular composition of the interstellar medium and are delivering an unprecedented, high quality survey of molecular lines, the physical and

physicochemical processes involved in the synthesis of these molecules are far from being completely determined. Presently, there is still much scope for investigation into the underlying processes involved in the formation of molecular species in the gas phase of the interstellar medium (including those occurring on interstellar ices). It is important to appreciate that formative processes analogous to those occurring within the gas phase of the interstellar medium may also be occurring in our solar system; the hydrocarbon containing atmospheres of Jupiter, Saturn, Uranus, Neptune, and especially Titan pose many challenges to the investigator in the unravelling of the processes that give rise to their molecular composition.

Table 1.1 123 Identified Interstellar and Circumstellar Molecules[#]

Number of Atoms	Molecular Species
Diatomic	H_2, HF, HCl, AlF, AlCl, C_2, CH, CN, CO, CP, CS, CSi, FeO, KCl, NH, NO, NS, NaCl, OH, PN, SO, SH, SiN, SiO, SiS
Triatomic	AlNC, C_3, C_2H, C_2O, C_2S, CH_2, HCN, HCO, H_2O, H_2S, HNC, HNO, MgCN, MgNC, N_2O, NaCN, OCS, *cyc*-SiC_2, SiCN, SO_2, CO_2, NH_2
4-atomic	*cyc*-C_3H, *l*-C_3H, C_3N, C_3O, C_3S, C_2H_2, HCCN, HNCO, HNCS, H_2CO, H_2CN, H_2CS, NH_3, SiC_3
5-atomic	C_5, C_4H, C_4Si, *l*-C_3H_2, *cyc*-C_3H_2, CH_2CN, CH_4, HC_2CN, HC_2NC, HCOOH, H_2CHN, H_2C_2O, H_2NCN, HNC_3, SiH_4
6-atomic	C_5H, C_5O, C_2H_4, CH_3CN, CH_3NC, CH_3OH, CH_3SH, HC_2CHO, $HCONH_2$, *l*-H_2C_4, C_5N
7-atomic	C_6H, CH_2CHCN, CH_3C_2H, HC_4CN, $HCOCH_3$, NH_2CH_3, *cyc*-C_2H_4O, CH_2CHOH
8-atomic	CH_3C_3N, $HCOOCH_3$, CH_3COOH,[§] C_7H, H_2C_6, CH_2OHCHO
9-atomic	CH_3C_4H, CH_3CH_2CN, $(CH_3)_2O$, CH_3CH_2OH, HC_7N, C_8H
10-atomic	CH_3C_4H, CH_3CH_2CN, $(CH_3)_2O$, CH_3CH_2OH, HC_7N, C_8H
11-atomic	CH_3C_5N,[§] $(CH_3)_2CO$, NH_2CH_2COOH [§]
12-atomic	HC_9N
13-atomic	$HC_{11}N$
Ions	H_3^+, CH^+, CO^+, SO^+, HCO^+, HCS^+, HOC^+, N_2H^+, CH_2D^+,[§] $HCNH^+$, $HOCO^+$, H_3O^+, H_2COH^+, HC_3NH^+

[#] From National Radio Astronomy Observatory online database.[1]
[§] Uncertain detection

The most significant bodies of molecules in outer space - cold molecular clouds and circumstellar envelopes (the shells of gas and dust that surround massive, old, red stars) - are tenuously connected to each other by vast intervening tracts of low density space. The physical conditions existing within these astronomical structures are also appreciably different (see Table 1.2 below). For this reason, it is surprising that many of the identified species listed in Table 1.1 are found to exist concurrently in what, on first analysis, appear to be rather divergent conditions. With respect to the energy available for chemical reactions, this tends to suggest that molecule formation occurs irrespective of the temperature conditions within the respective environments. This fact may be an important detail when one considers the likely gas phase chemistry that occurs in such environments (see section D below).

Table 1.2 Physical properties of various regions within the interstellar medium.[2]

Object	Properties[#]
H II region	T = 10 000 K. Dominant ion H^+, but C^+, N^+, and O^+ also present. $n \approx 10^2 - 10^3$ cm^{-3}. $r \approx 1 - 10$ pc. Line and continuum radiation emitted.
Intercloud medium	T = 10 000 K. Dominant ion H. Dominant ion C^+. All atoms with ionisation potential <13.6 eV ionised. $n \approx 0.1$ cm^{-3}. No molecules.
Diffuse clouds	T = 100 K. Partial conversion of H into H_2. Dominant ion C^+. Other atoms partially neutral. $n \approx 100$ cm^{-3}. Molecules CO, H_2CO, and some others observed.
Dark clouds	T = 10 - 20 K. Most H converted into H_2. Large optical depth in visible and ultraviolet. $n \approx 10^4$ cm^{-3}. Little internal motion. $M = 10^2 - 10^4$ $M_\odot$. $r \approx 5$ pc. Many molecules observed.
Molecular clouds	T = 50 K. Associated with regions of excitation. Large optical depth. Often emitters in infrared of thermal radiation. $n \approx 10^6$ cm^{-3}. $M = 10^6$ $M_\odot$. $r \leq 30$ pc. Many molecules observed but much turbulent motion produces wide lines.
Circumstellar shells	T = 100 - 1000 K. Associated with late type stars with low surface temperatures. Molecules and dust seen. Oxygen-rich stars show silicates, SiO. Carbon-rich stars show hydrocarbons, C_2H_2.
Compact H II regions	T = 100 - 1000 K. Hot stars in dense clouds of gas and dust. Infrared and radio emission of gas and dust including molecules. Maser sources SiO, H_2O, OH. $n \approx 10^3 - 10^4$ cm^{-3}.
Coronal gas	$T = 10^5 - 10^6$ K. $n = 10^{-2}$ cm^{-3}. Atoms highly ionised, e.g. O VI observed. May occupy ~20% of interstellar medium.
Giant molecular clouds	T = 10 K. Relatively low density ($n \approx 600$ cm^{-3}). Very large mass ($M \approx 5 \times 10^5$ $M_\odot$). Diameter 40 – 100 pc.

[#] T = kinetic temperature; n = number of H atoms cm^3 in all forms; M = mass ($M_\odot$ = solar masses); r = radius (pc = parsecs).

B. Stellar Evolution, Mass Outflow and Synthesis of Molecules

Cold molecular clouds are typically in a state of equilibrium with respect to two opposing forces: i) the tendency to collapse due to the gravitational attraction of the constituent matter, and ii) the pressure created by the motion of the particles of matter within the cloud. In various regions of the cloud, a localised density increase renders the pressure insufficient to prevent gravitational collapse, and the cloud spontaneously and slowly contracts under the action of its own gravity. This localised density increase may be due to the molecular constituents of the cloud; molecules capable of actively radiating energy away at radio wavelengths regulate the temperature of the cloud.[3] Energy loss can have a dramatic result in some of the densest regions of the cloud; with advanced heat depletion, the cloud gas pressure becomes insufficient to balance gravity, and the cloud undergoes gravitational collapse. Generally, the rate of collapse is proportional to cloud density; a collapse that occurs over about 100,000 years results in the birth of a new star, while, at the other extreme, gravitational collapse occurring in less than a second gives rise to a neutron star. A star first shines because the gravitational potential energy lost during the collapse is released as heat and light. Once the central density is sufficiently high, energy-releasing nuclear fusion reactions occur, and, in principle, almost all of the elements and isotopes in the periodic table up to those with the most strongly bound nuclei in the region of iron may be produced.

A consequence of gravitational collapse and star formation is that matter is constantly removed from the surrounding cloud. However, the flow of matter does not end with the birth of stars; mass outflows from the surfaces of stars in stellar winds of greater or lesser rates than from our own Sun have also been observed in many other stars and seems to highlight typical stellar behaviour. Mass outflows occurring during the stages of stellar evolution close matter flow into a cycle. The initial mass of the star determines the rate of mass outflow and also the evolutionary course the star follows. Main sequence stars (i.e. those that produce their energy by fusing hydrogen into helium in their cores) experience moderate rates of mass loss; the

continuous current of a typical stellar wind. This is in contrast to red giant stars, which expel enormous amounts of gas and dust from their uppermost layers in a strong current. Distinct structures can result from the various modes of mass outflow, depending on the intrinsic properties of the source star. In the case of a shell star, a cool circumstellar envelope may form. At the other extreme, supernova explosions, by which certain stars end their lives, involve the violent ejection of the outer layers of the star. These three events are important not only for providing a variety of sources and sinks by which matter is recycled within galactic environments, but also for creating different conditions whereby the synthesis of complex molecular species may occur.

Enormous quantities of matter are transported to interstellar space over the lifetimes of stars. The combination of vast quantities of matter and relatively cool (~100 K) and dense (~10^{10} cm^{-3}) conditions, as present in out flowing atmospheres of giant stars, provides an environment which is particularly conducive of the synthesis of complex molecules. These molecules, however, are created and destroyed within a relatively short radius from the progenitor stars, and are not thought to contribute to the contents of molecular clouds beyond the provision of simple atomic and diatomic raw material. This has been rationalised by considering the relative densities of the gas along the trajectory spanning from star to molecular cloud. For a parcel of gas close to a star at radius r where molecule formation occurred, the density may be expressed by n_0. The stellar atmosphere around this star is expanding radially outward with uniform velocity, so that the density of this parcel of gas when at distance $R > r$ is $n_0(r/R)^2$. A reasonable assumption sets $n_0 = 10^{10}$ cm^{-3} and $r = 10^{12}$ cm. The picture changes dramatically at a distance $R = 10^{16}$ cm, a relatively small distance on an astronomical scale since clouds are typically 3×10^{19} cm in diameter. At this distance from the progenitor star, the density has reduced to 100 cm^{-3}. The background interstellar radiation field can penetrate the gas at this density, reducing molecular lifetimes to a few hundred

years,* in which time the parcel of gas travels a negligible distance. Consequently, all molecules produced in the dense stellar atmospheres are destroyed in the passage from a region close to the star where molecule formation occurred out to interstellar space. The corollary of this is that for molecules to occur within molecular clouds, they must be synthesised *in situ*.[2]

C. Astronomical Detection of Molecules

The recent renewal of interest in the circumstellar environment of evolved stars has been driven by the progress in high resolution spatial and spectral techniques. Advances in spectroscopy, for example, have revealed the presence of a diverse range of molecules as constituents of interstellar and circumstellar atmospheres, and have provided evidence of complex chemistry. The gaseous interstellar molecules detected to date are predominantly organic in nature, ranging in complexity from diatomic species, to frequently observed linear carbon chains including some rather unusual neutral and ionic molecules. At the upper end of complexity, a thirteen-atom, unsaturated, linear organo-nitrogen species, $HC_{11}N$ (see Table 1.1) has been detected. This last example, and others like it, are of particular interest to the work herein, since they have acetylenic or cumulenic structures, displaying alternating triple and single carbon bonds or successive carbon double bonds respectively (in this thesis, they are collectively referred to as heterocumulenes).

---

* The photodissociation rate, β_0, for molecules exposed to the unattenuated interstellar radiation field is obtained by the following evaluation:

$$\beta_0 = 4\pi \int_{E=0}^{13.595} F(E)\sigma_{pd}(E)\mathrm{d}E$$

where $F(E)$ is the measured interstellar radiation flux, E is the photon energy in eV, and σ_{pd} is the photodissociation cross-section. The integration covers all absorption bands of the molecule between 0 and 13.595 eV. Typical values for β_0 lie between 10^{-9} and 10^{-11} s^{-1}. The molecular lifetime, τ, would then be the reciprocal of β_0.[2]

Some of the most abundant molecular sources have been detected in our own galaxy. The cyanopolyynes ($HC_{2n+1}N$), for instance, are most abundant in TMC-1, a cold (10 K) molecular cloud in the large constellation of Taurus. Similarly, the circumstellar envelopes of stars on the asymptotic giant branch (AGB)* show a remarkably rich variety of molecular species. One of the best examples is the carbon-rich envelope surrounding the nearby carbon-rich star IRC+10216, which has been shown by millimetre observation to contain cyanopolyynes ($HC_{2n+1}N$), the naked carbon chain molecules (C_n, n = 3, 5), and C_nH linear radicals. [5] Surprisingly, these highly unsaturated species are prevalent in regions in which the most abundant chemically reactive element is hydrogen. Moreover, diffuse interstellar clouds are characterised by low gas densities and high penetration by dissociative, external ultra-violet radiation from stars, and consequently have not been observed to contain any but the simplest diatomic species. The dense interstellar clouds, on the other hand, contain substantial quantities of dust that may act as an effective screen to molecules in the cloud interiors. Such screening furnishes the dense clouds with an environment that is more conducive to molecular development than would otherwise be found in the diffuse clouds.[6]

Electronic transitions can only be seen in absorption in the interstellar medium whereas vibrational transitions can also occur as emission bands in some hot regions. Rotational lines are most easily seen in emission in the cold interstellar clouds, and it is precisely via their low-energy transitions in emission that observers have been able to conclusively confirm the presence of interstellar molecules in these environments.

---

* The asymptotic giant branch, or AGB, are those stars such as the red giants and red super giants, which are positioned on the Hertzsprung-Russell (H-R) diagram asymptotically to the main sequence. The AGB phase of stellar evolution corresponds to the short stage during which intermediate-mass stars attain their highest luminosities, but also experience heavy mass loss. Whereas the stars on the main sequence fuse hydrogen into helium in their cores, AGB stars have depleted the hydrogen and helium fuel in their cores; instead they produce their energy by fusing helium and heavier elements in a relatively thin shell surrounding the core.[4]

It seems certain that inside the enormous interstellar molecular clouds there occurs a rich chemistry as evidenced by the ever-increasing number of molecules detected in space through rotational spectra characterisation. While many of these molecules are common in terrestrial laboratories, others are quite unusual and raise the exciting prospect of finding a great many more exotic molecules, of greater complexity and stranger properties.

Foremost among the more unusual molecules in terms of both molecular complexity and abundance are the long carbon chain molecules originally observed in the Taurus molecular cloud complex TMC-1. The polyyne series of molecules feature distinctly: the cyanopolyynes HC_2CN, including the longest known carbon chain molecule $HC_{11}N$, and the methyl polyyne species, CH_3C_2H. The study of carbon chain molecules has focussed on the evaluation of a key molecular property. Within the interstellar cloud, molecular abundance is integrally dependent on the quantum mechanical probability for rotational transition and on the emission signal strength as measured by the radio telescope.[7] The transition probability is proportional to the molecular dipole moment, and so the signal strength is converted into an abundance (in terms of a column density) by measurement of the dipole moment. Naturally, the laboratory measurement of dipole moments should precede the determination of a detected molecule's abundance, but where this is not the case,* the researcher makes use of *ab initio* calculations to produce reasonably accurate dipole moment values.[8]

D. Gas Phase Chemistry

One of the earliest, and simplest, models describing the chemistry of circumstellar envelopes is known as the 'freeze out' model.[9] It assumes that there are conditions of thermal equilibrium in regions close to the central star. In this case, a parallel decrease in the temperature occurs along with the decreasing circumstellar gas density, until some critical

* For instance $HC_{11}N$ was detected in interstellar molecular clouds before its dipole moment was accurately measured in the laboratory.

value is attained, beyond which there is no further chemical activity, and the molecular abundances are 'frozen'. While these models work well with simple CNO molecules (containing carbon, oxygen, and nitrogen), they cannot explain the formation of refractory compounds, chain molecules, and radicals.[10] A refinement of the freeze out model involves photodissociation and photoionisation as a result of action of interstellar and chromospheric ultraviolet radiation, and cosmic rays. Such processes can produce species such as $C_2H_2^+$, which can instantly react to build up large molecules.[11] A variation to this scheme involves cosmic ray ionisation of hydrogen that drives ion-electron dissociative recombination (*cf.* next paragraph and Scheme 1.1.1 below).[12] Schemes involving ion-molecule reactions were considered satisfactory explanations on energetic grounds due to the low activation barriers for these reactions, some of which are known to be near-zero. These models adequately account for the detection of the molecular ions HCO^+ [13] and HNN^+,[14] and have also gained support by the observation that complex molecules contained in circumstellar shells are actually found in the outer envelope, and not near the star.[15]

The ion-molecule chemistry suggested, for example, for the production of C_3O and propynal in the interstellar medium [16] follows a familiar pattern, and involves the radiative-stabilisation association reaction between $C_2H_3^+$ and CO, followed by the dissociative recombination of the $H_3C_3O^+$ ion (*cf.* Scheme 1.1.1).

SCHEME 1.1.1

Radiative-stabilisation association:	$C_2H_3^+ + CO$	$\rightarrow$	$H_3C_3O^+ + h\nu$	(a)
Dissociative Recombination:	$H_3C_3O^+ + e$	$\rightarrow$	$C_3O + H_2 + H$	(b) (i)
		$\rightarrow$	$HC_3HO + H$	(b) (ii)

In the same work, it was also established that the ions of the form $H_nC_mO^+$ are sufficiently unreactive toward the known neutral constituents of interstellar molecular clouds. This infers that the lifetime of these species is sufficiently long for dissociative recombination processes to be possible in the low densities and temperatures of these environments.

However, these schemes may not adequately explain the generation of large molecules in high abundance. Long chain heterocumulenic molecules such as HC_5N [17] within dark dust clouds, and $HC_{11}N$, along with pure carbon chains such as C_3 and C_5 [18] have been detected in circumstellar envelopes in high abundance. While it was known that neutral-neutral reactions are responsible for the formation of molecular hydrogen on dust grain surfaces, these reactions have much higher activation barriers and lower cross sections than ion-molecule reactions. The significance of this is that it is unlikely that neutral-neutral processes are responsible for the formation of large molecules. Recently, atomic carbon has been reported to be capable of inserting into unsaturated molecules, such as acetylene, with zero activation barriers and high probability.[19] While such findings are promising, it must be remembered that, according to the prevalent view, neutral-neutral reactions rapidly form small, stable molecules, thereby terminating the chain-lengthening process. This would seem to negate the possibility that such processes could result in large molecules. However, recent work on the reaction of ground-state carbon atoms with acetylene under single-collision conditions in crossed beam experiments has shown that cyclic and linear C_3H isomers can form via an atom-neutral reaction.[20]

SCHEME 1.1.2

Atom-neutral reaction: $^{\bullet}C^{\bullet} + C_2H_2 \rightarrow C_3H_2 \rightarrow l\text{-}^{\bullet}C_3H + H^{\bullet}$ (a)

$\rightarrow c\text{-}^{\bullet}C_3H + H^{\bullet}$ (b)

If negative ions are present in interstellar molecular clouds or in circumstellar envelopes, they have yet to be unequivocally detected. However, the absence of evidence does not necessarily negate the possibility that negative ions do indeed play a role in the chemistry of these environments. Initially, negative ion formation in interstellar clouds was thought to be an inefficient process, particularly for small molecules. Excess energy is gained during a radiative attachment-type process (Scheme 1.1.3), which needs to be dissipated; small molecules have too few vibrational and rotational modes through which to achieve this.[21]

SCHEME 1.1.3

Radiative attachment: $X + e^- \leftrightarrow [X^-]^{\ddagger} \rightarrow X^- + h\nu$

Electron detachment to a small molecule X, gives rise to an energetically excited intermediate $[X^-]^{\ddagger}$, which has a very short lifetime with respect to the reverse process (electron detachment). Since it was first proposed, this viewpoint has been elaborated to include consideration of larger molecular species such as polycyclic aromatic hydrocarbons (PAHs), which if present in the molecular cloud, may form negative ions upon radiative attachment more efficiently than smaller species.[22] Large cumulene anions of the form C_nH^- and $C_nH_2^{-\bullet}$ (n = 10-23) have been proposed to contribute in similar ways as PAHs to the hydrocarbon chemistry in these environments.[23] It has been suggested that large negatively charged molecules act as negative charge carriers in charge transfer processes involving relatively small neutral species possessing high electron affinities. For example, a recent model proposes that the cyanide anion, CN^-, which has been shown theoretically to occur in some interstellar gas clouds, is efficiently formed by charge transfer from large PAH anions [EA(CN) 3.82 ± 0.02 eV].[24] Analogously, C_3N^- and C_3H^- have also been postulated to contribute to the chemistry in these environments.[25]

E. Generation and Detection of Heterocumulenes in the Laboratory

Several studies, both experimental and theoretical, have been directed at the generation of heterocumulenes in the laboratory, with the aim of elucidating the possible synthetic pathways operating in interstellar environments. A common approach involves the detection by Fourier transform microwave spectroscopy of species generated in supersonic molecular beams. For example, the cyanopolyynes $HC_{2n+1}N$ are known up to $n = 5$,[26] or have been spectroscopically investigated up to $n = 8$.[27] Of the isocyanopolyynes, isocyanoacetylene (HC_2NC) has been studied spectroscopically, and its microwave spectrum reported,[28] while HC_4NC and HC_6NC were recorded and the ground state rotational constants were determined.[29]

A host of chemical species were produced by Thaddeus *et al.*[30] from acetylene and diacetylene diluted in an inert gas and subjected to a small dc discharge in the throat of a supersonic nozzle of a molecular beam spectrometer (Table 1.2).

Table 1.2 Twenty seven carbon chains generated in the laboratory.[30]

Carbon Chain		Chemical Formulae
Cyanopolyynes		HC_nN (n = 11, 13, 15, 17)
Isocyanopolyynes		HC_nNC (n = 4, 6)
Methylpolyynes		H_3C_nH (n = 9, 11)
Methylcyanopolyynes		H_3C_nN (n = 8, 10, 12)
Free Radicals:	Acetylenic	C_nH (n = 7, 9, 11, 13); H_2C_4N
	Cumulenic	C_nH (n = 8, 10, 12, 14)
Cumulene Carbenes		H_2C_n (n = 5,6)
Ring-Chain Carbenes		HC_3C_nH (n = 2, 4, 6); HC_3C_nCN (n = 0, 2)

While most of these molecules have not been astronomically detected, they are nevertheless good candidates for detection because for each type, a shorter member was astronomically detected once experimentally derived frequencies were obtained. These techniques, though capable of generating a great many chemical species with relative ease, do so non-selectively:

the reaction conditions are such that several types of molecule are generated simultaneously. The spectra thus obtained are exceedingly complex, requiring painstaking interpretation.

An alternative approach which enables a degree of structural selectivity whilst still permitting the capture and manipulation of transient species, involves the use of UV photolysis or flash vacuum pyrolysis of suitable precursor molecules, and trapping the products in a low temperature matrix. For example, some elusive bisimine and thione derivatives of iminopropadienones, RN=C=C=C=O, have been generated [31] from suitably substituted isoxazolopyrimidone precursors [Scheme 1.1.4 (a)] or dimethylaminomethylene-Meldrum's acid derivatives [Scheme 1.1.4 (b)] using flash vacuum pyrolysis, and monitoring the fragmentation reactions by matrix IR methods (and by NRMS, which is discussed later).

SCHEME 1.1.4

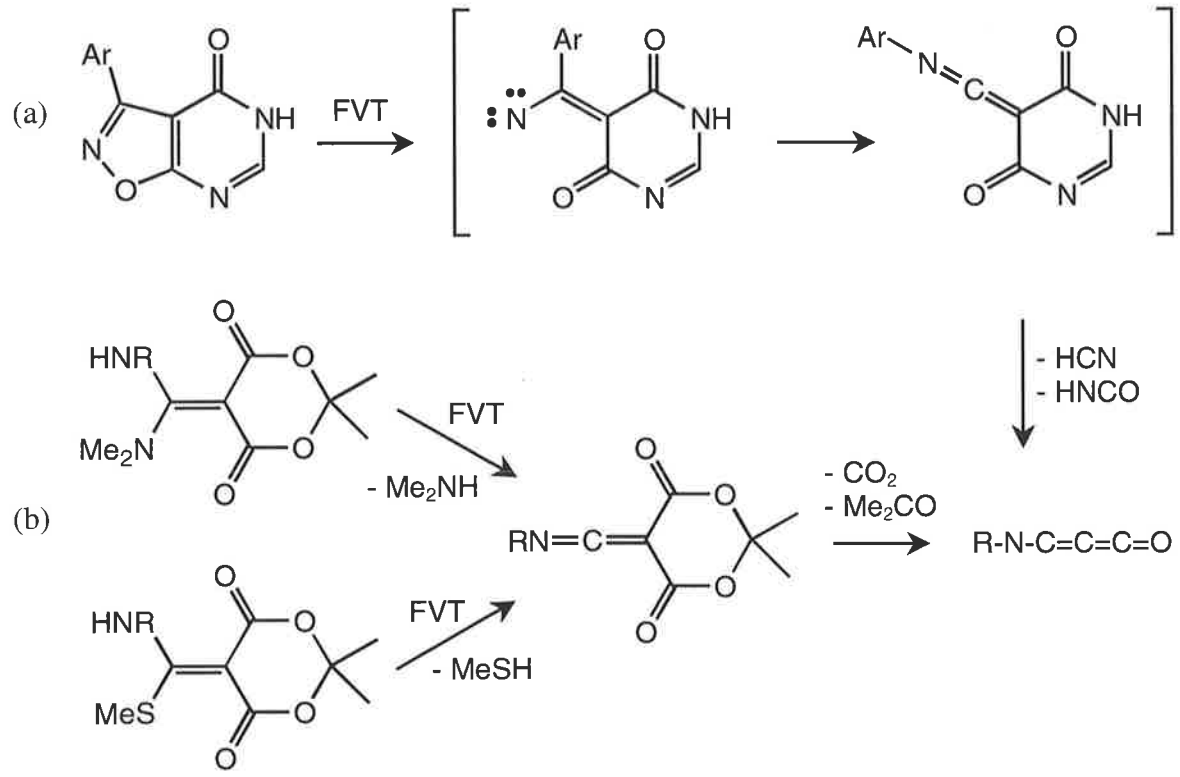

Another methodology by which transient ionic species can be generated and detected is mass spectrometry. Within the mass spectrometer, at low pressure, unstable ionic species may be generated at high dilution and relatively long lifetimes because the likelihood of destructive interaction with other reactive particles is significantly reduced. Moreover, the conditions within the mass spectrometer closely replicate the rarefied circumstellar and interstellar environments, making mass spectrometry an appropriate tool for the investigation of the chemistry in these environments. A particularly advantageous feature of mass spectrometry is that it enables the generation, detection, and further interrogation of the species under investigation, all within the same instrument. In the following sections, several gas phase techniques will be described that enable the examination of distinct structural isomers. When used in conjunction with other techniques such as neutralisation reionisation mass spectrometry (NRMS), or photoelectron spectroscopy (PES), transient neutrals may be exhaustively investigated and characterised.

1.2 Gas Phase Generation and Characterisation of Ions

I. Gas Phase Generation of Ions

A. Positive Ions

Electron Impact Ionisation

Electron impact (EI) ionisation is the traditional approach to ion generation in mass spectrometry.[32] Heating a tungsten wire or a rhenium ribbon *in vacuo* generates electrons that are then accelerated by applying a small voltage (generally 70 V).* The electron beam is confined to a narrow helical path by a weak magnetic field on the order of 300 G.† When an electron in the beam impacts with a volatilised compound (M) the electron may impart some of its kinetic energy into the neutral substrate. If the energy transferred is greater than the threshold for ionisation of M, then a molecular cation $M^{+\bullet}$ can be obtained (Scheme 1.2.1)

SCHEME 1.2.1

$$M + e^- \rightarrow M^{+\bullet} + 2e^-$$

However, ionisation in this manner is a relatively low probability occurrence, with 1 in 1000 gas molecules ionised. Electron impact ionisation can be described as a vertical process,‡ wherein electron removal from the neutral substrate molecule affords a product ion with an initial structure that is similar to that of the substrate (i.e. the nuclear geometry is similar in both neutral substrate and product ion). The radical cation thus formed may be stable with this structure, or conversely may be unstable and fragment into a number of dissociation products.

---

* Standard reference mass spectra are typically recorded with electrons accelerated to 70 eV.

† The Lorentz force, $ev \times B$, constrains electrons to spiral around magnetic field lines.

‡ However, electron impact ionisation is not a vertical process in the sense that photo-ionisation is; the IE onsets for molecules whose ions have significantly different geometries are gradual, indicating that non-vertical events have finite probability.

In the latter case the process is termed dissociative ionisation and is rationalised in terms of Figure 1.2.1.

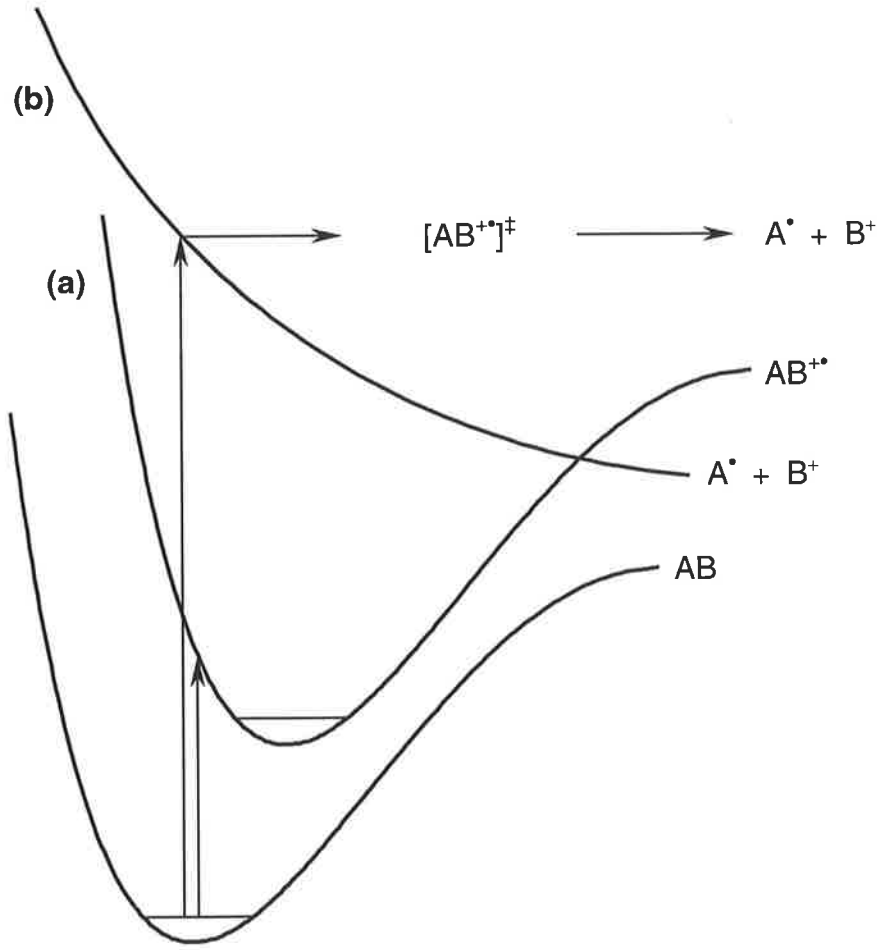

Figure 1.2.1 Morse potential energy curves for a diatomic neutral substrate molecule, AB. Vertical ionisation by electron impact (EI) results in access of (a) a stable (bound) radical cation, $AB^{+\bullet}$, and (b) an unbound potential energy surface whereby dissociation results in a neutral radical, $A^{\bullet}$, and an even electron cation, B^{+} (dissociative ionisation).

B. Even Electron Negative Ions

1. Resonance Capture

EI conditions may also be employed to produce negative ions through resonance electron capture. In this case, the volatilised substrate neutral, M, is required to have positive electron affinity such that an electron may be captured from the ionisation beam. Such an event results in the formation of a radical anion (Scheme 1.2.2).

SCHEME 1.2.2

$$M + e^- \rightarrow M^{-\bullet}$$

The probability for such an event occurring is smaller even than for electron removal (Scheme 1.2.1) by a factor of *ca.* 100.[33] Electron attachment too, like electron removal, is a vertical transition which involves transfer of excess energy (greater than or equal to the electron affinity of the neutral substrate) to the nascent ion. As in EI ionisation, formation of the nascent ion by electron capture may be followed by fragmentation and ion-pair formation [Scheme 1.2.3, (e) and (d)], in a process that is referred to as dissociative electron attachment. Conversely, for neutral substrates with high electron affinity and many internal degrees of freedom through which to dissipate the excess energy gained, electron attachment can produce a radical anion with a greater likelihood of surviving on the mass spectrometric timescale (*ca.* 10^{-6} s).[34]

SCHEME 1.2.3

$$AB + e^- \rightarrow [AB^{-\bullet}]^{\ddagger}$$

$$[AB^{-\bullet}]^{\ddagger} \rightarrow AB^{-\bullet} + h\nu \quad \text{(a)}$$

$$[AB^{-\bullet}]^{\ddagger} + X \rightarrow AB^{-\bullet} + [X]^{\ddagger} \quad \text{(b)}$$

$$[AB^{-\bullet}]^{\ddagger} \rightarrow AB + e^- \quad \text{(c)}$$

$$[AB^{-\bullet}]^{\ddagger} \rightarrow A^+ + B^- + e^- \quad \text{(d)}$$

$$[AB^{-\bullet}]^{\ddagger} \rightarrow A^- + B^{\bullet} \quad \text{(e)}$$

Electron capture may form energetically excited radical anions. In this instance, excess internal energy may be dissipated by radiative emission or by collisional transfer to other molecules [Scheme 1.2.3 (a) and (b)]. Other avenues of energy dissipation open to the excited radical anion may be electron ejection, fragmentation, or ion pair formation [Scheme 1.2.3

(c), (d), and (e) respectively], in which case the low energy electrons or even electron anions formed may participate in secondary reactions in the source of the mass spectrometer,[35] as discussed in the next section.

2. Negative Ion Chemical Ionisation

Increasing the source pressure (to *ca.* 0.1 Torr) results in a greater number of collisions between the electron beam and substrate molecules. Such conditions favour resonance capture processes, with a concomitant increase in the yield of low energy electrons [Scheme 1.2.3 (d) and (e)] mitigating further electron capture, resulting in an overall increase in negative ion yield. Negative ion chemical ionisation (NICI) is a technique which takes advantage of the fact that the higher-pressure conditions are also conducive of ion-molecule reactions between the nascent anions and the neutral gas molecules.[36] Typically, a small amount of substrate, M, is introduced into the ion source with a relatively high pressure of reagent gas (commonly water, but ammonia and methanol are also used). When water is used, the reagent gas undergoes dissociative resonance capture to give a hydride anion and a hydroxyl radical [Scheme 1.2.4 (a)]. The high-pressure conditions present in the source then induce the hydride anion to rapidly deprotonate another water molecule to produce a hydroxide ion [Scheme 1.2.4 (b)]. In this manner, high concentrations of hydroxide ions are produced which deprotonate the substrate molecules and generate even electron anions, denoted $[MH_{n-1}]^-$ in Scheme 1.2.4 (c).

SCHEME 1.2.4

$$H_2O + e^- \rightarrow [H_2O^{\bullet -}]^{\ddagger} \rightarrow HO^{\bullet} + H^- \quad \text{(a)}$$

$$H_2O + H^- \rightarrow HO^- + H_2 \quad \text{(b)}$$

$$HO^- + MH_n \rightarrow [MH_{n-1}]^- + H_2O \quad \text{(c)}$$

3. Decarboxylation and Desilylation

While NICI is a good general deprotonation technique, if more than one acidic proton is present on the substrate molecule, M, then a number of isomeric $[MH_{n-1}]^-$ anions may be formed. Conversely, in the absence of acidic protons, deprotonation cannot be effected in this manner. In the latter circumstance, an alternative method has been devised which involves decarboxylation of a carboxylate anion. This technique necessitates the selection of a precursor molecule that bears a carboxylic acid functionality at the location in which the negative charge is required.[37] Carboxylate anions are formed subsequent to deprotonation, and decarboxylation will result for those anions with sufficient internal energy (Scheme 1.2.5).* This procedure has been successfully employed in the generation of the alkenyl and alkyl anions, $H_2C{=}CH^-$ and $(CH_3)_2CH^-$.[38]

SCHEME 1.2.5

$$RCO_2H + HO^- \rightarrow RCO_2^- + H_2O$$
$$RCO_2^- \rightarrow R^- + CO_2$$

Alternatively, R^- anions may be generated using an S_N2 (Si) reaction between $RSiMe_3$ and an appropriate nucleophile (typically F^- and OH^-). Suitable precursor molecules are selected bearing a trimethyl silyl (TMS) moiety at the site that the negative charge is required, and are reacted with the gas phase nucleophile as shown in Scheme 1.2.6.

SCHEME 1.2.6

$$R\text{-}SiMe_3 + Nu^- \rightarrow R^- + Nu\text{-}SiMe_3$$

* In some instances, it may be necessary to collisionally activate the carboxylate anion.

The fluoride anion has been the nucleophile of choice as a result of its strong affinity for silicon.[39] As an alternative to F^-, hydroxide anions have also been shown to be effective gas phase TMS displacing agents,[40] and have been employed in the gas phase synthesis of the two isomeric C_3H_3 anions, $^-C{\equiv}CCH_3$ and $^-CH_2C{\equiv}CH$,[39] and in the preparation of the acetyl anion, CH_3CO^-.[41]

C. Radical Anions

1. Resonance Capture

Depending on the electron affinity of the substrate, radical anions can also be generated in the gas phase by electron capture under EI or CI conditions (as discussed on page 17). The various strategies employable have been the topic of a recent review.[42]

2. Radical Loss from Even Electron Anions

Even electron anion fragmentation under collisional activation has been extensively reported and has been the subject of review.[43] Radical anions can be generated from the homolytic cleavage of covalent bonds of a number of even electron anions via the loss of a radical. An example of this is the formation of the PhCHO radical anion by collisional activation of benzyl ethers of the form $[PhCHOR]^-$ to induce loss of R as a radical.[44] Fragmentations of this type are also known to occur in the source of the mass spectrometer, for instance, the C_5O radical anion has been formed by loss of the *tert*-butyl radical from the even electron precursor, $^-C{\equiv}CC{\equiv}CC(O)C(CH_3)_3$.[45]

3. Ion-molecule Reactions of the Oxygen Radical Anion

Dissociative electron attachment is employed in the generation of $O^{-\bullet}$ via the dissociative resonance capture of nitrous oxide [Scheme 1.2.7 (a)].[46] The oxygen radical anion has been demonstrated to be an effective chemical ionisation reagent, enabling the formation of radical

anions from the reactions between organic substrates and $O^{-\bullet}$[47] Organic substrates preferentially lose a proton and a hydrogen radical (the elements of $H_2^{+\bullet}$) over simple deprotonation [Scheme 1.2.7 (b) and (c) respectively].

SCHEME 1.2.7

$$N_2O + e^- \rightarrow N_2 + O^{-\bullet} \qquad (a)$$

$$RH_2 + O^{-\bullet} \rightarrow R^{-\bullet} + H_2O \qquad (b)$$

$$RH_2 + O^{-\bullet} \rightarrow RH^- + HO^{\bullet} \qquad (c)$$

This methodology has been employed to access a multitude of radical anions (for example the radical anion of vinylidene, an important organic intermediate). The reaction of $H_2C{=}CD_2$ with the oxygen radical anion was found to form $H_2C{=}C^{-\bullet}$ and $D_2C{=}C^{-\bullet}$ by loss of D_2O and H_2O respectively without producing $[DC{=}CH]^{-\bullet}$.[48] * The generally accepted mechanism for ion-molecule reactions of $O^{-\bullet}$ with organic substrates involving the elimination of $H_2^{+\bullet}$ has been argued along thermodynamic grounds. It is suggested that H-atom abstraction is followed by proton abstraction (Scheme 1.2.8), since the initial H· abstraction from ethylene is endothermic by < 1 kcal mol^{-1}, whereas H^+ abstraction is endothermic by almost 25 kcal mol^{-1}.[34,49,50]

SCHEME 1.2.8

$$H_2C{=}CH_2 + O^{-\bullet} \rightarrow [(H_2C{=}CH^{\bullet})\,HO^-] \rightarrow H_2C{=}C^{-\bullet} + H_2O$$

4. Diazo compounds

Scheme 1.2.9 depicts the dissociative resonance capture of diazo-substituted organic substrates, with facile loss of dinitrogen,[51] to afford the corresponding radical anion.

* See also R.N. McDonald, Tet., 1989, 45, 3993

SCHEME 1.2.9

$$RC(N_2)R' + e^- \rightarrow [RCR']^{-\bullet} + N_2$$

This method has been successfully used to access the radical anion of acetyl carbene (CH_3COCH), a reactive intermediate.[52]

5. Double-Desilylation

Double desilylation [53,54] is an extension to the desilylation method discussed previously. Here, the substrate molecule is required to be doubly substituted with TMS functional groups, which are then both lost upon reaction with an ion flux containing fluoride ions and molecular fluorine, forming the radical anion. In this manner, distonic [55] radical anions (i.e. where the charge and the unpaired electron reside on different atoms within the molecule) may be selectively generated. An example of the successful application of this method is the reaction of $(TMSCH_2)_2C{=}CH_2$ with F^-/F_2 in the gas phase to produce the trimethylene methane radical anion.[53] The general mechanism for this method is illustrated in Scheme 1.2.10 below, but radical anions of both *para*-benzyne [54] and oxyallyl [52] have also been generated using this methodology.

SCHEME 1.2.10

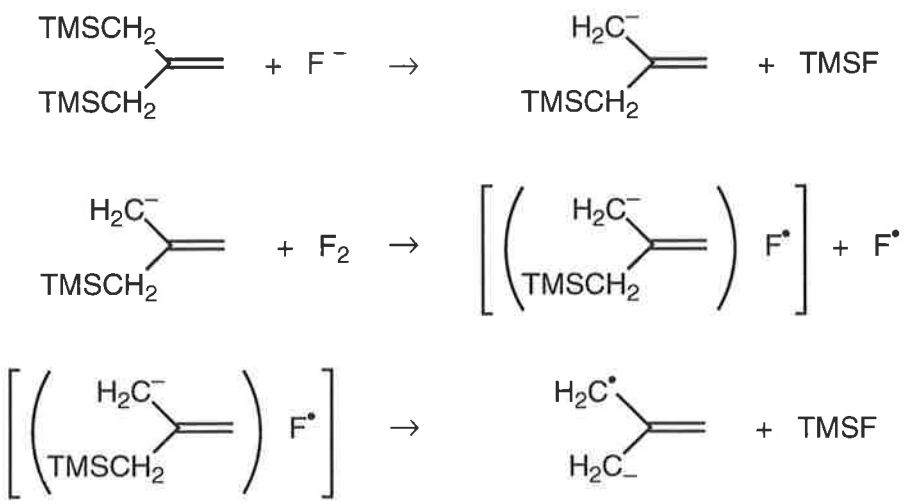

II. Mass Spectrometry

A. The VG ZAB 2HF Mass Spectrometer

The mass spectrometric techniques employed in this study of gas phase ions were performed on the VG ZAB 2HF mass spectrometer (ZAB) at the University of Adelaide (Figure 2.1). In a conventional Nier-Johnson (or EB)[56] two sector mass spectrometer, the electric sector (E), the energy (or velocity) focusing device, precedes the magnetic sector (B), the angular (or directional) focusing device. The ZAB is a two sector *reverse* geometry instrument [57] which differs from an EB mass spectrometer in the arrangement of the magnetic sector preceding the electric sector.

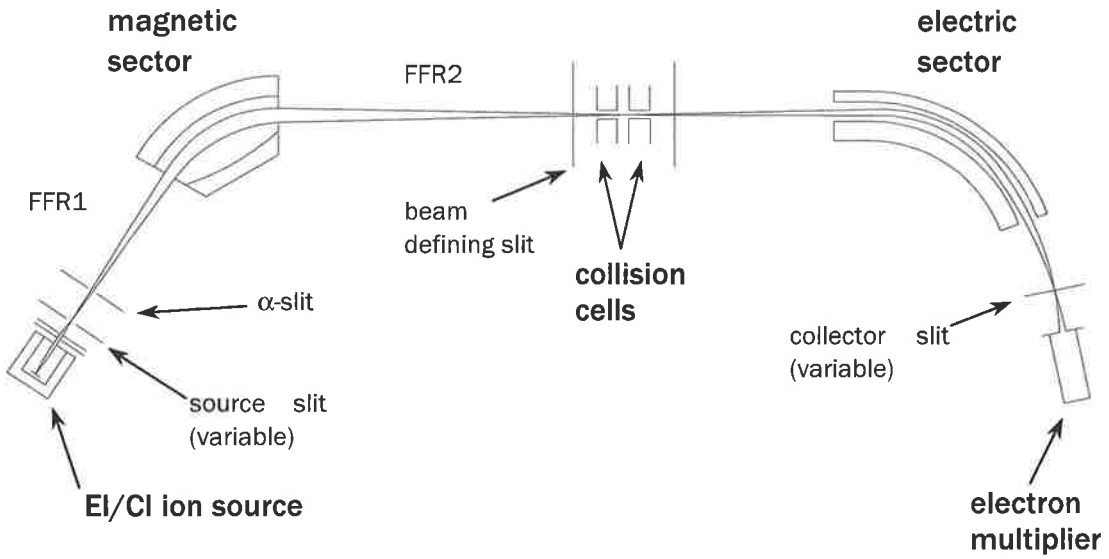

Figure 1.2.2 A simplified schematic representation of the VG ZAB 2HF (FFR denotes field-free region).

The main advantage of this arrangement is that parent ions may be mass selected within the magnetic sector by tuning the magnetic field strength to focus ions of a predetermined mass:charge ratio (*m/z*) within the second field free region (FFR), while the product ions may be resolved according to their masses by scanning the voltage across the electric sector. This technique is termed Mass-Analysed Ion Kinetic Energy (MIKE) spectrometry.[58]

B. Mass-Analysed Ion Kinetic Energy Spectrometry

The nascent ions are extracted out from the EI/CI source by an applied voltage and collimated into a beam by slits. The ions are accelerated through a potential of 7 kV (V) before passing through the magnetic sector. As has already been stated, mass selection within the magnetic sector is effected by adjusting the magnetic field strength (B) such that only an ion of mass to charge ratio m/z is permitted to traverse the circular radius of the sector (r), as is given in Equation 1.2.1 (e = 1.6 x 10^{-19} C).[33]

EQUATION 1.2.1

$$m/z = \frac{B^2 r^2 e}{2V}$$

In this way, a parent ion is mass selected and conveyed through the second field free region to the electric sector. In general, ions accelerated through a potential to a kinetic energy (V), and passing through a uniform strength field (E) in the electric sector, will only be transmitted through the electric sector if their trajectories have a radius of curvature that corresponds to the fixed electric sector radius (r), according to Equation 1.2.2.[33]

EQUATION 1.2.2

$$r = \frac{2V}{E}$$

The resultant spectrum shows peaks corresponding to the mass selected parent ion and any daughter ions formed from fragmentation of the parent ion in the second field free region. The kinetic energy of a parent ion AB (V_{AB}) of mass (M_{AB}) that decomposes in this region is divided between the charged and neutral fragments A and B in the ratio of their masses. Consequently, A having a mass (M_A) is formed with translational energy (V_A) given by Equation 1.2.3.

EQUATION 1.2.3

$$V_A = V_{AB} \times \frac{M_A}{M_{AB}}$$

III. Characterisation of Ions

A. Collisional Activation

The parent ion may undergo decomposition in the second field free region by two modes: (i) if during the generation of the parent ion sufficient energy is deposited into it by the generation process, this internal energy may cause the ion to decompose in a process known as *metastable decomposition*;[59] (ii) alternatively, a non-momentum transferring collision between the ion and a neutral gas can induce the ion to decompose, in a process known as either *collisional activation* (CA) or *collisionally induced decomposition* (CID).[60]

In a sufficiently energetic collision between a translationally energetic ion (AB^+ or AB^-) and a neutral gas (N), the ion may be either vibrationally or electronically excited. Energies of the order of several electronvolts are required to induce electronic transitions;[61] the translational energies employed in the ZAB are often as high as 7 kV, and as a result collisions with neutral gases generally induce vertical electronic excitation.[59,62] An ion that is electronically excited in this way may dissociate in order to dissipate the acquired internal energy (Scheme 1.2.11)

SCHEME 1.2.11

$$AB^- + N \rightarrow [AB^-]^{\ddagger} + N \rightarrow A^- + B + N$$

In a high energy, kilovolt collision, the energies of collision are predominantly less than 10 eV,[59,62] but in some CA spectra, processes requiring energies of the order of 16 eV have been observed.[63]

CA experiments are performed on the ZAB in one of the two collision cells that are located in the second field free region (Figure 1.2.2). The efficiency of the CA process depends on the nature and the pressure of the collision gas used. As well as the CA process, an accelerated ion and a neutral gas may also interact upon collision to result in neutralisation and ion

scattering (Scheme 1.2.12). These two alternate pathways have detrimental effects upon the efficiency of the decomposition processes, and while in certain circumstances neutralisation in this manner is a useful outcome,* its occurrence must be minimised in a simple CA experiment.[64]

SCHEME 1.2.12

$$AB^- + N \rightarrow AB + N + e^- \qquad (a)$$

$$AB^- + N \rightarrow AB^-(\text{scattered}) + N \qquad (b)$$

In order to maximise the efficiency of the CA process, selection of the collision gas is critical. The inert atomic gases helium and argon are the preferred collision reagents because they induce minimal neutralisation and scattering events in collision with ions compared with other gases.[65] The other pivotal consideration is the gas pressure in the collision cell. The probability of collision between a translationally energetic ion and a neutral gas molecule increases with increasing pressure, but this occurs with a concomitant increase in the probability of multiple collisions. Ideally, the conditions should be adjusted to maximise the incidence of single collisions between ions and neutral gas molecules, while keeping the incidence of multiple collisions to a minimum. Collision conditions can be further regulated by the attenuation of the parent ion beam (whereby the beam intensity is reduced). Attenuation of the parent ion beam by 10-20% results in about one in five ions undergoing collision with the neutral gas, and of these more than 90% of the collisions will be single collisions, while the remainder being double or multiple collisions.[66] For all practical purposes, such a degree of attenuation is considered to provide single collision conditions.

---

* Neutralisation processes are central to charge reversal and neutralisation reionisation mass spectrometry. See later discussion concerning these techniques.

During a MIKE experiment, it is possible for the fragment ions resulting from either metastable or CA decomposition in the second field free region to gain some of the kinetic energy released in the decomposition of the parent ion. This event is known as *kinetic energy release* and is evidenced by a detectable alteration in the peak shape of the MIKE spectrum. Such information can be useful in gaining insight into the unimolecular reactions of ions.[59]

B. **Charge Reversal**

Not all ions fragment under CA conditions. Among those resistant to fragmentation are negative ions, which are particularly pertinent to the work described herein. In the case of negative ions it becomes difficult to assign structure using conventional mass spectrometry techniques. However, it is possible to charge reverse negative ions under CA conditions [67,68] by a procedure known as *charge reversal* (CR). This is achieved by charge stripping of the incident negative ions (AB^-) in a high energy collision with a neutral gas (N). In the collision, two electrons are lost from the negative ion in a single step*[70] to form the corresponding positive ion [Scheme 1.2.13 (a)].[71] An estimate of the energy (E) imparted in the collision is obtained by taking the sum of the electron affinity (EA) and the ionisation energy (IE) of AB (Equation 1.2.4). Any energy lost in charge-stripping the anion to obtain the cation can be measured in a MIKE experiment.[70,72] All collision induced processes are considered vertical processes in the Franck-Condon sense, and in this regard, so is CR. As such, in the instance that the nascent cation is formed it has the same structure as the progenitor anion. A factor critical to the success of a CR experiment is the nature of the collision gas. If a "hard" target gas such as helium were used, extensive fragmentation of the charge inverted ion results. Conversely, oxygen captures electrons in collision events without

---

* There are documented examples of two-step, sequential losses of electrons.[69]

the consequent fragmentation observed when noble gases are used, and is therefore commonly employed as the collision gas.

SCHEME 1.2.13

$$AB^- + N \rightarrow AB + N + 2e^- \quad \text{(a)}$$

$$AB^- + N \rightarrow A + B + N + 2e^- \quad \text{(b)}$$

EQUATION 1.2.4

$$E = EA(AB^-) + IE(AB)$$

The cations thus produced are also known to fragment in ways that can be diagnostic in the identification of isomeric anions. [Scheme 1.2.13 (b)][72] Indeed, the charge reversal spectra of the three isomeric carbanions $CH_2{=}C{=}CH^-$, $CH_3C{\equiv}C^-$, and *cyc*-$CH_2CH{=}C^-$ are distinctively different.[73] The CR technique has also proven useful in the generation of various ionic species that have eluded attempts at their formation via conventional ionisation methods (*cf.* $H_2{\bullet}CHO^+$).[74]

Furthermore, the high energy collision of a positive ion and a neutral gas can also result in the production of a negative ion signal.[75] However, the attachment of two electrons in a collision process is a relatively low probability event, producing a feeble signal at best, and thereby severely limiting the usefulness of this method.

C. Neutralisation – Reionisation

It was previously pointed out that the neutralisation of an incident (positive or negative) ion is a process that can occur in conjunction with the collisionally induced decomposition of that ion (Scheme 1.2.12). Whilst this is an undesirable outcome during the collisional activation of an ionic species, the deliberate neutralisation of ionic precursors makes available the

possibility of using mass spectrometry to generate and investigate neutral species.* One of the advantages of the ZAB (Figure 1.2.2) is that by virtue of its two-sector reverse geometry, it can mass select a parent ion and then collisionally neutralise it in the first of the two collision cells in the second field free region. By applying a voltage perpendicular to the flight path immediately after the first collision cell, all ionic species may be deflected, while a pure beam of neutrals is transmitted. However, detection of a species is possible only if that species bears a charge, therefore the neutrals are reionised by a second collision in the second cell. Scanning the electric sector then allows the detection of reionised particles along with the fragment ions. This methodology, termed *neutralisation reionisation mass spectrometry* [77,78] (NRMS, Figure 1.2.3), is attributable to McLafferty *et al.*[79]

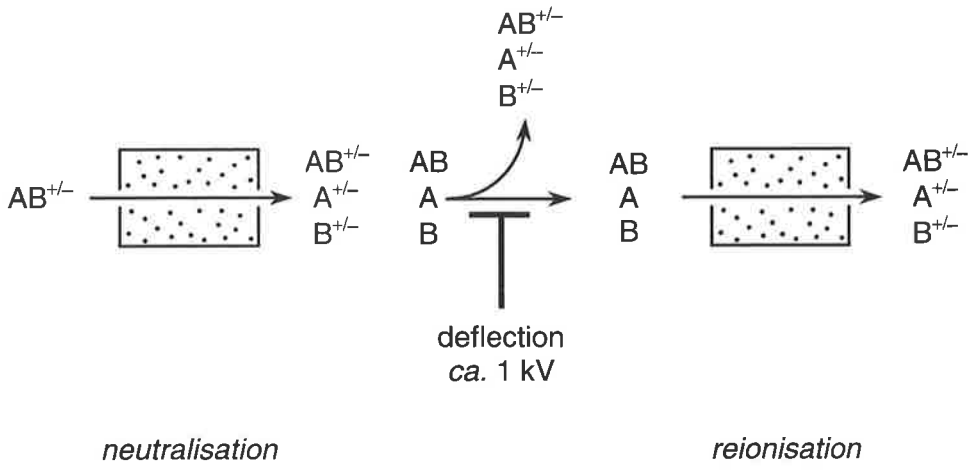

Figure 1.2.3 The neutralisation reionisation process.

All charge permutations are possible with NRMS. The most common are (i) neutralisation of an incident positive ion and the subsequent reionisation by charge stripping to regain a positive ion ($^{+}NR^{+}$), and (ii) the stepwise stripping of two electrons from an incident negative ion to form a positively charged species ($^{-}NR^{+}$). Though $^{+}NR^{-}$ and $^{-}NR^{-}$ experiments are

* However, the possibility that the stable neutral is a Rydberg state can never be wholly discounted. See [76]

possible, their applicability is limited due to the difficulty in inducing electron attachment to a neutral species in a binary collision.[80] As is the case with CR, choice of collision gas is of critical importance to the strength of the NRMS signal. In a typical $^{+}NR^{+}$ experiment, neutralisation of the cation in the first cell* is carried out using xenon [82] or benzene,[75] while reionisation in the second collision cell is achieved using oxygen. On the other hand, $^{-}NR^{+}$ typically makes use of oxygen in both collision cells. Oxygen is extensively used as a reionisation gas, as well as a neutralisation gas in $^{-}NR^{+}$, because of its ability to capture electrons in a collision, and because it minimises fragmentation of the reionised (or neutralised) species, thereby maximising the yield of that species.[83] It is because of this latter ability that oxygen has been described as a *soft* target gas. Oxygen owes this ability to the fact that it deposits minimal energy into the nascent neutral AB upon neutralisation. As a consequence, the fragmentation and rearrangement pathways of the neutral are less accessible.† Moreover, soft reionisation is necessary in order to maximise the signal corresponding to the reionised $AB^{+/-}$ (known as the *recovery signal*), relative to fragmentation of the ion.

The primary purpose of performing NRMS experiments is to demonstrate the stability or otherwise of a transient neutral in the gas phase. The obtainment of a recovery signal signifies that the neutral is stable for the time it takes to traverse a distance equal to the distance between the two collision cells.‡ Clearly, this distance will vary depending on the instrument used. In most instruments the two collision cells are configured with a distance, d, of *ca.* 50 mm between them. For an ion accelerated to voltage, V (typically 7 keV), the flight time, t, of

---

* Alternatively, vaporised metals such as mercury or sodium have also been successfully employed.[81]

† The fragmentation and rearrangement behaviour of transient neutrals is discussed in the following section.

‡ Provided that the transient neutral does not display any reactivity. Neutral reactivity is discussed in the following section.

the neutral is of the order of microseconds (10^{-6} s, Equation 1.2.5) depending on its mass (m, in kilograms).

EQUATION 1.2.5

$$t = \frac{d}{\sqrt{\frac{2eV}{m}}}$$

Hence, for a keV collision, the electron transfer proceeds in *ca.* 10^{-15} s, which can be considered as instantaneous. Consequently, electron transfer may be regarded as vertical, and geometry changes during neutralisation and reionisation phases of a NRMS experiment are effectively negligible.[84] It then follows that the efficiency of both steps is dictated by Franck-Condon factors, which also determine the internal energies of the species and the observed fragmentation patterns.[84,85] This can be graphically depicted in Figure 1.2.4 for the $^{+}NR^{+}$ case, but the principles are equally transposable to other charge permutations.

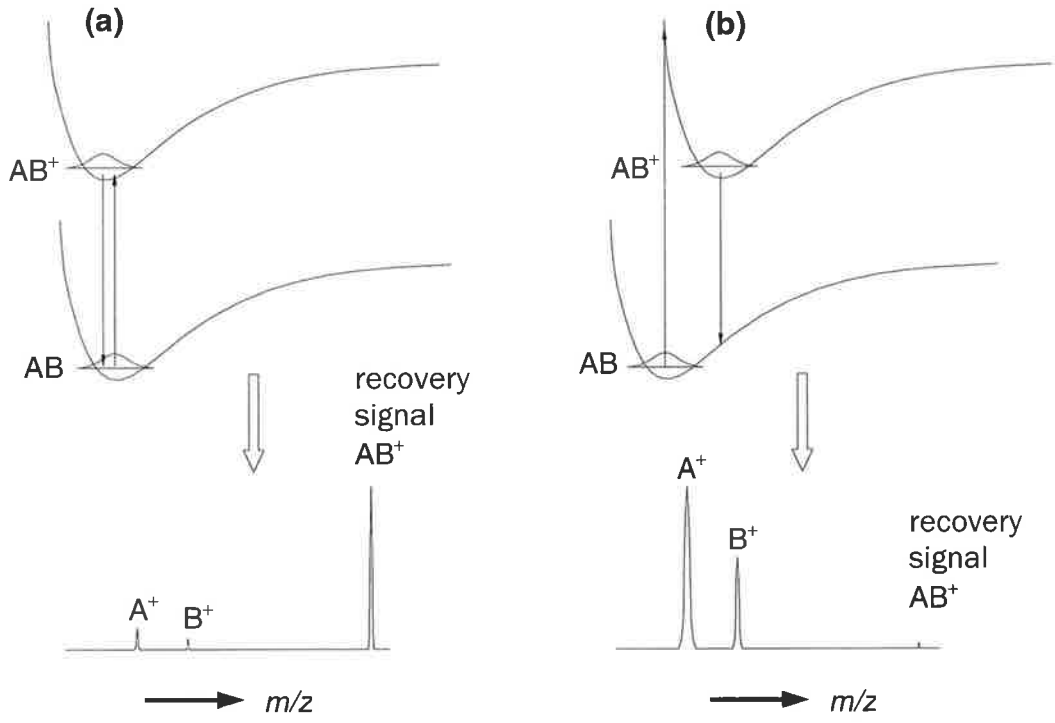

Figure 1.2.4 Franck-Condon diagrams depicting the effects of vertical electron transitions in a $^{-}NR^{+}$ experiment. (a) The geometries of AB and AB^{+} are similar; (b) the geometries of AB and AB^{+} are different.

For the situation where both the neutral and cationic charge states of AB are stable with respect to dissociation, the charge states will have similar geometries, and therefore a favourable Franck-Condon overlap [Figure 1.2.4 (a)]. As a consequence, neutralisation of AB^+ gives rise to energetically cold AB, and subsequent reionisation recovers AB^+ with little excitation. The upshot is that minimal fragmentation results and a large recovery signal is obtained. On the other hand, if AB and AB^+ have appreciably different geometries, poor Franck-Condon overlap between cation and neutral potential surfaces and the attendant excitation in both neutralisation and reionisation events results in increased fragmentation of AB and/or AB^+ and a concomitant decrease in recovery signal.[86]

Some of the intriguing reactive neutral intermediates that have been generated by NRMS include the neutral diradicals CO_3 [80] and CH_2OCH_2,[87] and the hypervalent species $HCNCH_2$.[88]

D. Neutral Reactivity

In addition to the extensive deployment of NRMS to the generation and detection of transient neutrals, the technique has also found recent application in the detection of unimolecular behaviour of neutrals in the gas phase. Several methodologies have been developed, and since most have been the subject of review, only two will be expounded below.[86]

1. Neutralisation Collisional Activation Reionisation (NCR)

This technique, principally developed in the late 1980s by McLafferty and co-workers,[89] is a modification to conventional NRMS that employs an instrument with three differentially pumped collision cells. The methodology involves a sequential process involving (i) neutralisation of incident ion in the first collision cell, followed by (ii) collisional activation of the neutral in a second collision cell, and finally (iii) reionisation in the third cell (Figure 1.2.5).

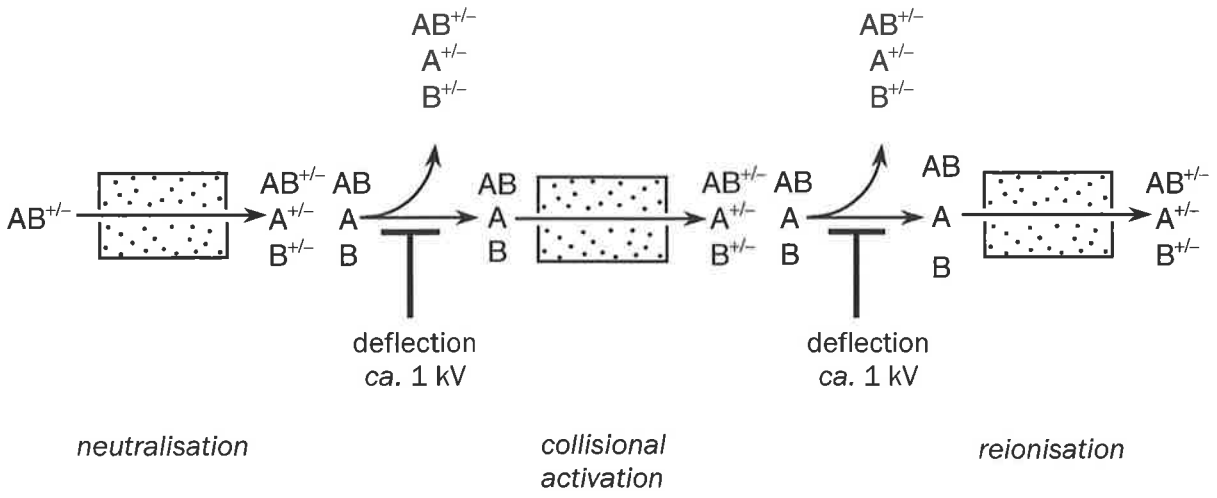

Figure 1.2.5 A schematic illustrating the NCR sequence.

The stability or otherwise of transient neutrals generated by NRMS can be examined with the NCR technique. Indeed, the diradical CH_2OCH_2 has been shown to be stable with respect to NRMS, but upon collisional activation of this neutral by NCR, isomerisation results with the oxirane being the major species obtained.[87]

2. Variable lifetime NRMS

Where a transient neutral rearranges or decomposes on a timescale which approximates that of the NR experiment (*ca.* 10^{-6} s), variable lifetime NRMS experiments can be conducted using an instrument with NCR capabilities. An NCR spectrum is obtained of a neutral traversing firstly a short distance (SD-NCR), and then a long distance (LD-NCR). When the two spectra are compared, any variations in peak abundance* in the latter can be attributable to the longer reaction time.[86] This inference holds only if similar collision conditions are employed in each experiment.

* Variations between spectra are usually subtle.[90]

IV. Fragmentation Behaviour

The fragmentation behaviour of an ion is diagnostic of its structure. As previously stated, an ion may spontaneously undergo fragmentation if it is formed with sufficient internal energy, or alternatively, fragmentation may be induced by collisional activation. The investigation of the decomposition pathways of both positive and negative ions by mass spectrometry has revealed several general patterns of decomposition behaviour. This section is a synopsis of this work.

A. Negative Ions

1. Homolytic Cleavages

The majority of anionic species, $[M\text{-}H]^-$, display various degrees of loss of the hydrogen radical. This loss may be more appreciable in systems that contain the stabilised radical anions as products. In these instances, the stability could provide the impetus for the loss of methyl, alkyl, and occasionally more complex radicals from the parent ion. An example of this is presented in Scheme 1.2.15 (b) below.

SCHEME 1.2.15

$$CH_3CO_2^- \rightarrow {}^{\bullet}CH_2CO_2^- + H^{\bullet} \quad \text{(a)}$$

$$[C_2H_5CCO_2CH_3]^- \rightarrow [C_2H_5CCO_2]^{-\bullet} + CH_3^{\bullet} \quad \text{(b)}$$

2. Ion-neutral Complex Formation

Decomposition of the $[M\text{-}H]^-$ ion may also yield an ion and a neutral as a result of charge-mediated heterolytic cleavage. The product ion and neutral have two possible fates: they either become separate from each other [Scheme 1.2.16 (a)], or conversely they may remain associated in an ion-neutral complex.[91] In the latter, the complex is loosely bound by hydrogen bonds and ion-induced dipole interactions. These interactions promote various

reactions of the anion upon the neutral, including deprotonation, S_N2 reaction, or hydride donation (Scheme 1.2.16).

SCHEME 1.2.16

$[(C_2H_5)_2CCO_2CH_3]^- \rightarrow [(C_2H_5)_2C{=}C{=}O \quad {}^-OCH_3]$

$\rightarrow \quad (C_2H_5)_2CCO + {}^-OCH_3 \qquad$ (a)

$\rightarrow \quad [C_2H_5(CH\ CH_3)CCO]^- + HOCH_3 \qquad$ (b)

$\rightarrow \quad C_2H_5CCO^- + C_2H_5OCH_3 \qquad$ (c)

$\rightarrow \quad [(C_2H_5)_2CCHO]^- + OCH_2 \qquad$ (d)

3. Rearrangements Preceding Fragmentation

The initially formed anion has been demonstrated in some cases to rearrange prior to the observed fragmentation. In these instances, the rearrangement may involve simple proton transfer, but a more complex skeletal rearrangement may also occur. When a rearrangement in this manner is suspected to have occurred, identification can be effected by comparing the spectra of the rearranged species with those of the independently derived suspected rearrangement product. An example of this type of rearrangement process is the deprotonation of alkenyl alkyl ethers at the acidic allylic position. The anion thus generated undergoes proton transfer to form an unstable alkyl anion, which subsequently decomposes by loss of an alkene, to yield the alkoxide anion [Scheme 1.2.17 (a)].[92] On the other hand, deprotonated diallyl ethers undergo skeletal rearrangement via sequential Wittig and Oxy Cope mechanisms to generate the more stable enolate anion [Scheme 1.2.17 (b)].[44]

SCHEME 1.2.17

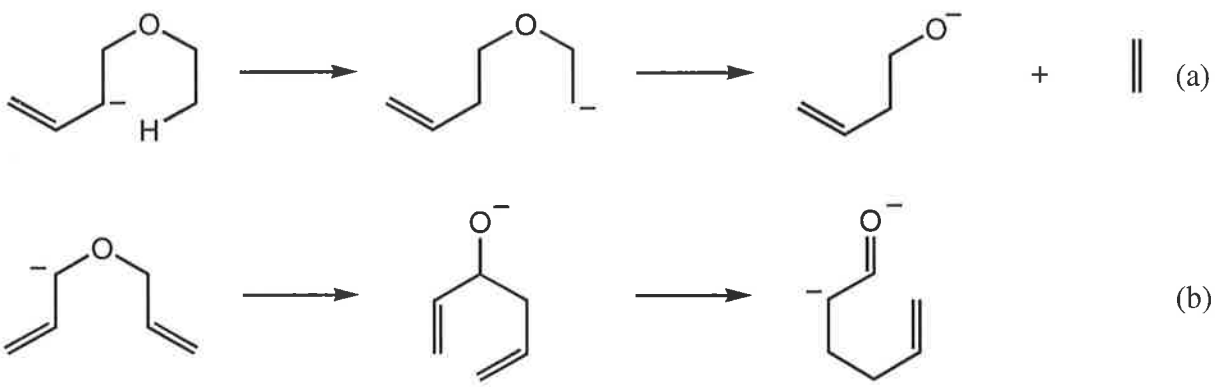

B. Charge Inverted Ions

1. Fragmentation of Positive Ions

This is a mature field of investigation which has been extensively reviewed.[93] in which particular emphasis has been placed on the fragmentations of radical cations generated from EI ionisation. Besides the issue of unimolecular decomposition by simple homolysis, the topic of positive ion fragmentation is somewhat beyond the scope of the work presented herein; therefore the reader is directed to the reviews for elaboration.

2. Simple Homolytic Cleavage

Ionisation techniques such as EI produce radical cations that routinely undergo facile homolysis of σ-bonds to yield a stable cation and a neutral radical (Scheme 1.2.18).

SCHEME 1.2.18

$$ABC^{+\bullet} \rightarrow AB^{+} + C^{\bullet}$$

Though theoretical mechanisms may be devised that demonstrate charge retention by either AB or C, the observed ratio of AB^+ and C^+ is determined by the relative stability of the two

possible product cations. To illustrate this point, homolysis of the C-OCH_3 bond of ionised methyl benzoate [$PhCO_2CH_3^{+\bullet}$] affords the phenyl acyl cation and the methoxide radical (Scheme 1.2.19).

SCHEME 1.2.19

$$[PhC(O)\text{-}OCH_3]^{+\bullet} \rightarrow PhCO^{+\bullet} + {}^{\bullet}OCH_3$$

3. Charge Inverted Ions

Charge inverted ions (i.e. those formed from either CR or NR procedures) exhibit fragmentation behaviour that is distinct from that observed in ions generated by direct ionisation. For instance, the CR spectra of nitrobenzene anion is markedly different from that of the nitrobenzene radical cation generated by EI,[67] which has been rationalised in terms of the variance in internal energies of the ions formed by each methodology. Although several categories of fragmentation behaviour have been described in this chapter, the treatment is not exhaustive. It is indeed possible that the fragmentations appearing in CR and NR spectra result from behaviour not described here.

1.3 Theoretical Methods for the Determination of Molecular Geometries and Energetics

I. Molecular Orbital Theory [61,94,95]

A. The Schrödinger Equation

Molecular orbital calculations find approximate solutions of the Schrödinger equation. A simplistic explanation of the Schrödinger equation is that it is an extended treatment of the *de Broglie* equation (Equation 1.3.1). de Broglie proposed that for any moving body there is an associated wave, and that the momentum of the particle and the wavelength are related properties. Momentum is a property of particles, and wavelength is a property of waves, and so the concept of *wave-particle duality* is introduced.

EQUATION 1.3.1

$$p = \frac{h}{\lambda}$$

The wave-particle (photon, electron, etc.) has wavelength λ, momentum p, while h is Planck's constant. With Planck's constant, the concept of the quantisation of energy is introduced. This concept makes the assumption that the energy of an oscillator of frequency ν is not continuously variable, but is restricted to integral multiples of the quantity $h\nu$, a quantum of energy (Equation 1.3.2).*

EQUATION 1.3.2

$$E = h\nu$$

---

* The frequency of radiation ν is related to the wavelength by $\nu = c / \lambda$ where c is the velocity of light.

The time-independent* Schrödinger equation, then, is essentially the fusion of the de Broglie relation with the classical differential equation describing the profile of a simple harmonic three-dimensional standing wave (Equation 1.3.3).

EQUATION 1.3.3

$$-\frac{\hbar}{2m}\nabla^2\,\psi + V\,\psi = E\,\psi$$

Here, $\hbar = h/2\pi$, and the term $-(\hbar / 2m)\,\nabla^2$ represents the kinetic energy of the system. The quantity ψ describes the profile of the wave associated with the particle of mass m moving in a field of potential V and having energy E, and because V may depend on the position of the particle in three-dimensional space, the *Laplacian* operator† $\nabla^2\,\psi$ is used.‡

The left-hand side of the equation can be simplified by introducing the Hamiltonian operator,§ H, which is the sum of the kinetic and potential energy of the system (Equation 1.3.4).

EQUATION 1.3.4

$$H\,\psi = E\,\psi$$

---

* Systems for which the potential energy does not depend on time are referred to as stationary states. The phase factor corresponding to the time-dependent component of the function can be subsequently appended to the Schrödinger equation if required.

† An operator carries out an operation on a function.

‡ The operator ∇^2, read "del-squared", is equivalent to partial differentiation with respect to x, y, and z components:

$$\nabla^2 = \frac{\partial^2}{\partial x^2} + \frac{\partial^2}{\partial y^2} + \frac{\partial^2}{\partial z^2}$$

§ A non-relativistic Hamiltonian is here described, which ceases to be valid when the velocities of the particles approach the velocity of light. Such a description, then, inadequately describes the inner shell electrons of heavy atoms.

The numerical value of the energy of the state, E, is the energy relative to a state in which the constituent particles (nuclei and electrons) are infinitely separated and at rest. Solutions to the Schrödinger equation are termed *wavefunctions* (atomic wavefunctions are called *atomic orbitals*, the cognate molecular solutions are called *molecular orbitals* which are distributed over multiple nuclei, except in the case of lone pairs of electrons). The wavefunction ψ is a function of the coordinates (space and spin) of all the particles in the system. The square of the wavefunction, ψ^2, or $|\psi|^2$ if ψ is complex, is a measure of the probability distribution of the particle in a given volume (or the electron density in the molecule).

The Schrödinger equation can be solved exactly for a hydrogen atom, however exact solutions are not possible in the case of larger, isolated molecular systems. As a consequence, Equation 1.3.4 is solvable only by adopting the *Born-Oppenheimer approximation*. In this approximation, electronic and nuclear motions are separated. This is justifiable because nuclei are thousands of times more massive than electrons and the nuclei will therefore move much more slowly relative to electrons (and may thus be considered stationary). When nuclear positions change, electrons instantaneously adjust their distribution. Therefore, at any given internuclear separation, the Schrödinger equation can be solved for the wavefunction of the electrons moving in the stationary potential generated by the nuclei, to give an *effective* electronic energy E_{eff} (**R**) which depends on the relative nuclear coordinates, denoted **R**. Hence, the Schrödinger equation for electrons in the field of stationary nuclei can be represented as in Equation 1.3.5.

EQUATION 1.3.5

$$H_{elec}\,\psi_{elec}(\mathbf{r},\mathbf{R}) = E_{eff}(\mathbf{R})\,\psi_{elec}(\mathbf{r},\mathbf{R})$$

The electronic wavefunction, ψ_{elec}, depends on the electronic coordinates, **r**, as well as the nuclear coordinates, **R**. In this case, the electronic Hamiltonian, H_{elec}, corresponds to the motion of electrons only in the field of fixed nuclei such that:

EQUATION 1.3.6

$$H_{elec} = T_{elec}(\mathbf{r}) + V_{nucl\text{-}elec}(\mathbf{r},\mathbf{R}) + V_{elec\text{-}elec}(\mathbf{r})$$

T_{elec} is the electronic kinetic energy, and the coulomb potential energy is now described by two terms: the first, $V_{nucl\text{-}elec}$ (**r,R**), corresponds to nuclear-electron attraction, while the second term, $V_{elec\text{-}elec}$ (**r**), corresponds to electron-electron repulsion. A full description of the energy would also include a third term corresponding to nuclear-nuclear repulsion, however this parameter is independent of the electronic coordinates and is a constant contribution to the energy for any particular nuclear configuration.

Note that the Schrödinger equation is an *eigenvalue** equation; eigenvalues are the energies corresponding to the different stationary states of the molecule. Put more succinctly, solutions to the electronic Schrödinger equation afford values for the effective nuclear potential function, E_{eff} (**R**), which depends on the specific nuclear coordinates (the *molecular conformation*). By solving the Schrödinger equation for different conformations of the molecule (i.e. altering bond length of a diatomic molecule), a curve can be constructed that exhibits this dependence: a *molecular potential energy curve* (or *surface* for polyatomic molecules in which the dependence of the total electronic energy and the total nuclear repulsion energy on geometrical parameters is represented). Since H, ψ, and E refer

---

* An *eigenvalue equation* is one in which an operator acting on a function delivers a multiple of the function itself as a result. It has the general form:

$$\mathbf{Op}\, f = c\, f$$

where **Op** is an operator, f is a function, and c is a constant. *Eigenfunctions* are the set of functions for which the equation holds, each having the associated constant c, referred to as its *eigenvalue*.

exclusively to electronic motion, being implicit functions of the relative nuclear coordinates, **R**, all superscripts can be disregarded.

The lowest energy solution of the electronic Schrödinger equation, $E(\mathbf{R})$, for a polyatomic molecule is the ground-state potential energy surface. Such a surface can exhibit a number of local minima, each of which represent equilibrium structures of the molecule. Other stationary points on the potential surface occur where there are one or more orthogonal directions where the energy is at a maximum. These points are termed *saddle points*, and are particularly pertinent to the analysis of chemical reaction processes if the second derivative matrix of E with respect to nuclear coordinates has a single negative eigenvalue, since this corresponds to a transition structure for a chemical reaction.

However, this definition of a minimum on the potential energy surface as being associated with a molecular equilibrium structure is possible only within the Born-Oppenheimer approximation, and equilibrium structural parameters thus obtained are purely theoretical. Because of quantum mechanics, physical measurements of structure are not absolute, but are reduced to averages. Moreover, the systems under analysis will necessarily be in motion because zero-point vibrational motion prevents nuclei from being at rest. In any case, the Born-Oppenheimer approximation, though seemingly a convenient and useful simplification, is only applicable to the hydrogen molecule-ion, $H_2^{+\bullet}$. For many electron systems, the interactions between electrons [the electronic Hamiltonian electron-electron repulsion term, $V_{elec\text{-}elec}(\mathbf{r})$, in Equation 1.3.6] need to be resolved, since the wavefunction depends on the coordinates of all the electrons. Analytical solutions to such complicated partial differential equations are exceedingly difficult to obtain, necessitating the application of various assumptions and approximate numerical procedures in an effort to simplify the acquisition.

B. **Hartree-Fock Theory**

An exact solution to the Schrödinger equation is only possible for the most trivial systems; for larger systems, an approximate solution is aimed for instead. The most commonly used technique for approximating a wavefunction for an atom or molecule is the *Hartree-Fock approximation*,[96] otherwise known as the *Self Consistent Field* (SCF) method. In the Hartree-Fock approximation, each electron is considered with respect to its interactions with all other electrons and nuclei. The many-electron wave function can be constructed approximately by assembling the product of one-electron wave functions, where each one-electron wave function corresponds to an individual electron. The *Pauli principle* (which states that a maximum of two electrons may occupy the same orbital, but they may do so only if their spins are paired), is included in the many-body wave function. Accordingly, the product of one-electron wave functions (orbitals) is generalized to a sum of such products with alternating sign. A molecular orbital, ϕ, is a function of the Cartesian coordinates x, y, z of a single electron. In practical applications of the theory, the individual molecular orbitals are themselves required to be expressed as linear combinations of one-electron functions known as *basis functions*, χ (the complete set of basis functions for all of the electrons of the system is called the basis set). The basis functions resemble atomic orbitals in that, like atomic orbitals, they are usually centred on atomic nuclei. In general, the molecular orbital is defined by Equation 1.3.7.

EQUATION 1.3.7

$$\phi_i = \sum_{\mu=1}^{N} c_{\mu i}\, \chi_\mu$$

The *molecular orbital expansion coefficients*, $c_{\mu\ i}$* are determined such that the total electronic energy (E^{elec}) calculated from the many-electron wavefunction is minimised and as close to the energy corresponding to the exact solution of the Schrödinger equation as possible. This is achieved in the following way. From Equation 1.3.6, it was seen that the Schrödinger equation consists of three parts: kinetic energy of electrons, nucleus-electron attractions, and electron-electron repulsions. The electron-electron repulsions are difficult to deal with in an accurate manner, so the Hartree-Fock approximation includes these repulsions only as an average. An individual electron is selected while initially neglecting the instantaneous electron-electron repulsions. The potential in which the electron moves is assumed to be a spherical average of the potential due to all other electrons. Hence, the electrons see each other as distributions rather than as distinct particles. By evaluating the average electron potential, the Schrödinger equation is then integrated numerically for the electron and the average potential, and a new orbital is obtained for the electron. The procedure is repeated for all the other electrons in the system, using this averaged spherical potential of the other electrons. At the end of one cycle, a set of orbitals is obtained which, in general, is unlike the original set. The cycle is repeated using the improved wavefunctions, to produce a new set of further improved functions. This iterative procedure is continued until processing a set of orbitals leaves them unchanged, in which case they are said to be *self-consistent*. The self-consistent procedures can be repeated for different nuclear positions thus allowing a point-by-point mapping of the total energy of a molecule as a function of its geometry.

The smallest possible basis set will accommodate all the electrons of the system, but increasing the size of the basis set improves the description of the molecular orbitals.

* Following the notational convention, Roman subscripts are used for molecular orbitals and Greek subscripts for basis functions. In Equation 1.3.8, the subscript i is an index which labels the particular molecular orbital, and μ is a running index 1, 2, 3 ... whose range will depend on the extent of the expansion taken.

However, the Hartree-Fock approach is not capable of giving the correct solution to the Schrödinger equation even if a very large and flexible basis set is selected; there is a limit to the quality of the description that can be achieved with the Hartree-Fock approach (termed the *Hartree-Fock limit*), beyond which increasing the basis set size results in no further improvement. This limit arises due to the absence of a description of the *correlation* between the motions of the electrons (recall that the potential the electron moves in is assumed to be a spherical average of the potential due to all the other electrons - in reality electrons in a molecular orbital move so as to keep away from each other). The difference in energy between the exact result and the Hartree-Fock limit energy is the correlation energy.

C. Electron Correlation

Correlated methods include more explicit interaction of electrons. Most begin with the Hartree-Fock wavefunction, and then incorporate varying amounts of electron-electron interaction by mixing in excited state determinants with ground state determinants. The limit of infinite basis set and complete electron correlation is the Schrödinger equation itself. The correlation energy E_{corr} is defined as the difference between the energy in the Hartree-Fock limit (E_{HF}) and the exact non-relativistic energy of a system (E_0), *viz.* Equation 1.38.

EQUATION 1.3.8

$$E_{corr} = E_0 - E_{HF}$$

This energy will always be negative because the Hartree-Fock energy is an upper bound to the exact energy. Hartree-Fock calculations with large basis sets show that correlation effects contribute about 25 kcal mol^{-1} to the binding energy in H_2, and generally ≈1 eV (23 kcal mol^{-1}) for a pair of electrons in a well-localized orbital.[97] For many pairs of electrons in close proximity, correlation effects become very large. For example, they contribute more than 100 kcal mol^{-1} to the bond energy in N_2.[97]

In most techniques, electron correlation effects are introduced by allowing the wave function to be a linear combination of many electron configurations. The other configurations are generated by replacing occupied spin orbitals in ψ_0 by virtual spin orbitals and may be classified as single, double, triple, quadruple , ... (S, D, T, Q, ...) excitations. T_1, T_2, T_3, T_4, ... are operators which generate linear combinations of all single, double, triple, quadruple, ... excitations involving expansion coefficients to be determined.

Coupled Cluster Method

Coupled cluster (CC) is one of the most accurate schemes available to evaluate electron correlation effects.[98,99] The CC method starts with the exponential form of wave function,

EQUATION 1.3.9

$$\psi = \exp(T)\,\psi_0$$

where $T = T_1 + T_2 + \ldots$ The exponential form of the operator introduces an efficient way of including the effects of higher excitations and also ensures size consistency in the calculated energy. The earliest implementation of coupled cluster theory used the wave function $\exp(T_2)\,\psi_0$ and was referred to as CCD (coupled cluster doubles).[100,101] More recently, the coupled cluster method is typically carried out including all single and double excitations (CCSD) with the wave function $\psi = \exp(T_1 + T_2)\,\psi_0$. The CCSD method is size consistent and exact for two electrons within the basis set space. The wave function and the energy are commonly solved iteratively by using a set of one projection equation for the correlation energy and another for each of the unknown coefficients in the T operators. The equations to be solved are nonlinear in the configuration expansion coefficients, but fast convergence is achieved relatively easily in most cases.[98] The contributions of triple excitations have to be included in any quantitative treatment of electron correlation. The CCSD method is exact for two electrons but still neglects these important three-electron correlations. One possible way to

evaluate these contributions effectively within coupled cluster theory is to formulate the CCSDT method [102,141] with the exponential form of the wave function [$\psi = \exp(T_1 + T_2 + T_3)\psi_0$]. Though accurate, the CCSDT method has an eighth-order dependence on the size of the system and is computationally too expensive to be generally applicable. Accordingly, a scheme referred to as CCSD(T) was proposed [103] in which, like CCSD, the three-electron correlations [triples, specified by (T)] correction formula has two terms, one each resulting from their interaction with single and double excitations. The CCSD(T) method is a highly accurate treatment of electron correlation for molecules near their equilibrium geometries, and provided that sufficiently large basis sets are employed, chemical accuracy in relative energies can be attained. In this thesis, the predicted molecular geometries are submitted for single point energy calculations using this coupled cluster approach.

Density Functional Theory

Density functional theory (DFT) is an exact theory (in principle) of electronic ground state structure, based on the electron density distribution $\rho(r)$, instead of the many-electron wave function $\psi(r_1, r_2, r_3,...r_N)$. Compared with traditional methods, DFT is preferable when the system under investigation contains 5-10 or more atoms and modest accuracy is acceptable - traditional quantum chemical methods are ordinarily preferable when dealing with few-atom systems, containing up to 5-10 atoms and when high accuracy is required.

DFT developed from the theorems of Hohenberg and Kohn.[104] The first theorem proves that the ground state electron density uniquely determines the Hamiltonian operator, which in turn characterises all the properties of the system. The second theorem states that the functional* that delivers the ground state energy of the system delivers the lowest energy if the input

* A *function*, which is the mapping of one number onto another number, needs a number as input and delivers a number. On the other hand, a *functional* is a function whose argument is itself a function; a functional needs a function as input, but again delivers a number.

density is the true ground state density, ρ_0. Hohenberg-Kohn theorems establish the existence of a universal functional which describes the kinetic, exchange, and correlation energy. All terms in the ground state electronic energy of a quantum system are functionals of the density,

With the aim of providing a way of approaching this universal functional (and for computing with greater accuracy the kinetic energy term - the most difficult aspect of direct density functionals), Kohn and Sham [105] proposed a *non-interacting* reference system built from a set of orbitals (i.e. one electron functions).* In this way, the shell structure of atoms is reproduced by the Kohn-Sham functional via the kinetic energy term which is expressed by a set of orbitals derived from a one-particle Schrödinger equation. These one-electron wave functions are solved iteratively until self-consistence is achieved, just as in Hartree-Fock theory. For molecular systems, the Kohn-Sham approximation leads to a molecular orbital picture analogous to the Hartree-Fock approach.

In practice, the Kohn-Sham functional must be supplemented by an approximation for the exchange and correlation term. This approximation is referred to as the *local density approximation* (LDA). The total energy is decomposed into three contributions: a kinetic energy, a Coulomb energy due to classical electrostatic interactions among all charged particles in the system, and a term called the exchange-correlation energy that captures all many-body interactions. This decomposition is formally exact, but the actual expressions for the many-body exchange and correlation interactions are unknown. The advantages of LDA are its computational convenience and high accuracy. In this approximation, the exchange-correlation energy is taken from the known results of the many-electron interactions in an electron system of constant density (described as a homogeneous electron gas). The LDA can

* The non-interacting electrons in these orbitals behave as uncharged fermions and do not interact with each other via Coulomb repulsion. This was an important device in Kohn and Sham's approach because a disastrous consequence of the electron kinetic energy term within the prevailing Thomas-Fermi model of atomic energy was that all molecular systems are not stable with respect to their fragments.[106]

be interpreted in the following manner: at each point in a molecule there exists a well defined electron density; it is assumed that an electron at such a point experiences the same many-body response by the surrounding electrons as if the density of these surrounding electrons had the same value throughout the entire space as at the point of the reference electron. The exchange-correlation energy of the total molecule is then the integral over the contributions from each volume element. The contributions are different from each volume element depending on the local electron density. The LDA is exact for a perfect metal (which has a constant electron density) and becomes less accurate for systems with varying electron density.

In response to these deficiencies, a variety of gradient corrected hybrid density functional methods [107,108] have been developed which give highly accurate results for a range of problems.[107,109] These typically fuse pure density functionals for exchange and exact Hartree-Fock exchange terms, and include DFT correlation. A method that has enjoyed wide-spread use is the B3LYP approach. This approach uses gradient corrected functionals. B3LYP is based on the earlier method denoted BLYP in which gradient corrections are added to the LDA method - specifically the exchange correction of Becke and the LYP correlation function. A linear combination of exchange and correlational functionals are assembled as in Equation 1.3.9, *viz.*

EQUATION 1.3.9

$$E_{xc}^{B3LYP} = 0.80\, E_x^{S} + 0.20\, E_x^{HF} + 0.74\, E_x^{B} + 0.19\, E_c^{VWN} + 0.81\, E_c^{LYP}$$

The terms E_x^{S}, E_x^{HF} and E_x^{B} are the Slater, HF and Becke exchange functionals; and E_c^{VWN} and E_c^{LYP} are the Vosko, Wilk and Nussair, and Lee, Yang and Parr correlation functionals respectively. The constants before each term are semi-empirical coefficients to determine the weights of the various components.

The major advantage of such methods is that computationally they are comparable to or less expensive than Hartree-Fock calculations, and they converge relatively rapidly with basis set expansion so that moderate polarized basis sets yield converged results. While not as accurate as CCSD(T), the combination of speed and sufficient accuracy makes them particularly effective for larger molecules. The B3LYP method has been chosen for the calculation of the molecular geometries of the systems investigated throughout this thesis.

D. Basis sets

Ab initio electronic structure computations are numerically carried out using a set of basis functions centred on the atoms, and as such are called atomic orbitals. Basis sets are mathematical functions that are used to approximate the size and shape of the one-electron atomic orbitals. A basis set should be large enough to adequately describe the molecular wave function. The orbital representations that commonly employed are called Slater type orbitals (STO) and Gaussian type orbitals (GTO). The difficulty of the calculation is approximately the same when either orbital type is used in the case of simple atomic structures. However, once several electrons are introduced, STOs greatly increase in mathematical complexity and their use becomes impractical. In this case, GTOs are used as the next best approximation of the actual wavefunction. However, once molecular size increases beyond a certain limit (approximately 30 atoms), even the GTO approximation is too computationally expensive to be used. Unlike hydrogen atom orbitals, GTOs do not have radial nodes; however, radial nodes can be obtained by combining different GTOs. An atomic basis function is often a fixed linear combination of GTOs; this is called a *contracted* Gaussian basis function.*

* The term *contraction* is used when several Gaussians are grouped together in one set of functions with constant coefficients relative to each other.

The smallest possible basis set is called the minimal basis set. It contains one orbital for every orbital usually associated with an atom (including unoccupied orbitals; for example, hydrogen has just one orbital, but carbon has 5: 1s, 2*s*, $2p_x$, $2p_y$, and $2p_z$). The minimal basis set approximates an atomic orbital well, but it lacks any flexibility to respond to the molecular environment (for example by expanding or shrinking in the presence of other atoms in the molecule). Hence, a minimal basis set does not produce a highly accurate result. The remedy to this situation is to add extra basis functions beyond the minimum number required to describe the system. One way to achieve this is to include two sizes of basis function in the minimum basis; such a basis set is called a *double zeta* basis set (designated DZ; the "zeta" refers to the two exponents in the GTO, called ζ). Hence, a double-zeta basis set for hydrogen would have two functions, and a true double-zeta basis set for carbon would have 10 functions. However, only a single orbital for the core (1*s*) is commonly used, giving 9 functions for carbon. Such basis sets are called *split-valence* basis sets. These schemes can be extended by increasing the number of functions in the various categories, resulting in triple- or quadruple-zeta basis sets. Additional flexibility is often built in by adding higher-angular momentum basis functions. Since the highest angular momentum orbital for carbon is a *p* orbital, the polarization of the atom can be described by adding a set of *d* functions. A hydrogen atom would use a set of 3 *p* functions as polarization functions. A double-zeta basis set including polarization is designated DZP. One of the most frequently used split-valence double-zeta plus polarization basis sets is the 6-31G(d) (or 6-31G*; the star indicates polarization functions on non-hydrogen atoms) basis, in which the core orbital is described by a contraction of 6 Gaussian orbitals, while the valence is described by two orbitals, one made of a contraction of 3 Gaussians, and one a single Gaussian function. Adding polarization to hydrogen atoms also would give the 6-31G(d,p) (or 6-31G** using the star notation) basis set.

The CCSD and CCSD(T) methods may employ polarized double- and triple-zeta *spd* basis sets for larger molecules. Though a direct and accurate evaluation of bond energies is not

possible with such basis sets, they are frequently adequate to provide reliable geometries, vibrational frequencies, and energy differences.[110] The cc-pVDZ basis is an all-electron basis designed for correlated calculations consisting of two large *s*-type contracted sets of Gaussians for the 1*s* electrons, an additional uncontracted *s*-type Gaussian, a single *p*-type contraction, an additional *p*-type Gaussian and a single *d*-type Gaussian. Dunning [111] also defined an augmented basis set, aug-cc-pVDZ which augments the cc-pVDZ basis by additional *s*, *p*, and *d* Gaussians.

In the interests of efficiency, a conventional theoretical methodology employs a level of theory that incorporates electron correlation (e.g. B3LYP), a modest basis set [e.g. 6-31G(d)] in the optimisation of the molecular structure. Using the optimized geometry, a high accuracy single point energy calculation utilising a more sophisticated treatment of electron correlation [e.g. CCSD(T)], and a larger basis set (e.g. aug-cc-pVDZ), is then performed on the optimised geometry. By convention, the model chemistry employs a methodology designated CCSD(T)/aug-cc-pVDZ//B3LYP/6-31G(d).

II. Transition State Theory of Unimolecular Reactions

Unimolecular fragmentations and isomerisations of gas phase ions (and neutrals) form the basis of analysis by mass spectrometry. What follows is a very brief discussion of one aspect of unimolecular reactions, in particular with regard to isomerisations in the gas phase. A comprehensive description of the mechanism of a chemical process requires accurate rate coefficients.[112] The rate coefficient of a reaction, in turn, can be predicted using *transition state theory*. This approach employs the fundamental properties of the geometry, vibrational frequencies, and relative energies in the reactants and transition states. However, although these may be obtained experimentally in the case of the reactants, it is very difficult to generate such data for transition states,[113] and as a result the various computational quantum chemistry approaches (utilising appropriate levels of theory) are indispensable in the determination of these fundamental properties.[95]

At the heart of transition state theory is a well developed concept in chemical dynamics that atoms within molecules move according to forces derived from a potential field which is determined by electronic interactions. The potential surface, then, is the energy of the system as a function of all possible coordinates of the atoms. The momenta and the positions of all atoms at any time, i.e., a trajectory, can be obtained by solving the classical equations of motion on the potential surface. It follows, then, that the rate coefficient may be classically determined by computing a large number of trajectories and averaging the velocities of the trajectories that start as reactants and end as products on the potential surface.[114] To simplify the mathematics, transition state theory focuses on the *reactive trajectories* on the potential surface, which are those trajectories which originate as reactants and end as products but pass through a geometry with a critical constraint. For dissociation and recombination reactions,

this constraint is the inter-fragment distance,* but for isomerisation and combination reactions the critical constraint is a complex function of coordinates representing stretches and bends of various bonds. The geometry with this constraint is the *transition state* and the energy is usually the maximum on the reaction pathway between the reactants and products.

A unimolecular rate coefficient, k, for a canonical ensemble (i.e., a collection of all possible classical states of reactant molecule possessing any energy or angular momentum) can thus be defined which is dependant only on the properties of the transition state and is given by Equation 1.3.10, the temperature-dependent, unimolecular reaction rate, or transition state expression.

EQUATION 1.3.10

$$k(T) = \frac{k_B T}{h} \frac{Q^{\ddagger}}{Q_R} \exp\left(\frac{-E_0}{k_B T}\right)$$

Here k_B is Boltzmann's constant, T is the temperature, h is Planck's constant, E_0 is the zero-point energy difference between reactants and transition state, and $Q^{\ddagger}$ and Q_R are the molecular partition functions for the transition state and reactants respectively. The Arrhenius frequency factor, A, and the activation energy, E_{act}, are related to the pre-exponential factor and E_0, respectively, and evaluation of both of these depends on a knowledge of the molecular partition functions. For the frequency factor, Equation 1.3.11 holds (see next page).

EQUATION 1.3.11

$$A = e\left(\frac{k_B T}{h}\right) \exp\left(\frac{\Delta S^{\ddagger}}{k_B}\right)$$

* For example, in a C-C bond-forming process, the inter-fragment separation is infinite in the reactants, while the bond length in the product is about 1.54 Å. Any trajectory where the carbon atoms approach closer than approximately 2 Å will react to form a bond, therefore the constraint is 2 Å.

In Equation 1.3.11, e is the base of the natural logarithm and $\Delta S^{\ddagger}$ is the entropy of activation, which is in turn related to the molecular partition functions, *viz.* Equation 1.3.12.

EQUATION 1.3.12

$$\Delta S^{\ddagger} = k_B \ln\left(\frac{Q^{\dagger}}{Q}\right) - \frac{k_B}{T}\frac{\partial \ln(Q^{\dagger}/Q)}{\partial T^{-1}}$$

The activation energy is related to the zero-point energy difference between reactants and transition state, E_0, by Equation 1.3.13, which demonstrates that the molecular partition functions must also be known to evaluate the activation energy.

EQUATION 1.3.13

$$E_{act} = E_0 - k_B \frac{\partial \ln(Q^{\ddagger}/Q)}{\partial T^{-1}} + k_B T$$

Combining Equations 1.3.11, 1.3.12, and 1.3.13 furnishes the familiar Arrhenius equation (Equation 1.3.14).

EQUATION 1.3.14

$$k(T) = A \exp^{-E_{act}/k_B T}$$

It is usually assumed that the Hamiltonians of the reactants and transition state are independent, so that the molecular partition function, Q, can be expressed as a product of translational, vibrational, rotational and electronic terms, *viz.* Equation 1.3.15.

EQUATION 1.3.15

$$Q = Q_{\text{Trans}} \times Q_{\text{Vib}} \times Q_{\text{Rot}} \times Q_{\text{Elec}}$$

The last term, Q_{Elec}, can be omitted from the factorisation if the reaction occurs on a single electronic surface (i.e. when the reactant, transition sate, and product have the same electronic

configuration. If the energy separations between electronic levels are assumed to be large (which is typically the case for separations from the ground state), and degenerate states are thermally inaccessible (at normal temperatures), then $Q_{Elec} = 1$. Furthermore, for unimolecular rearrangements, Q_{Trans} of both the reactant and transition state are identical, and we assume (to a first approximation) that the same is true for Q_{Rot}. Thus approximation of the A factor for each process simplifies to evaluating Q_{Vib} for the reactant and for the competing transition states. However it must be noted that anions in a mass spectrometer, especially following collisional activation, will not follow a Boltzmann (thermalised) distribution of internal energies. Thus these calculations must only be considered in a qualitative sense.

The approximate vibrational partition function for a polyatomic molecule is the product of the vibrational partition functions of separate vibrational modes, *viz*. Equation 1.3.16,

EQUATION 1.3.16

$$Q_{vib} = \prod_{i} Q_{vib,i}$$

and each separate vibrational mode, ω, is evaluated from the harmonic vibrational frequency, v, by Equation 1.3.17 (the term h is the Planck Constant).

EQUATION 1.3.17

$$\omega = \left(1 - \exp\frac{-hlv}{k_B T}\right)^{-1}$$

Because fundamental frequencies for transition states cannot be experimentally derived, they are generally acquired by quantum chemical calculation. There may be more than one frequency that is not included in this account. Foremost among these is the transition state's characteristic imaginary frequency corresponding to the geometric distortion along the reaction coordinate. In addition, the motions of some low frequencies approximate internal rotations.[115] Where this applies, the frequencies are excluded from the vibrational partition function and are included in the evaluation of the rotational partition function.[112]

2 Covalently Bound Complexes of CO and CO_2

I. Introduction*

The molecules CO and CO_2 are present in high abundance in the atmospheres of carbon-burning stars and interstellar gas clouds, and also in the planetary atmosphere of Earth. Carbon monoxide was one of the first heavy molecules produced within the Universe,[116] and continuous production has occurred via cold gas-phase chemistry within cold dark clouds. Indeed, much of the carbon present in the envelopes of carbon-rich late-type stars is locked in CO. CO has been found as a primary constituent even in the diffuse interstellar medium (those regions of interstellar space that are suffused by photons).[117] Carbon dioxide has been detected in cold molecular clouds and in stellar atmospheres, where it is thought to form as a result of the reaction of simple molecular species (including O_2, N_2, C_2H_2, and specifically by oxidation of CO) on grain surfaces,[118] and then is returned to the interstellar gas.[119]

Here on Earth, carbon monoxide is present as a trace pollutant in the troposphere, where it is released as a by-product of the incomplete combustion of carbon-containing materials, and by the photochemical conversion of atmospheric methane and other hydrocarbons.[120] It is an important link controlling the oxidizing capacity of the atmosphere. The reaction of CO with hydroxyl radical is widely considered as the most significant sink for carbon monoxide. The decomposition of carbon monoxide (in addition to essentially all reduced molecules such as methane and hydrogen sulfide) is initiated by reactions with OH and metastable oxygen. As the hydroxyl radical concentrations decrease, the lifetime of methane and its concentration increases and it leaks into the stratosphere. Once in the stratosphere, methane is a major catalytic ozone destruction agent.[120]

The importance of CO_2 to the terrestrial atmosphere has been primarily due to it being causally linked to the "greenhouse effect" and global warming. Carbon dioxide is an atmospheric gas that is distributed uniformly over the earth's surface at a concentration of

* A reviewer has requested more detail on carbon oxides. See appendix attached to last page of thesis.

about 0.033% or 330 ppm. The concentration of carbon dioxide is currently rising rapidly due to biomass and fossil fuel burning.

The prevalence of these molecules on Earth and throughout interstellar space and the high abundance at which they exist makes it reasonable to ask whether interactions occur between neutral CO and CO_2. The nature of these interactions is speculative but it may involve covalent bond formation. If this supposition is valid, among the many possible CO_2 and CO containing clusters imaginable, two simple complexes can be envisaged: a $O_2C{-}CO_2$ dimer, and a $OC{-}CO_2$ complex. Accordingly, the work detailed below is an experimental and theoretical investigation into the possible structures of such complexes.

II. Results and Discussion

Part A: Covalently bound CO_2 dimers ($O_2C{-}CO_2$)?

The covalent compound 1,2-dioxetane dione (C_2O_4) has been the focus of speculation for some time,[121] since it was suggested to be an elusive species involved in chemiluminescence (being an intermediate in the oxidation of oxalate esters by hydrogen peroxide). Initial attempts to identify C_2O_4 failed, which suggested that C_2O_4 must be an unstable species. Evidence for the existence of this intermediate was finally provided by the mass spectrometric analysis of the gaseous products of the hydrogen peroxide - oxalate ester reaction;[122] peaks were observed at *m/z* 88 indicating the generation of C_2O_4 [though the signal was only 0.1 percent abundance compared to that of *m/z* 44 $(CO_2)^{+\bullet}$].

The anions of CO_2 clusters also warrant consideration. Can $C_2O_4^{-\bullet}$ be made and charge-stripped in a neutralisation reionisation ($^{-}NR^{+}$) experiment (*cf.*[86,123]) to yield the corresponding neutral?

Several recent reports describe the generation of $(CO_2)_2^{-\bullet}$ cluster anions by electron attachment to CO_2 clusters.[124] The infrared [125] and photoelectron spectra [126] of these

negatively charged clusters of CO_2 have been recorded. A theoretical study by Fleischman and Jordan [127] at the MP3/6-31+G(d)//HF/6-31+G level of theory examined the various possible structures of the $(CO_2)_2^{-\bullet}$ species. The investigators showed that both a symmetrical D_{2d} form $\mathbf{1}^{-\bullet}$, and the C_S $CO_2 \cdot CO_2^{-\bullet}$ ion-induced dipole complex $\mathbf{2}^{-\bullet}$ are true local minima on the anionic potential surface, with $\mathbf{1}^{-\bullet}$ being more negative in energy by 3.4 kcal mol^{-1} at the level of theory used.

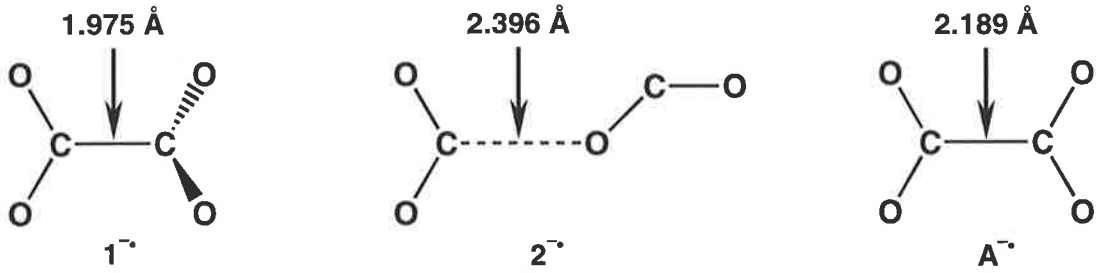

Though these two isomers are quite similar in energy, they have different calculated vertical electron detachment energies; 2.8 eV for $\mathbf{1}^{-\bullet}$ and 1.7 eV for $\mathbf{2}^{-\bullet}$. They have been distinguished experimentally using photoelectron spectroscopy. Accordingly, the photoelectron spectrum of $(CO_2)_2^{-\bullet}$ displays the maximum of the $(CO_2)_2^{-\bullet}$ band located above 2.3 eV, hence it is shifted more than 1 eV above the monomer peak, indicating that the dimer anion of CO_2 has molecular anion structure of $\mathbf{1}^{-\bullet}$.[128] A similar conclusion, i.e. that $(CO_2)_2^{-\bullet}$ clusters have the D_{2d} form ($\mathbf{1}^{-\bullet}$), was also reached in later photoelectron studies.[126]

The third structure identified in Fleischman and Jordan's study was a D_{2h} structure $\mathbf{A}^{-\bullet}$, corresponding to a first order transition state for rotation about the C-C bond of $\mathbf{1}^{-\bullet}$. At the CCSD(T)/aug-cc-pVDZ//B3LYP/6-31G(d) level of theory, our calculated geometries of $\mathbf{1}^{-\bullet}$, $\mathbf{2}^{-\bullet}$, and $\mathbf{A}^{-\bullet}$ are in agreement with previously reported geometries. Interestingly, Fleischman and Jordan concluded that on energetic grounds, the $(CO_2)_2^{-\bullet}$ species are unstable with respect to 2 CO_2 and an electron at all levels of theory employed.

The present study aims to investigate the generation of the neutral of a covalently bound CO_2 dimer and to investigate its stability. The plan is to form the neutral by one-electron oxidation of the corresponding anion, given that such a molecular anion can readily form (as is evident by the success of electron attachment experiments).

A. Generation of C_2O_4 Anions

In an attempt to synthesize the precursor anion $C_2O_4^{-\bullet}$ by an unequivocal route, oxalic acid-d_2, DO–CO–CO–OD, was allowed to react with $^-$OD in the source of our VG ZAB 2HF instrument. The source-formed fragment at *m/z* 90 corresponding to the de-deuterated oxalate was mass selected and the collision induced mass spectrum shown in Figure 2.1 was recorded.

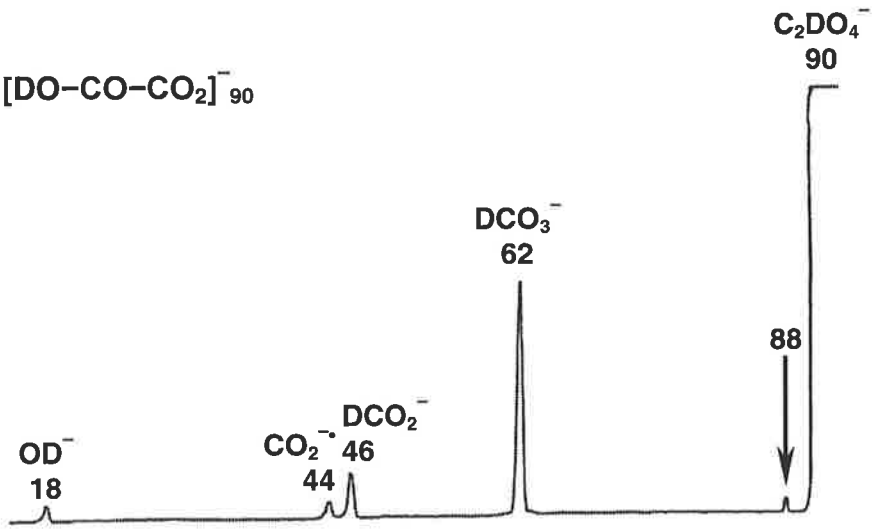

Figure 2.1 Collision-induced dissociation (CID) mass spectrum of $[DO–CO–CO–O]^-$. VG ZAB 2HF mass spectrometer. For experimental details see Experimental Section.

A small peak at *m/z* 88 can be seen which corresponds to a $C_2O_4^{-\bullet}$ fragment ion. The unusual peak at *m/z* 62 corresponds to $DO–CO_2^-$, the appearance of which can be rationalised as follows. The reaction between oxalic acid-d_2 and DO^- in the ion source of the mass spectrometer produces an $(M-D)^-$ ion. Collisional activation of this anion results in the loss of

CO (similar losses of CO have been previously reported).[129] This occurs as the incipient $DOCO^-$ ion acts as a DO^- donor within an anion-neutral ion complex.[130] The rupture of the C-C bond accounts for the occurrence of DCO_2^- at *m/z* 46 in the spectrum. Despite having an electron affinity of -0.60 eV,[131] $CO_2^{-\bullet}$ can clearly be seen (the generation of $CO_2^{-\bullet}$ under low energy conditions has been previously reported).[132,133] This is also unusual considering that the electron affinity of CO is 1.326 eV,[131] but fragment anions of $CO^{-\bullet}$ are not observed.

The dissociation of $\mathbf{1}^{-\bullet}$ into $^2CO_2^{-\bullet}$ + $^1CO_2$ was calculated at the CCSD(T)/aug-CC-pVDZ//B3LYP/6-31G(d) level of theory to be endothermic by + 20.7 kcal mol^{-1}. There is a barrier of 22.9 kcal mol^{-1} to this dissociation process, proceeding via transition state $\mathbf{B}^{-\bullet}$ (see Figure 2.2).

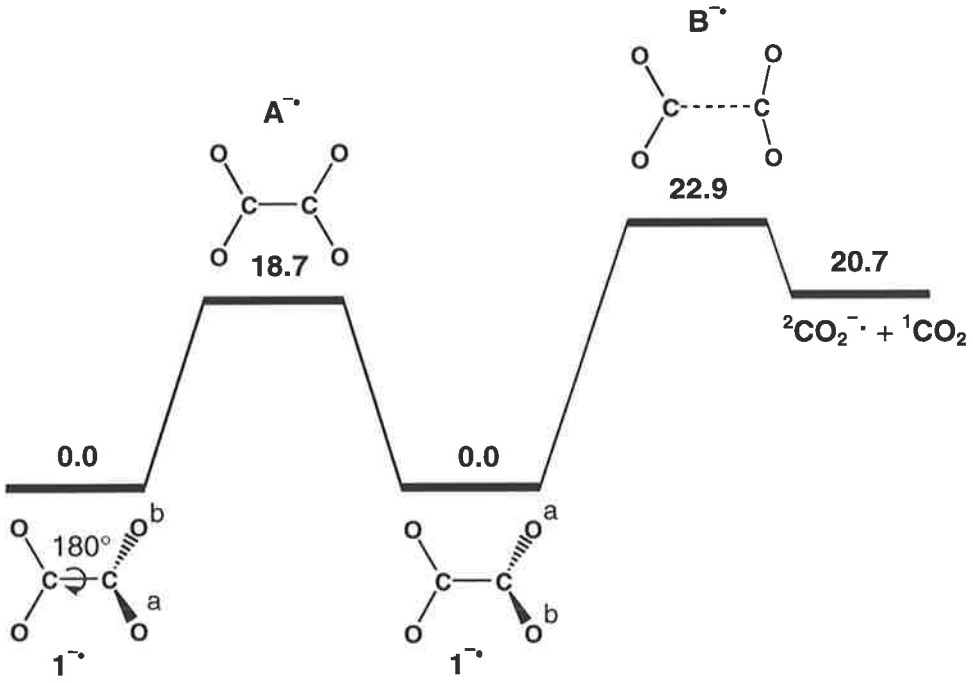

Figure 2.2 Relative energies for rotation of the O^aCO^b unit about the C-C bond of doublet anion, $1^{-\bullet}$, and the dissociation pathway of $1^{-\bullet}$. CCSD(T)/aug-cc-pVDZ//B3LYP/6-31G(d) level of theory - values are in kcal mol^{-1}.

The other transition state located on the doublet anionic surface is the planar D_{2h} saddle point $\mathbf{A}^{-\bullet}$ for rotation about the C-C bond of doublet anion $\mathbf{1}^{-\bullet}$. This transition state is in accord with

the findings of Fleischman and Jordan.[127] Transition state $\mathbf{A}^{-\bullet}$ lies 18.7 kcal mol^{-1} above the anion, therefore the 180° rotation of a CO_2 unit about the C-C bond competes favourably with the exothermic dissociation process (which must surmount a barrier of 22.9 kcal mol^{-1}).

B. Neutral C_2O_4

It is interesting to speculate what form(s) the neutral may have. Since the small signal corresponding to $(O_2C\text{-}CO_2)^{-\bullet}$ at *m/z* 88 in the collisional activation spectrum (Figure 2.1) is too weak to attempt neutralisation, a limited theoretical survey of the neutral potential surface was carried out. While the radical anion $\mathbf{1}^{-\bullet}$ is stable, the analogous neutral could not be found as a minimum on either the singlet or triplet neutral potential energy surfaces at the CCSD(T)/aug-CC-pVDZ//B3LYP/6-31G(d) level of theory. Other neutral structures were identified: (i) a 1,3-dioxetane-2,4-dionyl singlet neutral **5**, (ii) a planar $O_2C–CO_2$ triplet neutral **3**, 77.7 kcal mol^{-1} higher in energy than **5**, and (iii) a 1,2-dioxetane-3,4-dionyl singlet neutral **4**, 81.6 kcal mol^{-1} higher in energy than **5**.

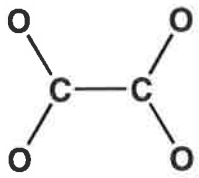

3

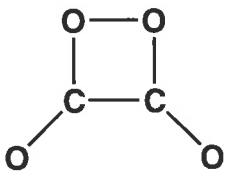

4

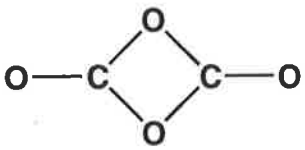

5

All three neutral isomers have been reported previously.[134] Both **3** and **4** are geometrically quite similar; the presence of a -O–O- linkage of **4** and the subsequent strain in the four-membered ring structure decreases the stability by 3.9 kcal mol^{-1} [MP3/6-31+G(d)//HF/6-31+G level of theory][127]. The formation of **5** from $\mathbf{1}^{-\bullet}$ involves rupture of the C-C bond and rotation of the CO_2 moieties with respect to each other, followed by the formation of two bonds.

Generation of a neutral from the radical anion $\mathbf{1}^{-\bullet}$ via a neutralisation reionisation experiment needs to be considered with respect to the possible dissociation channel(s) available to the nascent neutral. If the neutral is formed with sufficient internal energy, immediate fragmentation will result. Calculations at the CCSD(T)/aug-cc-pVDZ//B3LYP/6-31G(d) level of theory indicate that dissociation to $^3CO_2 + {}^1CO_2$ is an exothermic process (- 24.4 kcal mol^{-1}), although a small but distinct barrier of 5.0 kcal mol^{-1} must be overcome (Figure 2.3). One-electron Franck-Condon vertical oxidation of $\mathbf{1}^{-\bullet}$ yields a species corresponding to triplet $O_2C{-}CO_2$ (the triplet neutral with the same geometry as $\mathbf{1}^{-\bullet}$) formed with 11.7 kcal mol^{-1} excess energy. This is sufficient to overcome the barrier to dissociation. The triplet neutral **3** will not survive the NR experiment and immediate dissociation to $^3CO_2$ and $^1CO_2$ should result.

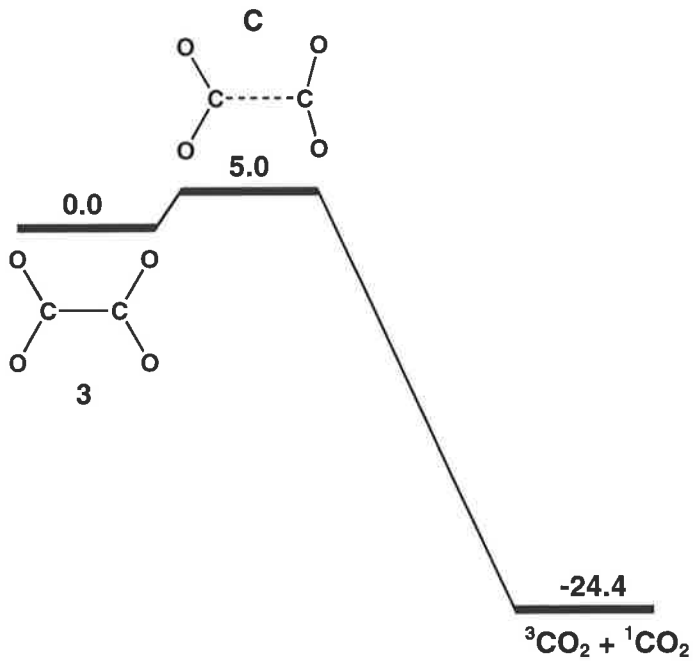

Figure 2.3 Dissociation pathway for triplet neutral $O_2C{-}CO_2$. CCSD(T)/aug-cc-pVDZ//B3LYP/6-31G(d) level of theory - values are in kcal mol^{-1}.

In conclusion, the radical anion $[O_2C{-}CO_2]^{-\bullet}$ $\mathbf{1}^{-\bullet}$ has been synthesized in the source of a modified ZAB 2HF mass spectrometer following D^+ loss from oxalic acid-d_2. A neutralisation reionisation experiment ($^-NR^+$) could not be performed on a source-formed precursor radical

anion $\mathbf{1}^{-\bullet}$ because of the weakness of the signal *m/z* 88 ($C_2O_4^{-\bullet}$). Theoretical calculations suggest that dissociation of the radical anion $\mathbf{1}^{-\bullet}$ into $^2CO_2^{-\bullet}$ + $^1CO_2$ is a process endothermic by 20.7 kcal mol^{-1}, and with a barrier of 22.9 kcal mol^{-1}. An assessment of the possible neutrals accessible by a neutralisation reionisation experiment suggests that the triplet neutral **3** is the most likely candidate. Theoretical calculations indicate that the triplet neutral **3** (if it were possible to access via $^-NR^+$) will be formed with excess energy following one-electron vertical oxidation of $1^{-\bullet}$. This excess energy is sufficient to effect the dissociation shown in Figure 2.3.

Part B: The Elusive Trioxydehydroethene Neutral (O_2C–CO)

Several gas phase studies have been carried out on clusters of carbon oxide neutrals and ions. These investigations have been predominantly spectroscopic in nature and have focussed on their photoelectron,[126,135] vibrational,[132,136] electron spin resonance,[137] and infrared [125,138] properties. The simplest cluster of carbon dioxide and carbon monoxide is the van der Waals complex **6**. This was first reported in 1989,[139] having been generated in a pulsed molecular beam using diode laser spectroscopy combined with Fourier transform microwave spectroscopy. Since then, several experimental and theoretical studies vis-à-vis the CO_2–CO complex have been carried out.[140,141] From the analysis of the Fourier transform IR absorption spectra from molecular beam experiments of the complex in argon matrices, researchers concluded that the CO_2–CO complex exists in three conformations. In the most stable conformation, the CO unit is oriented perpendicularly to CO_2 as shown in **6**, while two closely related less stable conformations also are suggested.[141] The energy differences between these conformations are small: ΔH = -140 J mol^{-1} and -337 J mol^{-1} between the T-shaped form and the other two forms.

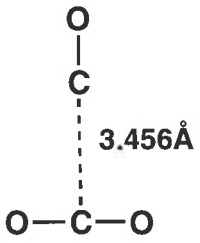

6

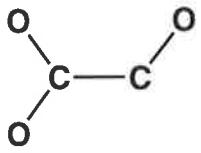

7

The formation and characterisation of short-lived neutrals in the gas phase may be investigated in a mass spectrometer using neutralisation/reionisation of negative ions ($^{-}NR^{+}$).[86,123] The covalently bound trioxydehydroethene structure **7** is one of the C_nO_m oxycarbon series (n = 2, m = 3), and is the next in sequence after ethylene dione, C_2O_2.

The singlet neutral ethylene dione (O=C=C=O) species has been calculated to be unstable with respect to dissociation into two singlet carbon monoxide molecules. The triplet neutral, which is predicted to be stable with respect to dissociation into singlet and triplet carbon monoxide, cannot be observed using either $^{-}NR^{+}$ or $^{-}NR^{-}$ experiments from $[O=C=C=O]^{-\bullet}$.[142] Efficient spin crossing from the triplet to the singlet neutral surface was suggested to prevent the detection of neutral O=C=C=O within the microsecond time-scale of this experiment. Whilst the van der Waals complex CO_2–CO **6** will certainly not be stable under the experimental conditions used for an NR experiment, a stable trioxydehydroethene with bond connectivity as shown in **7**, is a tentative proposition. Any C_2O_3 neutral detected during an NR experiment, must either be covalently bound or held together electrostatically. This study therefore seeks to achieve two objectives: (i), to make a precursor anion radical $C_2O_3^{-\bullet}$ with bond connectivity corresponding to **7**, and (ii), to determine whether vertical one-electron oxidation of this anion radical forms a detectable trioxydehydroethene neutral.

A. Experimental Approach Towards Neutral C_2O_3

In principle, the C_2O_3 neutral may be accessed via one electron oxidation of a suitable C_2O_3 precursor radical anion. The literature provides few reports of the formation of any anions of empirical formula C_2O_3. In an article by Cooper and Compton,[143] formation of a C_2O_3 radical anion is described as resulting from the capture of a low-energy electron by maleic anhydride followed by dissociation. Whilst the authors did not suggest a structure for the radical anion, the most likely bond connectivity for a species thus formed would initially be O–C–O–C–O.

Alternatively, a stable C_2O_3 radical anion has been reported to form by via laser ablation of transition metal targets (Pd and Ag) with concurrent 11 K co-deposition of CO_2/CO/Ar mixtures; the anion thus forms from the capture of ablated electrons by CO_2 and CO molecules during the condensation process.[144] Two structures of comparable energy were predicted by density functional theory (the highest level being B3LYP/aug-cc-pVDZ), and by an *ab initio* approach [MP2/6-311+G(d)]: an electrostatically bound complex **8**, and the non-planar, covalently bound radical anion **9** of C_S symmetry. Calculated isotopic vibrational frequencies indicated that certain features in the infrared spectrum were consistent with assignment of the covalently bonded structure to the radical anion **9**. The anion was suggested to form from electron capture of the T-shaped van der Waals complex **6**.

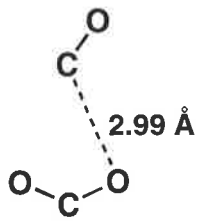

8

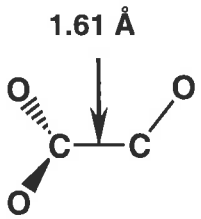

9

We were able to access the radical anion **9** via 1,3-dioxolane-2,5-dione, a neutral precursor for which the bond connectivity is known and unambiguous. Electron capture by this neutral precursor induced a retro-cleavage to yield the required radical anion, *viz.* Equation 1.

EQUATION 1

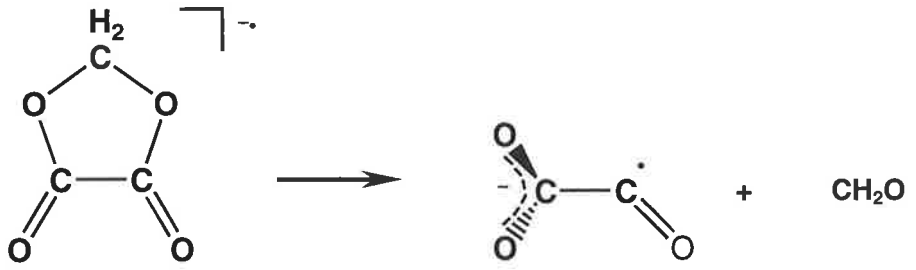

Interestingly, a pronounced molecular radical anion peak at *m/z* 72 is observed in the collision induced mass spectrum of $C_2O_3^{-\bullet}$, but despite the sizeable electron affinities of both $O^{\bullet}$ and CO (1.461 [145] and 1.326 eV [131] respectively), fragment anions of $O^{-\bullet}$ and $CO^{-\bullet}$ are not detected. The generation of $CO_2^{-\bullet}$, under low energy conditions has been previously reported,[132,133] which is surprising in view of the seemingly prohibitive electron affinity (-0.60 eV).[131] It is, however, highly improbable that such a fragment ion should be formed under the conditions of collisional activation. The $C_2O_3^{-\bullet}$ system is therefore robust enough to allow a radical anion of structure $\mathbf{9}^{-\bullet}$ to be formed under the conditions of collisional activation. The alternative structure $\mathbf{8}^{-\bullet}$ would be expected to readily decompose under the same conditions since the lowest energy dissociative pathway to CO_2 and CO is reported to be only some 3 kcal mol^{-1} endothermic.[144]

Table 2.1 Geometries and Energies of Anions $8^{-\bullet}$, $9^{-\bullet}$, and $10^{-\bullet}$.

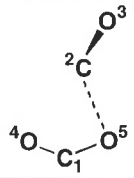

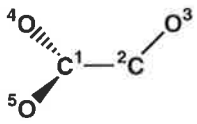

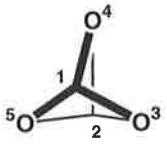

	$8^{-\bullet}$	$9^{-\bullet}$	$10^{-\bullet}$
State		$^2A'$	$^3A''$
Symmetry	C_1	C_S	D_{3h}
Energy (Hartrees)[a]	-301.22629	-301.23312	-301.04053
Rel. Energy (kcal mol^{-1})	4.3	0.0	120.9
Dipole Moment (Debye)[b]	2.89	1.31	0.00
Bond Length (Å)[b] or Angle (°)			
C^1C^2	3.03	1.62	1.64
C^2O^3	1.15	1.20	1.47
C^1O^4	1.24	1.24	1.47
C^2O^4	3.03	2.39	1.47
C^2O^5	2.57		
C^1O^5	1.25	1.24	1.47
$C^1C^2O^3$	106.4	124.4	56.3
$C^2C^1O^4$	78.1	112.6	56.3
$C^2C^1O^5$	56.6	112.6	56.3
$O^3C^2O^5$	104.5		
$O^4C^1O^5$	134.6	134.8	92.2
$O^3C^2C^1O^4$	89.3	91.3	120.0
$O^3C^2C^1O^5$	-88.8	-91.3	-120.0

[a] CCSD(T)/aug-cc-pVDZ level of theory including zero point energy correction (calculated from vibrational frequencies at the B3LYP/6-31G(d) level of theory and scaled by 0.9804).[146]

[b] B3LYP/6-31G(d) level of theory.

Details of the theoretical geometries and energies of $\mathbf{8}^{-\bullet}$ and $\mathbf{9}^{-\bullet}$ are listed in Table 2.1. Calculations were performed at the CCSD(T)/aug-cc-pVDZ//B3LYP/6-31G(d) level of theory. In a previous study, Zhou *et al.*[144] reported the geometries and energies of $\mathbf{8}^{-\bullet}$ and $\mathbf{9}^{-\bullet}$ calculated at the B3LYP level using a range of basis sets, and finally at the MP2/6-311+G(d) level of theory. The geometry values given in Table 2.1 are in reasonable agreement with the results of Zhou *et al.*[144] and in particular with those at the highest level of theory employed by these workers [MP2/6-311+G(d)].

10

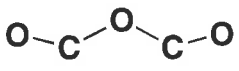

11

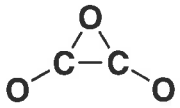

12

Stable structure **10** also occurs on the doublet anionic potential surface. It is more positive in energy than $\mathbf{9}^{-\bullet}$ by 121 kcal mol^{-1} at the CCSD(T)/aug-cc-pVDZ//B3LYP/6-31G(d) level of theory and is not considered further on energetic grounds. There were no minima found corresponding to structures $\mathbf{11}^{-\bullet}$ and $\mathbf{12}^{-\bullet}$ on the doublet anionic surface. Other possible isomers could feature the -O–O- functionality, but it is not expected that such species could be observable under the reaction conditions of the neutralisation experiments. Theory and experiment therefore indicate that the process shown in Equation 1 should yield the radical anion $\mathbf{9}^{-\bullet}$.

$^{-}CR^{+}$ and $^{-}NR^{+}$ Spectra

It is generally accepted that the synchronous two-electron oxidation event that produces a cation from the corresponding anion in the charge reversal experiment is a vertical process: the electronic transition occurs rapidly (vertically) and initially there is no change in the nuclear geometry.[123,147] Such a process will necessarily entail the involvement of Franck-Condon factors [the overlap integrals between the initial (in this case anionic), and the final (cationic) vibrational state wavefunctions].[123,147] The $^{-}CR^{+}$ spectrum of $[O_2C–CO]^{-\bullet}$ (Figure 2.4) lacks a peak for the parent radical cation; only decomposition peaks are observed. This implies that any attempt to produce a neutral C_2O_3 species must not involve identification of the neutral by positive ion mass spectrometry (as occurs in $^{-}NR^{+}$); the cation formed from ionisation of the neutral will immediately dissociate, and a recovery signal will not be

detectable [i.e., a peak corresponding to an ion $C_2O_3^{+\bullet}$ (*m/z* 72) will be absent].* The $^{-}NR^{+}$ experiment, in which a vertical process involving the stepwise one-electron oxidation of $C_2O_3^{-\bullet}$ to the neutral and then to the cation, is similar to the $^{-}CR^{+}$ spectrum (see Figure 2.5). The most important peaks in the $^{-}NR^{+}$ spectrum are those due to ionized CO and CO_2. No signal at *m/z* 72 is present.

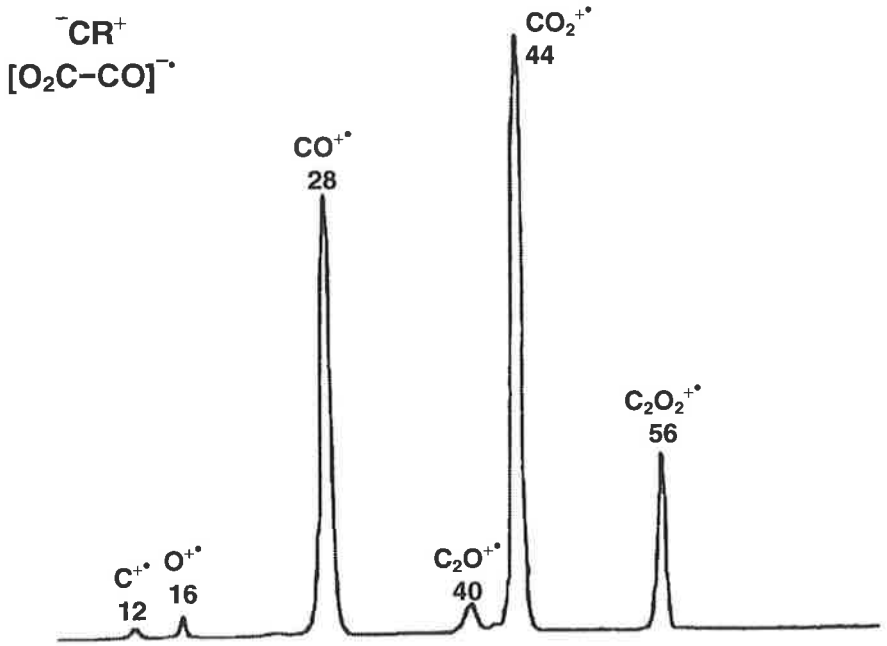

Figure 2.4 Charge reversal ($^{-}CR^{+}$) spectrum of $[O_2C-CO]^{-\bullet}$ $9^{-\bullet}$.VG ZAB 2HF mass spectrometer. For experimental details see Experimental Section.

*Notice that the $^{-}CR^{+}$ spectrum of $C_2O_3^{-\bullet}$ contains no peak due to $C_2^{-\bullet}$ (*m/z* 24), though the corresponding spectrum of $C_2O_2^{-\bullet}$ shows a distinct peak corresponding to *m/z* 24.[142] This is because there is essentially a double bond in $C_2O_2^{+\bullet}$ between the two carbon atoms [142] whereas the C–C bond in unstable $O_2C-CO^{+\bullet}$ is a 'long' single bond which undergoes facile cleavage to give CO and CO_2 species (see Table 2.2).

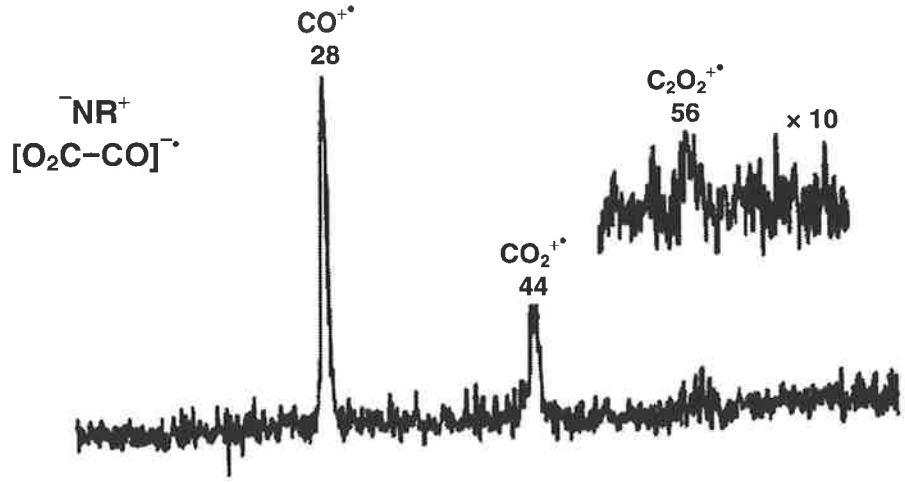

Figure 2.5 Neutralisation-reionisation ($^{-}NR^{+}$) mass spectrum of $[O_2C–CO]^{-\bullet}$ $\mathbf{9}^{-\bullet}$. VG ZAB 2HF mass spectrometer. For experimental details see Experimental Section.

However, a small peak at *m/z* 56 ($C_2O_2^{+\bullet}$) is (reproducibly) observable in the $^{-}NR^{+}$ spectrum. This signal must have arisen from the decomposition of the radical cation $C_2O_3^{+\bullet}$ because, whereas the radical anion and cation of O=C=C=O (ethylene dione) are stable species, the corresponding neutral cannot be detected under the conditions of the neutralisation reionisation experiment (the C_2O_2 neutral immediately dissociates into two CO units).[142] Accordingly, the positive ion signal at *m/z* 56 cannot have originated from ionised C_2O_2 neutral. Collisional activation of the $C_2O_3^{-\bullet}$ precursor anion does not give rise to $C_2O_2^{-\bullet}$, so the signal at *m/z* 56 (the $C_2O_2^{+\bullet}$ fragment) in the $^{-}NR^{+}$ spectrum is likely to be formed from the decomposition of the $C_2O_3^{+\bullet}$ radical cation. The $C_2O_3^{+\bullet}$ radical cation in turn, can only be formed by ionisation of a transient C_2O_3 neutral. We could not find a stable geometry corresponding to $[C_2O–CO]^{+\bullet}$ $\mathbf{9}^{+\bullet}$ on the radical cationic potential energy surface at the CCSD(T)/aug-cc-pVDZ//B3LYP/6-31G(d) level of theory. Of the three decomposition products observed in the $^{-}NR^{+}$ spectrum of $[O_2C–CO]^{-\bullet}$, namely $CO_2^{+\bullet}$, $CO^{+\bullet}$, and $C_2O_2^{+\bullet}$, two are formed by exothermic processes ($CO_2^{+\bullet}$ and $CO^{+\bullet}$ by 18.0 and 18.2 kcal mol^{-1} respectively), while $C_2O_2^{+\bullet}$ is formed by a process that is endothermic by 47 kcal mol^{-1} (Table 2.2).

Table 2.2 Thermochemical Data for Decompositions of C_2O_3.

cation process	ΔH (kcal mol^{-1})	neutral process	ΔH (kcal mol^{-1})
$^2C_2O_3^{+\bullet} \rightarrow {}^2C_2O_2^{+\bullet} + O^\bullet$	47.0	$^3\mathbf{9} \rightarrow {}^1CO + {}^3CO_2$	-6.80
$^2C_2O_3^{+\bullet} \rightarrow CO_2^{+\bullet} + CO$	-18.0	$^3\mathbf{9} \rightarrow {}^3CO + {}^1CO_2$	28.90
$^2C_2O_3^{+\bullet} \rightarrow CO_2 + CO^{+\bullet}$	-18.2	$^3\mathbf{11} \rightarrow {}^1CO + {}^3CO_2$	2.12

[a] Calculations at the CCSD(T)/aug-cc-pVDZ level of theory indicate that $\mathbf{9}^{+\bullet}$, the radical cation of O_2CCO, does not exist as a minimum on the potential energy surface, but undergoes immediate dissociation. The energy value for $C_2O_3^{+\bullet}$ given in the Table is that of a species with the geometry of neutral triplet **9** on the cation radical surface (following vertical Franck-Condon oxidation of the neutral). Energy values are determined from the following theoretically calculated values (Hartrees): $C_2O_3^{+\bullet}$ = -300.74294; $C_2O_2^{+\bullet}$ = -225.70604; $CO_2^{+\bullet}$ = -187.66628; $CO^{+\bullet}$ = -112.56104; $O^\bullet$ = -74.92565; ^1CO = -113.06894; ^3CO = -112.85212; $^1CO_2$ = -118.17443; $^3CO_2$ = -118.01450 [at CCSD(T)/aug-cc-pVDZ level of theory (calculated from vibrational frequencies at the B3LYP/6-31G(d) level of theory and scaled by 0.9804)].[146]

Because the cation radical $\mathbf{9}^{+\bullet}$ is not a stable species and cannot be used as a probe to detect the presence of neutral $O_2C{-}CO$ in a $^-NR^+$ experiment, perhaps a stable radical anion of structure $\mathbf{9}^{-\bullet}$ can be formed from the C_2O_3 neutral if the neutral exists for at least a microsecond.

If so, then the stable radical anion $\mathbf{9}^{-\bullet}$ can be used as a probe to detect neutral C_2O_3 in a $^-NR^-$ experiment. For the $^-NR^-$ experiment, the sensitivity of the instrument is first gauged by performing a standard experiment using PhCOCOPh. The radical anion $[PhCOCOPh]^{-\bullet}$ is first neutralised in the first collision cell, then the neutral PhCOCOPh captures an electron in the second collision cell reforming $[PhCOCOPh]^{-\bullet}$. The recovered radical anion produces an intense recovery signal in the $^-NR^-$ spectrum. Using this system as a standard, and with the instrument operating at optimal conditions of sensitivity, it is possible to increase the signal intensity by a factor of 100 times more than that used in the standard $^-NR^-$ experiment. $^-NR^-$ experiments with $[C_2O_3]^{-\bullet}$ were performed on numerous occasions. A very small signal at *m/z* 72 was observed on two occasions with the instrument set to maximum sensitivity. However,

the background noise under these conditions was unacceptably high, and the observation of a signal at *m/z* 72 was not reproducible. Thus, from repeated attempts at the $^{-}NR^{-}$ experiment using the instrument at maximum sensitivity and using various collision conditions in the tandem collision cell facility, it was concluded that the observation of a signal for $C_2O_3^{-\bullet}$ was not proven.* In spite of the non-observation of a recovery signal in NR experiments we conclude that a transient C_2O_3 species is produced because of the formation of *m/z* 56 ($C_2O_2^{+\bullet}$) in CR and NR spectra. However, the lifetime of this transient neutral must be less than 10^{-6} seconds.

* It is possible that some $(O_2C{-}CO)^{-\bullet}$ ions are 'metastable' with respect to electron loss. To check this possibility, we carried out a 'neutralisation' reionisation experiment as follows. The parent radical anion $(O_2C{-}CO)^{-\bullet}$ is fired through the first collision cell which contains no collision gas. The deflector between the two cells is charged, and the second cell contains O_2 (as in a normal $^{-}NR^{+}$ experiment). Thus only neutrals formed by 'metastable' electron loss from $(O_2C{-}CO)^{-\bullet}$ can enter the second collision cell. No positive ion signals result from this [$^{-}N_{metastable}R^{+}$] experiment. No conclusion can be drawn from the negative results of this experiment because it is possible that a small yield of such neutrals could be formed with the instrument not being sensitive enough to detect them.

Table 2.3 Geometries and Energies of Neutrals 6, 9, and 11.

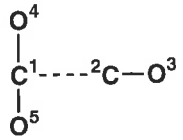
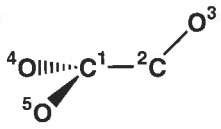
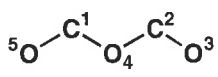

	6	**9**	**11**
State	$^1A'$	$^3A''$	$^3A'$
Symmetry	C_S	C_S	C_S
Energy (Hartrees)[a]	-301.24530	-301.07261	-301.08681
Rel. Energy (kcal mol^{-1})	0.0	180.4	99.5
Adiabatic Electron Affinity (eV)	-0.52	4.37	
Dipole Moment (Debye)[b]	0.235	0.950	1.350
Bond Length (Å)[b] or Angle (°)			
C^1C^2	3.19	1.51	2.34
C^2O^3	1.14	1.20	1.18
C^1O^4	1.17	1.26	1.39
C^2O^4	3.41	2.42	1.39
C^1O^5	1.17	1.26	1.18
$C^1C^2O^3$	179.9	133.8	156.7
$C^2C^1O^4$	90.5	122.0	32.4
$C^2C^1O^5$	90.4	122.0	156.7
$O^4C^1O^5$	179.1	116.0	124.3
$O^3C^2C^1O^4$	180.0	97.4	0.0
$O^3C^2C^1O^5$	180.0	-97.4	0.0
Total Atomic Charges			
C^1		0.278	
C^2		0.576	
O^3		-0.248	
O^4		-0.303	
O^5		-0.303	
Sum of Mulliken Charges		0.000	

[a] CCSD(T)/aug-cc-pVDZ level of theory including zero point energy correction (calculated from vibrational frequencies at the B3LYP/6-31G(d) level of theory and scaled by 0.9804).[146]

[b] B3LYP/6-31G(d) level of theory.

B. Theoretical Structures of the Isomers of C_2O_3

The singlet and triplet neutral potential energy surfaces feature several isomers of C_2O_3, *viz.* **6** and **9-12** at the CCSD(T)/aug-cc-pVDZ//B3LYP/6-31G(d) level of theory. Energy and geometry data of the stable neutral structures are presented in Tables 2.3 and 2.4. These isoforms are not all accessible via the neutralisation reionisation of $\mathbf{9}^{-\bullet}$. Some are either

structures with prohibitively high energies (for example the singlet and triplet propellane structures, ^{1}**10** and ^{3}**10** respectively) and can be disregarded, while others (such as the triplet neutral with the structure of **12**) are unstable with respect to dissociation. The remaining C_2O_3 neutrals, *viz.* the van der Waals complex **6**, the singlet and triplet of **9**, triplet **11**, and singlet **12**, will henceforth be the focus of the discussion.

Table 2.4 Geometries and Energies of Neutrals ^{1}10, ^{3}10, and 12.

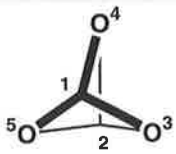

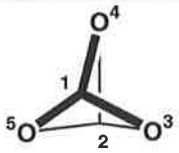

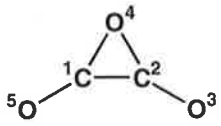

	^{1}10	^{3}10	12
State	^{1}A'	^{3}A$_1$"	^{1}A'
Symmetry	D_{3h}	D_{3h}	C_{2v}
Energy (Hartrees)[a]	-300.97142	-300.89094	-301.14828
Rel. Energy (kcal mol^{-1})	171.9	222.4	60.9
Adiabatic Electron Affinity (eV)	1.88	4.07	2.31
Dipole Moment (Debye)[b]	0.00	0.00	0.07
Bond Length (Å)[b] or Angle (°)			
C^1C^2	1.49	1.71	1.44
C^2O^3	1.43	1.46	1.18
C^1O^4	1.43	1.46	1.42
C^2O^4	1.43	1.46	1.42
C^1O^5	1.43	1.46	1.18
$C^1C^2O^3$	58.7	54.2	163.5
$C^2C^1O^4$	58.7	54.1	59.5
$C^2C^1O^5$	58.7	54.2	163.5
$O^4C^1O^5$	95.5	89.2	137.0
$O^3C^2C^1O^4$	120.0	120.0	180.0
$O^3C^2C^1O^5$	-120.0	-120.0	0.0

[a] CCSD(T)/aug-cc-pVDZ level of theory including zero point energy correction (calculated from vibrational frequencies at the B3LYP/6-31G(d) level of theory and scaled by 0.9804).[146]

[b] B3LYP/6-31G(d) level of theory.

Energetically, the van der Waals complex **6** is the most negative in energy but it needs only 1.2 kcal mol^{-1} [at the CCSD(T)/aug-cc-pVDZ//B3LYP/6-31G(d) level of theory] to effect dissociation to CO_2 and CO. Calculation of the minimum excess energy of one-electron oxidation of $\mathbf{9}^{-\bullet}$ to a neutral species corresponding to singlet $O_2C{-}CO$ (that is, the difference

in energy between the neutral minimum and that of the anion geometry on the ground-state neutral surface),[148] yields a value of 62.8 kcal mol^{-1} with respect to the van der Waals structure **6**. This is a considerable amount of excess energy, and it should be borne in mind that the calculated value is a *minimum* excess energy of formation of the neutral from the anion, and does not include any excess energy that the precursor anion itself may have, or extra energy imparted to the neutral as a consequence of the collisional process. The van der Waals neutral **6** will thus not be stable under the conditions required for a NR experiment. A minimum corresponding to **9** could not be identified on the singlet neutral potential energy surface of C_2O_3, but the triplet neutral potential surface does feature a minimum corresponding to triplet **9**. Energies and geometries of the stable neutrals are summarised in Table 2.3.

The O_2C–CO Radical Anion, $9^{-\bullet}$

The geometry data and the relative energies of the stable anionic species are given in Table 2.1. The O_2C–CO radical anionic structure $\mathbf{9}^{-\bullet}$ is a $^2A'$ electronic state of C_S symmetry. The C^1-C^2 bond length is 1.62 Å which is considerably longer than that of a sp^3 singly bonded system [e.g. 1.53 Å in ethane; all reference bond lengths were computed at the B3LYP/6-31G(d) level]. The C^2–O^3 bond length of 1.20 Å is almost identical to the carbonyl C–O bond length in formaldehyde (1.21 Å), while the C^1–$O^{4,5}$ bonds, 1.24 Å, are considerably shorter than those of CO_2 (1.17 Å) and are more akin to the carbonyl system in formaldehyde. The C^1-C^2-O^3 angle is 124.4°, and the C^2-C^1-$O^{4,5}$ angles are both 112.6°. The centres C^2, C^1, O^4, and O^5 do not lie on the same plane; dihedral angles indicate that O^4 and O^5 lie slightly below the plane upon which C^1 and C^2 lie (O^3-C^2-C^1-$O^{4,5}$ = 91.3° and -91.3° respectively).

The dipole moment is calculated to be 1.31 D at the B3LYP/6-31G(d) level of theory.

The O_2C–CO Triplet Neutral, 9

Neutral structure **9**, identified on the triplet neutral potential surface has a ^3A" electronic state of C_S symmetry (energy and geometry data are summarised in Table 2.3). Calculation at the B3LYP/6-31G(d) level of theory predicts a C^1-C^2 bond length of 1.51 Å - noticeably shorter than in the corresponding anion, and very similar to (though shorter than) the sp^3 C-C bond in ethane (1.53 Å). The C^2–O^3 bond length is 1.18 Å which is more like the doubly-bonded C-O linkages in CO_2 than the formaldehyde carbonyl. The equivalent C^1–$O^{4,5}$ bonds are 1.26 Å in length, and as such are slightly extended carbonyl bonds. The C^1-C^2-O^3 angle is 133.8°, and the C^2-C^1-$O^{4,5}$ angles are both 122.0°. As for $\mathbf{9}^{-\bullet}$, O^4 and O^5 lie below the plane upon which C^1 and C^2 lie, though more so (O^3-C^2-C^1-$O^{4,5}$ = 97.4° and -97.4° respectively).

Mulliken population analysis indicates that the unpaired electron is located equally on O^4 and O^5 (0.589 e), as is the charge density (-0.303 e on each), but a significant contribution of spin and charge density is also borne on C^1 (0.289 e). Finally, overlap population values C^1-$O^{4,5}$ and C^2-O^3 are 0.384 e and 0.520 e respectively, which are in accord with the calculated bond lengths.

The adiabatic electron affinity of the neutral **9** is calculated to be 4.37 eV at the CCSD(T)/aug-cc-pVDZ//B3LYP/6-31G(d) level of theory, and the dipole moment is 0.95 D at the B3LYP/6-31G(d) level of theory.

The OCOCO Triplet neutral, 11

Another structure identified as a minimum on the triplet potential surface is **11** (electronic state $^3B_2$, C_{2v} symmetry). In this planar neutral species, the two equivalent C^1-O^5 and C^2-O^3 bonds are each 1.18 Å long, and hence intermediate between the C-O bonds of CO_2 and in formaldehyde. The O^4-$C^{1,2}$ bonds are both 1.39 Å long and are of a similar length to the C-O bonds of dimethyl ether (1.41 Å). The angles O^5-C^1-O^4 and O^4-C^1-O^3 are 124.3°, and C^1-O^4-C^2 is 115.3° (by comparison, the C-O-C angle in dimethyl ether is 112.3°). The unpaired

electrons are mostly located on the carbon atoms (0.657 e), and the overlap populations (C^1-O^5, C^2-O^3 are 0.519 e, and O^4-$C^{1,2}$ are 0.098 e) agree with the calculated bond lengths.

At our chosen level of theory, the dipole moment of the neutral ~~5~~ 11 is calculated to be is ~~0.56~~ 1.350 Debye.

The Cyclic C_2O_3 Singlet neutral, 12

The only singlet neutral structure identified that, in principle, could be accessed by the one-electron oxidation of $\mathbf{9}^{-\bullet}$ (but in reality cannot be for the reasons given later) is a three-membered, oxygen-containing ring structure of $^1A_1$ electronic state and C_{2v} symmetry. The calculated C^1-C^2 bond length is 1.44 Å; this is both shorter than a model single bond (for example, the ethane C-C bond is 1.53 Å), yet longer than a pure double bond (1.34 Å in ethylene), but comparable to the C-C bond of ethylene oxide ring (1.47 Å). The equivalent O^4-$C^{1,2}$ bond lengths (1.42 Å) are also very similar to the analogous bonds in an ethylene oxide ring (1.43 Å), as are the C^1-C^2-O^4 and C^1-O^4-C^2 angles (59.48° and 61.04° respectively). The equivalent C^1-O^5 and C^2-O^3 bonds are 1.18 Å long, and hence only slightly longer than the C-O double bonds of CO_2 (1.17 Å).

The overlap population value for C^1-O^5 and C^2-O^3 are each 0.600 e, which are in accord with the calculated bond lengths. The overlap population of C^1-C^2 is 0.292 suggesting substantial electronic distribution between these two centres, while those for the two equivalent bonds O^4-$C^{1,2}$ are each 0.023 e and indicate the polarisation within each of the two C-O bonds.

The adiabatic electron affinity of the neutral **12** is calculated to be 2.31 eV at the CCSD(T)/aug-cc-pVDZ//B3LYP/6-31G(d) level of theory, and the dipole moment is 0.07 D at the B3LYP/6-31G(d) level of theory.

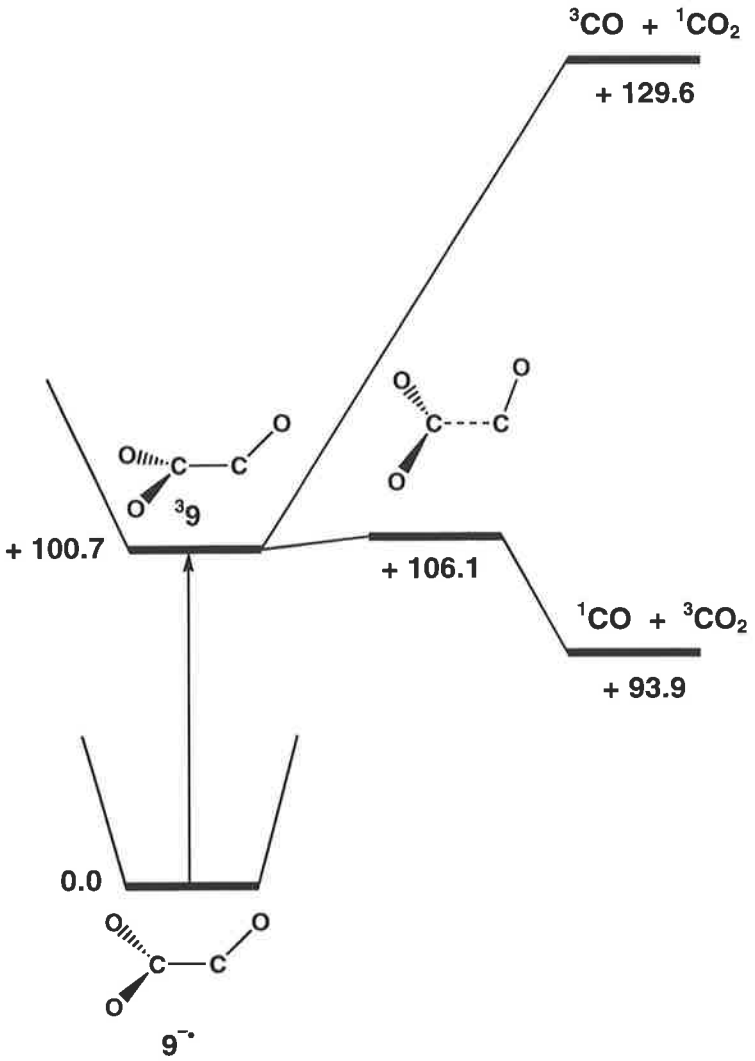

Figure 2.6 Vertical Franck-Condon oxidation of $[O_2C{-}CO]^{-\bullet}$ to triplet $O_2C{-}CO$, and dissociation pathways for triplet $O_2C{-}CO$. CCSD(T)/aug-cc-pVDZ//B3LYP/6-31G(d) level of theory. Energies in kcal mol^{-1}.

C. Theoretical Investigation into the Formation of Neutral C_2O_3

The vertical one-electron oxidation event whereby $\mathbf{9}^{-\bullet}$ is neutralised to triplet **9** imparts a negligible amount of excess energy into the nascent neutral. The fate of this neutral must then be considered with respect to two dissociative processes that it may undergo (calculated details of the neutralisation of $\mathbf{9}^{-\bullet}$ to triplet **9** are shown in Figure 2.6, and calculated energy and geometry data are listed in Tables 2.1 and 2.3). Firstly, the neutral may dissociate into ^3CO and $^1CO_2$. However, such a process is endothermic by + 28.9 kcal mol^{-1} and is therefore

unlikely to be accessible to a vibrationally cold neutral. Alternatively, dissociation may yield ^1CO and $^3CO_2$ by an exothermic process (- 6.8 kcal mol^{-1}). This process has a well defined barrier of 5.4 kcal mol^{-1} (see Figure 2.6 and Table 2.5). Consequently, if the triplet neutral of structure **9** could be formed vibrationally cold and without sufficient internal energy to surmount the 5.4 kcal mol^{-1} barrier to dissociation into ^1CO and $^3CO_2$, the neutral should be detectable in the NR experiment if the neutral lifetime is $\geq 10^{-6}$ seconds.

Table 2.5 Geometries and Energies of Transition State Structures

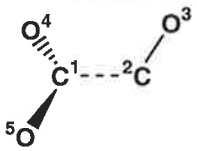

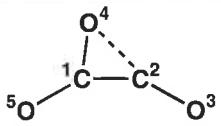

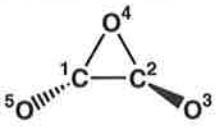

	See Figure 2.6	See Figure 2.7	13
State	$^3A''$	$^2A'$	
Symmetry	C_S	C_S	C_1
Energy (Hartrees)[a]	-301.06402	-301.14837	-301.01677
Bond Length (Å)[b] or Angle (°)			
C^1C^2	2.03	1.47	1.39
C^2O^3	1.15	1.16	1.21
C^1O^4	1.25	1.32	1.48
C^2O^4	2.84	1.66	1.48
C^2O^5	1.25	1.19	1.21
$C^1C^2O^3$	122.3	180.0	156.2
$C^2C^1O^4$	117.6	72.9	61.8
$C^2C^1O^5$	117.6	145.8	156.2
$O^4C^1O^5$	117.5	141.3	140.9
$O^3C^2C^1O^4$	-105.3	180.0	-164.8
$O^3C^2C^1O^5$	-105.3	0.0	30.5

[a] CCSD(T)/aug-cc-pVDZ level of theory including zero point energy correction (calculated from vibrational frequencies at the B3LYP/6-31G(d) level of theory and scaled by 0.9804).[146]

[b] B3LYP/6-31G(d) level of theory.

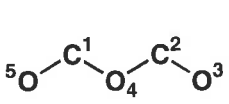

11

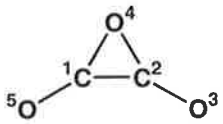

12

While the experimental evidence suggests that triplet neutral **9** (lifetime < 10^{-6} sec) has indeed been generated by neutralisation of $\mathbf{9}^{-\bullet}$ in an NR experiment, the same cannot be said of either triplet neutral **11** or singlet neutral **12**. We did not find a singlet neutral structure corresponding to $O_2C{-}CO$ (i.e. a singlet neutral with the same geometry as $\mathbf{9}^{-\bullet}$), nor was such a singlet neutral found on the reaction coordinate for the ring opening of singlet **12** followed by dissociation to CO_2 and CO (this process is depicted in Figure 2.7). A careful examination of the singlet neutral potential energy surface along the reaction coordinate for dissociation of singlet **12** revealed that during the ring opening of **12** and the subsequent dissociation, the CO_2 and CO units move apart, but otherwise do not break the plane along which they are oriented. The CO_2 and CO moieties do not assume the orthogonal orientation to each other as in structure $\mathbf{9}^{-\bullet}$.

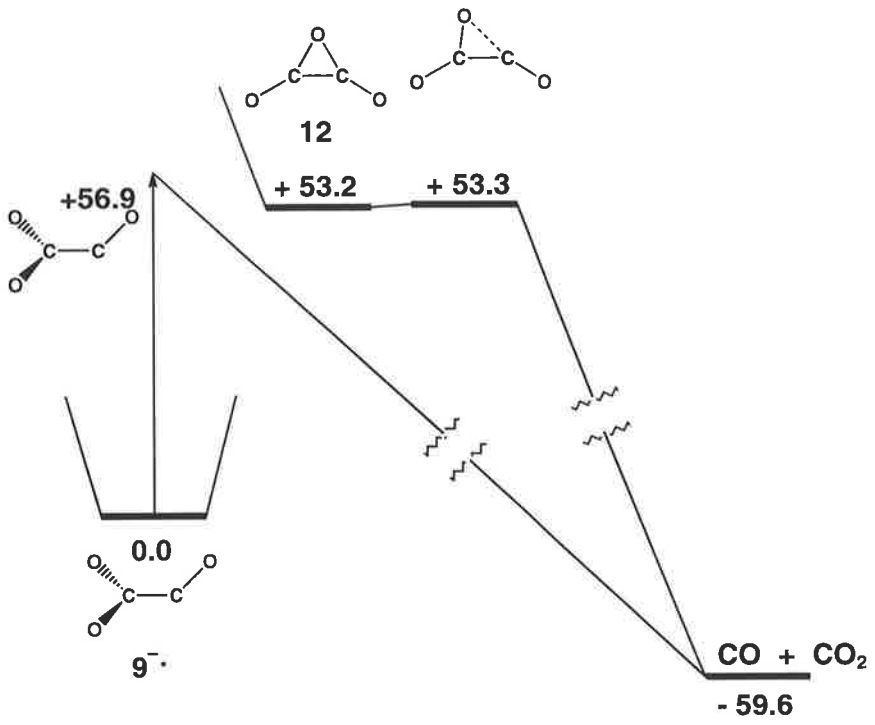

Figure 2.7 Dissociation pathways for singlet $O_2C{-}CO$ 9 and 12. CCSD(T)/aug-cc-pVDZ//B3LYP/6-31G(d) level of theory. Energies in kcal mol^{-1}.

OCOCO 11

Is triplet neutral **11** (OCOCO) accessible from doublet anion $\mathbf{9}^{-\bullet}$? For this to be possible, it is necessary that triplet neutral **9**, once formed, rearranges to **11**. It is possible, in principle, for triplet neutral **9** to rearrange to **11** if the barrier to rearrangement is less than the barrier to dissociation of the triplet **9** into ^{1}CO and ^{3}CO (+ 5.4 kcal mol^{-1}). Such a rearrangement could proceed via two possible pathways: (a) a synchronous rearrangement of triplet **9** to triplet **11**, and (b) a stepwise process which occurs by i) partial dissociation of triplet **9** into a loosely bound CO_2-CO intermediate; then ii) reorientation of the CO_2 and CO moieties within the CO_2-CO complex to form triplet **11**. We did not find evidence for this stepwise pathway towards triplet neutral **11**; the dissociation process to CO and CO_2, once begun, always proceeded towards complete separation between the two moieties. Neither could a concerted rearrangement pathway from triplet **9** to triplet **11** be found. A saddle point which corresponds to symmetrical but unstable triplet **12** was found, but this transition state is for a cyclisation process that leads directly to dissociation into CO and CO_2.

Moreover, we identified a non-planar cyclic saddle point for the degenerate rearrangement of triplet neutral O_2C–CO to triplet neutral OC–CO_2 (structure **13** below and detailed in Table 2.5). This transition state lies 30 kcal mol^{-1} above triplet neutral O_2C–CO. This degenerate rearrangement process therefore cannot compete on energetic grounds with the exothermic dissociation process (which has a barrier of 5.4 kcal mol^{-1}). A process whereby vertical one-electron oxidation of a $[O_2C–CO]^{-\bullet}$ radical anion $\mathbf{9}^{-\bullet}$ leads to formation of a triplet neutral of structure OCOCO **11** could not be found.

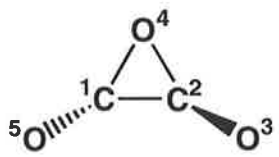

13

In conclusion, although the radical anion $[O_2C{-}CO]^{-\bullet}$ $\mathbf{9}^{-\bullet}$ was synthesized in the source of a modified ZAB 2HF mass spectrometer by electron capture of 1,3-dioxolane-2,5-dione followed by loss of CH_2O, neutralisation reionisation experiments (both $^{-}NR^{+}$ and $^{-}NR^{-}$) on the precursor radical anion $\mathbf{9}^{-\bullet}$ yielded spectra containing no recovery signals corresponding to ionized C_2O_3. The $^{-}NR^{+}$ spectrum of $[O_2C{-}CO]^{-\bullet}$ shows a peak corresponding to $[O{=}C{=}C{=}O]^{+\bullet}$, which can only originate from a decomposing $C_2O_3^{+\bullet}$ species. Both experimental and theoretical data suggest that neutralisation of $[O_2C{-}CO]^{-\bullet}$ $\mathbf{9}^{-\bullet}$ does produce a transient, covalently-bound species corresponding to triplet $O_2C{-}CO$ **9**, though this neutral triplet has a lifetime of less than 10^{-6} seconds.

III. Experimental Section

A. Mass Spectrometric Methods

Mass spectra were measured using a modified VG ZAB 2HF mass spectrometer with BE configuration (where B and E represent magnetic and electric sectors, respectively) equipped with tandem collision cells between the magnetic and electric sectors. The $C_2DO_4^-$ anion and $C_2O_3^{-\bullet}$ radical anion were generated with the instrument operating in the negative ion chemical ionisation (NICI) mode. Typical source conditions were as follows: source temperature 200°C; repeller voltage -0.5 V; ion extraction voltage 7 kV; mass resolution $m/\Delta m \geq 1500$. The precursor (either oxalic acid-d_2 or 1,3-dioxolane-2,5-dione), was placed in small glass capillary tube which was then drawn out in a flame to create a very fine aperture, allowing for a slow steady release of sample vapour upon heating. The capillary was inserted into the CI source via the direct probe; the probe tip was heated to 60-80 °C to generate a background pressure of *ca.* 10^{-5} Torr inside the source housing. The $C_2DO_4^-$ anion was formed by loss of D^+ from oxalic acid-d_2 using ^-OD (obtained from the reaction between D_2O and D^-. The $C_2O_3^{-\bullet}$ radical anion was formed by electron capture by 1,3-dioxolane-2,5-dione followed by loss of CH_2O (Scheme 2.1) with hexane as the CI reagent gas at a pressure of *ca.* 10^{-4} Torr inside the source housing. Collisional induced dissociation (CID) of mass selected anions was effected in the first of the two tandem collision cells positioned between B and E. Argon was used as a target gas. The pressure of the collision gas in the cell was maintained such that 80% of the parent ion beam was transmitted through the cell. This corresponds to an average of 1.1-1.2 collisions per ion.[66] Product ions resulting from CID were recorded by scanning E.

Neutralisation-reionisation [123,147] ($^-NR^+$ or $^-NR^-$ as appropriate) experiments were performed for mass-selected $C_2O_3^{-\bullet}$ utilising the dual collision cells located between sectors B and E. Neutralisation of the anions was achieved by collisional electron detachment using O_2 at 80% transmittance as collision gas, whereas reionisation to cations was achieved by collision of the neutrals with O_2, again at 80% transmittance. Ionisation to anions in the second cell was

performed using benzene as reagent gas at 80% transmittance. Any ions remaining after the first collision event were deflected from the primary neutral beam using an electrode maintained at a high voltage (1.5 kV) positioned before the second collision cell. To detect a reionisation signal due to the parent, the neutral species must be stable for approximately one microsecond. Charge reversal ($^{-}CR^{+}$) spectra [67,71,149] were recorded using single collision conditions in collision cell 1 (O_2, 80% T).

B. Synthetic Procedures

Oxalic acid-d_2 was prepared from anhydrous oxalic acid by dissolving the acid (2.22 mmol, 200 mg) in methanol-d_1 (5 cm^3) and stirring for 45 min at room temperature under an atmosphere of nitrogen. The solvent was then removed *in vacuo* and the procedure repeated 4 times. (d_2 = 99 %)

1,3-Dioxolane-2,5-dione was prepared by a reported method.[150]

C. Theoretical Methods

Molecular geometries were optimised and the vibrational frequencies computed according to the Becke 3LYP exchange-correlation functional.[151,152] This hybrid functional consists of the Lee-Yang-Parr correlation functional [153] and Becke's three-parameter exchange functional.[151] The exchange functional is a linear combination of the local density approximation, Becke's gradient correction,[154] and the "exact" Hartree-Fock exchange energy. This hybrid method has been shown to be more accurate than standard gradient-corrected methods.[155] The 6-31G(d) polarisation basis set was employed, which uses six primitive Gaussians for the core orbitals, a three/one split for the *s*- and *p*-valence orbitals, and a single set of six *d*-functions. All calculations were performed within the GAUSSIAN 98 [156] computational chemistry package. Stationary points on potential energy surfaces were characterised as either minima (no imaginary frequencies) or transition states (one imaginary frequency) by calculation of the

frequencies using analytical gradient procedures. The connection between minima and a given transition structure was established by examining the reaction path on the potential energy surface leading away from the transition structure in an intrinsic reaction coordinate (IRC) calculation. The calculated frequencies were also used to determine zero-point vibrational energies which were then scaled by 0.9804 [146] and used as a zero-point energy correction for the electronic energies calculated at this and higher levels of theory.

The B3LYP method has previously been used for geometry optimisations of anions and good agreement has been achieved with parameters calculated using high level coupled-cluster approaches.[157]

Higher accuracy energies for the B3LYP optimised geometries were obtained using the coupled cluster method, CCSD(T).[101,158] This method features all single and double substitutions [159]augmented by a quasi-perturbative account for triple excitations,[103] and is known to yield correlation energies very close to the exact *n*-particle solution within the given basis set as long as the Hartree-Fock determinant is a reasonably good zero-order reference wavefunction.[98] Single-point energy calculations employed the large augmented correlation-consistent polarised double-zeta basis set aug-cc-pVDZ of Dunning [111,160] which incorporates d functions [maximum angular momentum $l = 2$(d)] to heavy atoms.

Calculations were performed on the Silicon Graphics Power Challenge Super Computer at the Australian National University Super Computing Facility (Canberra), and on the 120 node 480 1GHz processor Compaq AlphaServer SC at the Australian Partnership for Advanced Computing National Facility (Canberra).

3 Formation of Two Isomeric C_3HO Radicals From Charged Precursors in The Gas Phase.

I. Introduction

There is continuing scientific interest in carbon chain molecules following the detection of several unsaturated hydrocarbon species in the interstellar medium at radio wavelengths. These molecular species often have cumulene-like structures and consist of some of the largest molecules identified in space, and also include polycarbon oxide molecules of the form C_nO (n = 1, 2, 3). Significantly, the HC_2CO radical, which can be thought of as a hydrogenated polycarbon monoxide, has recently been shown to be involved in a range of topical chemical processes: it is a probable intermediate in ethynyl combustion chemistry where it is formed by the reaction of the C_2H radical with CO;[161] it is an observed photodissociation product of propynal (HC_2CHO);[162] and it is likely to play a role in the chemistry of dense molecular clouds following the detection of propynal [163] and of several rotational lines of the related radical species tricarbon monoxide, CCCO, in the cold dark interstellar cloud TMC-1 where they occur in nearly equal abundance.[164-166]

There is some conjecture about the mechanism of formation of these hydrogenated polycarbon oxide species in interstellar molecular clouds, but in the model that has dominated the discussion, propynal, polycarbon oxide, and the analogous hydrogenated species are intertwined. It has been proposed [167] that the formation pathways involve ion-molecule reactions, *viz.*

$$C_2H_2^{+\bullet} + CO \rightarrow H_2C_2O^{+\bullet} + h\nu$$

followed by the dissociative electron recombination reactions,

$$H_2C_3O^{+\bullet} + e^- \rightarrow C_3O + H_2$$
$$\rightarrow HC_3O + H$$

Experimental [16] and theoretical [168] investigations suggest that $H_nC_3O^+$ ions are particularly unreactive toward the major constituents of interstellar clouds; this finding implies that the products of these reactions persist in interstellar clouds, and provides further validation for the on-going search for their occurrence in these media.* If HC_2CO is a natural intermediate in the interstellar production of C_2CO and HC_2CHO, it is possible that it exists in the same abundance as, or in greater abundance than both the known molecules if the unknown dissociative branching ratio is large.[171]

While attention has been focussed on the HC_3O radical, and in particular to its propynonyl H–C≡C–C=O, and/or propadienonyl H–C=C=C=O forms,[171-175] it is also valid to consider the other possible isomers of the HC_3O radical. To this end, a theoretical and experimental investigation is here described. Two thermodynamically less favourable, yet still stable connectivities are investigated and their energies relative to the global minimum, HC_2CO, are discussed with particular reference to the different isomerisation pathways. The gas-phase syntheses of HC_3O neutral isomers from charged precursors can be conveniently carried out using mass spectrometry. NR experiments in particular can establish the stability of corresponding neutrals in the microsecond timescale.

II. Results and Discussion

A. Theoretical Studies of HC_3O Isomers

Of the possible HC_3O isomers, three contain the carbonyl moiety other than HC_2CO, *viz.* C_2CHO, CCHCO, and (*cyclo*-C_3H)=O. All four isomers were analysed at the CCSD(T)/aug-cc-pVDZ//B3LYP/6-31G(d) level of theory. At our chosen level of theory, the CCHCO isomer was not found to be a local minimum on the neutral surface, and optimisation of a

*Propynal itself is predicted to be photolytically depleted via a gas-phase reaction involving a HCCHCO species, to form the isomers cyclopropenone and propadienone.[169] If so, then observed propynal in interstellar space must be produced by another route, namely the photolysis of $C_3{\cdot}H_2O$ clusters in the ice mantles of dust grains, and not in gas-phase ion-molecule reactions.[168-170]

suitable CCHCO starting geometry lead through cyclisation to yield the cyclic isomer (*cyclo*-C_3H)=O. The structures of the three stable HC_3O radicals, HC_2CO **1**, C_2CHO **2**, and (*cyclo*-C_3H)=O **3** are shown in Figure 3.1; full details of their geometries and energies are listed in Table 3.1. The geometries of all three neutrals **1**,[166,172,175] **2**,[176] and **3** [172] have been reported previously. Previous theoretical studies of the HC_3O neutral potential surface have been reported at a variety of levels of theory:[172,175] all found the HC_2CO isomer to be the global minimum. Our calculations are in agreement with this result. At the CCSD(T)/aug-cc-pVDZ//B3LYP/6-31G(d) level of theory as used by us, the relative energies of **2**, and **3** with respect to **1** are 41.1, and 12.2 kcal mol^{-1} respectively. To our knowledge, no previous study addressed the possibility of interconversion between the various carbonyl isomers. This will be discussed in detail later.

Table 3.1 Geometries and Energies of Neutral Isomers 1 - 3.

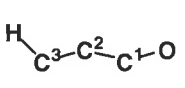
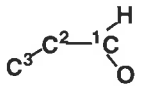
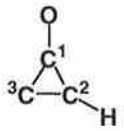

	1	2	3
State	$^2A'$	$^2A'$	$^2A'$
Symmetry	C_S	C_S	C_S
Energy (Hartrees)[a]	-189.51812	-189.45189	-189.49676
Rel. Energy (kcal mol^{-1})	0	41.6	13.4
Adiabatic electron affinity (eV)	1.06	3.72	1.9
Dipole Moment (Debye)[b]	2.65	1.31	2.71
Bond Length (Å)[b] or Angle (°)			
C^1C^2	1.38	1.44	1.45
C^2C^3	1.23	1.25	1.34
C^1C^3	2.57	2.67	1.46
C^1O	1.19	1.22	1.20
C^1H	3.64	1.10	2.41
C^2O	2.44	2.31	2.55
C^2H	2.29	2.18	1.08
C^3O	3.67	3.55	2.60
C^3H	1.07	3.20	2.36
$C^1C^2C^3$	162.5	162.7	63.0
$C^2C^1C^3$			54.9
C^2C^1O	143.9	119.9	149.2
C^2C^3H	169.1		
HC^1O		122.9	
HC^1C^2			
HC^2C^1			143.9
$C^1C^2C^3O$	0.0	0.0	0.0
$C^1C^2C^3H$	0.0	180.0	0.0

[a] CCSD(T)/aug-cc-pVDZ level of theory including zero point energy correction (calculated from vibrational frequencies at the B3LYP/6-31G* level of theory and scaled by 0.9804).[146]

[b] B3LYP/6-31G* level of theory.

1. HC_2CO

The structure of the $^2A'$ ground state neutral **1**, as computed at our chosen level of theory, exhibits a C^1-C^2 distance of 1.38 Å, indicating an elongated sp^2 double bond; by comparison, an ethylenic double bond is 1.34 Å (all reference bond lengths are computed at the B3LYP/6-31G* level). At 1.23 Å, the C^2-C^3 bond distance is greater than that of acetylene (1.20 Å), and is suggestive of an elongated *sp* triple bond. These computed values are in good agreement

with carbon-carbon bond lengths obtained from rotational spectra reported by Cooksy, *et al.*[174] of the ground state HC_2CO radical (1.39 Å and 1.22 Å, respectively). The carbon-oxygen bond length of 1.19 Å is longer than that of CO (1.14 Å), yet shorter than the C=O bond in formaldehyde (1.21 Å), and the 1.07 Å carbon-hydrogen bond is typical of a terminal C-H *sp* system. These computed carbon-oxygen and carbon-hydrogen distances also compare favourably with experimentally derived values (1.19 Å and 1.06 Å, respectively).[174] The C^1-C^2-C^3 carbon chain angle and the C^2-C^3-H angles are 162.4° and 169.1° respectively showing good agreement with the angles measured from rotational spectra (163° and 168° respectively), but the calculated O-C^1-C^2 angle of 144.0° is somewhat larger than the experimentally obtained value (136.5°).[174] The carbonyl carbon C^1 bears most of the spin density (0.518 e), with the majority of the remaining spin density located at C^3 and O (0.372 and 0.238 e respectively). The C^1-O, C^1-C^2, C^2-C^3, and C^3-H overlap populations are 0.531, 0.202, 0.641, and 0.271 e, respectively; the large relative values for C^1-O and especially C^2-C^3 strongly points to multiple bond character. The picture that emerges from this analysis is of an acetylenic carbon chain with the acetylenic centre at C^2-C^3, significant non-linearity in the C-C-O bond angle, and the unpaired electron localised on the terminal carbon carbonyl (C^1). This is in agreement with the conclusions of Cooksy, *et al.*[174] who observed only this acetylenic isomer of HC_2CO in their ground state rotational spectra.

The adiabatic electron affinity of **1** is calculated to be 1.06 eV at the CCSD(T)/aug-cc-pVDZ//B3LYP/6-31G(d) level of theory, and the dipole moment is 2.65 Debye at the B3LYP/6-31G(d) level of theory.

HC_2CO **1** been reported to be stable with respect to decomposition to CO and $^{\bullet}C_2H$, a process calculated to be endothermic by 33.6 kcal mol^{-1} at the CCSD(T)/DZP//CISD/DZP level of theory.[172]

2. C_2CHO

The structure of the $^2A'$ doublet state of C_2CHO **2** exhibits C^1-C^2 and C^2-C^3 bond lengths of 1.44 Å and 1.25 Å respectively. In the former case, the bond length is intermediate between a typical sp^2 double bond (ethylene, C=C bond length 1.34 Å), and an sp^3 single bond (ethane, C-C bond length 1.53 Å), while the latter appears to be an elongated *sp* triple bond (acetylene C-C bond length is 1.20 Å). The carbon-oxygen bond distance of 1.22 Å is very similar to the C-O bond in formaldehyde (1.21 Å), and the carbon-hydrogen bond length of 1.10 Å is slightly shorter than its formaldehyde counterpart (1.11 Å). These bond length values are different to previously reported values calculated at the MP2/6-31G(d) level of theory,[176] where the reported C^2-C^3 length is shorter (1.18 Å) and resembles more a pure acetylenic double bond, while the C^1-C^2 is longer (1.50 Å), approaching a pure single C–C bond. Bond angles also differ somewhat. At our chosen level of theory [B3LYP/6-31G(d)], the C^1-C^2-C^3, C^2-C^1-O, and C^2-C^1-H angles are 162.7°, 119.9°, and 117.3° respectively compared to 178.1°, 124.2°, and 112.2° respectively. C^3 bears most of the spin density (0.708 e), indicating that the unpaired electron is located mainly at this centre, but the value at C^2 (0.206 e) is not negligible. The C^2-C^3, C^1-O, C^1-H, and C^1-C^2 overlap populations are 0.774 e, 0.500 e, 0.368 e, and 0.278 e respectively, and are consistent with bond lengths.

The adiabatic electron affinity of **2** is calculated to be 3.72 eV at the CCSD(T)/aug-cc-pVDZ//B3LYP/6-31G(d) level of theory, and the dipole moment of is 1.31 Debye at the B3LYP/6-31G(d) level of theory.

3. (Cyclo-C_3H)=O

The (*cyclo*-C_3H)=O doublet neutral **3** structure corresponds to a $^2A'$ electronic state. The C^1-C^2, C^1-C^3, and C^2-C^3 bond lengths are 1.45 Å, 1.46 Å, and 1.34 Å respectively, and correspond to the two long sides (intermediate between the sp^3 single, and sp^2 double bonds of ethane and ethylene, respectively), and one short side (almost a typical ethylenic double bond) of a 3-membered carbon ring structure. These lengths and subsequent values are within

the range of the previously reported values calculated at higher levels of theory (CISD/DZP, SCF/DZP, and SCF/TZ2P).[172] The C^1-O bond length (1.20 Å) is very close to the reference C-O bond length (formaldehyde, 1.21 Å), and the C^2-H bond length (1.08 Å) is in line with an sp^2-s C-H bond. The population analysis indicates that the unpaired electron is located mainly at C^3 (0.469 e), but the oxygen also bears a significant proportion of spin density (0.250 e). The C^1-C^2, C^1-C^3, and C^2-C^3 overlap populations are 0.254 e, 0.292 e, and 0.280 e respectively, and 0.563 e and 0.331 e for C^1-O and C^2-H.

At the level of theory employed [CCSD(T)/aug-cc-pVDZ//B3LYP/6-31G(d)], the adiabatic electron affinity of **3** is calculated to be 1.90 eV, and the dipole moment is 2.71 Debye calculated at the B3LYP/6-31G(d) level of theory.

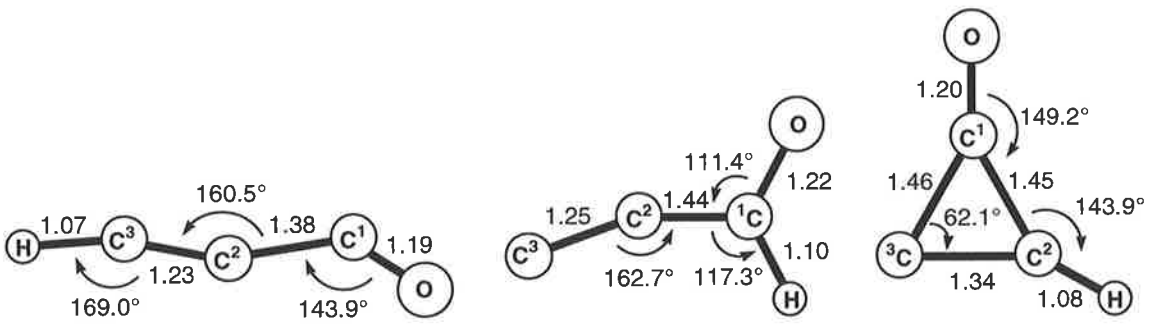

1 **2** **3**

Figure 3.1 Geometries of neutral radicals 1 - 3.

B. **The Syntheses of Ionic Precursors**

The neutral radicals **1**, **2**, and **3** were generated from either cationic or anionic precursors. The planned synthetic routes of these precursor ions are shown in Scheme 3.1. The positive ion HC_3O^+ is the simplest precursor to HC_3O **1**. It was made in the source of the mass spectrometer by loss of methanol from protonated methyl propiolate as shown in sequence (i) (Scheme 3.1). In contrast, the neutral C_2CHO **2** was generated from the negative ion

$^-C{\equiv}C{-}CHO$, formed by two methods, *viz.* (a) the S_N2 (Si) displacement reaction [39,40] shown in sequence (ii), and (b) the reaction sequence shown in sequence (iii) [the precursor $^-C{\equiv}C{-}CH(OH){-}C{\equiv}CH$ has also been used to synthesise C_2CHC_2].[177] The deuterium analogue ($^-C{\equiv}C{-}CDO$) was prepared in a similar manner [see sequence (iv) (Scheme 3.1)].

SCHEME 3.1

$$HC{\equiv}C{-}CO{-}{}^+O(H)(Me) \rightarrow HC{\equiv}C{-}C{\equiv}O^+ + MeOH \quad \text{(i)}$$

$$Me_3Si{-}C{\equiv}C{-}CHO + HO^- \rightarrow {}^-C{\equiv}C{-}CHO + Me_3SiOH \quad \text{(ii)}$$

$$HC{\equiv}C{-}CH(OH){-}C{\equiv}CH + HO^- \rightarrow {}^-C{\equiv}C{-}CH(OH){-}C{\equiv}CH + H_2O \rightarrow {}^-C{\equiv}C{-}CHO + C_2H_2 + H_2O \quad \text{(iii)}$$

$$HC{\equiv}C{-}CD(OH){-}C{\equiv}CH + HO^- \rightarrow {}^-C{\equiv}C{-}CDO + H_2O + C_2H_2 \quad \text{(iv)}$$

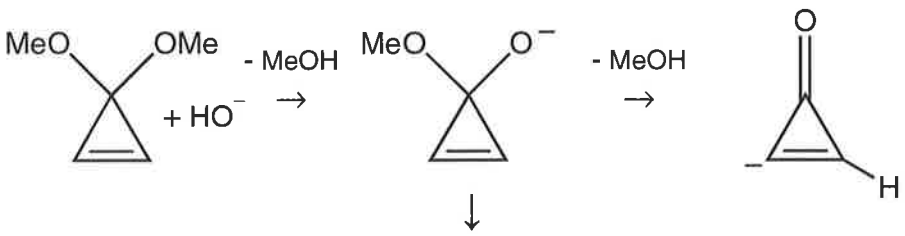

(v)

$$[(C_2H_2)\ MeO{-}{}^-CO] \rightarrow MeO{-}CH{=}CH^- + CO \quad \text{(vi)}$$

$$CH_2{=}CH{-}CO{-}SiMe_3 + O^{-\bullet} \rightarrow [C{=}CH{-}CO{-}SiMe_3]^{-\bullet} + H_2O \rightarrow [CCHCO]^{-\bullet} + Me_3Si^\bullet + H_2O \quad \text{(vii)}$$

$$CH_2{=}CH{-}CO{-}SiMe_3 + O^{-\bullet} \rightarrow CH_2{=}{}^-C{-}CO{-}SiMe_3 + HO^\bullet \rightarrow [CH_2{=}C{=}C{=}O]^{-\bullet} + Me_3Si^\bullet + HO^\bullet \quad \text{(viii)}$$

The formation of deprotonated cyclopropenone as shown in sequence (v), seemed a viable approach to the generation of the (*cyclo*-C_3H)=O species. Predictably, HO^- reacts with the dimethyl ketal of cyclopropenone via an S_N2 process, but the product alkoxide anion does not

eliminate methanol as expected; instead loss of carbon monoxide occurs [sequence (vi)]. This is not the first reported instance of the process shown in sequence (vi): deprotonated cyclopropanone was also not formed by an analogous reaction with the dimethyl ketal of cyclopropanone.[178] Because the methoxycarbonyl anion (generated subsequent to the deprotonation of the dimethyl ketal of cyclopropenone) is a good MeO^- donor [the reaction $MeO{-}{}^-CO \rightarrow MeO^- + CO$ is exothermic by 0.5 kcal mol^{-1}[179]], formation of $MeO{-}CH{=}CH^-$ with CO loss should readily occur.

Sequence (vii) illustrates how we attempted to form the anionic precursor of unstable CCHCO, reasoning that if it were possible to form the anion, charge stripping may proceed through CCHCO to the stable (cyclo-C_3H)=O **3**. Our reasoning is based on the observation that the reaction of $O^{-\bullet}$ with ethylene yields $CH_2{=}C^{-\bullet}$ and H_2O.[48] In reality, $O^{-\bullet}$ reacted exclusively as a base and formed the $[CH_2{=}C{=}C{=}O]^{-\bullet}$ radical anion as shown in sequence (viii) (Scheme 3.1; *cf.*[180]).

C. Formation of Neutrals HC_2CO and C_2CHO

The ion-molecule reactions involved in the soft ionisation techniques employed in the strategies detailed above should impart negligible excess energy into the required precursor ions ($H{-}C{\equiv}C{-}C{\equiv}O^+$ and ${}^-C{\equiv}C{-}CHO$). However, should the ionisation conditions employed yield energetically "hot" precursor ions, rearrangement could be induced in the ions prior to neutralisation, which precludes generation of the target neutrals. Accordingly, it is necessary to establish whether the precursor ions are stable towards rearrangement, or otherwise (see later). Furthermore, the required neutrals are obtained via electron capture by $H{-}C{\equiv}C{-}C{\equiv}O^+$, and electron detachment from ${}^-C{\equiv}C{-}CHO$ respectively (assuming that neither rearranges prior to neutralisation). The respective electron capture and detachment processes are followed by rapid electronic density re-distribution around the nuclear framework – an event

that occurs over the femtosecond timescale and is essentially instantaneous (termed "vertical" in the Franck-Condon sense). The nuclear structure adjusts to accommodate the re-distributed electron density much more slowly. Upon formation, the nascent neutral will initially possess the same geometry as the precursor ion. If this geometry is very close to the neutral's optimal geometry (in other words if the potential energy surfaces of both ion and nascent neutral are closely overlapped), the neutral gains minimal excess energy from the one-electron neutralisation. The converse also applies. The corollary is that an indication of the stability of the neutral obtained under the neutralisation conditions is provided by evaluating the amount of this excess energy. The excess energy of formation of the neutral from the precursor ion can be calculated as the difference in energy between the neutral minimum and that of the ion geometry on the ground-state neutral surface.[148] It should be emphasised that these calculated values are *minimum* excess energies of formation of the neutral from the ion, and do not include any excess energy that the precursor ion itself may have, or any energy imparted to the system by collision processes

Geometrically, the linearity of the HC_2CO singlet cation structure* is in contrast with the bent structure of the radical HC_2CO **1** (see Tables 3.1 and 3.2). Conversely, the structures of the C_2CHO singlet anion and the C_2CHO radical **2** are very similar. Hence, the minimum excess energy of formation of **1** following the vertical Franck-Condon transition should be appreciably more than the excess energy for formation of **2**. Indeed, the calculated values bear this prediction out: the minimum excess energy of formation by reduction of HC_3CO^+ to the radical HC_3CO **1** is 10.5 kcal mol^{-1}, whereas only 3.2 kcal mol^{-1} of energy is gained in the oxidation of ^-C_2CHO to C_2CHO **2**. Even so, these are relatively small figures; neutralisation

* The data listed in Table 2 describes the cation HC_3O^+ in the ground electronic state ($^1\Sigma$). We also located a triplet $^3A'$ state 80.3 kcal mol^{-1} higher in energy than the ground state.

of HC_2CO^+ and ^-C_2CHO should produce the stable isomers HC_2CO **1** and C_2CHO **2** respectively without inducing rearrangement or fragmentation of the neutral.

Table 3.2 Geometries and Energies of HC_3O^+ and ^-C_2CHO.

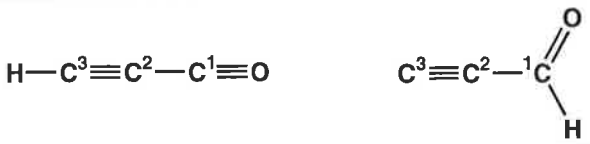

State	$^1\Sigma$	$^1A'$
Symmetry	$C_{\infty v}$	C_S
Energy (Hartrees)[a]	-189.24907	-189.58876
Dipole Moment (Debye)[b]	3.62	4.05
Bond Length (Å)[b] or Angle (°)		
C^1C^2	1.34	1.41
C^2C^3	1.22	1.23
C^1O	1.13	1.21
C^1H		1.10
C^3H	1.08	
$C^1C^2C^3$	180.0	174.8
C^2C^1O	180.0	120.1
C^2C^1H		113.7
C^2C^3H	180.0	
OC^3H		117.1
$C^3C^2C^1O$	0.0	180.0
$C^3C^2C^1H$		0.0
$C^1C^2C^3H$	0.0	

[a] CCSD(T)/aug-cc-pVDZ level of theory including zero point energy correction (calculated from vibrational frequencies at the B3LYP/6-31G* level of theory and scaled by 0.9804).[146]

[b] B3LYP/6-31G(d) level of theory.

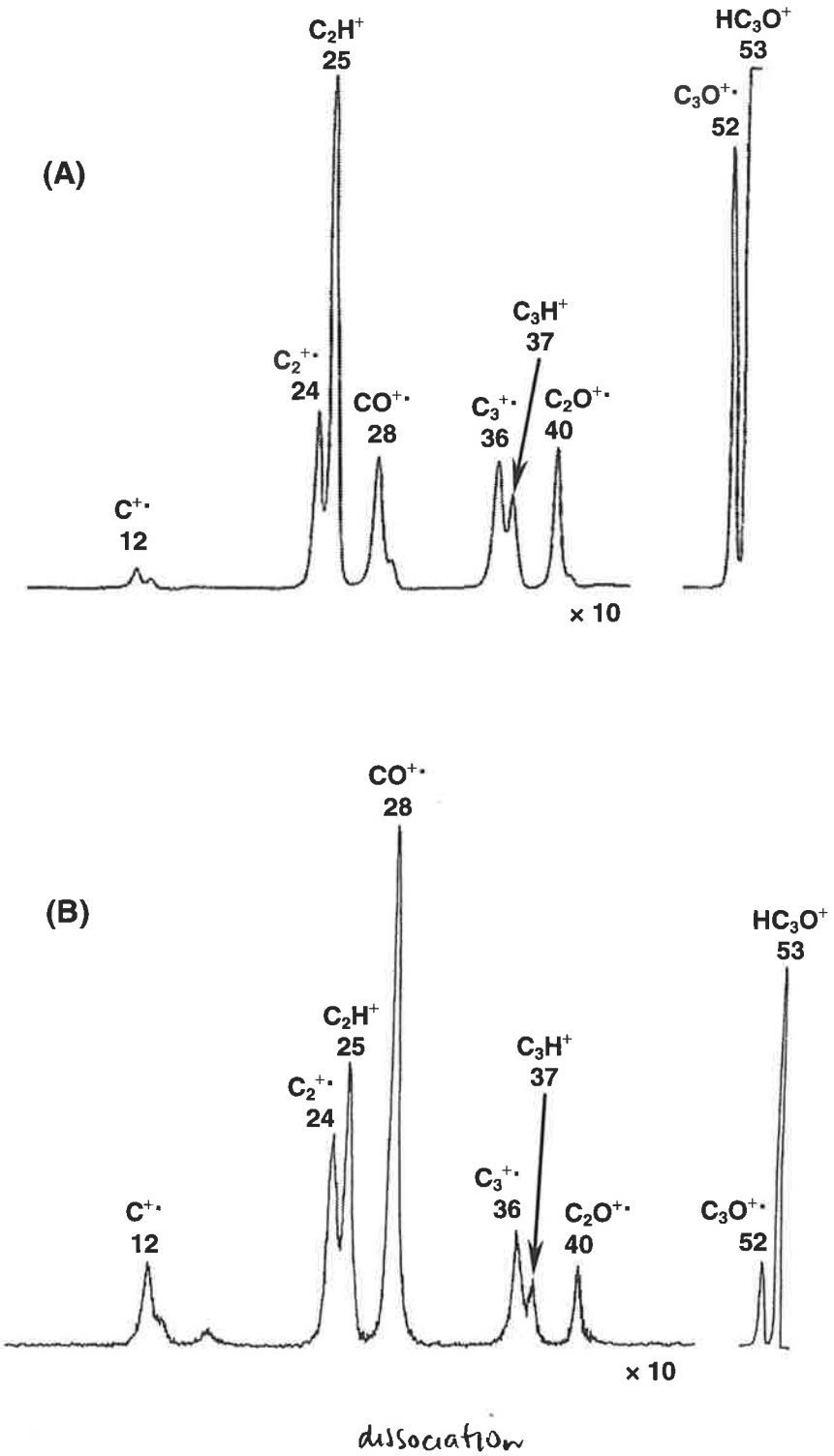

Figure 3.2 (A) Collision-induced dissociation mass spectrum (MS/MS) of HC_2CO^+. VG ZAB 2HF instrument.
(B) Neutralisation reionisation ($^+NR^+$) mass spectrum of HC_2CO^+. For experimental conditions see Experimental Section.

CID Spectrum of HC_2CO^+

Confirmation of the structure of the precursor ion HC_2CO^+ can be obtained by inspection of the collisional-induced (CID) mass spectrum (MS/MS) of HC_2CO^+ (Figure 3.2A). Fragmentations corresponding to losses of $H^\bullet$, $HC^\bullet$, $HC_2^\bullet$, and CO are consistent with the structural assignment. Identical CID spectra as shown in Figure 3.2A featuring the HC_3O^+ ion were also obtained for uracil, fumaroyl chloride, and by introducing C_2H_2 and CO into the CI source of the ZAB spectrometer (emulating on our instrument the flowing afterglow experiment of Dheandhanco *et al.*[181]) and analysing the source-formed HC_3O^+ ion, mirroring the previously reported results of the positive ion spectra of this ion.[66,181,182]

$^+NR^+$ Spectrum of HC_2CO^+

The neutralisation-reionisation ($^+NR^+$) spectrum of HC_2CO^+ depicted in Figure 3.2B shows a recovery signal (in this case, the base peak at *m/z* 53) that corresponds to the parent cation, and a variety of fragment peaks, including $C_3O^{+\bullet}$ at *m/z* 52, $CO^{+\bullet}$ at *m/z* 28, and C_2H^+ at *m/z* 25. Again, identical $^+NR^+$ spectra of the HC_3O^+ ion were obtained from uracil, fumaroyl chloride, and the experiment described above. The CID and $^+NR^+$ spectra of HC_2CO^+ show a high degree of similarity; fragment peak abundances in the both spectra are comparable, apart from an enlarged fragment ion peak at *m/z* 28 representing $CO^{+\bullet}$ and a correspondingly reduced C_2H^+ peak at *m/z* 25. This occurrence can be understood by comparing the decomposition channels available to HC_2CO^+. The major fragmentation pathways of HC_2CO^+ evident in the CID spectrum result in the production of $C_3O^{+\bullet} + H^\bullet$ and $HC_2^+ + CO$. These are the least endothermic decomposition channels available to HC_2CO^+ (see Table 3.3).

Table 3.3 Thermochemical Data for Decompositions of C_3HO Cations and Neutrals

cation process	ΔH (kcal mol^{-1})	neutral process	ΔH (kcal mol^{-1})
$HCCCO^+ \rightarrow CCCO^{+\bullet} + H^\bullet$	120	$HCCCO^\bullet \rightarrow CCCO + H^\bullet$	66
$HCCCO^+ \rightarrow HCCC^+ + O$	210	$HCCCO^\bullet \rightarrow HCCC^\bullet + O$	174
$HCCCO^+ \rightarrow HCC^\cdot + CO^{+\bullet}$	198	$HCCCO^\bullet \rightarrow HCC^\bullet + CO$	34 [172]
$HCCCO^+ \rightarrow HCC^+ + CO$	142		
$CCCHO^+ \rightarrow CCCO^{+\bullet} + H^\bullet$	-88	$CCCHO^\bullet \rightarrow CCCO + H^\bullet$	24
$CCCHO^+ \rightarrow CCC^{+\bullet} + HO^\bullet$	65	$CCCHO^\bullet \rightarrow CCC + HO^\bullet$	99
$CCCHO^+ \rightarrow CHO^+ + CC$	-42	$CCCHO^\bullet \rightarrow CHO^\bullet + CC$	104
$CCCHO^+ \rightarrow CC^{+\bullet} + CHO^\bullet$	33	$CCCHO^\bullet \rightarrow CCH + CO$	−76 ?

ΔH values are determined from the following thermochemical data [ΔH°_f (kcal mol^{-1}), ionisation energy (eV)]. HC_3O^+ (232[a]), $HC_3O^\bullet$ (64[c], 7.3[b]), C_2CHO^+ (440[c]), $C_2CHO^\bullet$ (106[c], 14.5[b]), $C_3O^{+\bullet}$ (300[a]), $C_3O^\bullet$ (78[a], 9.6[c]), HC_3^+ (383[f]), $HC_3^\bullet$ (178[c], 8.9[c]), $C_3^{+\bullet}$ (496[c]), C_3 (196[d], 13.0[d]), HC_2^+ (401[c]), $HC_2^\bullet$ (133[d], 11.6[d]), $CO^{+\bullet}$ (297[d]), CO (-26[d], 14.0[d]), HO^+ (310[c]), $HO^\bullet$ (9[d], 13.0[d]).

a From [16]

b From theoretical calculations presented in this work (see Tables 3.1 and 3.2); also HC_3O^- = -189.55699 and C_2CHO^+ = -189.05500 Hartrees [at CCSD(T)/aug-cc-pVDZ level of theory (calculated from vibrational frequencies at the B3LYP/6-31G* level of theory and scaled by 0.9804)].[146]

c From combination of thermochemical data presented above.

d From NIST database.[179]

e From [183]

f Estimated from the proton affinity of C_3 : $PA(C_3)$ = 184 kcal mol^{-1}.[184]

Turning now to the $^+NR^+$ experiment, neutralisation events which are effected by collision are inevitably accompanied by the fragmentation of a proportion of the population of neutrals. Neutral fragment species are thus produced (in line with the CID fragmentation processes) along with the neutralised parent ions. All the neutrals are transmitted together while the charged species are deflected away from the beam of neutral species. This neutral beam must comprise a sizeable proportion of C_3O and CO neutrals that are subsequently reionised together with the parent $HC_2CO^\bullet$, with the consequence that the $^+NR^+$ spectrum exhibits a larger abundance of $CO^{+\bullet}$ fragment peak at *m/z* 28 (contributions of neutral fragments to NR

spectra are termed Neutral fragment Reionisation, N_fR). [185] On the other hand, direct decomposition of neutral $HC_2CO^{\bullet}$ could account for the observed peak abundance differences in the $^{+}NR^{+}$. However, the thermochemically most favourable decomposition channel available to $HC_2CO^{\bullet}$ produces $HC_2^{\bullet}$ + CO in a process that is endothermic by 34 kcal mol^{-1} (see Table 3.3 and [172]). The ionisation energies of $HC_2^{\bullet}$ and CO are 11.6 and 14.0 eV, respectively (see also Table 3.3), therefore if direct decomposition of neutral $HC_2CO^{\bullet}$ is occurring, the $^{+}NR^{+}$ spectrum should show a more pronounced peak at *m/z* 25 (HC_2^{+}) rather than at *m/z* 28 ($CO^{+\bullet}$). Instead the converse is observed. Thus, the possibility that the neutral is directly decomposing is ruled out, and the greater part of $HC_2CO^{\bullet}$ is stable over the timescale of the NR experiment (*ca* 10^{-6} sec.).

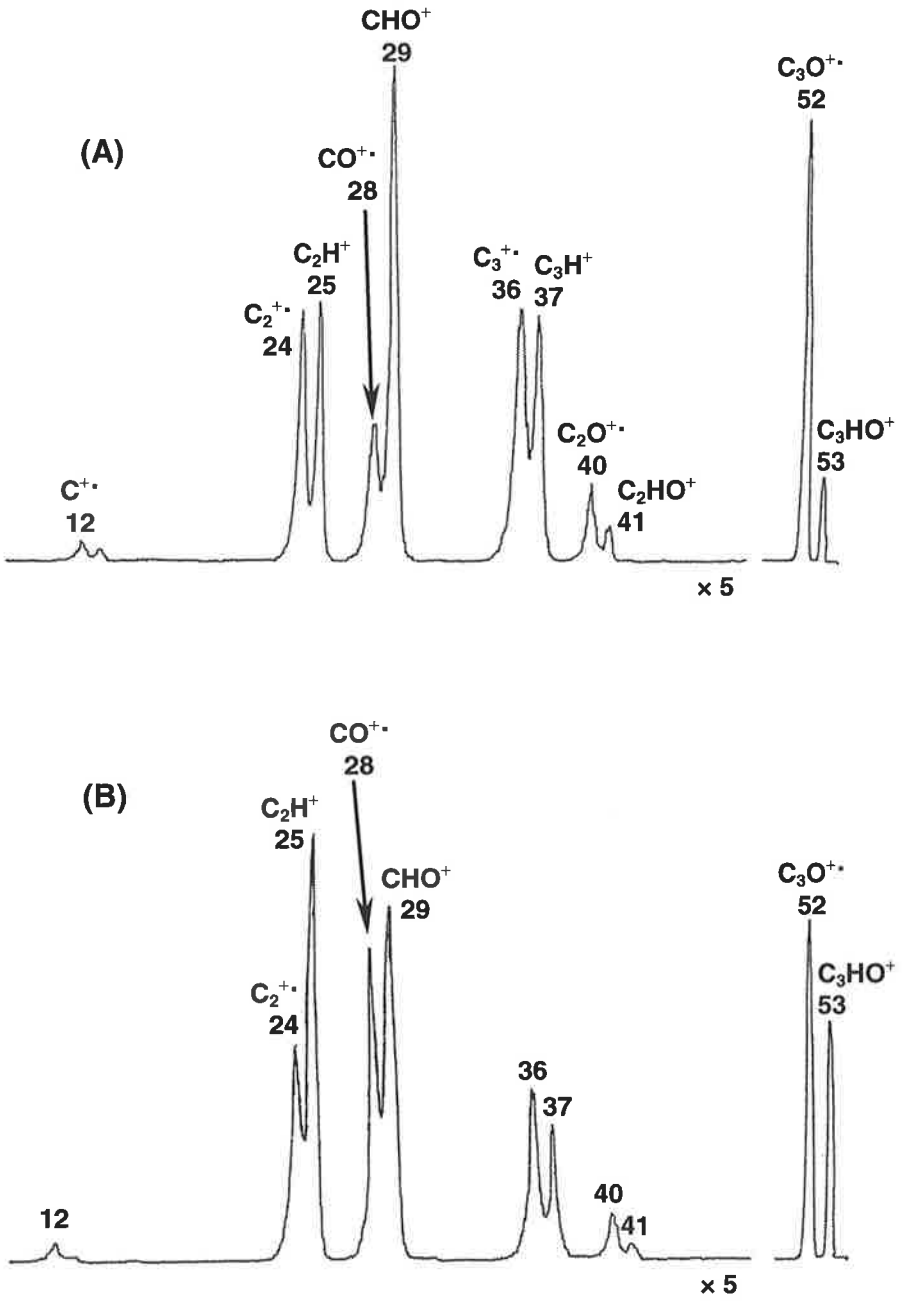

Figure 3.3 (A) Charge reversal ($^-CR^+$) mass spectrum of ^-C_2CHO. VG ZAB 2HF instrument.
(B) Neutralisation reionisation ($^-NR^+$) mass spectrum of ^-C_2CHO. For experimental conditions see Experimental Section.

CR Spectrum of $^-C{\equiv}C{-}CHO$

Figure 3.3A depicts the CR spectrum of $^-C{\equiv}C{-}CHO$. The most prominent features of the spectrum are the fragmentations of the parent cation corresponding to the exothermic losses of $H^\bullet$ and C_2, and the endothermic loss of $^\bullet CHO$ (by 33 kcal mol^{-1} - see Table 3.3). These processes are mirrored in the corresponding spectrum of $^-C{\equiv}C{-}CDO$ (see Table 3.4), being diagnostic of the proposed C–C–CXO (X = H, D) connectivity, and are in line with the known connectivity of the precursor anion. These observations indicate that the anion does not rearrange upon collisional activation.

$^-NR^+$ Spectrum of $^-C{\equiv}C{-}CHO$

There are considerable differences observed in the $^-NR^+$ spectrum of $^-C{\equiv}C{-}CHO$ (Figure 3.3B) compared with the $^+NR^+$ spectrum of HC_2CO^+ (Figure 3.2B). The neutralisation-reionisation and the corresponding charge reversal spectra of $^-C{\equiv}C{-}CHO$ are similar with respect to the fragment ion peaks observed. Fragmentation of C_2CHO^+ to give $C_3O^{+\bullet} + H^\bullet$ and $C_2^\bullet + CHO^+$ are exothermic processes (see Table 3.3) so it is not surprising to see peaks corresponding to loss of $H^\bullet$ and $C_2^\bullet$ from C_2CHO^+. The observable differences between the $^-NR^+$ and $^-CR^+$ spectra are in the relative abundances of the peaks at *m/z* 25 corresponding to loss of CO, and at *m/z* 28 corresponding to loss of $^\bullet C_2H$; both are more abundant in the $^-NR^+$ than in the $^-CR^+$ spectrum. These observations suggest that while charge-stripping of $^-C{\equiv}C{-}CHO$ does produce neutral C_2CHO **2**, the collision-induced vertical oxidation effected during charge stripping of the precursor anion imparts sufficient excess energy to a proportion of neutrals to cause them to rearrange. The positive ion spectrum of the neutral that results from this isomerisation exhibits strong peaks corresponding to charged CO and C_2H. If this isomerisation involves H migration, the probable product would be either $HC_2CO^\bullet$ **1** or (*cyclo*-C_3H)=O **3**. Generation of **3** experimentally by methodologies analogous to those

employed in the generation of **1** and **2** was unsuccessful; hence, the possible rearrangement channels available to **2** have been investigated by theoretical means.

Table 3.4 $^-CR^+$ and $^-NR^+$ Mass Spectra of $^-C{\equiv}C{-}CDO$ [*m/z* (Relative Abundance)]

charge reversal (CR)	peak composition	neutralisation reionisation ($^-NR^+$)
54 (46)	C_3DO	54 (100)
52 (100)	$C_3O^{\bullet}$	52 (98)
42 (2)	C_2DO	42 (4)
40 (3)	$C_2O^{\bullet}$	40 (7)
38 (14)	C_3D	38 (15)
36 (12)	$C_3^{\bullet}$	36 (14)
30 (21)	CDO	30 (20)
28 (8)	$CO^{\bullet}$	28 (12)
26 (13)	C_2D	26 (31)
14 (1)	CD	14 (1)
12 (1)	$C^{\bullet}$	12 (1)

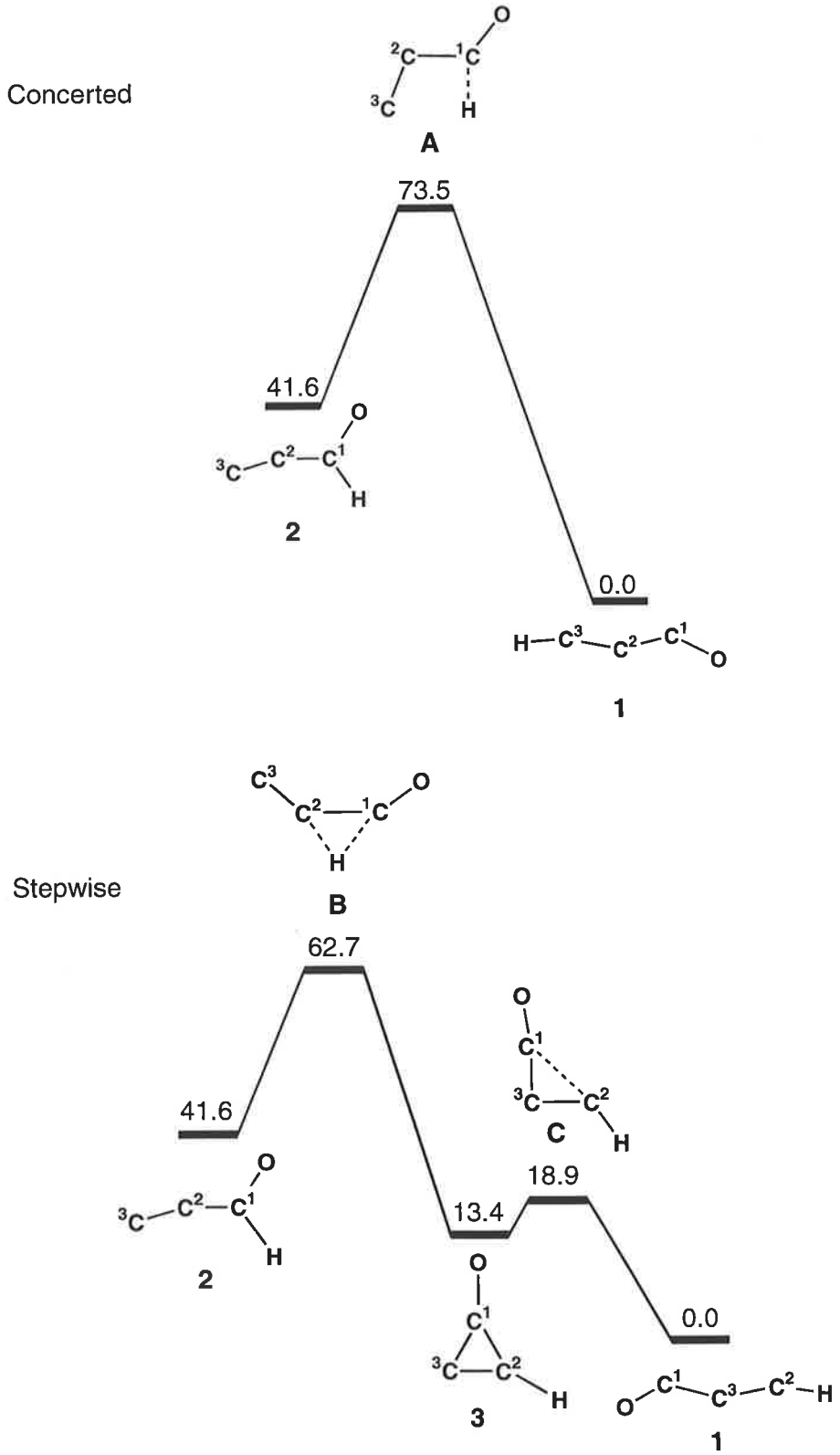

Figure 3.4 Concerted and stepwise rearrangements of C_2CHO 2. CCSD(T)/aug-cc-pVDZ//B3LYP/6-31G(d) level of theory. Relative energies (kcal mol^{-1}) in relation to 1 (0.0 kcal mol^{-1}). Full data for neutrals: see Figure 3.1 and Table 3.1. Data for transition states A - C: see Table 3.5.

D. Theoretical Studies of the Rearrangement of Neutral C_2CHO.

The results of a computational study of various isomerisation processes of the C_2CHO radical are illustrated in Figure 3.4. The geometries of the local minima and the transition states were optimised at the B3LYP/6-31G(d) level of theory. Energies were subsequently refined at the CCSD(T)/aug-cc-pVDZ level. Geometries of three stable HC_3O isomers **1**, **2** and **3** and their energies (including energies relative to HC_2CO, the global minimum on the doublet neutral potential surface, set at 0.0 kcal mol^{-1}) are listed in Table 3.1, and geometry data pertaining to the three transition states **A**, **B** and **C** involved in the two competitive rearrangement channels investigated are summarised in Table 3.5.

Neutral C_2CHO **2** may rearrange to form HC_2CO **1** by means of H-migration. Accordingly, we have identified two possible rearrangement channels for this isomerisation. The first is a synchronous pathway involving H-migration from C^1 to C^3. This rearrangement occurs via the four-membered transition state **A** and with a calculated activation energy barrier of 31.9 kcal mol^{-1}. The other rearrangement pathway involves a series of isomerisation steps in which the first occurs via 1,2 H transfer (from C_1 to C_2) via transition sate **B** over a barrier of 21.1 kcal mol^{-1}. The product of this isomerisation would seem to be $^{\bullet}$CCHCO, however no local minimum that corresponds to this geometry could be identified on the neutral surface. Instead, 1,2 H migration is immediately followed by ring closure to yield the cyclic isomer (cyclo-C_3H)=O **3**. Should isomer **3** form with sufficient excess energy to overcome the barrier to ring cleavage (5.5 kcal mol^{-1}), it will form HC_2CO **1**. This can proceed through transition state **C** for specific C^1-C^2 bond cleavage, located 18.9 kcal mol^{-1} above the global minimum. The two pathways have as the end result a neutral with the same HC_2CO geometry, except that the product of the stepwise pathway also exhibits a rearrangement in the carbon backbone (see Figure 3.4). Therefore, it remains to be established which of the two processes occurs preferentially. A conventional approach at resolving such a conundrum would involve ^{13}C-

labelling at either C^2 or C^3 of the precursor anion and then analysing the resultant $^-NR^+$ spectrum. However, after considering the fragmentations obtained from the neutralised-reionised ^-C_2CHO (Figure 3.3B), no key fragment is evident that could be used as a definitive mechanistic probe. Consequently, a labelling study was not attempted.

The two primary factors governing reaction rates of gas phase reactions are (i) the barrier to the transition state, and (ii) the probability of reaction (the frequency factor, or pre-exponential Arrhenius factor)[186] in the rate equation. These will be considered in turn.

Barriers to Transition States

Regardless of mechanism, each step in the rearrangement process has an activation energy barrier that must be overcome in order for the isomerisation to proceed. From a thermochemical standpoint, the stepwise pathway seems energetically more accessible; in the rate determining step of the stepwise process (the 1,2 H migration prior to cyclisation), the activation energy barrier is lower by 10.9 kcal mol^{-1} than that of the synchronous pathway. Clearly, since the minimum excess energy gained by vertical Franck-Condon oxidation of ^-C_2CHO to the corresponding neutral is only 3.2 kcal mol^{-1}, the system must acquire sufficient energy via the collision event during neutralisation.

Table 3.5 Geometries and Energies of Transition States A – C (see Figure 3.4).

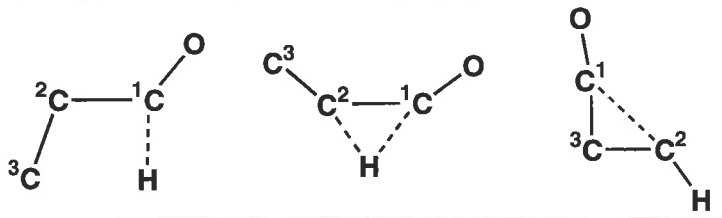

	A	B	C
State	$^2A'$	$^2A'$	$^2A'$
Symmetry	C_s	C_s	C_s
Energy (Hartrees)[a]	-189.40092	-189.41813	-189.48794
Rel. Energy (kcal mol^{-1})	73.5	62.7	18.9
Bond Length (Å)[b] or Angle (°)			
C^1C^2	1.39	1.32	1.83
C^1C^3			1.38
C^2C^3	1.32	1.32	1.34
C^1O	1.19	1.18	1.16
C^1H	1.28	1.38	
C^2H			1.09
$C^1C^2C^3$	92.7	176.7	
$C^1C^3C^2$			85.0
C^2C^1O	150.8	170.8	
C^3C^1O			172.6
OC^3H	113.5		
C^2C^1H	95.7		
C^3C^2H		119.8	137.7
C^1C^2H		63.4	
$C^3C^2C^1O$	180.0	0.0	180.0
$C^2C^3C^1O$			180.0
$C^3C^2C^1H$	180.0	180.0	180.0
$C^1C^2C^3H$	180.0	180.0	180.0

[a] CCSD(T)/aug-cc-pVDZ level of theory including zero point energy correction (calculated from vibrational frequencies at the B3LYP/6-31G* level of theory and scaled by 0.9804).[146]

[b] B3LYP/6-31G(d) level of theory.

Table 3.6. Vibrational Partition Functions for Transition States A and B (Figures 3.4 and 3.5)

A		B	
frequency	Q'_{vib}	frequency	Q'_{vib}
301.9337	1.3025	213.7079	1.5524
474.1521	1.1124	295.1187	1.3159
695.5204	1.0359	596.7254	1.0591
761.5058	1.0258	783.6761	1.0231
1121.7496	1.0044	918.4504	1.0119
1498.5768	1.0007	1595.4821	1.0005
1687.5169	1.0003	1669.9188	1.0003
1935.8658	1.0001	2204.6719	1.0000
total	**1.5481**	total	**2.2417**

Pre-exponential Arrhenius factor

In general, the 'looser' (more disordered) the transition state, the higher the rate of reaction. To determine the relative abilities of the neutral to access the various rearrangement channels requires an intimate knowledge of the potential surface maps for those processes. In the absence of this knowledge, the entropic natures of the two transition states may be determined by calculating the relative pre-exponential Arrhenius factors, *A*. An assessment of the relative *A* factors for the various competing rearrangement channels can be made using transition state theory (see pp 55-59 and),[114] *viz.* Equation 1.3.10,

EQUATION 1.3.10

$$k(T) = (k_B T/h)\,(Q^{\ddagger}/Q_R)\exp(E_o/k_B T)$$

where k_B is Boltzmann's constant, h is Planck's constant, E_o is the energy difference between reactant and transition state at 0 K, and $Q^{\ddagger}$ and Q_R are the molecular partition functions of transition state and reactants respectively. The partition function can be factorised into partition functions for translation, rotation, vibration and electronic state,[114] *viz.* Equation 1.3.15.

EQUATION 1.3.15

$$Q = Q_{Trans} \times Q_{Rot} \times Q_{Vib} \times Q_{Elec}$$

The rearrangements are occurring on a neutral potential energy surface; if we assume large electronic energy separations between energy levels, and thermally inaccessible degenerate states (at normal temperatures, at least), then $Q_{Elec} = 1$. These are unimolecular rearrangements, in which case Q_{Trans} of both the reactant and transition state are identical, and we assume (to a first approximation) that the same is true for Q_{Rot}. Thus approximation of the *A* factor for each process simplifies to evaluating Q_{Vib} for the reactant and for the competing transition states. However it must be noted that the anions in a mass spectrometer, especially following collisional activation, will not follow a Boltzmann (thermalised) distribution of internal energies. Thus the following calculations must only be considered in a qualitative sense. The methodology adopted for this calculation has been described previously. The results are displayed in Table 3.6. The vibrational partition function for transition state **A** (Figure 3.4) is 1.55, whereas that for **B** (Figure 3.4) is 2.24, with the result that the stepwise process shown in Figure 3.4 is favoured both by the smaller barrier to the transition state in the rate determining step and by the larger Arrhenius factor.

Finally, the HC_3O products of the reaction sequence shown in Figure 3.4 could have minimum formation energies of up to 62.6 kcal mol^{-1} unless they are being de-energised either by collision or radiation* in the collision cell. It may be, therefore, that some of the HC_3O neutrals formed in the isomerisation process have sufficient energy to decompose to yield CO and $\cdot C_2H$ (a process which is endothermic by 33.6 kcal mol^{-1}).[172]

* While radiative processes are common for cations, they have not been specifically reported for neutralisation reionisation processes. See, e.g.[187]

E. Conclusions

An experimental and theoretical study has been carried out in which evidence is presented for the formation of $HC_2CO^{\bullet}$ from HC_2CO^+ and $^{\bullet}C_2CHO$ from ^-C_2CHO. Since the neutral species are formed via collision processes, energy imparted into the nascent C_2CHO neutral **2** induces a proportion to rearrange to $HC_2CO^{\bullet}$ **1**. The evidence indicates that some of these energised HC_2CO radicals decompose to yield CO and $^{\bullet}C_2H$. On energetic grounds, rearrangement seems more likely than straight cleavage of C_2CHO since all cleavage processes are endothermic by at least 24 kcal mol^{-1} (see Table 3.3), compared with a barrier of 21 kcal mol^{-1} in the rate determining step of the most probable rearrangement pathway (see Figure 3.4). The isomerisation may proceed via (i) a synchronous rearrangement of C_2CHO and/or (ii) a stepwise pathway via the intermediacy of (*cyclo*-C_3H)=O. The second of the two isomerisation processes is suggested to occur with the higher rate ~~is~~ because it exhibits a lower barrier in the rate determining step and a higher calculated Arrhenius pre-exponential *A* factor.

III. Experimental Section

A. Mass Spectrometric Methods

All mass spectra were measured using a modified VG ZAB 2HF mass spectrometer with BE configuration (where B and E represent magnetic and electric sectors, respectively) equipped with tandem collision cells between the magnetic and electric sectors. The instrument was used in both the positive ion chemical ionisation (PICI) mode, and the negative ion chemical ionisation (NICI) mode, as appropriate. The MH^+ ion of methyl propiolate was formed using methanol as the protonating agent, and negative ions were formed in the chemical ionisation source using either deprotonation of the sample with HO^- or by an S_N2 (Si) reaction between HO^- and a trimethylsilyl derivative ($HO^- + Me_3SiR \rightarrow R^- + Me_3SiOH$).[39] Samples were introduced through the septum inlet (maintained at 100°C) to a measured pressure of 5×10^{-7} Torr, together with the reagent gas (either methanol for PICI, or water for NICI) at a measured pressure of 1×10^{-5} Torr. The estimated total pressure in the chemical ionisation source is 10^{-1} Torr.[188] The ion source temperature was 200°C, the accelerating voltage was 7 kV, and the slits were fully open to obtain maximum sensitivity. Collisional activation MS/MS experiments were carried out using the magnet to focus and transmit the ion beam under study, the ion beam was intercepted at the first of the tandem collision cells which contained argon as collision gas at a measured pressure of 1×10^{-6} Torr [reducing the beam transmission to 80% (equivalent to single collision conditions)]. Ionic dissociation products were detected by scanning the electric sector. The same experimental parameters were used for CR experiments,[67,71,149] except that polarity of the sector voltage was reversed to allow the detection of positive ions, and O_2 was used as the collision gas. Neutralisation reionisation [$^+NR^+$ (magnet set for transmission of positive ions) or $^-NR^+$ (magnet set for transmission of negative ions)] experiments [78,86] were carried out as for CR experiments. Dioxygen was used as the collision gas in both collision cells (pressure measured outside each cell = 1×10^{-6} Torr, 80% beam transmission through collision cells) for $^-NR^+$ experiments. For $^+NR^+$ experiments,

benzene was used in the first collision cell, while O_2 was used in the second cell (pressures as for $^{-}NR^{+}$ experiments). For both $^{-}NR^{+}$ and $^{+}NR^{+}$ experiments, the deflector plate between the two collision cells was switched on in order to deflect all ions before they enter the second collision cell.

B. Computational Methods

Molecular geometries were optimised and the vibrational frequencies computed exclusively according to the Becke 3LYP exchange-correlation functional. This hybrid functional consists of the Lee-Yang-Parr correlation functional [153] and Becke's three-parameter exchange functional.[151] The exchange functional is a linear combination of the local density approximation, Becke's gradient correction,[154] and the "exact" Hartree-Fock exchange energy. This hybrid method has been shown to be more accurate than standard gradient-corrected methods.[155] The 6-31G(d) polarisation basis set was employed, which uses six primitive Gaussians for the core orbitals, a three/one split for the *s*- and *p*-valence orbitals, and a single set of six *d*-functions. All calculations were performed within the GAUSSIAN 98 [156] computational chemistry package. Stationary points on potential energy surfaces were characterised as either minima (no imaginary frequencies) or transition states (one imaginary frequency) by calculation of the frequencies using analytical gradient procedures. The connection between minima and a given transition structure was established by examining the reaction path on the potential energy surface leading away from the transition structure in an intrinsic reaction coordinate (IRC) calculation. Zero-point vibrational energies were also determined from calculated frequencies and used as a zero-point energy correction for the electronic energies calculated at this and higher levels of theory.

Higher accuracy energies for the B3LYP optimised geometries were obtained using the coupled cluster method, CCSD(T).[101,158] This method features all single and double substitutions [159] augmented by a quasi-perturbative account for triple excitations,[103] and is

known to yield correlation energies very close to the exact *n*-particle solution within the given basis set as long as the Hartree-Fock determinant is a reasonably good zero-order reference wavefunction.[98] Single-point energy calculations employed the large augmented correlation-consistent polarised double-zeta basis set aug-cc-pVDZ of Dunning [111,160] which incorporates d functions [maximum angular momentum $l = 2(d)$] to heavy atoms.

Experimental electron affinity values are still not available for HC_3O, so it is not possible to compare calculated values with experimental values. However we have compared calculated values of electron affinities at this level of theory with experimental values in previous studies, *viz.* for C_3H (calculated 1.79 eV, experimental 1.86 eV)[12] and C_2CH_2 (calculated 1.67 eV, experimental 1.79 eV).[177]

Calculations were performed on the Power Challenge Super Computer at the South Australian Super Computing Centre (Adelaide) and the Silicon Graphics Power Challenge Super Computer at the Australian National University Super Computing Facility (Canberra).

C. Synthetic Procedures

Methyl propiolate used was a commercial sample. **3-Hydroxypenta-1,4-diyne** and **3-$^1H_1$-3-hydroxypenta-1,4-diyne** were available from a previous study.[189] **Trimethylsilyl vinyl ketone**,[190] and **Cyclopropenone dimethyl ketal** [191] were made by reported methods.

IV. Appendix

Table A3.1 **Harmonic frequencies (in cm^{-1}) and infrared intensities (in km mol^{-1}) for the doublet ground state of the HC_3CO neutral 1. Harmonic frequencies are unscaled.**

mode	symmetry	frequency	intensity
ω_1	A'	3481	73.4
ω_2	A'	2078	172.2
ω_3	A'	1942	187.1
ω_4	A'	882	0.3
ω_5	A"	744	30.4
ω_6	A'	461	0.9
ω_7	A'	364	60.3
ω_8	A"	242	0.2
ω_9	A'	135	12.1

Table A3.2 **Harmonic frequencies (in cm^{-1}) and infrared intensities (in km mol^{-1}) for the quartet state of the C_2CHO neutral 2. Harmonic frequencies are unscaled.**

mode	symmetry	frequency	intensity
ω_1	A'	3017	77.2
ω_2	A'	17697	186.1
ω_3	A'	15417	262.0
ω_4	A'	1397	4.7
ω_5	A"	973	2.9
ω_6	A'	925	325.1
ω_7	A'	538	79.6
ω_8	A"	218	0.9
ω_9	A'	206	35.6

Table A3.3 Harmonic frequencies (in cm^{-1}) and infrared intensities (in km mol^{-1}) for the doublet ground state of the (*cyclo*-C_3H)=O neutral 3. Harmonic frequencies are unscaled.

mode	symmetry	frequency	intensity
ω_1	A'	3259	4.9
ω_2	A'	1948	295.6
ω_3	A'	1556	7.9
ω_4	A'	1025	18.4
ω_5	A'	874	1.2
ω_6	A"	783	46.4
ω_7	A'	732	37.9
ω_8	A"	529	0.5
ω_9	A'	428	9.6

Table A3.6 Dipole moments and rotational constants for the three stable HC_3O neutrals and for the HC_2CO cation and C_2CHO anion. Parameters are given for the ground electronic states only and are calculated from the equilibrium geometry at the B3LYP/6-31G(d) level of theory.

Parameters†	**1** $HC_2CO^{\cdot}$	**2** $^{\cdot}C_2CHO$	**3** $^{\cdot}$*cyc*-(C_3H)=O	HC_2CO^+	^-C_2CHO
μ_z	0.000	0.000	0.000	0.000	0.000
μ_y	2.638 [a]	0.610	-2.352 [c]	-3.5812 [d]	4.0049 [e]
μ_x	-0.246	-1.159 [b]	-1.357	0.0011	0.6315
$\|\|\mu\|\|$	2.649	1.310	2.715	3.5812	4.0544
A	362307	74750	37700	-	79535
B	4489	5176	8107	4426	5000
C	4435	4841	6672	4426	4704

† Dipole moments are given in Debye and rotational constants are given in MHz.

[a] The molecule is oriented as depicted in Figure 3.1 with the x and y axes defining the plane of the page. Positive x axis is to the bottom and positive y axis is to the right of the figure.

[b] The molecule is oriented as depicted in Figure 3.1 with the x and y axes defining the plane of the page. Positive x axis is to the bottom right and positive y axis is to the top right of the figure.

[c] The molecule is oriented as depicted in Figure 3.1 with the x and y axes defining the plane of the page. Positive x axis is to the bottom left and positive y axis is to the bottom right of the figure.

[d] The molecule is oriented as depicted in Table 3.1 with the x and y axes defining the plane of the page. Positive x axis is to the right and positive y axis is to the top of the figure.

[e] The molecule is oriented as depicted in Table 3.1 with the x and y axes defining the plane of the page. Positive x axis is to the bottom and positive y axis is to the figure.

4 Gas Phase Generation of Neutral HC_3S Isomers from Charged Precursors: An Experimental and Theoretical Study

I. Introduction

The elements hydrogen, carbon, oxygen, and sulfur are among the most abundant atoms in the universe,[192] however comparatively few sulfur-containing molecules have been detected within interstellar or circumstellar regions of space. Amongst the identified interstellar sulfur-containing species are the polycarbon sulphide radicals C_2S and C_3S, which where found in the Taurus Molecular Cloud (TMC-1) in 1987 in significant abundance,[193,194] and within the circumstellar envelope of the carbon-rich star IRC+10216.[194,195] Larger polycarbon sulphides, C_4S and C_5S, have been characterised spectroscopically [196] but have not yet been unequivocally identified within interstellar clouds. C_4S has nevertheless been proposed as a plausible interstellar species, while there has been tentative assignment of C_5S within IRC+10216.[194] Given that many of the C_nS series have either been identified or are strong candidates for detection within interstellar or circumstellar media, it is conceivable that the hydrogenated carbon-chain-sulfur radicals of the form HC_nS ~~are~~ may also be present.

The cosmic abundance of the element sulfur is 1.5 orders of magnitude below that of oxygen,[197] yet it is surprising that CCS and CCCS occur at unusually large abundances within TMC-1 with respect to the corresponding oxygen-containing carbon-chain molecules, CCO [198] and CCCO [165] (indeed the CCCS abundance is significantly larger than CCCO).[199] Any proposed synthetic pathway to these sulfur-containing carbon-chain molecules must be able to take into account the observed high abundances. In this regard, the existing models that have focussed on ion-molecule reaction mechanisms [200,201] have been found to have limitations.[202] A viable mechanism suggested to operate within the circumstellar envelope IRC + 10216 (but not necessarily in the interstellar cloud TMC-1, where the calculated abundance of $C_2H_2^+$ may be too low)[203] involves reactions of hydrocarbon ions with sulfur-containing neutrals,[204] *viz.*

$C_2H_2^{+\bullet} + CS \rightarrow HCCCS^+ + H^\bullet$

followed by dissociative recombination:

$HCCCS^+ + e \rightarrow CCCS + H^\bullet$

However, the dissociation process itself is endothermic by 63.5 kcal mol^{-1}; this implies that neutral HC_3S may have a significant lifetime if the energy of the captured electron is lower than the dissociation threshold.

Many reactions of radicals, with other radicals or with unsaturated neutrals have been found to lack activation energy barriers,[201,205] and as such these processes may be viable processes at cold interstellar molecular cloud temperatures (~10K). Accordingly, radical-neutral pathways to C_nS have been put forward.[202,206] The continuing debate in the literature over the synthetic pathways towards sulfur-containing carbon-chain molecules, is not, however, mirrored by one concerning their neutral hydrides, for which there seems to be a conspicuous lack of discussion. One recent theoretical study of the potential energy surfaces of the S + *c*-C_3H and S + *l*-C_3H reactions [207] highlights a number of doublet and quartet minima of the neutral HC_3S class of molecules which are simply presented as reaction intermediates in these reactions. Our aim in the work presented below is to prepare HC_3S neutral radicals from charged precursors and to investigate their stability.

II. Results and Discussion

A. Theoretical Studies of HC_3S Isomers

The singlet anionic and the doublet neutral surfaces of HC_3S feature a number of minima. The geometry data for the ground states and the relative energies of the stable neutral species are given in Table 4.1, and the structures of the ground state neutrals are depicted in Figure 4.1. The relative energies of the stable anionic species are given in Table 4.2 and their structures are represented in Figure 4.2.

Table 4.1 Geometries and Energies of Neutral Isomers 1 - 4.

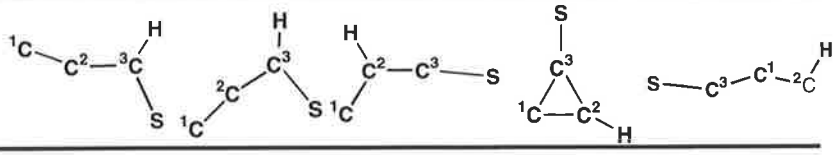

	1	1q	2	3	4
State	$^2A'$	$^4A'$	$^2A''$	$^2A'$	$^2A'$
Symmetry	C_S	C_S	C_S	C_S	C_S
Energy (Hartrees)[a]	-512.06863	-512.14679	-512.05375	-512.10763	-512.13058
Rel. Energy (kcal mol^{-1})	38.87	-10.17	48.21	14.39	0.00
Adiabatic electron affinity (eV)	7.76	5.63	8.16	6.70	6.07
Dipole Moment (Debye)[b]	4.04	3.85	2.00	2.42	1.24
Bond Length (Å)[b] or Angle (°)					
C^1C^2	1.29	1.33	1.35	1.35	1.26
C^2C^3	1.37	1.36	1.38	1.42	2.56
C^1C^3	2.66	2.69	2.53	1.47	1.31
C^2H			1.09	1.09	1.08
C^3S	1.68	1.75	1.57	1.62	1.57
C^3H	1.09	1.08			
$C^1C^2C^3$	179.2	173.7	124.3	64.0	
$C^2C^1C^3$				60.2	172.1
$C^2C^3C^1$				55.8	
C^2C^3S	111.4	96.5	179.1	144.2	
C^1C^3S					176.8
C^2C^3H	125.0	134.3			151.6
SC^3H	123.6	129.1			
C^1C^2H			104.6	154.2	
$C^1C^2C^3S$	180.0	0.0	0.0	180.0	
$C^3C^2C^1S$					180.0
$C^1C^2C^3H$	0.0	180.0	180.0		
$C^2C^3C^1H$				180.0	180.0

[a] CCSD(T)/aug-cc-pVDZ level of theory including zero point energy correction (calculated from vibrational frequencies at the B3LYP/aug-cc-pVDZ level of theory).

[b] B3LYP/aug-cc-pVDZ level of theory.

Table 4.2 Geometries and Energies of Anions.

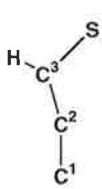
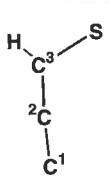
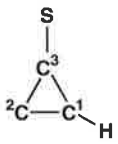
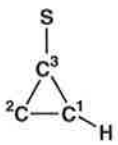
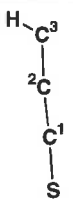
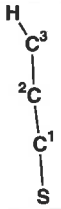

	1^-	$1t^-$	3^-	$3t^-$	4^-	$4t^-$
State	$^1A'$	$^3A''$	$^1A'$	$^3A''$	$^1A'$	$^3A''$
Symmetry	C_s	C_s	C_s	C_s	C_s	C_s
Energy (Hartrees)[a]	-512.35374	-512.13419	-512.19668	-512.10853	512.18672	-512.18260
Rel. Energy (kcal mol^{-1})	0.00	137.77	98.56	153.87	104.81	107.39
Dipole Moment (Debye)[b]	4.92	5.25	1.46	0.87	2.98	0.87
Bond Length (Å)[b] or Angle (°)						
C^1C^2	1.27	1.29	1.40	1.35	1.28	1.29
C^2C^3	1.38	1.38	1.46	1.46	1.34	1.30
C^1C^3	2.65	2.67	1.37	1.42	2.61	2.59
C^1S					1.64	1.64
C^1H			1.09	1.09		
C^3S	1.69	1.76	1.69	1.63		
C^3H	1.10	1.09			1.12	1.08
$C^1C^2C^3$	174.8	178.8	64.0	60.7	171.2	172.2
$C^2C^1C^3$			57.0	63.4		
$C^2C^3C^1$			59.0	55.9		
C^2C^1S					177.5	178.6
C^2C^3S	129.2	109.6	149.7	154.9		
C^2C^1H			146.3	154.9		
C^2C^3H	115.4	127.2			111.4	140.7
SC^3H	115.4	123.3				
$C^1C^2C^3S$	180.0	0.0	180.0	180.0		
$C^3C^2C^1S$					180.0	180.0
$C^1C^2C^3H$	0.0	180.0			180.0	180.0
$C^2C^3C^1H$			180.0	180.0		

[a] CCSD(T)/aug-cc-pVDZ level of theory including zero point energy correction (calculated from vibrational frequencies at the B3LYP/aug-cc-pVDZ level of theory).

[b] B3LYP/aug-cc-pVDZ level of theory.

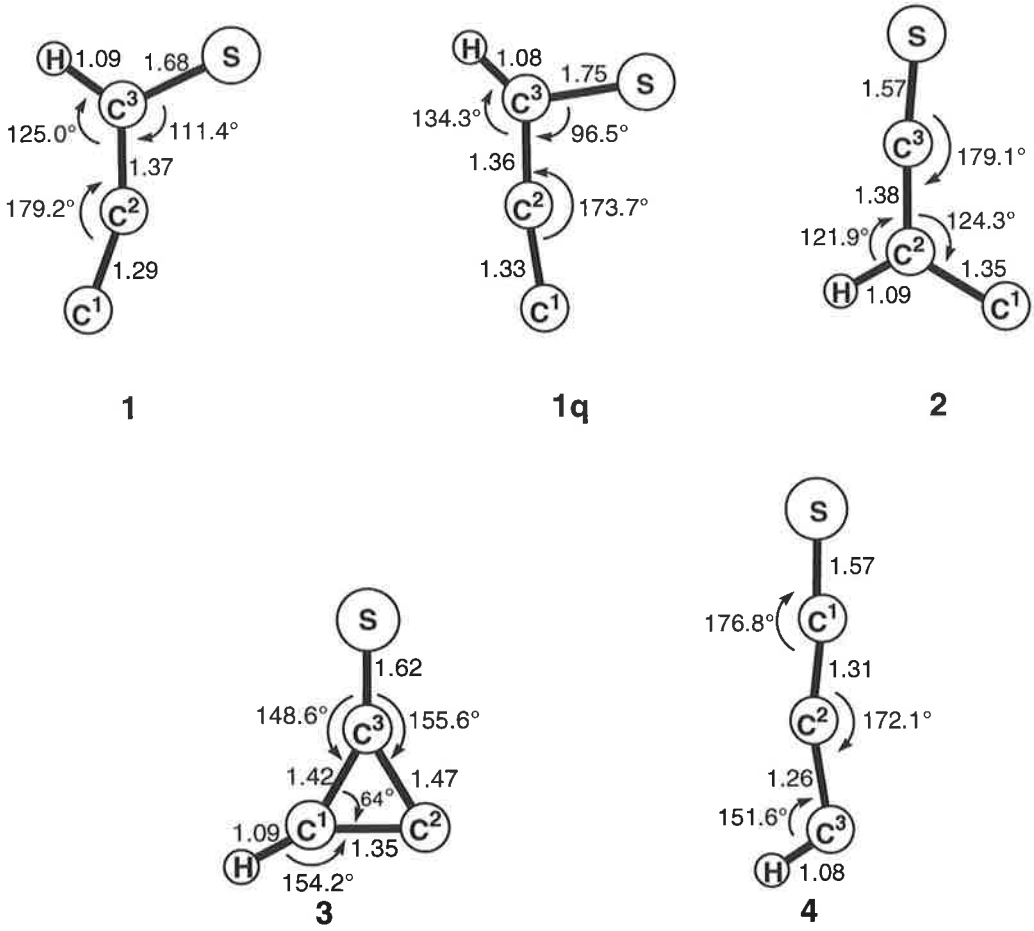

Figure 4.1. Geometries of neutral radicals 1 - 4.

1a. HC_2CS Anion

The ground state HC_2CS anion structure was found to be the $^1A'$ electronic state, but a corresponding triplet anion structure $\mathbf{4t}^-$ 2.6 kcal mol^{-1} higher in energy was also found. Geometry optimisations of both the singlet and the triplet anions produce planar structures of C_S symmetry. These structures (Figure 4.2) demonstrate the limitations of the valence bond approach in describing these systems. In the singlet anion $\mathbf{4}^-$ the C^1-C^2 bond length is 1.28 Å which is intermediate between a model *sp* triple bonded system (e.g. 1.21 Å in acetylene; all reference bond lengths are computed at the B3LYP/aug-cc-pVDZ level), and an sp^2 double bonded system (e.g. 1.34 Å in ethylene). The C^2-C^3 bond length is 1.34 Å which is almost identical to that of an ethylenic double bond. The C^1-C^2-C^3 carbon chain angle is 171.2°.

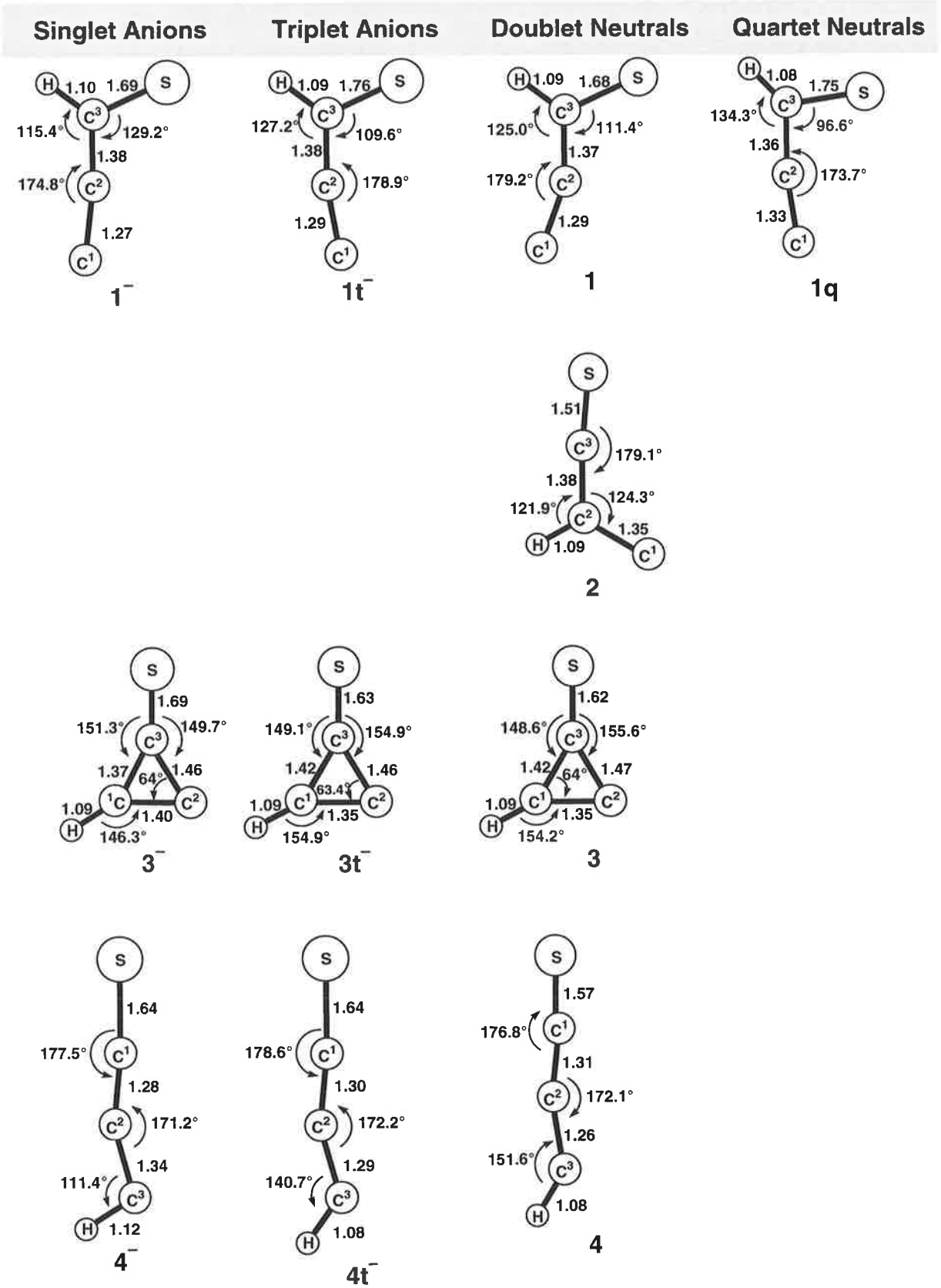

Figure 4.2. Comparison of the geometries of anions and neutrals.

The carbon-hydrogen bond length of 1.12 Å is longer than that of a typical terminal sp^2 system (1.09 Å), while the C^2-C^3-H bond angle of 111.4° is rather acute when compared to a terminal sp^2 system. The carbon-sulfur bond distance of 1.64 Å is considerably larger than that of CS (1.55 Å), but very similar to thioformaldehyde (1.62 Å), while the C^2-C^1-S angle is almost linear at 177.5°.

The triplet structure **4t**$^-$ (electronic state ^{3}A") in Figure 4.2 is less explicable in terms of the valence bond approach than is the singlet. The C^1-C^2 and C^2-C^3 bond lengths of 1.30 Å and 1.29 Å respectively are both longer than an acetylene triple bond, and shorter than an ethylene double bond. The C^1-S bond distance in the triplet anion is almost identical to that of the singlet (1.64 Å), and at 1.08 Å the C-H bond suggests that the carbon it is attached to exhibits some *sp* character. The C^1-C^2-C^3 carbon chain angle in the triplet anion is 171.2°, while the C^2-C^3-H and C^2-C^1-S angles are 140.7° and 178.6° respectively.

1b. HC_2CS Neutral

Rotational spectra of HC_3S (generated by a pulsed discharge in a supersonic free jet of argon-diluted mixtures of C_2H_2 and CS_2) have been measured with a Fabry-Perot type Fourier-transform microwave spectrometer.[208] The spectra indicated that the structures of the free radical species in their ground electronic states are linear with $^2\Pi$ symmetry. Coupling between orbital and vibrational angular momenta in the linear $^2\Pi$ state of neutral HC_2CS (the Renner-Teller effect)[209] involves degenerate electronic states.

A linear ^{2}A" state is the lowest energy experimentally located electronic state of HC_3S neutral, as reported by both McCarthy *et al.*[209] and Hirahara *et al.*[208] in millimetre-wave studies. The other is a planar, lower energy ^{2}A' state - the theoretical minimum. The ^{2}A' isomer was also found by us to be the most stable isomer on the doublet radical surface, represented by

structure **4** in Figure 4.1. This result is in agreement with previous, higher-level studies by both McCarthy and co-workers (at the QCISD level of theory)[209] and Flores and co-workers (at the QCISD/6-311G** level of theory)[207]. The structure of **4** (Figure 4.1), as computed at our chosen level of theory has the carbon-carbon bond lengths in the doublet neutral reverse the pattern seen in the anion $\mathbf{4}^-$ (Figure 4.2). The C^1-C^2 distance of 1.31 Å is slightly shorter than the C-C length in ethylene (1.34 Å), while C^2-C^3 at 1.26 Å is intermediate between the C-C distances of ethylene (1.34 Å) and acetylene (1.21 Å) calculated at the B3LYP/aug-cc-pVDZ. The carbon-sulfur bond length of 1.57 Å is similar to the calculated carbon-sulfur bond length in CS (1.55 Å), and the 1.08 Å carbon-hydrogen bond is intermediate between a typical terminal *sp*, and an sp^2 system. The C^1-C^2-C^3 carbon chain angle of 172.1° is in agreement with the angles calculated at higher levels of theory (172.0° at QCISD/6-311G**), but the S-C^1-C^2 and C_2-C_3-H angles, at 176.8° and 151.6° respectively, show considerable divergence from the higher-level geometries of McCarthy *et al.*[209] (S-C-C = 150.6° and C-C-H = 174.8°) and Flores *et al.*[207] (S-C-C = 155.5° and C-C-H = 179.7°).

Mulliken population analysis indicates that the unpaired electron is mostly located on C^3 (0.565 e), but a significant amount of spin density is also borne on S (0.292 e). The high relative value of spin density on C^1 (0.372 e) may indicate that the electron can be found to a large extent on this centre. It could also be a result of the spin polarisation of the C^2-C^3 bond, since the spin density on C^2 is -0.220 e. Finally, analysis of overlap populations provides an ambiguous account of the bonding in this system (overlap population values do not show close agreement with the calculated bond lengths). The overlap population values C^1-C^2, C^2-C^3, and C^1-S are -0.240 e, -0.054 e, and 0.264 e respectively. The picture that emerges from this electronic analysis suggests a structure intermediate between the two valence bond structures shown below. The first representation is of a heterocumulenic SCCC chain with the unpaired electron located in an orbital on the terminal sp^2 hybridised carbon. The highest

occupied molecular orbital in each structure is symmetric with respect to the plane defined by S-C-C-C-H, consistent with the predicted $^2A'$ electronic term.

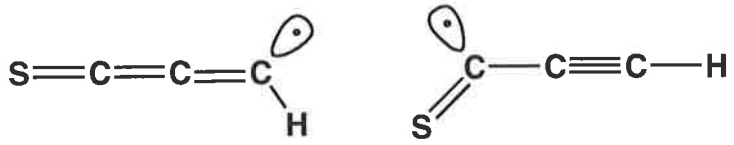

The adiabatic electron affinity of the neutral **4** is calculated to be 6.07 eV at the CCSD(T)/aug-cc-pVDZ//B3LYP/aug-cc-pVDZ level of theory, and the dipole moment is 1.24 D at the B3LYP/aug-cc-pVDZ level of theory.

2. CCHCS

A survey of both the singlet and triplet anionic surfaces did not produce a minimum of structure $[CCHCS]^-$. The doublet neutral surface however features a minimum that does display CCHCS connectivity (see **2**, Figure 4.1). This neutral lies 48.2 kcal mol^{-1} above HC_2CS **4** in energy and corresponds to a $^2A''$ electronic state. The C^1-C^2 bond length is calculated to be 1.35 Å, typical of doubly-bonded sp^2 systems. The C^2-C^3 bond (1.38 Å) is a slightly elongated double bond. The C-S bond distance 1.57 Å is shorter than the calculated bond length of SC (1.55 Å, at the B3LYP/aug-cc-pVDZ level of theory), whereas the C^2-H bond distance (1.09 Å) is very close to the C-H bond distance of ethylene. The H-C^2 moiety makes an angle of 121.9° with C^2-C^3, and contributes to the angle in the carbon chain (C^1-C^2-C^3 = 124.3°). On the other hand, the configuration of C^2-C^3-S is almost linear (179.1°).

C^1 has a calculated spin density of 0.555 e, and because spin polarisation of the C^1-C^2 bond is negligible (C_2 is calculated to have -0.186 e), this suggests that the unpaired electron resides predominantly at C^1, particularly in light of the low relative C^1-C^2 overlap population (-0.008 e). The unpaired electron also resides to some extent at C^3 (0.391 e), and at S (0.243 e). The

C^2-C^3 overlap population is 0.127 e, while the C^3-S value of 0.219 e strongly points to multiple bond character, and is consistent with the calculated C-S bond length.

The adiabatic electron affinity of the neutral **2** is 8.16 eV at the CCSD(T)/aug-cc-pVDZ//B3LYP/aug-cc-pVDZ level of theory, and the dipole moment is 2.00 D at the B3LYP/aug-cc-pVDZ level of theory.

3. (*Cyclo*-C_3H)=S

Cyclic (C_3 ring) structures, (*cyclo*-C_3H)=S, were also found. Among the possible anionic minima, the two lowest electronic states consisted of a singlet $^1A'$ and a triplet $^3A''$ electronic state. The singlet $\mathbf{3}^-$ was found to be more stable than the triplet $\mathbf{3t}^-$ by 56.7 kcal mol^{-1}. Because the energy separation between singlet and triplet states is large (56.7 kcal mol^{-1}), the triplet anion can be disregarded for the purposes of this investigation, and the discussion henceforth will focus only on the ground state singlet anion. The structure of the singlet anion is shown in Figure 4.2. The C^1-C^2 bond distance is 1.40 Å, is intermediate between the ethylene double bond length (1.34 Å) and the single bond length of ethane (1.53 Å). The C^3-C^1 bond length of 1.46 Å is longer than a typical double bond, and displays significant single bond character. Conversely, the C^3-C^1 bond length is 1.37 Å is almost a pure double bond. The C^3-S bond length in the anion (1.69 Å) is longer than the thioformaldehyde C-S bond (1.62 Å). The C^1-H distance (1.09 Å) is characteristic of an sp^2 hybridised system.

The structure of the doublet neutral **3** (Figure 4.1) is very similar to that of the corresponding singlet anion species just described. The C^1-C^2, C^2-C^3, and C^3-C^1 bond lengths are 1.35 Å, 1.47 Å, and 1.42 Å respectively. The C^3-S bond length (1.62 Å) matches the reference C-S bond length (thioformaldehyde) exactly, and the C^1-H bond length (1.09 Å) demonstrates the sp^2 nature at this carbon centre. The population analysis indicates that the unpaired electron is located mainly at sulfur (0.536 e), but C^2 also has a significant spin density (0.369 e).

The adiabatic electron affinity of **3** is calculated to be 6.70 eV at the CCSD(T)/aug-cc-pVDZ//B3LYP/aug-cc-pVDZ level of theory, and the dipole moment is 2.42 D at the B3LYP/aug-cc-pVDZ level of theory.

4. C_2CHS

The C_2CHS anion exhibits two electronic states: a planar singlet $^1A'$ state of C_S symmetry ($\mathbf{1}^-$), and a planar triplet $^3A''$ state ($\mathbf{1t}^-$) also of C_S symmetry but more positive in energy than the singlet anion structure by 137.8 kcal mol^{-1} (Table 4.1). The triplet state anion is disregarded for the purposes of this investigation on energetic grounds. The structure of the singlet anion $\mathbf{1}^-$ (Figure 4.2) again demonstrates the limitations of the valence bond approach in describing the structure of this system. The C^1-C^2 and C^2-C^3 bond lengths are 1.27 Å and 1.38 Å respectively. In the former case, the bond length is intermediate between a model *sp* triple bonded system (e.g. 1.21 Å in acetylene; all reference bond lengths are computed at the B3LYP/aug-cc-pVDZ level), and an sp^2 double bonded system (e.g. 1.34 Å in ethylene). The C^2-C^3 bond length (1.38 Å) shows some single bond character. The carbon-hydrogen bond length of 1.02 Å is somewhat shorter than in a typical terminal sp^2 thiocarbonyl system (thioformaldehyde C-H, 1.10 Å), and the C^2-C^3-H bond angle is 115.4°. The carbon-sulfur bond distance of 1.69 Å is greater than that of thioformaldehyde but is shorter than that found in methanethiol (1.62 Å and 1.84 Å respectively, calculated at the B3LYP/aug-cc-pVDZ level of theory).

One electron oxidation of $\mathbf{1}^-$ may produce a doublet $^2A'$ state **1** and a quartet $^4A'$ state **1q** (Figure 4.2). The quartet state isomer is more negative in energy than the doublet state by 49.2 kcal mol^{-1}. The ground state quartet is noteworthy due to its stability relative to the doublet neutral. A survey of the quartet neutral potential energy surface did not reveal quartet minima

of any other connectivity (except CCHCS) at the level of theory employed.* As a consequence, we focussed our attention on the doublet neutral surface. The gross structure of the $^2A'$ doublet **1** (Figure 4.1 and *cf.* Figure 4.2) is very similar to that of the singlet anion $\mathbf{1}^-$; the C^1-C^2 and C^2-C^3 bond lengths of 1.29 Å and 1.37 Å respectively again display intermediate triple/double bond character in the former case and lengthened double bond character in the latter. The carbon-hydrogen bond length is 1.09 Å, but in this case the C^2-C^3-H bond angle of 125° is much larger than that found in typical aldehydes. In a similar manner to the analogous anion, the carbon-sulfur bond (1.68 Å) is elongated. Population analysis indicates that the unpaired electron is localised predominantly on C^1, but some charge also is seen to reside on hydrogen.

The adiabatic electron affinity of **1** is calculated to be 7.76 eV at the CCSD(T)/aug-cc-pVDZ//B3LYP/aug-cc-pVDZ level of theory, and the dipole moment of is 4.04 D at the B3LYP/aug-cc-pVDZ level of theory.

B. The Syntheses of Ionic Precursors

The negative ion HC_2CS^- is the most obvious precursor to neutral HC_2CS **4**. It was generated in the source of the mass spectrometer by the reaction of the oxygen radical anion, $O^{-\cdot}$(formed from the dissociative resonance capture of nitrous oxide)[46] with 3-(ethylsulfanyl)-1-propyne, *viz.* sequence (i) (Scheme 4.1). This reaction is mediated by the removal of a proton and a hydrogen radical from the central methylene (adjacent to the ethynyl moiety) in a reaction found to produce radical anions in many other organic substrates.[47,49] Another of the possible isomers of HC_3S contains the thioaldehyde moiety, namely $C_2CH{=}S$ **1**. However, gas phase **1** cannot be directly accessed via a stable condensed

* This is in contrast to the work of Flores and Gómez who report several minima on the quartet surface corresponding to the HC_2CS, C_2CHS, CCHCS, and C_3SH planar geometries, and to various cyclic geometries at the QCISD/6-311** level of theory.[207]

phase thioaldehyde since thioaldehydes are generally too unstable to be isolated in pure form, even at low temperatures.[210] In the gas phase, however, some thioaldehydes have sufficient lifetimes against decomposition to make possible characterisation by various techniques, for example by photoelectron spectroscopy.[211] The simplest precursor to neutral $C_2CH{=}S$ **1** is the negative ion $^-C_2CH{=}S$. Our approach towards this elusive thioaldehyde species therefore involved generation of the negative ionic precursor in the source of the mass spectrometer via the S_N2 (Si) displacement reaction [39] shown in sequence (ii) (Scheme 4.1).

SCHEME 4.1

$$HC{\equiv}C{-}CH_2{-}S{-}C_2H_5 + O^{-\bullet} \rightarrow HC{\equiv}C{-}{}^-C{=}S + H_2O + C_2H_5 \quad \text{(i)}$$

$$Me_3Si{-}C{\equiv}C{-}CH(\textit{cyclo}\text{-}SCH_2{-}CH_2S) + F^- \rightarrow {}^-C{\equiv}C{-}CH(\textit{cyclo}\text{-}SCH_2CH_2S) + Me_3Si{-}F$$

$$\downarrow$$

$$^-C{\equiv}C{-}CH{=}S + SC_2H_4 \quad \text{(ii)}$$

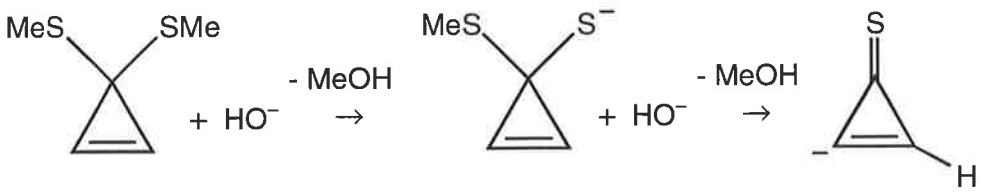

(iii)

Two other isomers of HC_3S were considered in this work. The neutral CCHCS is not accessible via the anion (at the level of theory employed by us, a local minimum that corresponds to the CCHCS geometry on the anionic surface could not be found), and a convenient cationic precursor was not obvious. The final isomer, (*cyclo*-C_3H)=S could in theory be obtained by deprotonation of cyclopropenthione via the route shown in Sequence (iii) (Scheme 4.1). However, a similar strategy in which HO^- reacts with the dimethyl ketal of cyclopropenone via an S_N2 process, followed by elimination of methanol from the product alkoxide anion, has been previously applied by us without success in the attempted generation

of the analogous (*cyclo*-C_3H)=O neutral.[212] Thus we did not proceed with the synthesis outlined in Sequence (iii) (Scheme 4.1).

The precursor anions $\mathbf{1}^{-\bullet}$ and $\mathbf{4}^{-\bullet}$ were prepared in the ion source of the mass spectrometer by the processes shown in Scheme 4.1. Evidence to confirm the atom connectivities of HC_2CS^- and C_2CHS^- is provided by the conventional collision-induced negative ion mass spectra (MS/MS) shown respectively in Figures 4.3 (A) and 4.4 (A). Major fragmentations observed in the negative ion spectrum of HC_2CS^- involve losses of $H^\bullet$, CS, $^\bullet CH$, $^\bullet C_2H$, and $S^\bullet$ from the parent anion, in agreement with structure $HCCCS^-$. The negative ion spectrum of C_2CHS^- is also diagnostic: losses of $H^\bullet$, $CHS^\bullet$, C_2, and C are observed, in line with C_2CHS^- anion connectivity. Importantly, both spectra indicate that the precursor anions show predictable fragmentation behaviour, and do not rearrange upon collisional activation.

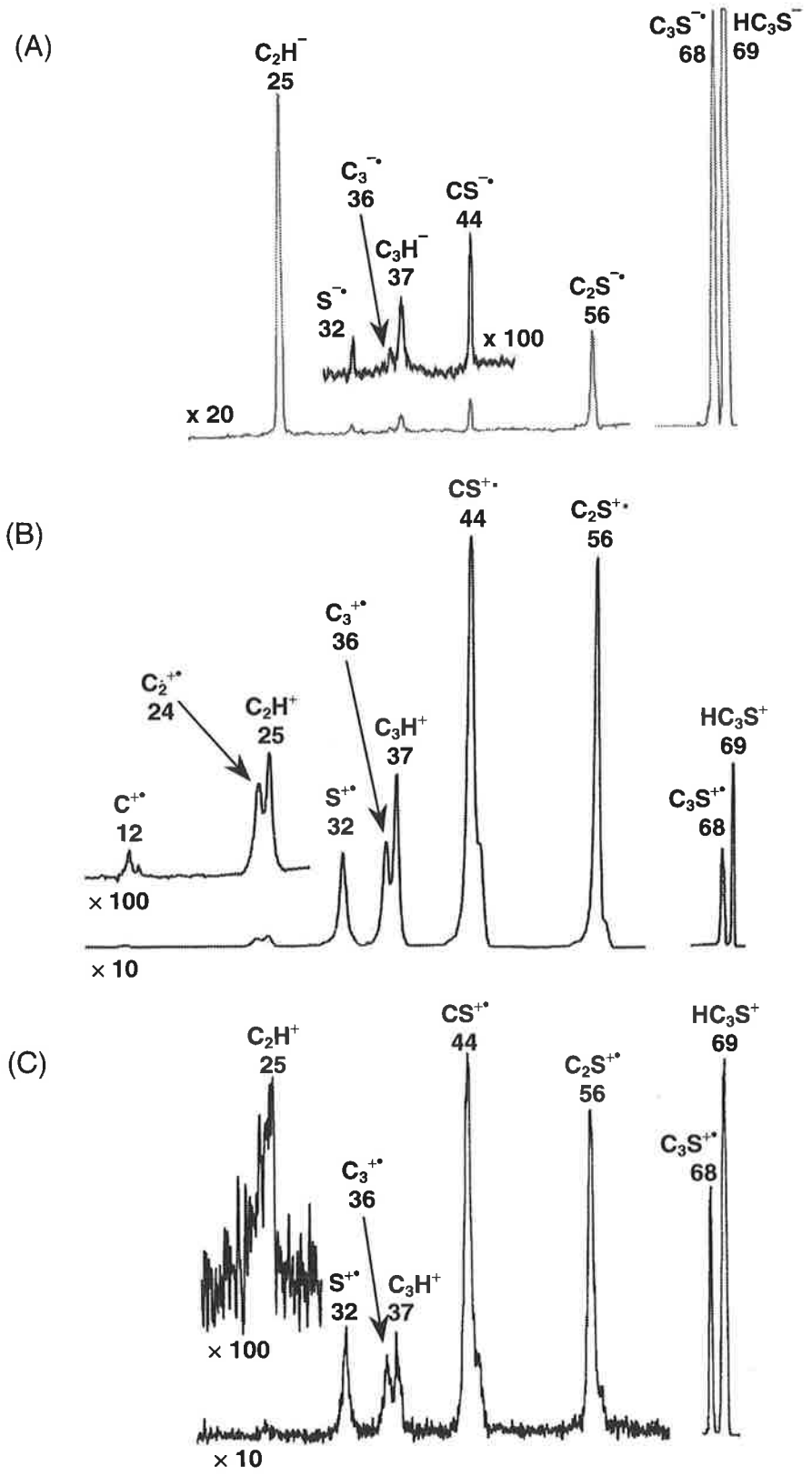

Figure 4.3. (A) Collision-induced mass spectrum (MS/MS) of HC_2CS^-.
(B) Charge reversal mass spectrum ($^-CR^+$) of HC_2CS^-.
(C) Neutralisation reionisation ($^-NR^+$) mass spectrum of HC_2CS^-. VG ZAB 2HF instrument. For experimental conditions see Experimental Section.

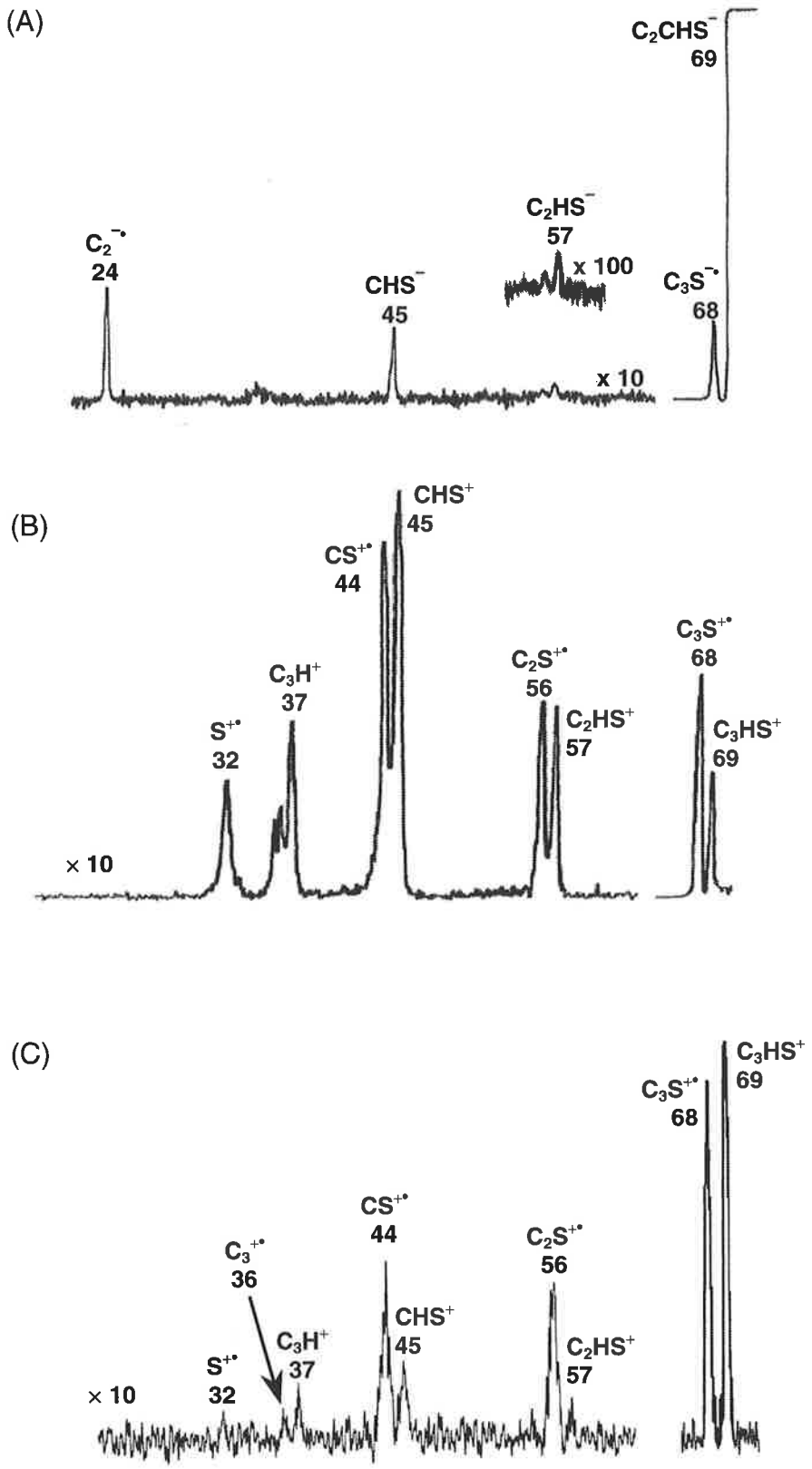

Figure 4.4. (A) Collision-induced mass spectrum (MS/MS) of C_2CHS^-.
(B) Charge reversal mass spectrum ($^-CR^+$) of C_2CHS^-.
(C) Neutralisation reionisation ($^-NR^+$) mass spectrum of C_2CHS^-. VG ZAB 2HF instrument. For experimental conditions see Experimental Section.

C. Formation of Neutrals HC_2CS and C_2CHS

Single electron oxidation from $\mathbf{1}^-$ and $\mathbf{4}^-$ respectively should form the required neutral radicals C_2CHS **1** and HC_2CS **4**. Both of the precursor anions have been formed by soft ionisation techniques that impart little excess energy into the system and they have been shown not to rearrange under the conditions of collisional activation (Figures 4.3A and 4.4A). We now need to know the minimum excess energy contained by each neutral following vertical one-electron oxidation of the precursor anion. This excess energy should give an indication as to whether the neutral is likely to be stable under the conditions of the planned neutralisation experiment. Where the ion and neutral potential surfaces show good Franck-Condon overlap, i.e. where the neutral is produced from vertical, one-electron oxidation of the anion, the excess energy of formation of each neutral from the precursor anion can be calculated as the difference in energy between the neutral minimum and that of the anion geometry on the ground-state neutral surface.[148] It should be emphasised that these calculated values are *minimum* excess energies of formation of the neutral from the ion, and do not include any excess energy that the precursor anion itself may have, or extra energy imparted to the neutral as a consequence of collisional processes.

The data provided in Tables 4.1 and 4.2 show that the structures of the HC_2CS anion and the radical HC_2CS **4** are quite similar: both the anion and the radical are planar. Similarly, the structures of ^-C_2CHS and C_2CHS **1** are comparable. The consequence is that the minimum excess energy of formation of each neutral following the vertical Franck-Condon transition is small. For oxidation of the HC_2CS ground state anion to HC_2CS **4**, the minimum excess energy of the radical on formation is calculated to be a very modest 8.3 kcal mol^{-1}, while for oxidation of ^-C_2CHS to C_2CHS **1** the corresponding minimum excess energy is only 8.4 kcal mol^{-1}. Both of these energies are modest and should not by themselves be sufficient to induce rearrangement or fragmentation of the neutral. These calculations suggest that neutralisation

of HC_2CS and C_2CHS anions should produce the stable isomers HC_2CS **4** and C_2CHS **1**, respectively. The charge-reversal ($^-CR^+$) mass spectrum of HC_2CS anion is shown in Figure 4.3(B). Major fragmentations observed in this positive ion spectrum involve losses of $H^\bullet$, $HC^\bullet$, $HC_2^\bullet$, and CS from the parent cation, consistent with structure $[HC_2CS]^+$.

The characteristic neutralisation-reionisation spectrum ~~Goldberg, 1994 #110; Schalley, 1998 #236~~ ($^-NR^+$) of the HC_2CS anion is shown in Figure 4.3(C). The base peak (*m/z* 69) in the $^-NR^+$ spectrum of HC_2CS^- corresponds to the parent cation (the recovery signal), with major fragment peaks at *m/z* 68 ($C_3S^{+\bullet}$), 56 ($C_2S^{+\bullet}$), 44 ($CS^{+\bullet}$), 37 (C_3H^+), 36 ($C_3^{+\bullet}$), and 32 ($S^{+\bullet}$). The fragment peak abundances in the $^-NR^+$ spectrum are comparable to those observed in the $^-CR^+$ spectrum. The conclusion to be drawn from this is that $HCCCS^\bullet$ is stable for the duration of the NR experiment (*ca.* 10^{-6} s). The $^-CR^+$ and $^-NR^+$ spectra of $^-C{\equiv}C{-}CHS$ are shown in Figure 4.4(B) and (C) respectively. Major peaks in the $^-CR^+$ spectrum (Figure 4.4(B) correspond to losses of $H^\bullet$, C_2, $^\bullet C_2H$, $^\bullet CH$, and C from the parent cation. All of these processes are endothermic (see Table 4.3).

Table 4.3 Thermochemical Data for Decompositions of HC_2CS and C_2CHS Cations and Neutrals

cation process	ΔH (kcal mol^{-1})	neutral process	ΔH (kcal mol^{-1})
$HCCCS^+ \rightarrow CCCS^{+\bullet} + H^\bullet$	136.4	$HCCCS^\bullet \rightarrow CCCS + H^\bullet$	63.5
$HCCCS^+ \rightarrow HCCC^+ + S$	180.6	$HCCCS^\bullet \rightarrow HCCC^\bullet + S$	136.4
$HCCCS^+ \rightarrow HCC^\bullet + CS^{+\bullet}$	170.2	$HCCCS^\bullet \rightarrow HCC^\bullet + CS$	71.7
$HCCCS^+ \rightarrow HCC^+ + CS$	190.5		
$CCCHS^+ \rightarrow CCCS^{+\bullet} + H^\bullet$	138.1	$CCCHS^\bullet \rightarrow CCCS + H^\bullet$	24.6
$CCCHS^+ \rightarrow CHS^+ + CC$	146.2	$CCCHS^\bullet \rightarrow CHS^\bullet + CC$	94.3
$CCCHS^+ \rightarrow CC^{+\bullet} + CHS^\bullet$	326.5	$CCCHS^\bullet \rightarrow HCC + CS$	32.8

ΔH values are determined from the following theoretically calculated values (Hartrees): HC_3S^+ = -511.87388; $HC_3S^\bullet$ = -512.13058; C_2CHS^+ = -511.87658; $C_2CHS^\bullet$ = -512.06863; $C_3S^{+\bullet}$ = -511.15723; C_3S = -511.53003; HC_3^+ = -114.02798; $HC_3^\bullet$ = -114.35497; $C_3^{+\bullet}$ = -113.31547; C_3 = -113.74731; HC_2^+ = -75.95193; $HC_2^\bullet$ = -76.39797; $CS^{+\bullet}$ = -435.20464; CS = -435.61841; $C_2^{+\bullet}$ = -75.16825; C_2 = -75.73035 [at CCSD(T)/aug-cc-pVDZ level of theory including zero point energies (calculated from vibrational frequencies at the B3LYP/aug-cc-pVDZ level of theory)].

The $^-NR^+$ spectrum of $^-C{\equiv}C{-}CHS$ [Figure 4.4(C)] is similar to the $^-CR^+$ spectrum (Figure 4.4B), except that peaks at *m/z* 56 (- $^\bullet CH$) and *m/z* 44 (- $^\bullet C_2H$) are more pronounced in the $^-NR^+$ spectrum. The presence of these two peaks in the $^-NR^+$ and $^-CR^+$ spectra indicates that some C_2CHS neutrals and cations are rearranging to an isomer, possibly HC_2CS (**4**) or (*cyclo*-C_3H)=S (**3**) (for dissociation energies of HC_2CS and C_2CHS neutrals and cations, see Table 4.3). The experimental observation that the abundances of *m/z* 56 and 44 are larger in the $^-NR^+$ spectrum indicates that the rearrangement is more prevalent for the neutral form of C_2CHS.

These experimental observations indicate that charge stripping of $^-C{\equiv}C{-}CHS$ gives rise to C_2CHS **1**, with collision-induced vertical oxidation producing a proportion of neutrals with

sufficient excess energy to instigate rearrangement into another isomer.* The isomerisation produces a neutral whose positive ion spectrum is dominated by peaks corresponding to charged CS and C_2S. This isomerisation must involve either H or S migration, and the product is most likely to be $HC_2CS^{\cdot}$ **4**, but (*cyclo*-C_3H)=S (**3**) must also be considered in this context. Since we have been unable to prepare **3**, the possible rearrangements of **1** have been investigated theoretically.

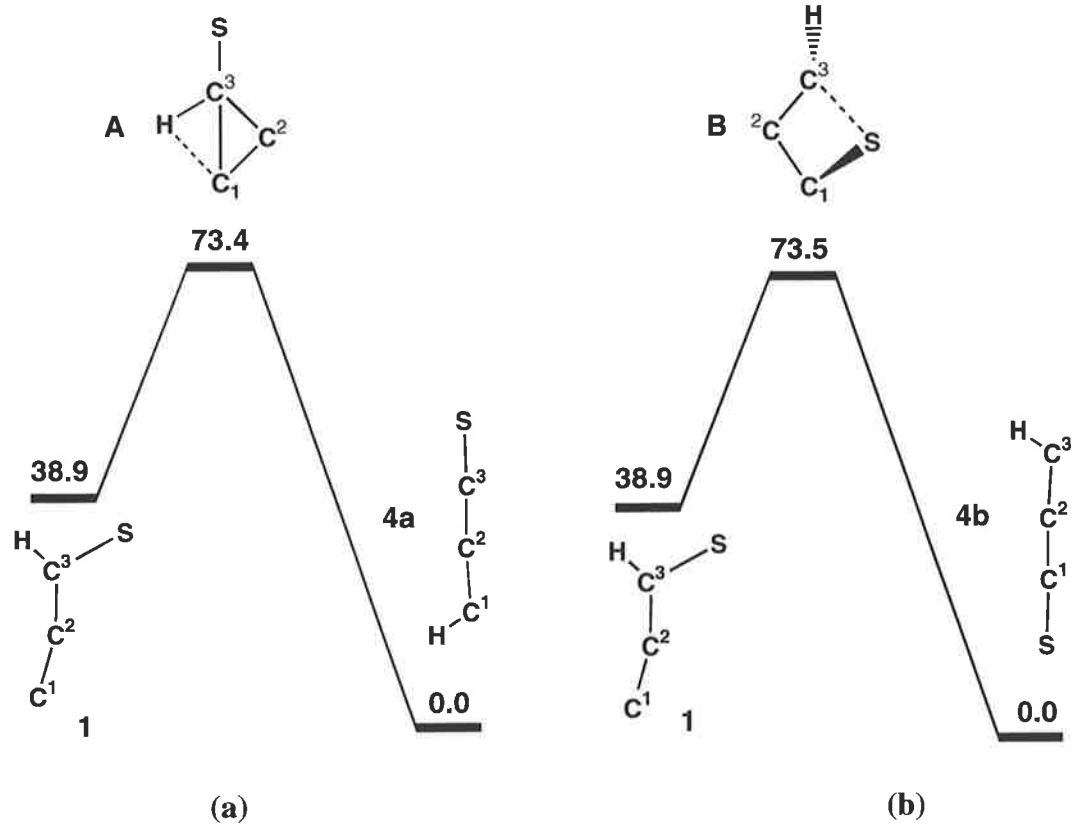

Figure 4.5. Concerted rearrangements of C_2CHS 1 to HC_2CS 4 via (a) H-migration, and (b) S-migration. CCSD(T)/aug-cc-pVDZ//B3LYP/aug-cc-pVDZ level of theory. Relative energies (kcal mol^{-1}) in relation to 4a or 4b (0.0 kcal mol^{-1}). Full data for neutrals: see Figure 4.1 and Table 4.1. Data for transition states A and B: see Table 4.4

* It must be emphasised that while the evidence provided in Figure 4.4 clearly indicates that some of the neutral rearranges, the spectra also suggest that positive ion rearrangement is occurring [strong signals for $CS^{+\cdot}$ (*m/z* 44) and C_3H^+ (*m/z* 37) in $^{-}CR^{+}$]. We have focussed solely on neutral phenomena in this system.

D. Theoretical Studies of the Rearrangement of Neutral C_2CHS.

Calculations of possible rearrangements of radical C_2CHS have been investigated at the CCSD(T)/aug-cc-pVDZ//B3LYP/aug-cc-pVDZ level of theory. There are three competitive rearrangements of C_2CHS: these are summarized in Figures 4.5 and 4.6. Structure and energy data for the four isomers **1-4** are shown in Figure 4.1 and Table 4.1; the data for the five transition states **A-E** are recorded in Table 4.4. The relative energy data shown in Figures 4.5 and 4.6 conform to the values listed earlier in the text; i.e., HC_3CS (energy designated as 0.0 kcal mol^{-1}) is the global energy minimum on the neutral potential surface. There are three isomerisation pathways for C_2CHS **1**, all terminating with the formation of the stable isomer HC_2CS **4**. The first rearrangement is a synchronous reaction in which the C^1 hydrogen transfers, via transition state **A**, to form HC_2CS **4a** directly. The barrier for this reaction is computed as 34.5 kcal mol^{-1} at the level of theory used. The second isomerisation is also a synchronous reaction which occurs by the C^1-C^3 sulfur migration, via transition state **B**, to form HC_2CS **4b**. The barrier for this reaction is computed as 34.6 kcal mol^{-1} at the level of theory used. Finally, a stepwise sequence in which the rate determining first step involves 1,2 H transfer through transition state **C** over a barrier of 24.0 kcal mol^{-1}. This reaction forms $^{\bullet}$CCHCS, which lies in a very shallow potential well on the HC_3S radical surface (see Figure 4.6) and readily undergoes rearrangement with very little surplus energy imparted to it via transition state **D**. The product of this cyclisation step is (*cyclo*-C_3H)=S **3**, which specifically ring opens (because of its excess energy) via transition state **E** to form HC_2CS **4c**.

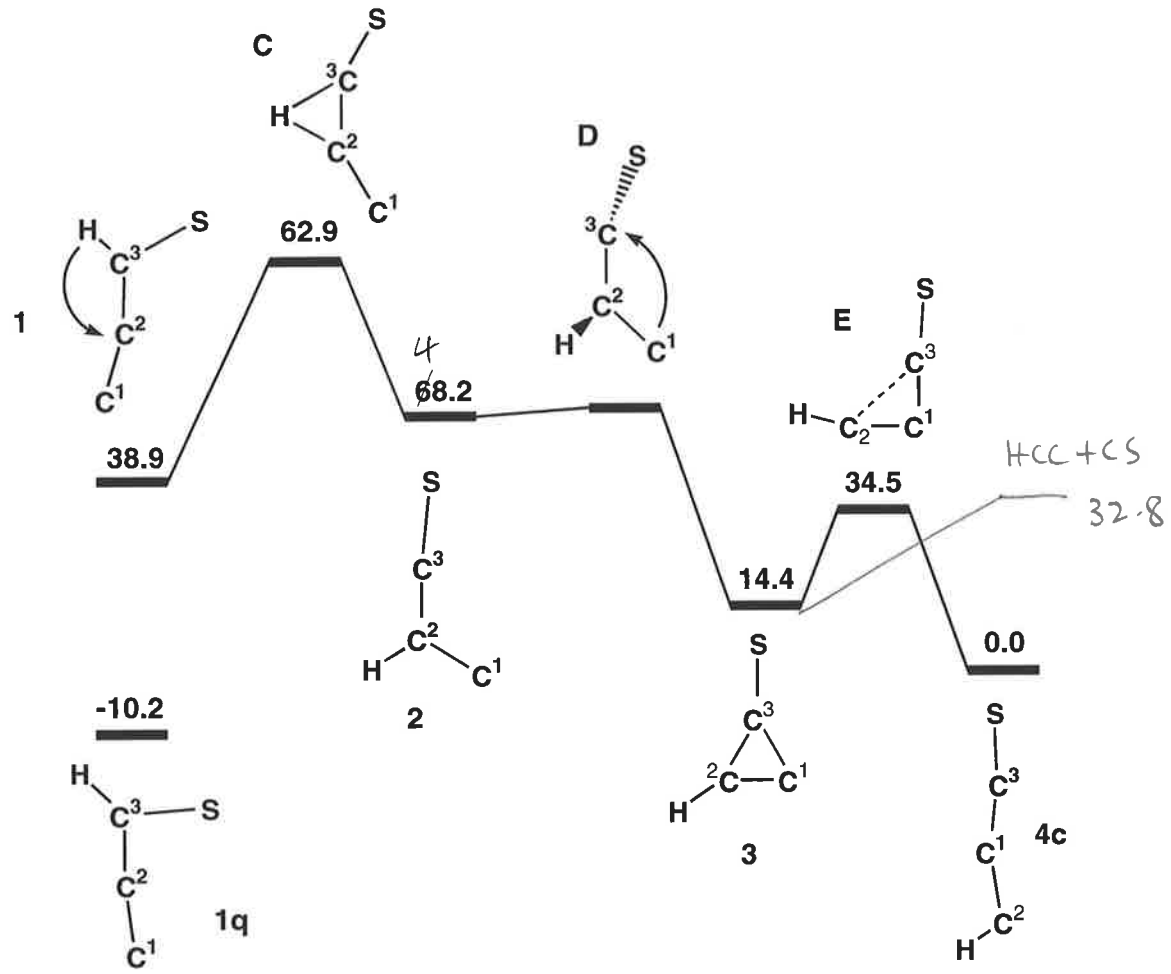

Figure 4.6. Stepwise rearrangements of C_2CHS 1 to HC_2CS 4. CCSD(T)/aug-cc-pVDZ//B3LYP/aug-cc-pVDZ level of theory. Relative energies (kcal mol^{-1}) in relation to 4 (0.0 kcal mol^{-1}). Full data for neutrals: see Figure 4.1 and Table 4.1. Data for transition states C - E: see Table 4.4.

Table 4.4 Geometries and Energies of Transition States A - E.

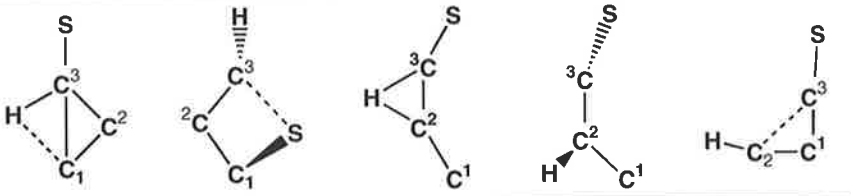

	A	B	C	D	E
State	$^2A'$	-	$^2A'$	-	$^2A'$
Symmetry	C_S	C_1	C_S	C_1	C_S
Energy (Hartrees)[a]	-512.01378	-512.01342	-512.03029	-512.05700	-512.07644
Bond Length (Å)[b] or Angle (°)					
C^1C^2	1.34	1.49	1.33	1.31	1.34
C^2C^3	1.43	1.30	1.33	1.41	1.88
C^1C^3	1.66	2.36	2.66		1.36
C^1S		1.73			
C^1H	1.55				
C^2H			1.30	1.14	1.09
C^3S	1.65	2.14	1.59	1.58	1.58
C^3H	1.19	1.09	1.37		
$C^1C^2C^3$	73.7	115.4	176.5	148.5	
$C^2C^1C^3$					87.9
$C^2C^3C^1$		29.9			
C^2C^3S	139.1	79.7	175. 5	141.2	
C^1C^3S					176.1
C^2C^3H	113.7	147.4	57.9	120.7	
SC^3H	107.2	132.8	126.6		
C^1C^2H			120.8		150.3
C^3C^1H	43.3				
$C^1C^2C^3S$	180.0	-0.07	0.0	54.7	180.0
$C^3C^2C^1S$		0.008			
$C^1C^2C^3H$	180.0	179.897	180.0	-154.1	180.0
$C^2C^3C^1H$	180.0				

[a] CCSD(T)/aug-cc-pVDZ level of theory including zero point energy correction (calculated from vibrational frequencies at the B3LYP/aug-cc-pVDZ level of theory).

[b] B3LYP/aug-cc-pVDZ level of theory.

The similarity between the geometries of the singlet anion $\mathbf{1}^-$ and the doublet neutral **1** have important consequences for the neutralisation-reionisation experiments conducted. Since the electronic transitions in such an experiment are considered vertical,[84,85] good Franck-Condon overlap between the singlet anion and doublet neutral surfaces, and the consequent favourable Franck-Condon factors will result in the formation of a neutral with little excess energy (8.4 kcal mol^{-1}). However, the step-wise rearrangement of C_2CHS shown in Figure 4.6 has a

barrier of 24 kcal mol^{-1} in the rate determining step, i.e. migration of the hydrogen from C_3 to C_2 to produce the isomer CCHCS **2**.

Conversely, in the two concerted mechanisms, involving in the first case, a 1-3 hydrogen migration between C_3 and C_1 in neutral **1**, and in the other, a 1-3 sulfur migration also between C_3 and C_1 (see Figure 4.5 a and b), activation energy barriers of 34.5 and 34.6 kcal mol^{-1} respectively must be surmounted. These are considerable barriers. Finally, the HC_3S products of the reaction sequence shown in Figures 4.5 and 4.6 could be formed with excess energy. Unless these products are de-energised by either collision or radiation [187] in the collision cell, some of the HC_3S neutrals formed in the isomerisation process have sufficient energy to decompose to yield CS and HC_2 [a process that is endothermic by 71.7 kcal mol^{-1} (Table 4.3)].

Gas phase reactions are generally kinetically controlled, and reaction rates are governed primarily by two factors: (i) the barrier to the transition state, and (ii) the probability of reaction (the frequency factor, or pre-exponential Arrhenius factor)[186] in the rate equation. With regards to the first issue, the situation is made more complex by the matter concerning the amount of excess energy actually imparted into the nascent neutral upon one electron oxidation of the progenitor anion.

The *minimum* excess energy of formation of each neutral from the ion (excluding any excess energy that the precursor ion itself may have, or extra energy given to the neutral as a consequence of the collisional process) can be calculated as the difference in energy between the neutral minimum and that of the ion geometry on the ground-state neutral surface: this assumes vertical Franck-Condon overlap of the ion and neutral potential surfaces.[148] To consider the role that the probability of reaction has on the reaction rate, a deeper understanding of the nature of the transition state is required. In general, the 'looser' (more disordered) the transition state, the higher the rate at which a reaction will proceed. To

determine the relative abilities of the neutral to access the various rearrangement channels requires an intimate knowledge of the potential energy surfaces for those processes. In the absence of this knowledge, the entropic natures of the two transition states may be determined by calculating the relative pre-exponential Arrhenius *A* factors. Approximation of the *A* factor for each process simplifies to evaluating Q_{Vib}, the relative vibrational partition functions for the competing transition states. The methodology adopted for this calculation has been described previously in chapters 1.3 and 3.

Table 4.5. Vibrational Partition Functions for Transition States A, B, and C (Figures 4.4 and 4.5)

A		B		C	
frequency	Q'_{vib}	frequency	Q'_{vib}	frequency	Q'_{vib}
268.1871	1.37631	192.0646	1.65311	128.327	2.16301
299.9721	1.30628	580.9382	1.06413	229.1845	1.49291
704.8469	1.03424	633.7005	1.04898	412.1914	1.15778
754.1097	1.02679	777.5750	1.02385	575.3130	1.06602
783.7844	1.02312	795.1751	1.02186	690.6398	1.03676
1167.8391	1.00354	1013.0072	1.00752	1370.7800	1.00132
1529.6990	1.00061	1569.4120	1.00051	1841.5835	1.00014
2303.8585	1.00001	3261.7399	1.00000	2021.0860	1.00006
total	1.96152	total	1.94611	total	4.13830

The harmonic vibrational frequencies of each of the transition states **A** - **C** (Figures 4.5 and 4.6) were calculated at the B3LYP/aug-cc-pVDZ level of theory, using Gaussian 98 [*cf.*[156]] These values are listed in the Appendices to this chapter and in Table 4.5. The value of $Q^{\ddagger}_{Vib}$ for the transition state **A** involving H-migration leading to the linear product **4** in a concerted fashion is 1.96, the transition sate for concerted S-migration **B** is 1.95, whereas for the step-wise pathway, the transition state **C** for the rate determining step which involves a 1-2 H-migration to give CCHCS intermediate, the value of $Q^{\ddagger}_{Vib}$ is 4.14. This may be interpreted thus: the transition state **C** for the rate determining step (which involves a 1-2 H-migration) is 'looser' than either **A** or **B**, the two transition states for the concerted rearrangement (Figures

4.6, and see Appendix for details). The *A* factor for the formation of **C** is thus larger than that for the formation of **A** or **B**, within the approximations we have employed. The stepwise rearrangement is therefore the most favourable mechanism in entropic terms. Taken together, these values suggest that the step-wise pathway (Figure 4.6) should be the major pathway for rearrangement of the neutral C_2CHS **1** to HC_2CS **4c**.

An interesting issue that arises from this theoretical analysis of the possible HC_3S neutral rearrangement pathways is that the carbon chain remains intact during both of the synchronous isomerisations, but rearranges during the stepwise process (see Figures 4.5 and 4.6). Moreover, the connectivity of the rearrangement product of H migration is different to that of S migration. In principle, if we label the precursor anion with ^{13}C at either positions 1, 2, or 3 we should be able to differentiate between either H-migration or S-migration, *viz.*,

^{13}C at Position 1:

$$[CC^{13}CHS]^{\bullet} \xrightarrow{\text{H-migration}} [H\text{-}C^3\text{-}C^2\text{-}^{13}C^1\text{-}S]^{\bullet} \quad \text{(a)}$$

$$\xrightarrow{\text{S-migration}} [S\text{-}C^3\text{-}C^2\text{-}^{13}C^1\text{-}H]^{\bullet} \quad \text{(b)}$$

$$\xrightarrow{\text{stepwise rearrangement}} [H\text{-}C^2\text{-}C^3\text{-}^{13}C^1\text{-}S]^{\bullet} \quad \text{(c)}$$

By introducing a label at position 1, it would possible to differentiate between H-migration (d) or S-migration (e) pathways. If H-migration occurs, the $^{-}NR^{+}$ spectrum should show $^{13}CS^{+\bullet}$ (*m/z* 45), and $CS^{+\bullet}$ (*m/z* 44) if S-migration occurs. However, there are no characteristic fragmentations to differentiate between H-migration and the stepwise pathway for this labelled system. This labelling experiment therefore can only determine whether the rearrangement occurs via (i) a concerted S-migration pathway, or (ii) either a concerted H-migration *or* a stepwise isomerisation mechanism.

^{13}C at Position 2:

$$[C^{13}CCHS]^{\bullet} \xrightarrow{\text{H-migration}} [H{-}C^3{-}{}^{13}C^2{-}C^1{-}S]^{\bullet} \quad \text{(d)}$$

$$\xrightarrow{\text{S-migration}} [S{-}C^3{-}{}^{13}C^2{-}C^1{-}H]^{\bullet} \quad \text{(e)}$$

$$\xrightarrow{\text{stepwise rearrangement}} [H{-}{}^{13}C^2{-}C^3{-}C^1{-}S]^{\bullet} \quad \text{(f)}$$

With position 2 labelled, the $^{-}NR^{+}$ spectra for both concerted pathways and the stepwise rearrangement mechanism would be identical, and cannot differentiate between the competing pathways.

^{13}C at Position 3:

$$[{}^{13}CCCHS]^{\bullet} \xrightarrow{\text{H-migration}} [H{-}{}^{13}C^3{-}C^2{-}C^1{-}S]^{\bullet} \quad \text{(g)}$$

$$\xrightarrow{\text{S-migration}} [S{-}{}^{13}C^3{-}C^2{-}C^1{-}H]^{\bullet} \quad \text{(h)}$$

$$\xrightarrow{\text{stepwise rearrangement}} [H{-}C^2{-}{}^{13}C^3{-}C^1{-}S]^{\bullet} \quad \text{(i)}$$

Introducing ^{13}C at position 3 would enable differentiation between all three competing pathways. If H-migration (g) occurs, the characteristic fragment $CCS^{+\bullet}$ (*m/z* 56) will be observable in the $^{-}NR^{+}$ spectrum. Concerted S-migration will yield $^{13}CS^{+\bullet}$ (*m/z* 45) process (i), the $CS^{+\bullet}$ peak (*m/z* 44) will be present together with *m/z* 57 (- $^{12}C^{13}CH^{\bullet}$). Labelling with ^{13}C at position 3 would be very difficult but the formation of the precursor to $(CC^{13}CHS)^{-}$ should be possible by the following method (Scheme 4.2).

SCHEME 4.2

$$(CH_3)_3Si{-}C{\equiv}CH + H^{13}CON(CH_3)_2 \xrightarrow{n\text{-BuLi}} (CH_3)_3Si{-}C{\equiv}C{-}{}^{13}CHO$$

$$\downarrow \begin{matrix} HS{-}(CH_2)_2{-}SH \\ BF_3.OEt_2 \end{matrix}$$

$$(CH_3)_3Si{-}C{\equiv}C{-}{}^{13}CH(\textit{cyclo}\text{-}SCH_2{-}CH_2S)$$

The synthetic summary recorded in Scheme 4.2 (see also ref. [39]) demonstrates the generation of the stable ^{13}C-labelled dithiolanyl precursor. The requisite labelled anionic precursor

$(C{\equiv}C{-}^{13}CH{=}S)^-$ can then be generated by the ion-molecule reaction between the fluoride anion, F^-, and the ^{13}C-labelled dithiolanyl precursor in the chemical ionisation source of the mass spectrometer as indicated in Scheme 4.1 (pp. 133 and 134, see also Experimental Section).

Unfortunately, time did not allow the synthesis of this ^{13}C labelled precursor.

In summary, (i) *ab initio* calculations indicate that the barriers to the formation of **4** from **1** via the transition states **A**, **B** and **C** are sizeable, though the barriers to **A** and **B**, are significantly larger than the barrier to **C**; (ii) the relative Arrhenius factors indicate that **C** is the looser transition state by a significant factor. Taken together, these calculations suggest that the step-wise pathway shown in Figure 4.6 should be the major rearrangement pathway.

In conclusion, a consideration of both the experimental and the theoretical evidence indicates that (i) $HC_2CS^{\bullet}$ has been formed from HC_2CS^- and $^{\bullet}C_2CHS$ from ^-C_2CHS, and (ii) under the collision conditions used, some of the initially formed C_2CHS radicals rearrange to HC_2CS [a reaction more favourable than simple cleavage of C_2CHS (see Table 4.3 and compare with Figures 4.5 and 4.6)], and it is likely that some of these energised HC_2CS radicals decompose to yield CS and C_2S.

III. Experimental Section

A. Mass Spectrometric Methods

All mass spectra were measured using a two-sector modified VG ZAB 2HF mass spectrometer with BE configuration (where B and E represent magnetic and electric sectors, respectively) equipped with tandem collision cells between the magnetic and electric sectors. The instrument was used in the negative ion chemical ionisation (NICI) mode. Negative ions of 3-thioxo-1-propynyl, $^{-}C{\equiv}C{-}CH{=}S$, were formed in the chemical ionisation source by an S_N2 (Si) reaction [39] between F^- and a neutral trimethylsilyl substrate {$F^- + Me_3SiR \rightarrow R^- + Me_3SiF$; R = [2-(1,3-dithiolan-2-yl)-1-ethynyl](trimethyl)silane}. The 1-thioxo-2-propynyl negative ion, $HC{\equiv}C{-}^{-}C{=}S$, is formed by the ion-molecule reaction between the oxygen radical anion, $O^{-\bullet}$ (generated via dissociative resonance capture of nitrous oxide),[47] and 3-(ethylsulfanyl)-1-propyne in the chemical ionisation source. Samples were introduced through the septum inlet (maintained at 100°C) to a measured pressure of 5×10^{-7} Torr, together with the reagent gas (either SF_6 or N_2O) at a measured pressure of 1×10^{-6} Torr. The estimated total pressure in the chemical ionisation source is 10^{-1} Torr.[188] The ion source temperature was 200°C, the accelerating voltage was 7kV, and the slits were fully open to obtain maximum sensitivity. Collisional activation MS/MS experiments [213] were carried out using the magnet to focus and transmit the ion beam under study, the ion beam was intercepted at the first of the tandem collision cells which contained argon as collision gas at a measured pressure of 1×10^{-6} Torr. Ionic dissociation products were detected by scanning the electric sector. The same experimental parameters were used for CR experiments,[67,70,71] except that polarity of the sector voltage was reversed to allow the detection of positive ions, and O_2 was used as the collision gas. The CR process can be regarded under these conditions as a single step, vertical, two-electron oxidation, occurring in a time scale of a few femtoseconds (however, some species may undergo multiple collisions). Neutralisation reionisation [$^{-}NR^+$ (magnet set for transmission of negative ions)] experiments [78,86] were carried out as for $^{-}CR^+$ experiments

except that dioxygen was used as the collision gas in both collision cells (pressure measured outside each cell = 1×10^{-6} Torr, 80% beam transmission through collision cells). Ions were deflected away from the beam of neutral species by applying a voltage of 1.5 kV to a deflector electrode located between the two collision cells.

B. Computational Methods

Molecular geometries were optimised and the vibrational frequencies computed according to the Becke 3LYP method [151,152] initially using the 6-31G(d) basis within the GAUSSIAN 98 [156] computational chemistry package. The larger augmented correlation-consistent polarised double-zeta basis set of Dunning, aug-cc-pVDZ,[111,160] which incorporates d functions [maximum angular momentum l = 2(d)] to heavy atoms, was used to further optimise minima on the anion, neutral, and cation surfaces. Stationary points on potential energy surfaces were characterised as either minima (no imaginary frequencies) or transition states (one imaginary frequency) by calculation of the frequencies using analytical gradient procedures. The connection between minima and a given transition structure was established by examining the reaction path on the potential energy surface leading away from the transition structure in an intrinsic reaction coordinate (IRC) calculation. Zero-point vibrational energies were also determined from calculated frequencies and used as a zero-point energy correction for the electronic energies calculated at this and higher levels of theory. Some problems with the planar HC_3S radical structure **4** and the transition state structure for concerted 1-3 S-migration **B** were encountered using these methods. In the former case, a bent structure of ^{2}A' electronic state was predicted for **4** in agreement with the higher level geometry optimisations (in particular QCISD) reported by other investigators.[207,209] Calculations at higher levels of theory also predict small departures from linearity in the HCCC backbone but significant CCS angles; at the B3LYP methods employed by us, small CCCS angles and a comparatively large CCH angle are produced. Additionally, the B3LYP methods predict a geometry for the transition state structure (**B**) that only marginally deviates from planarity (dihedral angles of

less than a degree). With C_S symmetry imposed, a first order saddle point could not be found, and a frequency calculation on an identical but otherwise planar (**B**) structure resulted in a number of imaginary frequencies, the most significant of which was an out-of-plane vibration. Accordingly, the non-planar geometry is reported.*

The B3LYP method has previously been used [214] to obtain good agreement between computed properties of the ground states and experimental observations of C_nS (n = 2-9) optimised structures at low computational costs, which compare favourably with higher level calculations (stretching frequencies of C_3S obtained by this method are in better agreement than correlated *ab initio* methods). The coupled cluster method, CCSD(T)[101,158] employing the Dunning aug-cc-pVDZ basis set was used to obtain higher accuracy energies for the B3LYP optimised geometries.

Calculations were performed on the 120 node 480 1GHz processor Compaq AlphaServer SC at the Australian Partnership for Advanced Computing National Facility (Canberra).

C. Synthetic Procedures

[2-(1,3-dithiolan-3-yl)-1-ethynyl](trimethyl) silane was prepared by adapting the method of Furth *et al.*[215] Boron trifluoride etherate (6.34 mmol, 899 mg) was added dropwise to a stirred solution of trimethylsilyl propiolaldehyde (1.98 mmol, 250 mg) and 1,2-ethanedithiol (2.18 mmol, 205.2 mg, 1.1 equiv.) in dichloromethane (9 cm^3) and methanol (9 cm^3) at 0°C. This mixture was stirred for 6 h at room temperature. The reaction was quenched with aqueous sodium hydrogen carbonate (saturated, 15 cm^3) and the solution was extracted with diethyl ether (10 cm^3, 3 times). The organic layer was washed with aqueous sodium hydrogen

* A theoretical study of the potential energy surface of the S + C_3H reaction at the QCISD(T)/ 6-311+G(3df,2p)//QCISD/6-311G** level of theory by Flores and Gómez [207] makes no mention of a transition state of structure resembling **B**. Instead, a local minimum on the potential energy surface was observed with a non-planar SC_3 ring structure which approximates **B** but is of ^2A electronic state.

carbonate (saturated, 15 cm^3) and aqueous sodium chloride (saturated, 15 cm^3) , dried over $MgSO_4$, filtered and concentrated to give a yellow oil (1.24 mmol, 250 mg, 62 %; warning: any 1,2-ethanedithiol residue present at this stage will confer a powerful stench to product!). $[M-H]^-$ (ZAB 2HF instrument) = 202.0323 $C_8H_{14}S_2Si$ requires 202.0306. ^1H NMR 200 MHz, $CDCl_3$ δ 0.09 (s, 9H); 2.60 (s 4H); 5.08 (s, 1H).

1-thioethyl-

~~3-(ethylsulfanyl)-~~1-propyne [216] was prepared by a reported method.

IV. Appendix

Table A4.1 Harmonic frequencies (in cm^{-1}) and infrared intensities (in km mol^{-1}) for the doublet ground state of the C_2CHS neutral 1. Harmonic frequencies are unscaled.

mode	symmetry	frequency	intensity
ω_1	?A	136.8516	7.1532
ω_2	?A	193.7026	0.1012
ω_3	A'	401.5143	13.8303
ω_4	?A	838.3417	10.1926
ω_5	A'	907.6365	37.3304
ω_6	?A	1055.8172	11.2469
ω_7	A'	1253.4592	36.5482
ω_8	A'	1929.6381	458.1226
ω_9	A'	3147.9308	0.9779

Table A4.2 Harmonic frequencies (in cm^{-1}) and infrared intensities (in km mol^{-1}) for the quartet state of the C_2CHS neutral 1q. Harmonic frequencies are unscaled.

mode	symmetry	frequency	intensity
ω_1	?A	160.1600	4.5778
ω_2	?A	291.4369	6.7393
ω_3	?A	377.6785	53.4087
ω_4	?A	385.3009	0.6085
ω_5	A'	782.0859	2.2715
ω_6	A'	1046.4013	15.0160
ω_7	A'	1154.4249	52.7624
ω_8	A'	1686.3029	62.5075
ω_9	A'	3257.0943	5.7930

Table A4.3 Harmonic frequencies (in cm^{-1}) and infrared intensities (in km mol^{-1}) for the doublet ground state of the CCHCS neutral 2. Harmonic frequencies are unscaled.

mode	symmetry	frequency	intensity
ω_1	?A	168.6284	10.7335
ω_2	?B	379.4991	2.5403
ω_3	?B	450.9631	8.9755
ω_4	?A	560.9561	12.3205
ω_5	?B	751.6267	21.7270
ω_6	?B	932.2523	2.2887
ω_7	?B	1349.7001	24.1871
ω_8	?B	1655.7939	157.9354
ω_9	A'	3013.0476	47.8924

Table A4.4 Harmonic frequencies (in cm^{-1}) and infrared intensities (in km mol^{-1}) for the doublet ground state of the (*cyclo*-C_3H)=S neutral 3. Harmonic frequencies are unscaled.

mode	symmetry	frequency	intensity
ω_1	A'	318.9153	2.4273
ω_2	A"	416.6332	1.6451
ω_3	A'	666.8498	0.0653
ω_4	A"	771.0797	18.6585
ω_5	A'	843.1654	123.2538
ω_6	A'	968.1537	17.3480
ω_7	A'	1218.8676	6.2215
ω_8	A'	1624.7053	52.9184
ω_9	A'	3256.4023	9.9848

Table A4.5 Harmonic frequencies (in cm^{-1}) and infrared intensities (in km mol^{-1}) for the doublet ground state of the HC_2CS neutral 4. Harmonic frequencies are unscaled.

mode	symmetry	frequency	intensity
ω_1	A'	158.4788	1.2749
ω_2	A"	183.1836	1.2661
ω_3	A'	349.5078	7.9866
ω_4	A"	495.6870	0.3802
ω_5	A'	650.0461	17.4801
ω_6	A'	989.4949	46.6689
ω_7	A'	1334.5868	109.9274
ω_8	A'	1973.5991	220.0676
ω_9	A'	2877.9836	295.9787

Table A4.6 Dipole moments and rotational constants for the four stable HC_3S neutrals 1 - 4 and for the C_2CHS and HC_2CS anions 1^- and 4^-. Parameters are calculated from the equilibrium geometry at the B3LYP/aug-cc-pVDZ level of theory.

Parameters†	μ_z	μ_y	μ_x	$\|\|\mu\|\|$	A	B	C
(1) $^{\bullet}C_2CHS$	0.0000	2.2997	-3.3248[a]	4.0426	30.6598	3.7208	3.3181
(1Q) $^{\bullet}C_2CHS$	0.0000	2.2917	-3.0940[a]	3.8502	20.1079	4.5187	3.6896
(2) $^{\bullet}CCHCS$	0.0000	1.4918[b]	-0.5831	1.6017	80.7409	2.9095	2.8083
(3) $^{\bullet}$*cyc*-(C_3H)=S	0.0000	-0.0061	2.4175[c]	2.4175	36.9757	4.2123	3.7815
(4) $HC_2CS^{\bullet}$	0.0000	-0.5565	-2.9255[d]	2.9780	536.5059	2.5693	2.5571
^-C_2CHS	0.0000	1.8779	-4.5425[e]	4.9154	52.1309	3.0677	2.8972
HC_2CS^-	0.0000	-1.2356[d]	-0.1014	1.2398	2388.1595	2.6390	2.6361

† Dipole moments are given in Debye and rotational constants are given in GHz.

[a] The molecule is oriented as depicted in Figure 4.1 with the x and y axes defining the plane of the page. Positive x axis is to the bottom left of the figure, and positive y axis is to the top left of the figure.

[b] The molecule is oriented as depicted in Figure 4.1 with the x and y axes defining the plane of the page. Positive x is to the bottom of the figure, and positive y axis is to the left of the figure.

[c] The molecule is oriented as depicted in Figure 4.1 with the x and y axes defining the plane of the page. Positive x is to the bottom left of the figure, and positive y axis is to the bottom right of the figure.

[d] The molecule is oriented as depicted in Figures 4.1 and 4.2 with the x and y axes defining the plane of the page. Positive x is to the bottom right of the figure, and positive y axis is to the top right of the figure.

[e] The molecule is oriented as depicted in Figure 4.2 with the x and y axes defining the plane of the page. Positive x is to the bottom of the figure, and positive y axis is to the left of the figure.

5 Summary and Conclusions

Experimental and theoretical studies have been carried out on a number of unusual organic molecules of potential astronomical significance. Stable, neutral precursors of the molecular systems investigated have been accessed experimentally via unequivocal pathways by the application of conventional synthetic chemical techniques. The molecules, once prepared by these means, were then probed by mass spectrometry, and specific use has been made of the two-sector modified VG ZAB 2HF mass spectrometer with BE configuration (where B and E represent magnetic and electric sectors, respectively).

The experimental work was corroborated by various theoretical approaches and by utilising computer-based quantum chemical calculations. The theoretical methods used throughout this work include density functional theory (specifically the B3LYP approach), which was employed to generate accurate predictions of structure, and coupled-cluster theories [in particular the CCSD(T) approach] to estimate thermochemical properties of the B3LYP-optimised geometries.

Accordingly, calculations at the CCSD(T)/aug-CC-pVDZ//B3LYP/6-31G(d) level of theory indicate that the radical anion of structure $[O_2C–CO_2]^{-\bullet}$ $\mathbf{1}^{-\bullet}$ (Chapter 2, pp. 63) is stable, but the analogous neutral could not be found on any neutral potential energy surface examined. Conversely, other neutral structures were identified: (i) a 1,3-dioxetane-2,4-dionyl singlet neutral **5** (Chapter 2, pp. 67), (ii) a planar $O_2C–CO_2$ triplet neutral **3** (Chapter 2, pp. 67), 77.7 kcal mol^{-1} higher in energy than **5**, and (iii) a 1,2-dioxetane-3,4-dionyl singlet neutral **4** (Chapter 2, pp. 67), 81.6 kcal mol^{-1} higher in energy than **5**. The anion could not be generated in the source of the mass spectrometer by the reaction of oxalic acid-d_2 with DO^-, but mass-selection of a source-formed anionic fragment at *m/z* 90 corresponding to mono-deuterated oxalate, gave rise to a small signal corresponding to $(O_2C\text{-}CO_2)^{-\bullet}$ at *m/z* 88 in the collisionally-induced dissociation (CID) spectrum. This signal

was, however, too weak to attempt mass selection and vertical one-electron oxidation. Theoretical calculations conducted in concert with experiment showed that dissociation of the anion into $^2CO_2^- + {}^1CO_2$ is an endothermic process by 20.7 kcal mol^{-1}, if an energy barrier of 22.9 kcal mol^{-1} can be overcome. It is unlikely that a stable neutral could be produced by a vertical, one-electron oxidation of the anion, because such a planar neutral would require less than 5 kcal mol^{-1} to overcome the barrier to exothermic dissociation (by -24.4 kcal mol^{-1}) into $^3CO_2 + {}^1CO_2$.

The covalently bound radical anion $[O_2C–CO]^{-\bullet}$ was formed through the one-electron capture by 1,3-dioxolane-2,5-dione followed by retro-cleavage of CH_2O. There are a number of neutral isomers with formula C_2O_3, as suggested by calculation at the CCSD(T)/aug-CC-pVDZ//B3LYP/6-31G(d) level of theory, *viz.* the van der Waals complex $O_2C{\cdot}CO$ **6** (relative energy 0 kcal mol^{-1}; Chapter 2, pp. 69), singlet oxiran dione (+60.9 kcal mol^{-1}), triplet OCOCO (+99.4 kcal mol^{-1}), covalently bound triplet $O_2C–CO$ (+ 107.6 kcal mol^{-1}), singlet trioxapropellane (+171.9 kcal mol^{-1}) and triplet trioxapropellane (+ 222.4 kcal mol^{-1}). Of these, only triplet $O_2C–CO$ is accessible by vertical Franck-Condon one-electron oxidation of $[O_2C–CO]^{-\bullet}$. Neutralisation reionisation spectra of $[O_2C–CO]^{-\bullet}$ (both $^-NR^+$ and $^-NR^-$) do not feature recovery signals corresponding to reionised C_2O_3, which means that neutral C_2O_3, if stable, must have a sub-10^{-6} second lifetime (i.e. less than the timeframe of an NR experiment). The $^-NR^+$ spectrum of $[O_2C–CO]^{-\bullet}$ reveals signals corresponding to $CO^{+\bullet}$, $CO_2^{+\bullet}$ and to $[O=C=C=O]^{+\bullet}$. The last of these species can only be formed from a decomposing $C_2O_3^{+\bullet}$ radical cation by a process endothermic by 47 kcal mol^{-1} [at the CCSD(T)/aug-CC-pVDZ//B3LYP/6-31G(d) level of theory]. Calculations at this same level of theory indicate that the vertical one-electron oxidation of $[O_2C–CO]^{-\bullet}$ anion produces the triplet neutral $O_2C–CO$ with a negligible amount of excess energy. There are two dissociation pathways available to this triplet

neutral: (i) an endothermic process yielding $^3CO + {}^1CO_2$ (+ 28.9 kcal mol^{-1}), and (ii) an exothermic process (-6.8 kcal mol^{-1}) with a barrier of 5.4 kcal mol^{-1} yielding $^1CO + {}^3CO_2$. A combination of experimental and theoretical data suggests that vertical oxidation of $[O_2C–CO]^{-\bullet}$ produces only one neutral C_2O_3 isomer; a transient triplet $O_2C–CO$ neutral whose lifetime is less than 10^{-6} seconds.

Theoretical calculations of the C_3HO potential surface at the CCSD(T)/aug-CC-pVDZ//B3LYP/6-31G(d) level indicate that the three radicals HC_2CO, C_2CHO, and (*cyclo*-C_3H)=O are stable, with HC_2CO being the most stable of the three. A fourth isomer, CCHCO, is unstable with respect to cyclisation to (*cyclo*-C_3H)=O. Two isomers were prepared by neutralisation of charged precursors: (i) HC_2CO, by $HC{\equiv}C–C(O)–{}^+O(H)(Me) \rightarrow HC_3O^+ + MeOH$, and (ii) C_2CHO, by (a) $Me_3Si–C{\equiv}C–CHO + HO^- \rightarrow {}^-C{\equiv}C–CHO + Me_3SiOH$ and (b) $^-C{\equiv}C–CH(OH)–C{\equiv}CH \rightarrow {}^-C{\equiv}C–CHO + C_2H_2$. A comparison of the CR and $^-NR^+$ spectra of ^-C_2CHO indicate that $^\bullet C_2CHO$ doublet neutral is partially rearranging to an isomer that shows significant formation of $CO^{+\bullet}$ in the $^-NR^+$ spectrum of the anion. *Ab initio* calculations indicate that HC_2CO is the product of the isomerism and that a proportion of these isomerised neutrals dissociate to CO and C_2H. The neutral $HC_2CO^\bullet$ may be formed by (i) synchronous rearrangement of $^\bullet C_2CHO$ and/or (ii) stepwise rearrangement of $^\bullet C_2CHO$ through (*cyclo*-C_3H)=O. The second of these processes should have the higher rate, as it has the lower barrier in the rate-determining step and the higher Arrhenius pre-exponential *A* factor.

Calculations at the CCSD(T)/Aug-CC-pVDZ//B3LYP/Aug-CC-pVDZ level indicate the existence of four isomers with empirical formula HC_3S as energy minima on the doublet neutral potential energy surface: a linear HC_2CS (relative energy 0 kcal mol^{-1}), (*cyclo*-C_3H)=S (+14.4 kcal mol^{-1}), C_2CHS (+38.9 kcal mol^{-1}), and CCHCS (+ 46.4 kcal mol^{-1}). Of these, the doublet neutral isomers HC_2CS and C_2CHS were generated by neutralisation of

anionic precursors in the following way: (i) HC_2CS, by $HC{\equiv}C{-}CH_2{-}S{-}C_2H_5 + O^{-\bullet} \rightarrow HC_2CS + H_2O + {}^{-}C_2H_5$, and (ii) C_2CHS, by $Me_3Si{-}C{\equiv}C{-}CH(-SCH_2CH_2S-) + F^{-}$ (generated from SF_6) $\rightarrow {}^{-}C{\equiv}C{-}CH(-SCH_2CH_2S-) \rightarrow {}^{-\bullet}C{\equiv}C{-}CH{=}S + SC_2H_5$. A comparison of the CR and $^{-}NR^{+}$ spectra of $^{-}C_2CHS$ indicates that $^{\bullet}C_2CHS$ doublet neutral is (partially) rearranging to an isomer that shows significant formation of $CS^{+\bullet}$ in the $^{-}NR^{+}$ spectrum of the anion. Calculations indicate that HC_2CS is the product of the isomerism and that a proportion of these isomerised neutrals dissociate to CS and $^{\bullet}C_2H$. The neutral $HC_2CS^{\bullet}$ may be formed by (1a) synchronous rearrangement of $^{\bullet}C_2CHS$ via a 1-3 H migration with an energy barrier of 34.5 kcal mol^{-1}, and/or (1b) synchronous rearrangement of $^{\bullet}C_2CHS$ via a 1-3 S migration with an essentially identical energy barrier of 34.6 kcal mol^{-1}, or (2) stepwise rearrangement of $^{\bullet}C_2CHS$ through 1-2 H migration to yield $[CCHCS]^{\bullet}$ with a barrier of 24 kcal mol^{-1}, followed by cyclisation to yield (*cyclo*-$C_3H){=}S$ via a negligible energy barrier, and then ring-cleavage with a barrier of 20.1 kcal mol^{-1} to yield HC_2CS. Calculation of the Arrhenius pre-exponential *A* factor for each isomerisation mechanism indicates that the stepwise pathway has the highest *A* factor. It also has the lowest barrier in the rate-determining step.

References

1 National Radio Astronomy Observatory, *http://www.cv.nrao.edu/~awootten/allmols.html*, **2002**.

2 Duley, W. W.; Williams, D. A. *Interstellar Chemistry*; Academic Press Inc.: London, **1984**.

3 Williams, D. A. *Chem. Eur. J.* **1997**, *3*, 1929.

4 Zeilik, M.; Gregory, S. A.; Smith, E. v. P. *Introductory Astronomy and Astrophysics*; Harcourt Brace Jovanovich College Publishers: Orlando, **1992**.

5 Omont, A. *Polyynes and Polycyclic Aromatic Molecules in C-rich Circumstellar Envelopes.* In *Molecules in the Stellar Environment*; Jørgensen, U. G., Ed.; Springer-Verlag: Copenhagen, Denmark, **1993**; Vol. 428.

6 Herbst, E. *Interstellar Chemistry in the Last Two Decades.* In *The Structure and Content of Molecular Clouds*; Wilson, T. L. and Johnston, K. J., Ed.; Springer-Verlag: Schloss Ringberg, Tegernsee, Germany, **1993**; Vol. 439.

7 Dykstra, C. E. *An Initio Calculation of The Structures and Properties of Molecules*; Elsevier: Amsterdam, **1988**; Vol. 58.

8 Snyder, L. E.; Dykstra, C. E.; Bernholdt, D. *Calculated Dipole Moments and Resulting Column Densities of Carbon Long Chain Molecules in TMC-1.* In *Masers, Molecules and Mass Outflows in Star Forming Regions*; Haschick, A. D., Ed.: Haystack Observatory, Massachusetts, **1985**.

9 McCabe, E. M.; Smith, R. C.; Clegg, R. E. S. *Nature* **1979**, *281*, 263; Lafont, S.; Lucas, R.; Omont, A. *Astron. Astrophys.* **1982**, *106*, 201.

10 Hinkle, K. H. *Infrared Spectroscopy and Molecules in Circumstellar Envelopes.* In *Molecules in the Stellar Environment*; Jørgensen, U. G., Ed.; Springer-Verlag: Copenhagen, Denmark, **1993**; Vol. 428.

11 Nejad, L. A. M.; Millar, T. J.; Freeman, A. *Astron. Astrophys.* **1984**, *134*, 129.

12 Woods, R. C.; Dixon, T. A.; Saykally, R. J.; Szanto, P. G. *Phys. Rev. Lett.* **1975**, *35*, 1269.

13 Buhl, D.; Snyder, L. E. *Nature* **1970**, *228*, 267.

14 Green, S.; Montgomery, J. A.; Thaddeus, P. *Astrophys. J.* **1974**, *193*, L89.

15 Bieging, J. H.; Tafalla, M. *Astrophys. J.* **1993**, *105*, 576.

16 Petrie, S.; Bettens, R. P.; Freeman, C. G.; McEwan, M. J. *J. Phys. Chem.* **1993**, *97*, 13673.

17 Avery, L. W.; al., e. *Astrophys. J.* **1975**, *205*, L173.

18 Bernath, P. F.; Hinkle, K. H.; Keady, J. J. *Science* **1989**, *244*, 562.

19 Haider, N.; Husain, D. *Z. Phys. Chem.* **1992**, *176*, 133.

20 Kaiser, R. I.; Ochsenfeld, C.; Head-Gordon, M.; Lee, Y. T.; Suits, A. G. *Science* **1996**, *274*, 1508.

21 Herbst, E. *Nature* **1981**, *289*, 656.

22 Omont, A. *Astron. Astrophys.* **1986**, *164*, 159; Lepp, S.; Dalgarno, A. *Astrophys. J.* **1988**, *324*, 553.

23 Bettens, R. P. A.; Herbst, E. *Astrophys. J.* **1996**, *468*, 686.

24 Petrie, S. *Mon. Not. R. Astron. Soc.* **1996**, *281*, 137.

25 Petrie, S.; Herbst, E. *Astrophys. J.* **1997**, *491*, 210.

26 Bell, M. B.; Feldmann, P. A.; Travers, M. J.; McCarthy, M. C.; Gottlieb, C. A.; Thaddeus, P. *Astrophys. J.* **1997**, *483*, L61.

27 McCarthy, M. C.; Grabow, J.-U.; Travers, M. J.; Chen, W.; Gottlieb, C. A.; Thaddeus, P. *Astrophys. J.* **1998**, *994*, L231.

28 Krüger, M.; Dreizler, H.; Preugschat, D.; Lentz, D. *Angew. Chem.* **1991**, *103*, 1674.

29 Botschwina, P.; Heyl, Ä.; Chen, W.; McCarthy, M. C.; Grabow, J.-U.; Travers, M. J.; Thaddeus, P. *J. Chem. Phys.* **1998**, *109*, 3108.

30 Thaddeus, P.; McCarthy, M. C.; Travers, M. J.; Gottlieb, C. A.; Chen, W. *Faraday Discussions* **1998**, *109*, 121.

31 Wolf, R.; Stadtmüller, S.; Wong, M. W.; Barbieux-Flammang, M.; Flammang, R.; Wentrup, C. *Chem. Eur. J.* **1996**, *2*, 1318; Wentrup, C.; Kappe, C. O.; Wong, M. W. *Pure Appl. Chem.* **1995**, *67*, 749.

32 Dempster, A. J. *Phys. Rev.* **1918**, *18*, 415.

33 Rose, M. E.; Johnstone, R. A. W. *Mass Spectrometry for Chemists and Biochemists*; Cambridge University Press: Cambridge, **1982**.

34 Budzikiewicz, H. *Angew. Chem., Int. Ed. Engl.* **1981**, *20*, 624.

35 Dillard, J. G. *Chem. Rev.* **1973**, *73*, 589.

36 Harrison, A. G. *Chemical Ionization Mass Spectrometry*; CRC Press: Boca Raton, **1983**.

37 Froelicher, S. W.; Freiser, B. S.; Squires, R. R. *J. Am. Chem. Soc.* **1986**, *108*, 2853.

38 Graul, S. T.; Squires, R. R. *J. Am. Chem. Soc.* **1988**, *110*, 607.

39 DePuy, C. H.; Bierbaum, V. M.; Flippin, L. A.; Grabowski, J. J.; King, G. K.; Schmitt, R. J.; Sullivan, S. A. *J. Am. Chem. Soc.* **1980**, *102*, 5012.

40 Klass, G.; Trenerry, C.; Sheldon, J. C.; Bowie, J. H. *Aust. J. Chem.* **1981**, *34*, 519.

41 DePuy, C. H.; Bierbaum, V. M.; Damrauer, R.; Soderquist, J. A. *J. Am. Chem. Soc.* **1985**, *107*, 3385.

42 Born, M.; Ingemann, S.; Nibbering, N. M. M. *Mass Spectrom. Rev.* **1997**, *16*, 181.

43 Bowie, J. H. *Mass Spectrom. Rev.* **1990**, *9*, 349; Bowie, J. H. *The Fragmentations of (M-H)⁻ Ions Derived from Organic Compounds.* In *Experimental Mass Spectrometry*; Russell, D. H., Ed.; Plenum Press: New York, **1994**.

44 Eichinger, P. C. H.; Bowie, J. H. *J. Org. Chem.* **1986**, *51*, 5078.

45 Dua, S.; Blanksby, S. J.; Bowie, J. H. *Int. J. Mass Spectrom.* **1999**, *195-196*, 45.

46 Chantry, P. J. *J. Chem. Phys.* **1969**, *51*, 3369; Chantry, P. J. *J. Chem. Phys.* **1969**, *51*, 3380.

47 Dawson, J. H. J.; Jennings, K. R. *J. Chem. Soc. Faraday Trans. 2* **1976**, *72*, 700.

48 Goode, G. C.; Jennings, K. R. *Adv. Mass Spectrom.* **1974**, *6*, 797.

49 Lee, J.; Grabowski, J. J. *Chem. Rev.* **1992**, *92*, 1611.

50 Nibbering, N. M. M. *Recl. Trav. Chim. Pays-Bas.* **1981**, *100*, 297.

51 McDonald, R. N.; Chowdhury, A. K.; Sester, D. W. *J. Am. Chem. Soc.* **1980**, *102*, 6491.

52 Schalley, C. A.; Blanksby, S. J.; Harvey, J. N.; Schröder, D.; Zummack, W.; Bowie, J. H.; Schwarz, H. *Eur. J. Org. Chem.* **1998**, 987.

53 Wenthold, P. G.; Hu, J.; Squires, R. R. *J. Am. Chem. Soc.* **1994**, *116*, 6961.

54 Wenthold, P. G.; Hu, J.; Squires, R. R. *J. Am. Chem. Soc.* **1996**, *118*, 11865.

55 Yates, B. F.; Bouma, W. J.; Radom, L. *J. Am. Chem. Soc.* **1984**, *106*.

56 Johnson, E. G.; Nier, A. O. *Phys. Rev.* **1953**, 10.

57 Beynon, J. H.; Caprioli, R. M.; Ast, T. *Org. Mass Spectrom.* **1971**, *5*, 229.

58 Beynon, J. H.; Cooks, R. G.; Amy, J. W.; Baitinger, W. E.; Ridley, T. Y. *Anal. Chem.* **1973**, *45*, 1023A.

59 Cooks, R. G.; Beynon, J. H.; Caprioli, R. M.; Lester, G. R. *Metastable Ions*; Elsevier: Amsterdam, **1973**.

60 Haddon, W. F.; McLafferty, F. W. *J. Am. Chem. Soc.* **1968**, *90*, 4745.

61 Atkins, P. W. *Physical Chemistry*; 5th ed.; Oxford University Press: Oxford, **1994**.

62 Kim, M. S.; McLafferty, F. W. *J. Am. Chem. Soc.* **1978**, *100*, 3279.

63 Wysocki, V. H.; Kenttämaa, H. I.; Cooks, R. G. *Int. J. Mass Spectrom. Ion Processes* **1987**, *75*, 181.

64 Todd, P. J.; McLafferty, F. W. *Collisionally Activated Dissociation of High Kinetic Energy Ions.* In *Tandem Mass Spectrometry*; McLafferty, F. W., Ed.; John Wiley and Sons: New York, **1983**.

65 Laramée, J. A.; Cameron, D.; Cooks, R. G. *J. Am. Chem. Soc.* **1981**, *103*, 12.

66 Holmes, J. L. *Org. Mass Spectrom.* **1985**, *20*, 169.

67 Bowie, J. H.; Blumenthal, T. *J. Am. Chem. Soc.* **1975**, *97*, 2959.

68 Bowie, J. H.; Blumenthal, T. *Aust. J. Chem.* **1976**, *29*, 115.

69 DeLange, W.; Nibbering, N. M. M. *Int. J. Mass Spectrom. Ion Processes* **1986**, *68*, 111.

70 Szulejko, J. E.; Bowie, J. H.; Howe, I.; Beynon, J. H. *Int. J. Mass Spectrom. Ion Phys.* **1980**, *34*, 99.

71 Bursey, M. *Mass Spectrom. Rev.* **1990**, *9*, 555.

72 Howe, I.; Bowie, J. H.; Szulejko, J. E.; Beynon, J. H. *Journal of the Chemical Society Chemical Communications* **1979**, 983.

73 Burgers, P. C.; Holmes, J. L.; Mommers, A. A.; Szulejko, J. E. *J. Am. Chem. Soc.* **1984**, *106*, 521.

74 Bursey, M. M.; Haas, J. R.; Harvan, D. J.; Parker, C. E. *J. Am. Chem. Soc.* **1979**, *101*, 5485.

75 Keough, T.; Beynon, J. H.; Cooks, R. G. *J. Am. Chem. Soc.* **1973**, *95*, 1695.

76 Kuhns, D. W.; Turecek, F. *Org. Mass Spectrom.* **1994**, *29*, 463; Sirois, M.; George, M.; Holmes, J. L. *Org. Mass Spectrom.* **1994**, *29*, 11; Bordas-Nagy, J.; Holmes, J. L.; Hop, C. E. C. A. *Int. J. Mass Spectrom. Ion Processes* **1988**, *85*, 241; Selgren, S. F.; Gellene, G. I. *J. Chem. Phys.* **1987**, *87*, 5804.

77 Terlouw, J. K.; Schwarz, H. *Angew. Chem., Int. Ed. Engl.* **1987**, *26*, 805; McLafferty, F. W. *Science* **1990**, *247*, 925; Zagorevskii, D. V.; Holmes, J. H. *Mass Spectrom. Rev.* **1994**, *13*, 133.

78 For an account of neutralisation reionisation of negative ions, and definitions of nomenclature, see: Goldberg, N.; Schwarz, H. *Acc. Chem. Res.* **1994**, *27*, 347, and references therein.

79 McLafferty, F. W.; Todd, P. J.; McGilvery, D. C.; Baldwin, M. A. *J. Am. Chem. Soc.* **1980**, *102*, 3360.

80 McMahon, A. W.; Chowdhury, S. K.; Harrison, A. G. *Org. Mass Spectrom.* **1989**, *24*, 620.

81 Danis, P. O.; Feng, R.; McLafferty, F. W. *Anal. Chem.* **1986**, *56*, 348.

82 Villeneuve, S.; Burgers, P. C. *Org. Mass Spectrom.* **1986**, *21*, 733.

83 Danis, P. O.; Feng, R.; McLafferty, F. W. *Anal. Chem.* **1986**, *58*, 355.

84 Lorquet, J. C.; Leyh-Nihaut, B.; McLafferty, F. W. *Int. J. Mass Spectrom. Ion Processes* **1990**, *100*, 465.

85 Nguyen, V. G.; Turecek, F. *J. Mass Spectrom.* **1996**, *31*, 842.

86 For an account of the application of the comparison of $^{-}NR^{+}$ and $^{-}CR^{+}$ spectra of an anion, see: Schalley, C. A.; Hornung, G.; Schröder, D.; Schwarz, H. *Chem. Soc. Rev.* **1998**, *27*, 91.

87 Wesdemiotis, C.; Leyh, B.; Fura, A.; McLafferty, F. W. *J. Am. Chem. Soc.* **1990**, *112*, 8655.

88 Goldberg, N.; Iraqi, M.; Schwarz, H. *Chem. Ber.* **1993**, *126*, 2353.

89 Feng, R.; Wesdemiotis, C.; Baldwin, M. A.; McLafferty, F. W. *Int. J. Mass Spectrom. Ion Processes* **1988**, *86*, 95.

90 Schalley, C. A.; Schröder, D.; Schwarz, H. *Int. J. Mass Spectrom. Ion Processes* **1996**, *153*, 173.

91 Longevialle, P. *Mass Spectrom. Rev.* **1992**, *11*, 157.

92 Waugh, R. J.; Hayes, R. N.; Eichinger, P. C. H.; Downard, K. M.; Bowie, J. H. *J. Am. Chem. Soc.* **1990**, *112*, 2537.

93 McLafferty, F. W. *Decompositions and Rearrangements of Organic Ions.* In *Mass Spectrometry of Organic Compounds*; McLafferty, F. W., Ed.; Academic Press: New York, **1963**; Budzikiewicz, H.; Djerassi, C.; Williams, D. H. *Mass Spectrometry of Organic Compounds*; Holden-Day: San Francisco, **1967**; Williams, D. H.; Howe, I. *Principles of Organic Mass Spectrometry*; McGraw Hill: London, **1972**; Williams, D. H.; Fleming, I. *Spectroscopic Methods in Organic Chemistry*; 4th ed.; McGraw-Hill: London, **1989**.

94 Foresman, J. B.; Frisch, Æ. *Exploring Chemistry with Electronic Structure Methods*; 2nd ed.; Gaussian Inc.: Pittsburgh, **1993**; Born, M.; Oppenheimer, J. R. *Ann. Phys.* **1927**, *84*, 457; Richards, W. G.; Cooper, D. L. *Ab Initio Molecular Orbital Calculations For Chemists*; Oxford University Press: Oxford, **1983**.

95 Hehre, W. J.; Radom, L.; Schleyer, P. v. R.; Pople, J. A. *Ab Initio Molecular Orbital Theory*; Wiley-Interscience: New York, **1986**.

96 Hartree, D. R. *Proceedings of the Cambridge Philosphical Society* **1928**, *24*, 426; Fock, V. *Z. Physik* **1930**, *61*, 126.

97 Hurley, A. C. *Electron Correlation in Small Molecules*; Academic Press: New York, 1976.

98 Lee, T. J.; Scuseria, G. E. *Quantum Mechanical Electronic Structure Calculations With Chemical Accuracy*; Langhoff, S. R., Ed.; Kluwer: Dordrecht, The Netherlands, **1995**.

99 Lee, T. J.; Scuseria, G. E. *J. Chem. Phys.* **1990**, *93*, 489; Scuseria, G. E.; Lee, T. J. *J. Chem. Phys.* **1990**, *93*, 5851.

100 Taylor, P. R.; Bacskay, G. B.; Hush, N. S.; Hurley, A. C. *Chem. Phys. Lett.* **1976**, *41*, 444; Bartlett, R. J.; Purvis, G. D. *Int. J. Quantum Chem.* **1978**, *14*, 561; Chiles, R. A.; Dykstra, C. E. *J. Chem. Phys.* **1981**, *74*, 4544; Paldus, J.; Cizek, J.; Shavitt, I. *Pys. Rev. A* **1972**, *5*, 50.

101 Pople, J. A.; Krishnan, R.; Schlegel, H. B.; Binkley, J. S. *Int. J. Quantum Chem.* **1978**, *XIV*, 545.

102 Noga, J.; Bartlett, R. J. *J. Chem. Phys.* **1987**, *86*, 7041; Noga, J.; Bartlett, R. J. *J. Chem. Phys.* **1988**, *89*, 3401 (E); Hoffmann, M. R.; Schaefer, H. F. *Adv. Quantum Chem.* **1986**, *18*, 207; Scuseria, G. E.; Schaefer, H. F. *Chem. Phys. Lett.* **1988**, *152*, 382; Watts, J. D.; Bartlett, R. J. *J. Chem. Phys.* **1990**, *93*, 6104.

103 Raghavachari, K.; Trucks, G. W.; Pople, J. A.; Head-Gordon, M. *Chem. Phys. Lett.* **1989**, *157*.

104 Hohenberg, P.; Kohn, W. *Phys. Rev. B* **1964**, *136*, 864.

105 Kohn, W.; Sham, L. J. *Phys. Rev.* **1965**, *140*, A1133.

106 Koch, W.; Holthausen, M. C. *A Chemist's Guide to Density Functional Theory*; 2nd ed.; Wiley-VCH: Weinheim, **2001**.

107 Becke, A. D. *Pys. Rev. A* **1988**, *38*, 3098; Becke, A. D. *J. Chem. Phys.* **1992**, *96*, 2155; Becke, A. D. *J. Chem. Phys.* **1992**, *97*, 9173; Becke, A. D. *J. Chem. Phys.* **1993**, *98*, 1372.

108 Perdew, J. P. *Phys. Rev. B* **1986**, *33*, 8822; Lee, C.; Yang, W.; Parr, R. G.; Perdew, J. P. *Phys. Rev.* **1988**, *37*, 785; Perdew, J. P.; Wang, Y. *Phys. Rev. B* **1992**, *45*, 13244.

109 Gill, P. M. W.; Johnson, B. G.; Pople, J. A.; Frisch, M. J. *Int. J. Quantum Chem. Symp.* **1992**, *26*.

110 Raghavachari, K.; Anderson, J. B. *J. Phys. Chem.* **1996**, *100*, 12960 .

111 Dunning, T. H. *J. Chem. Phys.* **1989**, *90*, 1007.

112 Heuts, J. P. A.; Gilbert, R. G.; Radom, L. *Macromolecules* **1995**, *28*, 8771.

113 Neumark, D. M. *Acc. Chem. Res.* **1993**, *26*, 33; Polanyi, J. C.; Zewail, A. H. *Acc. Chem. Res.* **1995**, *28*, 119.

114 Gilbert, R. G.; Smith, S. C. *Theory of Unimolecular and Recombination Reactions*; Blackwell: Oxford, **1990**.

115 Wilson, E. B.; Decius, J. C.; Cross, P. C. *Molecular Vibrations*; McGraw-Hill: New York, **1955**.

116 Dalgarno, A. *Astrochemistry: Historical Perspective and Future Challenges.* In *Astrochemistry: From Molecular Clouds to Planetary Systems*; Minh, Y. C. and Dishoeck, E. F. v., Ed.; Kluwer Academic Publishers: Sogwipo, Rep. of Korea, **1999**.

117 Lucas, R.; Liszt, H. S. *Molecules in Astrophysics: Probes and Processes*; Dishoeck, E. F. v., Ed.; Kluwer Academic Publishers: Dordrecht, **1997**.

118 Ehrenfreund, P.; Charnley, S. B. *Annu. Rev. Astron. Astrophys.* **2000**, *38*, 427.

119 Tielens, A. G. G. M.; Hagen, W. *Astron. Astrophys.* **1982**, *114*, 245 ; Schutte, W. A. *Water Ice on Comets and Satellites.* In *Laboratory Astrophysics and Space Research*; Ehrenfreund, P., Krafft, K., Kochan, H. and Pirronello, V., Ed.; Kluwer Academic Publishers: Dordrecht, **1999**.

120 Baird, C. *Environmental Chemistry*; W. H. Freeman and Company: New York, **1995**.

121 Rauhut, M. M. *Acc. Chem. Res.* **1969**, *2*, 80, and references cited therein.

122 Cordes, H. F.; Richter, H. P.; Heller, C. A. *J. Am. Chem. Soc.* **1969**, *91*, 7209.

123 Wesdemiotis, C.; McLafferty, F. W. *Chem. Rev.* **1987**, *87*, 485; Holmes, J. L. *Mass Spectrom. Rev.* **1989**, *8*, 513; Zagorevskii, D. V.; Holmes, J. L. *Mass Spectrom. Rev.* **1999**, *18*, 87.

124 Klots, C. E.; Compton, R. N. *J. Chem. Phys.* **1977**, *67*, 1779; Klots, C. E.; Compton, R. N. *J. Chem. Phys.* **1978**, *69*, 1636; Klots, C. E. *J. Chem. Phys.* **1979**, *71*, 4172; Stamatovic, A.; Leitner, K.; Ritter, W.; Stephan, K.; Mark, T. D. *J. Chem. Phys.* **1985**, *83*, 2942; Knapp, M.; Kreisle, D.; Echt, O.; Sattler, K.; Recknagel, E. *Surf. Sci.* **1983**, *156*, 313; Kondow, T.; Mitsuke, K. *J. Chem. Phys.* **1985**, *83*, 2612; Alexander, M. L.; Johnson, M. A.; Levinger, N. E.; Lineberger, W. C. *Phys. Rev. Lett.* **1986**, *57*, 976.

125 Zhou, M.; Andrews, L. *J. Chem. Phys.* **1999**, *110*, 6820.

126 DeLuca, M. J.; Niu, B.; Johnson, M. A. *J. Chem. Phys.* **1988**, *88*, 5857 .

127 Fleischman, S. H.; Jordan, K. D. *J. Phys. Chem.* **1987**, *91*, 1300 .

128 Bowen, K. H.; Eaton, J. G. *The Structure of Small Molecules and Ions*; Naaman, R. and Vagar, Z., Ed.; Plenum: New York, **1987**.

129 Raftery, M. J.; Bowie, J. H. *Aust. J. Chem.* **1987**, *47*, 711; Eichinger, P. C. H.; Hayes, R. N.; Bowie, J. H. *J. Am. Chem. Soc.* **1991**, *113*, 1949.

130 McAnoy, A. M.; Dua, S.; Blanksby, S. J.; Bowie, J. H. *J. Chem. Soc. Perkin Trans. 2* **2000**, 1665.

131 Refaey, K. M. A.; Franklin, J. L. *Int. J. Mass Spectrom. Ion Phys.* **1976**, *20*, 19.

132 Thompson, W. E.; Jacox, M. E. *J. Chem. Phys.* **1999**, *111*, 4487.

133 Schröder, D.; Schalley, C. A.; Harvey, J. N.; Schwarz, H. *Int. J. Mass Spectrom. Ion Processes* **1999**, *187*, 25.

134 Frapper, G.; Saillard, J.-Y. *J. Am. Chem. Soc.* **2000**, *122*, 5367, and references cited therein; Pyykkö, P. *J. Chem. Soc. Chem. Commun.* **1999**, 495 ; Lewars, E. *J. Mol. Struct. (Theochem)* **1996**, *363*, 1 .

135 Smith, G. P.; Cosby, P. C.; Mosely, J. T. *J. Chem. Phys.* **1977**, *67*, 3838; Jones, G. G.; Taylor, J. W. *J. Chem. Phys.* **1978**, *68*, 1768; Linn, S. H.; Ng, C. Y. *J. Chem. Phys.* **1981**, *75*, 4921; Illies, A. J.; Jarrod, M. F.; Inagner-Redeker, W.; Bowers, M. T. *J. Chem. Phys.* **1988**, *88*, 5204; Tsukuda, T.; Johnson, M. A.; Nagata, T. *Chem. Phys. Lett.* **1997**, *268*, 429.

136 Jacox, M. E.; Thompson, W. E. *J. Chem. Phys.* **1989**, *91*, 1410; Thompson, W. E.; Jacox, M. E. *J. Chem. Phys.* **1991**, *95*, 735; Jacox, M. E.; Thompson, W. E. *J. Phys. Chem.* **1991**, *95*, 2781.

137 Knight, L. B.; Steadman, J. *J. Chem. Phys.* **1982**, *77*, 1750; Giamello, E.; Murphy, D.; Marchese, L.; Marta, G.; Zeechina, A. *J. Chem. Soc. Faraday Trans.* **1993**, *89*, 3715; Knight, L. B.; Hill, D.; Berry, K.; Babb, R.; Fetter, D. *J. Chem. Phys.* **1996**, *105*, 5672.

138 Zhou, M.; Andrews, L. *J. Chem. Phys.* **1999**, *110*, 2414.

139 Legon, A. C.; Suckley, A. P. *J. Chem. Phys.* **1989**, *91*, 4440.

140 Randall, R. W.; Summersgill, J. P. L.; Howard, B. J. *J. Chem. Soc. Faraday Trans.* **1990**, *86*, 1943; Xu, Y.; McKellar, A. R. W.; Howard, B. J. *J. Mol. Spectrosc.* **1996**, *179*, 345; Muenter, J. S.; Bhattacharjee, R. *J. Mol. Spectrosc.* **1998**, *190*, 290; Raducu, V.; Gauthier-Roy, B.; Dahoo, R.; Abouaf-Marguin, L.; Langlet, J.; Caillet, J.; Allavena, M. *J. Chem. Phys.* **1996**, *105*, 10092 .

141 Raducu, V.; Gauthier-Roy, B.; Dahoo, R.; Abouaf-Marguin, L.; Langlet, J.; Caillet, J.; Allavena, M. *J. Chem. Phys.* **1995**, *102*, 9235; Langlet, J.; Caillet, J.; Allavena, M.; Raducu, V.; Gauthier-Roy, B.; Dahoo, R.; Abouaf-Marguin, L. *J. Mol. Struct.* **1999**, *484*, 145.

142 Schröder, D.; Heinemann, C.; Schwarz, H.; Harvey, J. N.; Dua, S.; Blanksby, S. J.; Bowie, J. H. *Chem. Eur. J.* **1998**, *4*, 2550.

143 Cooper, C. D.; Compton, R. N. *J. Chem. Phys.* **1973**, *59*, 3550 .

144 Zhou, M.; Zhang, L.; Chen, M.; Qin, Q. *J. Chem. Phys.* **2000**, *112*, 7089 .

145 Neumark, D. M.; Lykke, K. R.; Andersen, T.; Lineberger, W. C. *Phys. Rev.* **1985**, *32*, 1890.

146 Wong, M. W. *Chem. Phys. Lett.* **1996**, *256*, 391.

147 Schalley, C. A.; Hornung, G.; Schröder, D.; Schwarz, H. *Int. J. Mass Spectrom. Ion Processes* **1998**, *172*, 181.

148 For discussions of Franck-Condon overlap of potential surfaces of neutral and charged systems, see: Hornung, G.; Schalley, C. A.; Dieterle, M.; Schröder, D.; Schwarz, H. *Chem. Eur. J.* **1997**, *3*, 1866.

149 Szulejko, J. E.; Bowie, J. H.; Howe, I.; Beynon, J. H. *Int. J. Mass Spectrom. Ion Phys.* **1980**, *13*, 76.

150 Serck-Hanssen, K. *Acta Chem. Scand.* **1969**, *23*, 2900.

151 Becke, A. D. *J. Chem. Phys.* **1993**, *98*, 5648.

152 Stevens, P. J.; Devlin, F. J.; Chablowski, C. F.; Frisch, M. J. *J. Phys. Chem.* **1994**, *98*, 11623.

153 Lee, C.; Yang, W.; Parr, R. *Phys. Rev. B* **1988**, *37*, 785.

154 Becke, A. D. *J. Chem. Phys.* **1988**, *88*, 1053.

155 Barone, V.; Adamo, C.; Mele, F. *Chem. Phys. Lett.* **1996**, *249*, 240.

156 Frisch, M. J.; Trucks, G. W.; Schlegel, H. B.; Scuseria, G. E.; Robb, M. A.; Cheeseman, J. R.; Zakrzewski, V. G.; J. A. Montgomery, J.; Stratmann, R. E.; Burant, J. C.; Dapprich, S.; Millam, J. M.; Daniels, A. D.; Kudin, K. N.; Strain, M. C.; Farkas, O.; Tomasi, J.; Barone, V.; Cossi, M.; Cammi, R.; Mennucci, B.; Pomelli, C.; Adamo, C.; Clifford, S.; Ochterski, J.; Petersson, G. A.; Ayala, P. Y.; Cui, Q.; Morokuma, K.; Malick, D. K.; Rabuck, A. D.; Raghavachari, K.; Foresman, J. B.; Cioslowski, J.; Ortiz, J. V.; Baboul, A. G.; Stefanov, B. B.; Liu, G.; Liashenko, A.; Piskorz, P.; Komaromi, I.; Gomperts, R.; Martin, R. L.; Fox, D. J.; Keith, T.; Al-Laham, M. A.; Peng, C. Y.; Nanayakkara, A.; Challacombe, M.; Gill, P. M. W.; Johnson, B.; Chen, W.; Wong, M. W.; Andres, J. L.; Gonzalez, C.; Head-Gordon, M.; Replogle, E. S.; Pople, J. A. *Gaussian 98*; Revision A.9 ed.; Gaussian, Inc.: Pittsburgh PA, **1998**.

157 Szczepanski, J.; Ekern, S.; Vala, M. *J. Phys. Chem. A* **1997**, *101*, 1841 .

158 Cizek, J. *Adv. Chem. Phys.* **1969**, *14*, 35; Hampel, C.; Peterson, K.; Werner, H.-J. *Chem. Phys. Lett.* **1992**, *190*, 1; Knowles, P.; Hampel, C.; Werner, H.-J. *J. Chem. Phys.* **1993**, *99*, 5219; Watts, J. D.; Gauss, J.; Bartlett, R. J. J. *Chem. Phys.* **1993**, *98*, 8718.

159 Purvis, G. D.; Bartlett, R. J. *J. Chem. Phys.* **1982**, *76*, 1910.

160 Woon, D. E.; Dunning, T. H. *J. Chem. Phys.* **1993**, *98*, 1358; Dunning, T. H.; Peterson, K. A.; Woon, D. E. *Basis Sets: Correlation Consistent.* In *Encyclopedia of Computational Chemsitry*; Schleyer, P. v. R., Ed.; Wiley: Chichester, **1998**.

161 Lander, D. R.; Unfried, K. G.; Glass, G. P.; Curl, R. F. *J. Phys. Chem.* **1990**, *94*, 7759.

162 Haas, B. M.; Minton, T. K.; Felder, P.; Huber, J. R. *J. Phys. Chem.* **1991**, *95*, 5149.

163 Irvine, W. M.; Brown, R. D.; Cragg, D. M.; Friberg, P.; Godfrey, P. D.; Kaifu, N.; Matthews, H. E.; Ohishi, M.; Suzuki, H.; Takeo, H. *Astrophys. J.* **1988**, *355*, L89.

164 Winnewisser, G. *J. Mol. Spectrosc.* **1973**, *46*, 16.

165 Matthews, H. E.; Irvine, W. M.; Friberg, P.; Brown, R. D.; Godfrey, P. D. *Nature* **1984**, *310*, 125.

166 Brown, R. D.; Godfrey, P. D.; Elmes, P. S.; Podler, M.; Tack, L. M. *J. Am. Chem. Soc.* **1985**, *107*, 4112.

167 Herbst, E.; Smith, D.; Adams, N. G. *Astron. Astrophys.* **1984**, *138*, L13.

168 Maclagan, R. G. A. R.; McEwan, M. J.; Scott, G. B. *Chem. Phys. Lett.* **1995**, *240*, 185.

169 Ekern, S.; Szczepanski, J.; Vala, M. *J. Phys. Chem.* **1996**, *100*, 16109.

170 Petrie, S.; Bettens, R. P. A.; Freeman, C. G.; McEwan, M. J. *J. Phys. Chem.* **1993**, *97*, 13673.

171 Cooksy, A. L.; Watson, J. K. G.; Gottlieb, C. A.; Thaddeus, P. *Astrophys. J.* **1992**, *386*, L27.

172 Tomasic, Z. A.; Scuseria, G. E. *J. Phys. Chem.* **1991**, *95*, 6905.

173 Jiang, Q.; Graham, W. R. M. *J. Chem. Phys.* **1993**, *98*, 9251; Cooksy, A. L.; Watson, J. K. G.; Gottlieb, C. A.; Thaddeus, P. *J. Mol. Spectrosc.* **1992**, *153*, 610.

174 Cooksy, A. L.; Watson, J. K. G.; Gottlieb, C. A.; Thaddeus, P. *J. Chem. Phys.* **1994**, *101*, 178.

175 Wang, H.; Cooksy, A. L. *Chem. Phys.* **1996**, *213*, 139.

176 Ekern, S.; Vala, M. *J. Phys. Chem. A* **1997**, *101*, 3601.

177 Blanksby, S. J.; Dua, S.; Bowie, J. H.; Schröder, D.; Schwarz, H. *J. Phys. Chem. A* **1998**, *102*, 9949.

178 Noest, A. J.; Nibbering, N. M. M. *J. Am. Chem. Soc.* **1980**, *102*, 6427.

179 Thermochemical data from the NIST Chemistry Web book. http://webbook.nist.gov

180 Dua, S.; Sheldon, J. C.; Bowie, J. H. *Rapid Commun. Mass Spectrom.* **1994**, *8*, 533.

181 Dheandhanco, S.; Forte, L.; Fox, A.; Bohme, D. K. *Can. J. Chem.* **1986**, *64*, 641.

182 Nelson, C. C.; McCloskey, J. A. *J. Am. Soc. Mass Spectrom.* **1994**, *5*, 339.

183 Ikuda, S. *J. Chem. Phys.* **1997**, *106*, 4536.

184 Raksit, A. B.; Bohme, D. K. *Int. J. Mass Spectrom. Ion Phys.* **1983**, *49*, 275.

185 Polce, M. J.; Beranova, S.; Nold, M. J.; Wesdemiotis, C. *J. Mass Spectrom.* **1996**, *32*, 1073.

186 Okada, S.; Abe, Y.; Tanaguchi, S.; Yamabe, S. *J. Am. Chem. Soc.* **1987**, *109*, 295.

187 Hansen, K.; Campbell, E. E. B. *J. Chem. Phys.* **1996**, *104*, 5012; Ho, Y.-P.; Yang, Y.-C.; Klippenstein, S. J.; Dunbar, R. C. *J. Phys. Chem.* **1995**, *99*, 12115; Mitzner, R.; Campbell, E. E. B. *J. Chem. Phys.* **1995**, *103*, 2445.

188 Stringer, M. G.; Bowie, J. H.; Holmes, J. L. *J. Am. Chem. Soc.* **1986**, *108*, 3888.

189 Blanksby, S. J.; Dua, S.; Bowie, J. H. *J. Phys. Chem. A* **1999**, *103*, 5161.

190 Danheiser, R. L.; Fink, D. M.; Okano, K.; Tsai, Y. M.; Szezepanski, S. W. *Org. Synth. Coll. Vol. VIII* **1993**, 501.

191 Breslow, R.; Pecorar, J.; Sugimoto, T. *Org. Syn. Coll. Vol. VI* **1981**, 361.

192 Scheffler, H.; Elsässer, H. *Physics of the Galaxy and Interstellar Matter*; Springer: Berlin, **1988**.

193 Saito, S.; Kawaguchi, K.; Yamamoto, S.; Ohishi, M.; Suzuki, H.; Kaifu, N. *Astrophys. J. Lett.* **1987**, *317*, L115; Yamamoto, S.; Saito, S.; Kawaguchi, K.; Kaifu, N.; Suzuki, H.; Ohishi, M. *Astrophys. J. Lett.* **1987**, *317*; Fuente, A.; Cernicharo, J.; Barcia, A.; Gómez-González, J. *Astron. Astrophys.* **1990**, *231*, 151.

194 Bell, M. B.; Avery, L. W.; Feldman, P. A. *Astrophys. J.* **1993**, *417*, L37.

195 Cernicharo, J.; Guélin, M.; Hein, H.; Kahane, C. *Astron. Astrophys.* **1987**, *181*, L9.

196 Hirahara, Y.; Ohshima, Y.; Endo, Y. *Astrophys. J.* **1993**, *408*, L113; Gordon, V. D.; McCarthy, M. C.; Apponi, A. J.; Thaddeus, P. *Astrophysics Journal Supplement Series* **2001**, *134*, 311; Kasai, Y.; Kinichi, O.; Ohshima, Y.; Hirahara, Y.; Endo, Y.; Kawaguchi, K.; Muramaki, A. *Astrophys. J.* **1993**, *410*, L45.

197 Trimble, V. *Rev. Mod. Phys.* **1975**, *47*, 877.

198 Ohishi, M.; Suzuki, H.; Ishikawa, S.; Yamada, C.; Kanamori, H.; Irvine, W. M.; Brown, R. D.; Godfrey, P. D.; Kaifu, N. *Astrophys. J.* **1991**, *380*, L39.

199 Brown, R. D. *Astrophys. J.* **1985**, *297*, 302.

200 Suzuki, H.; Ohishi, M.; Kaifu, N.; Kasuga, T.; Ishikawa, S.; Miyaji, T. *Vistas Astron.* **1988**, *31*, 459; Millar, T. J.; Herbst, E. *Astron. Astrophys.* **1990**, *231*, 466.

201 Smith, D.; Adams, N. G.; Giles, K.; Herbst, E. *Astron. Astrophys.* **1988**, *200*, 191.

202 Petrie, S. *Mon. Not. R. Astron. Soc.* **1996**, *281*, 666, and references therein.

203 Herbst, E.; Leung, C. M. *Astrophys. J. Suppl. Series* **1989**, *69*, 271.

204 Howe, D. A.; Millar, T. J. *Mon. Not. R. Astron. Soc.* **1990**, *244*, 444.

205 Smith, I. W. M. *Int. J. Mass Spectrom. Ion Processes* **1995**, *149/150*, 231; Clary, D. C.; Stoecklin, T. S.; Wickham, A. G. *J. Chem. Soc. Faraday Trans.* **1993**, *89*, 2185; Rowe, B. R.; Canosa, A.; Sims, I. R. *J. Chem. Soc. Faraday Trans.* **1993**, *89*, 2193.

206 Millar, T. J.; Flores, J. R.; Markwick, A. J. *Mon. Not. R. Astron. Soc.* **2001**, *327*, 1173.

207 Flores, J. R.; Gómez, F. J. *J. Phys. Chem. A* **2001**, *105*, 10384.

208 Hirahara, Y.; Ohshima, Y.; Endo, Y. *J. Chem. Phys.* **1994**, *101*, 7342.

209 McCarthy, M. C.; Vrtilek, J. M.; Gottlieb, E. W.; Tao, F.-M.; Gottlieb, C. A.; Thaddeus, P. *Astrophys. J.* **1994**, *431*, L127.

210 Wazneh, L.; Guillemin, J. C.; Guenot, P.; Vallée, Y.; Denis, J. M. *Tetrahedron Lett.* **1988**, *29*, 5899.

211 Bock, H.; Hirabayashi, T.; Mohmand, S. *Chem. Ber.* **1982**, *115*, 492; Mohmand, S.; Bock, H. *Phosphorus Sulfur* **1983**, *14*, 185; Vallée, Y.; Ripoll, J. L.; Lafon, C.; Pfister-Guillouzo, G. *Can. J. Chem.* **1987**, *65*, 290.

212 Peppe, S.; Blanksby, S. J.; Dua, S.; Bowie, J. H. *J. Phys. Chem. A* **2000**, *104*, 5817.

213 Busch, K. L.; Glish, G. L.; McLuckey, S. A. *Mass Spectrometry/Mass Spectrometry: Techniques and Applications of Tandem Mass Spectrometry*; VCH Publishers: Weinheim, **1988**.

214 Lee, S. *Chem. Phys. Lett.* **1997**, *268*, 69.

215 Furth, P. S.; Hwu, J. R. *J. Am. Chem. Soc.* **1989**, *111*, 8842.

216 Brandsma, L. *Preparative Acetylenic Chemistry*; 2nd ed.; Elsevier Scientific Publishing Co.: New York, **1988**.

Publications

The Formation of the Neutral isomers NCCCCO and CCC(O)CN in the Gas Phase from Ionic Precursors: a Joint Experimental and Theoretical Study. Dua, S.; Peppe, S.; Bowie, J. H. *J. Phys. Chem. A* **2002**, in press.

(reprint unavailable at time of publication of thesis)

Is the Elusive Trioxydehydroethene Neutral (O_2C-CO) Detectable in the Gas Phase? Peppe, S.; Dua, S.; Bowie, J. H. *J. Phys. Chem. A* **2001**, *105,* 10139.

The unusual neutral OCOCO and possible charged analogues. A theoretical investigation. Dua, S.; Peppe, S.; Bowie, J. H. *J. Chem. Soc., Perkin Trans. 2*, **2001**, 2244.

Formation of Two Isomeric C_3HO Radicals from Charged Precursors in the Gas Phase. Potential Interstellar Molecules. Peppe, S.; Blanksby, S. J.; Dua, S.; Bowie, J. H. *Journal of Physical Chemistry A* **2000**, *104*, 5817.

The unusual neutral OCOCO and possible charged analogues. A theoretical investigation

Suresh Dua, Salvatore Peppe and John H. Bowie

Department of Chemistry, The University of Adelaide, South Australia, 5005

Received (in Cambridge, UK) 17th September 2001, Accepted 12th October 2001
First published as an Advance Article on the web 9th November 2001

Calculations at the CCSD(T)/aug-cc-pVDZ//B3LYP/6-31+G(d) level of theory indicate that singlet neutral OCOCO is unstable with respect to dissociation to CO_2 and CO. In contrast, triplet OCOCO is a stable species provided it can be formed with excess energy of less than 41 kJ mol^{-1} [the process ^{3}OCOCO $\longrightarrow$ ^{1}CO + $^3CO_2$ is endothermic by only 9 kJ mol^{-1}, but the barrier for this process is 41 kJ mol^{-1}]. Triplet OCOCO is not accessible by one-electron oxidation from [OCOCO]$^-$· or one-electron reduction from [OCOCO]$^+$· because neither of these charged species is stable at the level of theory used for these calculations. A report by Cooper and Compton indicates that dissociative electron capture by maleic anhydride results in loss of the elements of C_2H_2 yielding an anion $C_2O_3^-$·. Calculations at the CCSD(T)/aug-cc-pVDZ//B3LYP/6-31+G(d) level of theory suggests that the ion radical $C_2O_3^-$· may be the stable species [O_2C–CO]$^-$· provided that the dissociating maleic anhydride radical anion has excess energy of at least 260 kJ mol^{-1}.

Introduction

Carbon monoxide and carbon dioxide cluster ions are important in atmospheric chemistry. Carbon dioxide cluster neutrals and ions have been studied extensively in the gas phase: these studies include their photoelectron,[1–6] vibrational,[7–10] electron spin resonance,[11–13] and infrared[14,15] spectra. The van der Waals complex between carbon dioxide and carbon monoxide was first formed in a pulsed molecular beam using diode laser spectroscopy combined with Fourier-transform microwave spectroscopy.[16] This CO_2–CO complex has since been studied extensively both experimentally and theoretically.[17–21] The complex is proposed to have the T-shaped geometry shown in **1**,[22] but infrared spectroscopy suggests that there may be two stable conformers of the complex.[20,21]

We have calculated at the CCSD(T)/aug-cc-pVDZ//B3LYP/6-31+G(d) level of theory that there are six C_2O_3 neutral structures which occupy minima on the C_2O_3 potential surface.[23] Structures which contain O–O bonds have not been considered in either the earlier report[23] or this paper. The six stable structures are shown (with relative energies in kJ mol^{-1}) in Scheme 1.

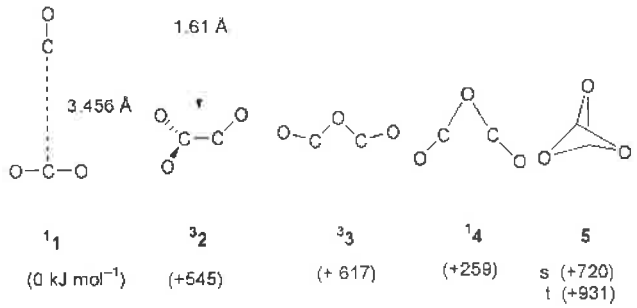

Scheme 1

The singlet state of the van der Waals complex **1** is the structure most negative in energy, but it decomposes to CO_2 and CO when the excess energy is only 6 kJ mol^{-1}. The other structures are all covalently bound. Only bond connectivities are shown in Scheme 1, full geometric data have been reported previously.[23]

We have used neutralisation/reionisation of negative ions ($^-NR^+$)[24] in a mass spectrometer to investigate the formation and characterisation of short-lived neutrals in the gas phase. The anion radical corresponding to neutral **2** was synthesised by electron capture of 1,3-dioxolane-2,5-dione, followed by a retro cleavage as shown in eqn. (1). One-electron oxidation by

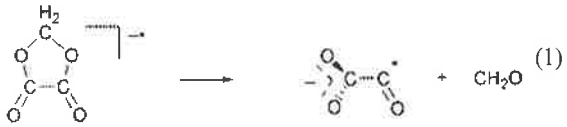

(1)

a Franck–Condon process of this anion radical should produce the triplet neutral **2**, but ionisation of the neutrals formed from [O_2CCO]$^-$· does not give a detectable parent cation [O_2CCO]$^+$·, and we concluded that any transient triplet neutral O_2CCO, if formed during this experiment, must have a lifetime less than 10^{-6} s.[23] Another conclusion reached in this study was that none of the other neutrals shown in Scheme 1 were accessible following one-electron oxidation of the radical anion [O_2CCO]$^-$·. This raises an interesting question. Could any of the other neutrals shown in Scheme 1 be synthesised in a mass spectrometer by way of a suitable neutralisation–ionisation experiment? Although the syntheses of charged precursors of neutral **4**† and **5** seem unlikely processes, the formation of a neutral corresponding to triplet OCOCO does, at first sight, appear to be worth consideration.

This paper investigates the triplet neutral system OCOCO and possible precursors, either positively or negatively charged.

Results and discussion

Data concerning the geometry of triplet OCOCO [calculated at the B3LYP/6-31+G(d) level of theory] and energy [at the CCSD(T)/aug-cc-pVDZ//B3LYP/6-31+G(d) level] are listed in Table 1. The end and central C–O bond lengths are 1.18 and 1.39 Å, respectively, with OCO and COC angles being 124.3

† Singlet **4** is only 'stable' using the definition of theoretical stability: *i.e.* the occupation of a potential minimum on the neutral potential surface. Increasing the bond length of either C–C or C–O bonds of the ring of **4** by only 0.1 Å results in immediate decomposition to CO_2 and CO in a process exothermic by 250 kJ mol^{-1} at the level of theory used in this study.

 DOI: 10.1039/b108425a

Table 1

	$O^5-C^1-O^4-C^2-O^3$	$O^5-C^1-O^4-C^2-O^3$ TS
State	$^3A'$	$^3A'$
Symmetry	C_s	C_s
Energy (Hartree)[a]	−301.08681	−301.07120
Rel. energy (kJ mol^{-1})	0.00	40.93
Adiabatic electron affinity/eV	0.00	0.42
Dipole moment/Debye [a]	0.65	2.11
Bond length/Å [b] or angle/° [b]		
C^1C^2	2.35	2.74
C^2O^3	1.18	1.14
C^1O^4	1.38	1.31
C^2O^4	1.38	1.95
C^1O^5	1.18	1.20
$C^1C^2O^3$	156.4	147.4
$C^2C^1O^4$	31.9	41.2
$C^2C^1O^5$	156.4	163.8
$O^4C^1O^5$	124.4	122.6
$O^3C^2C^1O4$	0.0	0.0
$O^3C^2C^1O^5$	0.0	0.0
Total atomic charges		
C^1	0.444	0.387
C^2	0.444	0.280
O^3	−0.300	−0.144
O^4	−0.289	−0.240
O^5	−0.300	−0.283
Sum of Mulliken charges	0.000	0.000

[a] CCSD(T)/aug-cc-pVDZ level of theory including zero point energy (calculated from vibrational frequencies at the B3LYP/6-31+G(*d*) level of theory and scaled by 0.9804.) [b] Geometries at B3LYP/6-31+G(d) level of theory.

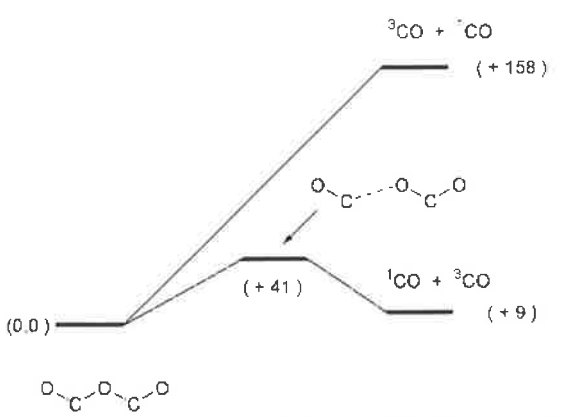

Fig. 1 Decompositions of triplet OCOCO. CCSD(T)/aug-cc-pVDZ//B3LYP/6-31+G(d) level of theory. Relative energies in kJ mol^{-1}. Geometries and energies of triplet OCOCO and transition state shown in this figure are listed in Table 1.

and 111.4°, respectively. This is consistent with the end CO bonds being double bonds and the two central bonds being single bonds. Thus the structure of triplet OCOCO may be represented as the classical valence bond structure O=C–O–C=O. The dipole moment of triplet OCOCO is calculated to be 1.35 D.

Of the possible decomposition pathways of triplet OCOCO, those forming CO_2 and CO are the most likely: these processes are depicted [energies determined using the CCSD(T)/aug-cc-pVDZ//B3LYP/6-31+G(d) level of theory] in Fig. 1. Decomposition to ^3CO plus $^1CO_2$ is endothermic by 158 kJ mol^{-1}. The alternative decomposition to ^1CO and $^3CO_2$ is endothermic by only 9 kJ mol^{-1}, but this dissociation process has a barrier of 41 kJ mol^{-1}. Details of the transition state for this process are given in Table 1. We conclude from these data that triplet OCOCO should, in principle, be accessible in a neutralisation–

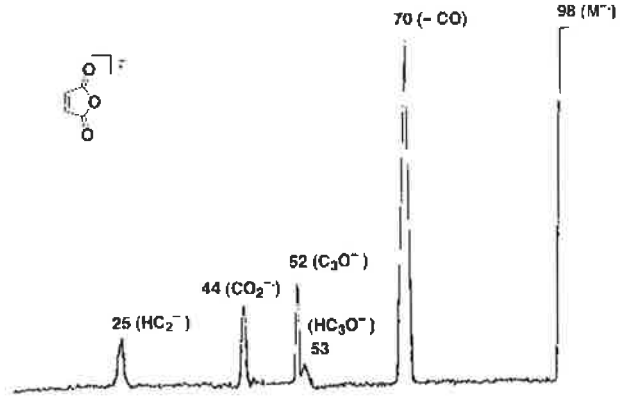

Fig. 2 The collision induced mass spectrum (MS/MS) of the molecular radical anion of maleic anhydride. Micromass VG ZAB 2HF mass spectrometer. For experimental details see the Experimental section.

reionisation experiment from either a negative or positive ion precursor provided any excess energy of the neutral is less than 41 kJ mol^{-1}.

In order to form OCOCO by a neutralisation–reionisation experiment, we must first synthesise either $[OCOCO]^{-\bullet}$ or $[OCOCO]^{+\bullet}$. There are no literature reports of a radical cation corresponding to this structure, but Cooper and Compton[25] have reported that maleic anhydride, which has an electron affinity of about 1.4 eV, captures a low-energy electron to form a molecular radical anion $C_4H_2O_3$, together with four fragment ions formed by dissociative electron attachment; these are $C_2H_2CO_2^-$, $C_2H_2CO^-$, $C_2O_3^{-\bullet}$ and $CO_2^{-\bullet}$. The C_2O_3 radical anion is formed at 0.1, 1.2, 2.2 and 2.7 eV, with the lifetime of the ion formed at 1.2 eV being 117 μs. The $C_2O_3^{-\bullet}$ ion was not observed in the negative ion spectra of any other anhydrides.[25] The authors do not propose a structure for $C_2O_3^{-\bullet}$ (*m/z* 72) formed from maleic anhydride, but, at least initially, it must correspond to a radical anion with bond connectivity OCOCO.

We next attempted to calculate the structures of both $[OCOCO]^{-\bullet}$ and the radical cation analogue $[OCOCO]^{+\bullet}$ at the CCSD(T)/aug-cc-pVDZ//B3LYP/6-31+G(d) level of theory. We find that neither ion occupies a potential minimum on the appropriate potential surface. Each structure is unstable with respect to dissociation to form charged and/or neutral (as appropriate) CO_2 and CO. Since neither of the charged species corresponding to OCOCO is stable, we will not be able to use neutralisation–reionisation to effect the synthesis of the desired triplet neutral OCOCO.

Since the radical anion $[OCOCO]^{-\bullet}$ is an unstable species, what then is (are) the structure (structures) of the $C_2O_3^{-\bullet}$ species(s) formed on dissociative electron capture of maleic anhydride? We do not have the experimental facilities to allow us to repeat the experiment of Cooper and Compton, so we are unable to determine whether the peak at *m/z* 72 corresponds to $C_2O_3^{-\bullet}$ or to some source-formed impurity. We have, however, measured the collision induced spectrum of the maleic anhydride molecular anion: this is shown in Fig. 2.

The collision induced spectrum of the maleic anhydride radical anion shows fragment peaks corresponding to $C_3H_2O_2^{-\bullet}$, $C_3HO^{-\bullet}$, C_3O^-, $CO_2^{-\bullet}$ and C_2H^-. No peak at *m/z* 72 ($C_2O_3^{-\bullet}$) is noted in this spectrum. This observation by itself does not imply that *m/z* 72 formed in the experiment of Cooper and Compton is an impurity. It may be that a $C_2O_3^{-\bullet}$ species is formed on collisional activation of the molecular anion of maleic anhydride, but that it has sufficient excess energy to effect decomposition, and, as a consequence not be observable in Fig. 2. However, in this context, it needs to be noted that a peak corresponding to low-energy $CO_2^{-\bullet}$ ions is observed in Fig. 2. The $CO_2^{-\bullet}$ story is a complex one, but in summary, carbon dioxide has an electron affinity of −0.6 ± 0.2 eV (−59 ± 19 kJ mol^{-1}),[26,27] but there is a small barrier of *ca.* 15 kJ mol^{-1}

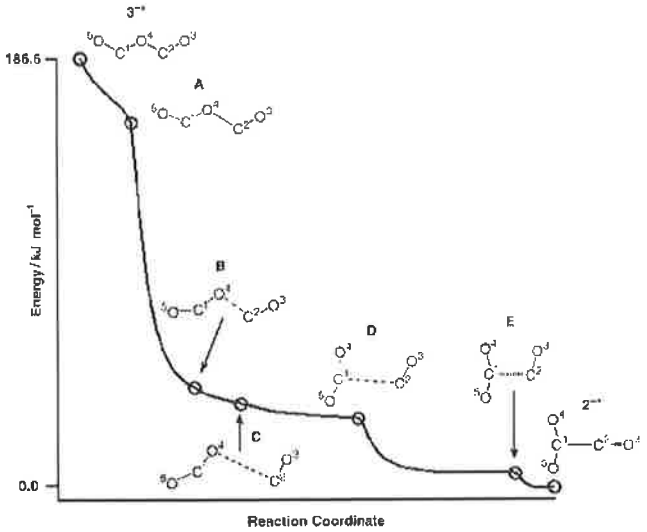

Fig. 3 MOLDEN projections of the reaction coordinate of the $[OCOCO]^{-\bullet}$ to $[O_2CCO]^{-\bullet}$ rearrangement. CCSD(T)/aug-cc-pVDZ//B3LYP/6-31+G(d) level of theory. Internuclear lengths (Å): $\mathbf{3}^{-\bullet}$, C^1C^2 (2.29), C^2O^4 (1.40); **A**, C^1C^2 (2.35), C^2O^4 (1.85); **B**, C^1C^2 (3.38), C^2O^4 (2.97); **C**, C^1C^2 (4.07), C^2O^4 (4.02); **D**, C^1C^2 (2.44), C^2O^4 (3.16); **E**, C^1C^2 (1.79), C^2O^4 (2.52); $\mathbf{2}^{-\bullet}$, C^1C^2 (1.61), C^2O^4 (2.38).

to electron detachment which enables the detection of $CO_2^{-\bullet}$ provided that the ion does not have sufficient energy (≥15 kJ mol^{-1}) to surmount the barrier for electron detachment.[25]

If there is a species $[C_2O_3]^{-\bullet}$ formed from maleic anhydride following or accompanying dissociative electron capture, then it does not correspond to $[OCOCO]^{-\bullet}$ but to some rearranged structure. We have carried out calculations at the CCSD(T)/aug-cc-pVDZ//B3LYP/6-31+G(d) level of theory on this system and have used the MOLDEN program,[28] to track the reaction coordinate of any such rearrangement. The results of these computations are shown in Fig. 3. The data in Fig. 3 show that, on formation, unstable $[OCOCO]^{-\bullet}$ ($\mathbf{3}^{-\bullet}$) rearranges to the isomer $[O_2CCO]^{-\bullet}$ ($\mathbf{2}^{-\bullet}$). The only potential minimum shown in Fig. 3 is that of product $\mathbf{2}^{-\bullet}$; all other indicated structures are points on the reaction coordinate chosen to illustrate the mechanistic course of the rearrangement. The intimate details of the rearrangement are interesting. The radical anion begins to dissociate at a region corresponding to structure **A**. Instead of dissociating further at this point, the system, essentially now CO_2 and $CO^{-\bullet}$, rotates within the plane to form **D** which is held together by weak electrostatic interactions. Mulliken analysis indicates that the OCO and $CO^{-\bullet}$ carbons have Mulliken charge densities of +0.749 and −0.757, respectively. Thus the δ^+ C^1 and δ^- C^2 come together to form planar **E**, which then undergoes rotation of the CC bond to form $\mathbf{2}^{-\bullet}$. Radical anion $\mathbf{2}^{-\bullet}$ is formed with an excess energy of 187 kJ mol^{-1}, so unless this radical anion is collisionally stabilised, it will dissociate by one, or both of the processes shown in Scheme 2.

$$[O_2CCO]^{-\bullet} \rightarrow CO^{-\bullet} + CO_2 \ (+126 \text{ kJ mol}^{-1})$$
$$[O_2CCO]^{-\bullet} \rightarrow CO + CO_2^{-\bullet} \ (+59 \text{ kJ mol}^{-1})$$

Scheme 2

If an energised maleic anhydride molecular anion fragments *via* a decomposing species $[OCOCO]^{-\bullet}$, the three processes shown in Scheme 3 might, in principle, be operative. We have calculated the thermochemistry for these three overall processes from the maleic anhydride radical anion at the CCSD(T)/aug-cc-pVDZ//B3LYP/6-31+G(d) level of theory. Results are shown in Scheme 3.

Peak maxima for *m/z* 72 (from dissociation of maleic anhydride radical anions) were observed by Compton and Cooper using electrons of energies 0.1 eV (10 kJ mol^{-1}), 1.2 eV

$$[C_4H_2O_3]^{-\bullet} \xrightarrow{-C_2H_2} [OCOCO]^{-\bullet} \begin{cases} \rightarrow [O_2C\text{-}CO]^{-\bullet} & (+262 \text{ kJ mol}^{-1}) \\ \rightarrow CO_2^{-\bullet} + CO & (+329 \text{ kJ mol}^{-1}) \\ \rightarrow CO_2 + CO^{-\bullet} & (+393 \text{ kJ mol}^{-1}) \end{cases}$$

Scheme 3

(116 kJ mol^{-1}), 2.2 eV (212 kJ mol^{-1}) and 2.7 eV (260 kJ mol^{-1}). Insufficient energy is available to effect either of the dissociation processes shown in Scheme 3, however the peak at *m/z* 72 could, in principle, correspond to $[O_2CCO]^{-\bullet}$ [rearrangement process, Scheme 3, +262 kJ mol^{-1}] when the energy of the captured electrons is 2.7 eV. It must be stressed that the results of calculations shown in Scheme 3 provide the thermochemistries of the three overall processes; they do not provide data concerning individual steps or barriers.

Conclusions

Theoretical calculations indicate that: (*i*) triplet OCOCO should be a stable species provided it can be formed with an excess energy less than 41 kJ mol^{-1}; (*ii*) the radical anion and radical cation of OCOCO are unstable species, and as a consequence cannot be used as precursors of triplet OCOCO using neutralisation–reionisation; (*iii*) the species *m/z* 72 observed by Compton and Cooper following dissociative electron capture from maleic anhydride cannot be $[OCOCO]^{-\bullet}$. If electrons captured by maleic anhydride have energies of ≥2.7 eV (≥260 kJ mol^{-1}) the initially formed (and unstable) species $[OCOCO]^{-\bullet}$ could, in principle, rearrange *via* a barrierless exothermic process to yield the isomer $[O_2CCO]^{-\bullet}$.

Experimental

A Mass spectrometric methods

For a detailed description of the experiment and the instrument used see ref. 29. In brief, the experiments were performed using a two-sector modified VG ZAB 2HF mass spectrometer with BE configuration, where B and E represent magnetic and electric sectors, respectively. The maleic anhydride radical anion was generated by electron capture in the chemical ionisation source operating in the negative ion mode, with typical source conditions as follows: source temperature 200 °C, repeller voltage −0.5 V, ion extraction voltage 7 kV, mass resolution $m/\Delta m$ ≥ 1500. Maleic anhydride (available commercially) was placed in a small glass capillary tube which was then drawn out in a flame to create a very fine aperture, allowing for a slow steady release of sample vapour upon heating. The capillary was inserted into the CI source *via* the direct probe; the probe tip was heated to 60 °C to generate a background pressure of *ca.* 10^{-5} Torr inside the source housing. The collision induced spectrum of the maleic anhydride radical anion was effected using argon as the target gas in the first collision gas after the magnetic sector. The pressure of argon in the cell was maintained such that 80% of the parent ion beam was transmitted through the cell. This corresponds to an average of 1.1–1.2 collisions per ion.[30] Product ions resulting from CID were recorded by scanning E.

B Theoretical methods

Geometry optimizations were carried out with the Becke 3LYP method[31,32] using a modest 6-31+G(d) basis within the GAUSSIAN 98 suite of programs.[33] Stationary points were characterised as either minima (no imaginary frequencies) or transition structures (one imaginary frequency) by calculation of the frequencies using analytical gradient procedures. The minima connected by a given transition structure were confirmed by

intrinsic reaction coordinate (IRC) calculations. The calculated frequencies were also used to determine zero-point vibrational energies which were then scaled[34] by 0.9804 and used as a zero-point correction for the electronic energies calculated at this and higher levels of theory. B3LYP/6-31+G(d) has previously been used for geometry optimizations of anions and has demonstrated good correlation with structures calculated using high level coupled-cluster approaches.[35,36] Some problems have been highlighted in the literature regarding the use of the B3LYP method for the accurate prediction of molecular energies for carbon clusters,[37] even though the method continues to be used with success.[38,39] More accurate energies for the B3LYP geometries were determined using the CCSD(T) method[40–45] together with the Dunning aug-cc-pVDZ basis set.[46,47] The CCSD(T)/aug-cc-pVDZ//B3LYP/6-31+G(d) approach predicts the adiabatic electron affinity of linear C_4 to be 3.65 eV[29] which is in reasonable agreement with the experimentally measured value of 3.88 eV.[48,49] All calculations were carried out on the AlphaServer SC at the Australian National University Supercomputing Facility (Canberra).

Acknowledgements

We thank the Australian Research Council for continuing financial support of our ion chemistry program, and the Australian National University for a generous allocation of time on their AlphaServer super computer.

References

1 G. P. Smith, P. C. Cosby and J. T. Mosely, *J. Chem. Phys.*, 1977, **67**, 3838.
2 G. G. Jones and J. W. Taylor, *J. Chem. Phys.*, 1978, **68**, 1768.
3 S. H. Linn and C. Y. Ng, *J. Chem. Phys.*, 1981, **75**, 4921.
4 A. J. Illies, M. F. Jarrod, W. Inagner-Redeker and M. T. Bowers, *J. Chem. Phys.*, 1988, **88**, 5204.
5 M. J. DeLuca, B. Niu and M. A. Johnson, *J. Chem. Phys.*, 1988, **88**, 5857.
6 T. Tsukuda, M. A. Johnson and T. Nagata, *Chem. Phys. Lett.*, 1997, **268**, 429.
7 M. E. Jacox and W. E. Thompson, *J. Chem. Phys.*, 1989, **91**, 1410.
8 W. E. Thompson and M. E. Jacox, *J. Chem. Phys.*, 1991, **95**, 735.
9 M. E. Jacox and W. E. Thompson, *J. Phys. Chem.*, 1991, **95**, 2781.
10 W. E. Thompson and M. E. Jacox, *J. Chem. Phys.*, 1999, **111**, 4487, and references cited therein.
11 L. B. Knight and J. Steadman, *J. Chem. Phys.*, 1982, **77**, 1750.
12 E. Giamello, D. Murphy, L. Marchese, G. Marta and A. Zeechina, *J. Chem. Soc., Faraday Trans.*, 1993, **89**, 3715.
13 L. B. Knight, D. Hill, K. Berry, R. Babb and D. Fetter, *J. Chem. Phys.*, 1996, **105**, 5672.
14 M. F. Zhou and L. Andrews, *J. Chem. Phys.*, 1999, **110**, 2414.
15 M. F. Zhou and L. Andrews, *J. Chem. Phys.*, 1999, **110**, 6820.
16 A. C. Legon and A. P. Suckley, *J. Chem. Phys.*, 1989, **91**, 4440.
17 R. W. Randall, J. P. L. Summersgill and B. J. Howard, *J. Chem. Soc., Faraday Trans.*, 1990, **86**, 1943.
18 Y. Xu, A. R. W. McKellar and B. J. Howard, *J. Mol. Spectrosc.*, 1996, **179**, 345.
19 J. S. Muenter and R. Bhattacharjee, *J. Mol. Spectrosc.*, 1998, **190**, 290.
20 V. Raducu, B. Gauthierroy, R. Dahoo, L. Abouafmarguin, J. Langlet, J. Caillet and M. Allavena, *J. Chem. Phys.*, 1995, **102**, 9235.
21 J. Langlet, J. Caillet, M. Allavena, V. Raducu, B. Gauthier-Roy, R. Dahoo and L. Abouaf-Marguin, *J. Mol. Struct.*, 1999, **484**, 145.
22 Structures drawn in the text or the figures indicate the bond connectivity and the overall geometry. These structures do not indicate the bond order except when indicated to the contrary [*e.g.* in eqn. 1]. Bond lengths are listed in Tables 1 and 3–5. S. Peppe, S. Dua and J. H. Bowie, *J. Chem. Phys. A.*, in the press.
23 S. Peppe, S. Dua and J. H. Bowie, *J. Chem. Phys. A*, in the press.
24 C. Wesdemiotis and F. W. McLafferty, *Chem. Rev.*, 1987, **26**, 805; J. L. Holmes, *Mass Spectrom. Rev.*, 1989, **8**, 513; for recent reviews of the neutralisation–reionisation technique and nomenclature see; C. A. Shalley, G. Hornung, D. Schröder and H. Schwarz, *Int. J. Mass Spectrom. Ion Processes*, 1998, **172**, 181; D. V. Zagorevskii and J. L. Holmes, *Mass Spectrom. Rev.*, 1999, **18**, 87.
25 C. D. Cooper and R. N. Compton, *J. Chem. Phys.*, 1973, **59**, 3550.
26 R. N. Compton, P. W. Reinhardt and C. D. Cooper, *J. Chem. Phys.*, 1975, **63**, 3821.
27 D. Yu, A. Rauk and D. A. Armstrong, *J. Phys. Chem.*, 1992, **96**, 6031.
28 A. Schaftenaar and J. H. Noordik, *J. Comput.-Aided Mol. Des.*, 2000, **14**, 123.
29 S. J. Blanksby, D. Schröder, S. Dua, J. H. Bowie and H. Schwarz, *J. Am. Chem. Soc.*, 2000, **122**, 7105 and references cited therein.
30 J. L. Holmes, *Org. Mass Spectrom.*, 1985, **20**, 169.
31 A. D. Becke, *J. Phys. Chem.*, 1993, **98**, 5648.
32 P. J. Stevens, F. J. Devlin, C. F. Chablowski and M. J. Frisch, *J. Phys. Chem.*, 1994, **98**, 11623.
33 M. J. Frisch, G. W. Trucks, H. B. Schlegel, P. M. W. Gill, B. G. Johnson, M. A. Robb, J. R. Cheeseman, T. Keith, G. A. Peterson, J. A. Montgomery, K. Raghavachari, M. A. Al-Laham, V. G. Zakrzewski, J. V. Ortiz, J. B. Foresman, C. Y. Peng, P. Y. Ayala, W. Chen, M. W. Wong, J. L. Andres, E. S. Replogle, R. Gomperts, R. L. Martin, D. J. Fox, J. S. Binkley, D. J. Defrees, J. Baker, J. P. Stewart, M. Head-Gordon, C. Gonzales and J. A. Pople, GAUSSIAN 98, Gaussian Inc., Pittsburgh, PA, 1998.
34 M. W. Wong, *Chem. Phys. Lett.*, 1996, **256**, 391.
35 J. Szczepanski, S. Ekern and M. Vala, *J. Phys. Chem.*, 1997, **101**, 1841.
36 T. D. Crawford, J. F. Stanton, J. C. Saeh and H. F. Schaefer, *J. Am. Chem. Soc.*, 1999, **121**, 1902.
37 D. A. Plattner and K. N. Houk, *J. Am. Chem. Soc.*, 1995, **117**, 4405.
38 L. M. L. Martin, J. El-Yazal and J.-P. Trancois, *Chem. Phys. Lett.*, 1996, **252**, 9.
39 E. E. Masqualine and M. Lopez, *Chem. Phys. Lett.*, 2000, **320**, 415.
40 J. Cizek, *Adv. Chem. Phys.*, 1969, **14**, 35.
41 J. A. Pople, R. Krishnan, H. B. Schlegel and J. S. Binkley, *Int. J. Quantum Chem.*, 1978, **4**, 545.
42 C. Hampel, K. Peterson and H.-J. Werner, *Chem. Phys. Lett.*, 1992, **190**, 1.
43 J. D. Watts, J. Gauss and R. J. J. Bartlett, *J. Chem. Phys.*, 1993, **98**, 8718.
44 P. J. Knowles, C. Hampel and H.-J. Werner, *J. Chem. Phys.*, 1993, **99**, 5219.
45 M. J. O. Deegan and P. J. Knowles, *Chem. Phys. Lett.*, 1994, **227**, 321.
46 T. H. Dunning, *J. Chem. Phys.*, 1989, **90**, 1007.
47 D. E. Woon and T. H. Dunning, *J. Chem. Phys. A*, 1993, **98**, 1358.
48 D. W. Arnold, S. E. Bradforth, T. N. Kitsopoulos and D. M. Neumark, *J. Chem. Phys.*, 1991, **95**, 8753.
49 C. Xu, G. R. Burton, T. R. Taylor and D. M. Neumark, *J. Chem. Phys.*, 1997, **107**, 3428.

Peppe, S., Dua, S., and Bowie, J.H., (2001) Is the elusive trioxydehydroethene neutral ($O_2C{-}CO$) detectable in the gas phase?
Journal of Physical Chemistry A, v. 105 (44), pp. 10139-10145.

Peppe, S., Blanksby, S.J., Dua, S., and Bowie, J.H., (2000) Formation of two isomeric C_3HO radicals from charged precursors in the gas phase. Potential interstellar molecules.
Journal of Physical Chemistry A, v. 104 (24), pp. 5817-5824.

Appendix

Oxides of Carbon

Carbon monoxide and carbon dioxide are almost universal in terrestrial and extraterrestrial environs; conversely, other known carbon oxides are comparatively scarce. Of these, the best known is carbon suboxide, C_3O_2, whose structure and properties have been extensively studied both experimentally [217] and theoretically.[218] However, the smaller related molecule ethylene dione, C_2O_2, has eluded all attempts at generating and unequivocally characterising it.[219,142]

Other studies of oligomers of carbon monoxide, i.e. the radical anions $C_nO_n^{-\bullet}$ (where n = 3–6), have been carried out (these C_nO_n species are referred to as oxocarbons according to the terminology introduced by West [220]). Of particular relevance to the work described in this thesis are the those investigations which have made use of metastable ion (MI) and collisional activation (CA) techniques,[221] charge-reversal,[71] and neutralisation-reionisation (NR)[78] mass spectrometry, as well as the neutral-and-ion decomposition difference (NIDD) scheme.[222]

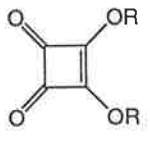

Ia, R = CH_3
Ib. R = *i*-C_3H_7

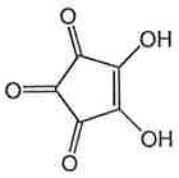

II

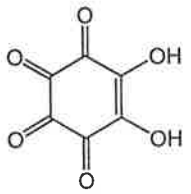

III

Such polyones may either exist as open-chain diradicals or as cyclic compounds in which the open valences are saturated by cyclisation; accordingly, it is not possible to distinguish by mass-spectrometry and the analysis of fragmentation patterns alone between the two isomeric structures, e.g. **1**, **2**.

Radical anions of oligomeric carbon monoxide, i.e. the oxocarbon ions [220,90,223] $C_nO_n^{-\bullet}$ (n = 2 - 6), can be generated by ionisation of a variety of precursors. Thus, ionisation of cyclic carbonyl compounds (dimethyl and di-iso-propyl squaric acid, **Ia** and **Ib** respectively, croconic acid, **II**, and the dihydrate of rhodizonic acid, **III**) in the negative ion mode [224] gave rise to a series of $C_nO_n^{-\bullet}$ ions whose mass spectra are identical within experimental error irrespective of the precursor used.[224] From these anions, the corresponding neutral counterparts were generated.

Oxocarbons with structures that can generally be described as cyclic polyketones, were formed without disruption of the gross structure of the precursor molecules.[224] The neutral and charged C_nO_n species showed a predominant tendency towards complete dissociation into CO molecules. This situation was evident in particular for the neutral polyones of n = 4 and 6. In the case where n = 3, however, a decent NR recovery signal was observed. However, the expected cyclopropanetrione **1** was not observed; instead, partial rearrangement (by means of an internal disproportionation) yielded an oxycarboxylate, i.e. $^{\bullet}O–C{\equiv}C–CO_2^-$, **3**.

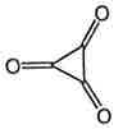

1

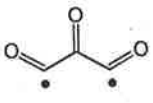

2

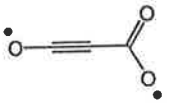

3

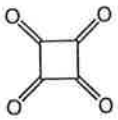

4

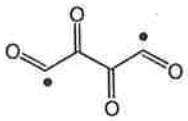

5

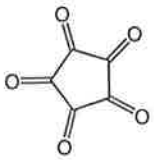

6

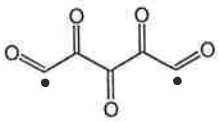

7

8

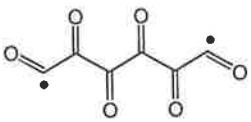

9

In the MI and CA spectra of $C_4O_4^{-\bullet}$, the major processes observed were the consecutive losses of carbon monoxide to afford $C_3O_3^{-\bullet}$ and $C_2O_2^{-\bullet}$, respectively, whereas decarboxylation to yield $C_3O_2^{-\bullet}$ was seen to be a minor process. In addition, the CR and NR spectra of $C_4O_4^{-\bullet}$ exhibited weak $CO_2^{+\bullet}$ signals. On this basis, and as implied by the precursors (and the previous observation of the anion radical $\mathbf{4}^{-\bullet}$ in the condensed phase [223]), structures **4** and/or **5** were assigned to the ions. Attempts to generate a carboxylate type ion in analogy to $\mathbf{3}^{-\bullet}$, i.e. $^{\bullet}O_2C–C{\equiv}C–CO_2^{-}$, by ionisation of acetylene dicarbonic acid esters failed.

Consecutive losses of CO were observed as major pathways in the MI and CA spectra of $C_5O_5^{-\bullet}$, suggesting the polyone structures **6** and/or **7**. The CR and NR spectra of $C_5O_5^{-\bullet}$ showed distinct recovery signals, which was in contrast to the other $C_nO_n^{-\bullet}$ investigated.[224] The recovery signal in the CR and NR spectra was assigned to an intact polyone instead of the carboxylate type structure due to the series of other $C_nO_n^{+\bullet}$ ions (n = 1 - 4) observed in these spectra, and because of the weakness of the observed $CO_2^{-\bullet}$ signal. Moreover, the distinct recovery signal observed for this species as compared to the other oligomers (n = 2, 4, 6) disfavors the acyclic structure **7**, because there is no reason to expect a particular stability for

n = 5. The latter result suggests that matrix isolation experiments may be successful in the isolation of free cyclopentanepentaone.

In the MI and CA spectra of $C_6O_6^{-\bullet}$, as in $C_4O_4^{-\bullet}$ and $C_5O_5^{-\bullet}$, consecutive losses of CO are the major processes observed. By analogy to the results obtained for $C_5O_5^{-\bullet}$, structure **8** was assigned to the anion radical formed upon ionisation of rhodizonic acid instead of **9**. The CR and NR spectra of $C_6O_6^{-\bullet}$ are, however, more analogous to those of $C_4O_4^{-\bullet}$ which show large abundances of low mass fragments, whereas the series of $C_nO_n^{+\bullet}$ ions (n = 2 - 6) are of minor abundance.

These experiments suggested an odd/even alternation in the stability of the free carbon oxides in the gas phase, but theoretical studies are required to shed more light on this apparent trend.

References

217 Lafferty, W. J.; Maki, A. G.; Plyler, E. K. *J. Chem. Phys.* **1964**, *40*, 224. Tanimoto, M.; Kuchitsu, K.; Morino, Y. *Bull. Chem. Soc. Jpn.* **1970**, *43*, 2776. Carreira, L. A.; Carter, R. O.; Durig, J. R.; Lord, R. C.; Milionis, C. C. *J. Chem. Phys.* **1973**, *59*, 1028. Duckett, J. A.; Mills, I. M.; Robiette, G. *J. Mol. Spectrosc.* **1976**, *63*, 249. Weber, W. H.; Maker, P. D.; Peters, C. W. *J. Chem. Phys.* **1976**, *64*, 2149. Weber, W. H.; Maker, P. D.; Peters, C. W. *J. Mol. Spectrosc.* **1979**, *77*, 139. Burenin, A. V.; Karyakin, E. N.; Krupnov, A. F.; Shapin, S. M. *J. Mol. Spectrosc.* **1979**, *78*, 181. Lolck, J.-E.; Brodersen, S. *J. Mol. Spectrosc.* **1978**, *72*, 445. Lolck, J.-E.; Brodersen, S. *J. Mol. Spectrosc.* **1979**, *75*, 234. Fusina, L.; Mills, I. M.; Guelachvili, G. *J. Mol. Spectrosc.* **1980**, *79*, 101. Fusina, L.; Mills, I. M. *J. Mol. Spectrosc.* **1980**, *79*, 123. Weber, W. H. *J. Mol. Spectrosc.* **1980**, *79*, 396. Bunker, P. *J. Mol. Spectrosc.* **1980**, *80*, 422.

218 Sabin, J. R.; Kim, H. *J. Chem. Phys.* **1972**, *56*, 2195. Jensen, H. H.; Nilssen, E. W.; Seip, H. M. *Chem. Phys. Lett.* **1974**, *27*, 338. Osamura, Y.; Nishimoto, K.; Yamabe, S.; Minato, T. *Theoret. Chim. Acta* **1979**, *52*, 257. Amos, R. D. *Chem. Phys. Lett.* **1984**, *108*, 347. Lozes, R. L.; Sabin, J. R.; Oddershede, J. *J. Mol. Spectrosc.* **1981**, *86*, 357. Janoschek, R. *J. Mol. Struct. THEOCHEM* **1991**, *232*, 147. Mosandl, T.; Stadtmuller, S.; Wong, M. W.; Wentrup, C. *J. Phys. Chem.* **1994**, *98*, 1080.

219 Sulzle, D. Technische Universität Berlin D83. Berlin. **1991**. Sulzle, D.; Weiske, T.; Schwarz, H. *Int. J. Mass Spectrom. Ion Processes* **1993**, *125*, 75. Chen, H.; Holmes, J. L. *Int. J. Mass Spectrom. Ion Processes* **1994**, *133*, 111. Schröder, D.; Schwarz, H. *Int. J. Mass Spectrom. Ion Processes* **1995**, *146/147*, 183. Dawson, D.; Chen, H.; Holmes, J. L. *Eur. Mass Spectrom.* **1996**, *2*, 373.

220 West, R.; Niu, J. *The Chemistry of the Carbonyl Group*. Interscience. New York. **1970**, *11* 241. West, R. *Oxocarbons*. In Academic. New York. **1980**,

221 Busch, K. L.; Glish, G. L.; McLuckey, S. A. *Mass Spectrometry/Mass Spectrometry: Techniques and Applications of Tandem Mass Spectrometry*. VCH Publishers. Weinheim. **1988**,

222 Schalley, C. A. Technische Universität Berlin D83. Shaker, Herzogenrath/Germany. **1997**.

223 Patton, E. V.; West, R. *J. Phys. Chem.* **1973**, *77*, 2652. Lednor, P. W.; Versloot, P. C. *J. Chem. Soc., Chem. Commun.* **1983**, 284.

224 Schröder, D.; Schwarz, H.; Dua, S.; Blanksby, S. J.; Bowie, J. H. *Int. J. Mass Spectrom.* **1999**, *188*, 17.